IL
NUOVO CIMENTO
ORGANO DELLA SOCIETÀ ITALIANA DI FISICA
SOTTO GLI AUSPICI DEL CONSIGLIO NAZIONALE DELLE RICERCHE

VOL. XIX, N. 6 *Serie decima* 16 Marzo 1961

On the Observation of Fast Σ-Hyperons Emitted from the Interactions of K^--Mesons with Emulsion Nuclei.

B. D. JONES, B. SANJEEVAIAH (*) and J. ZAKRZEWSKI (**)

H. H. Wills Physical Laboratory - Bristol

P. G. BIZZETI (***), J. P. LAGNAUX and M. RENÉ (***)

Laboratoire de Physique Nucléaire, Université Libre de Bruxelles

M. J. BENISTON, S. A. BROWN (†), E. H. S. BURHOP, D. H. DAVIS, D. FERREIRA, E. FROTA-PESSOA (§), W. B. LASICH and N. N. RAINA

Physics Department, University College - London

M. C. AMERIGHI, A. BONETTI, M. DI CORATO, C. C. DILWORTH, C. A. FEDRIGHINI, E. QUERCIGH, A. E. SICHIROLLO and G. VEGNI

Istituto di Scienze Fisiche dell'Università - Milano
Istituto Nazionale di Fisica Nucleare - Sezione di Milano

(ricevuto il 26 Agosto 1960)

Summary. — A study of fast baryons emitted from 12150 K^- meson interactions at rest in emulsion has been made in order to determine the nature and extent of K^- meson-multinucleon capture processes. Fast Σ hyperons are produced in at least 9 per cent of all interactions while direct fast Λ^0 hyperon production is indicated by the presence of 3 protons with energies exceeding 200 MeV. An upper limit of 30% is ob-

(*) On leave from the University of Mysore.
(**) On leave from the University of Warsaw.
(***) Now at Istituto di Fisica dell'Università, Firenze.
(***) Now at Centre d'Etudes Nucléaires, Saclay.
(†) Now at University College, Ibadan, Nigeria.
(§) Now at Centro Brasileiro de Pesquisas Físicas and Faculdade Nacional de Filosofia, Rio de Janeiro.

tained for multinucleon processes (not producing π mesons) from consideration of π meson emission. The energy spectra for fast Σ hyperons and fast protons are given and mass determinations on a sample of so-called fast protons have revealed about 10% of deuterons and tritons. The suggestion in K^- European Collaboration Part II of an apparent infrequency of the reaction $K^- + n + n \to \Sigma^- + n$ has been confirmed and an α-particle model of K^- meson multinucleon interaction has been put forward to explain both this and the emission of deuterons and tritons.

1. – Introduction.

In continuation of the work of the K^- European Collaboration an effort has been made to study K^- meson multi-nucleon interactions at rest with emulsion nuclei. For this purpose a search has been made for fast Σ hyperons of energies exceeding 60 MeV, since the presence of such a fast hyperon is the only certain indication that the capture has not taken place via a one-nucleon process. The experimental procedure and the result of the study of fast Σ hyperons are given below.

2. – Experimental method.

A stack of Ilford K-5 emulsion of dimensions 18 cm $\times$ 20 cm $\times$ 18 cm exposed to the filtered 300 MeV/c K^- meson beam from the Bevatron was used for this experiment. Grey tracks in the beam direction were picked up at about 1 cm from the entrance edge of the stack and followed to their end points. Those track endings falling within 50 μm (un processed) of either emulsion interface were discarded, as were also K_ρ^-'s or K_σ^-'s whose only charged secondary was found to be a π meson. The number of K_σ^- stars so obtained has been corrected using the results presented elsewhere [1].

The aim of this study was the identification of every baryon which had, at emission, a residual range in emulsion exceeding 1 cm. In order to distinguish between tracks of baryons and π mesons the scanning procedure was as follows:

i) The dip angle of each track which was possibly due to a fast baryon was measured. Since previous experience [2] has shown that it is difficult both to identify hyperons dipping steeply, and to measure their energies, tracks

[1] M. C. Amerighi, M. J. Beniston, A. Bonetti, D. H. Davis, M. Di Corato, C. C. Dilworth, D. Ferreira, E. Frota-Pessoa, W. B. Lasich, N. N. Raina, M. René J. Sacton and A. E. Sichirollo: *Nuovo Cimento*, **12**, 91 (1959).

[2] K^- European Collaboration, Part II: *Nuovo Cimento*, **14**, 315 (1959).

for which the dip angle exceeded 40° were discarded from the analysis. However, in the stars in which a fast baryon of dip $< 40°$ was emitted, all prongs were followed to their ends.

ii) 200 blobs of each light track were counted in the first instance. If the blob density was less than 25/100 μm, the track was taken to be that of a π meson. If the blob density exceeded 25/100 μm a further 400 blobs were counted. If the blob density was less than 30/100 μm the track was again taken as that of a π meson, if greater than 30/100 μm, the track was followed to its end point.

The blob density of the most energetic hyperon expected is 36/100 μm and all tracks with blob densities greater than 30/100 μm were followed. Therefore it is concluded that the loss of fast hyperons by these procedures is negligible.

All baryon tracks whose lengths exceed 1 cm, or would have exceeded 1 cm, had the baryons not decayed or interacted in flight, were followed under high magnification and these features recorded:

i) All changes in direction, greater than 10° for a residual range exceeding 2 mm, or greater than 45° for residual range less than 2 mm, whether or not accompanied by a change in grain density.

ii) All observable changes in grain density.

iii) Length of track followed in emulsion.

iv) Co-ordinates and depth of each ending.

The grain densities of tracks of particles decaying or interacting in flight were measured by appropriate methods at the end points such that the energies at emission could be determined with standard errors less than 10% whenever possible. (For $F\Sigma_{\pi}^{+}$, in 27 cases the error was less than 5%, in 20 cases it lay between 5% and 10% and in 8 cases it was greater than 10%). For $F\Sigma_{p}^{+}$ events the energies were also obtained from decay dynamics and the better estimates are quoted.

The endings of these tracks have been examined for evidence of either a nuclear interaction or a decay secondary. All recorded changes in grain density and/or direction have been checked for compatibility with the dynamics of $F\Sigma_{p}^{+}$ decay.

In order to reduce the effects of observational loss of fast hyperons, the following cut-offs have been applied to their end points:

i) For $F\Sigma_{\pi}^{\pm}$ and $R\Sigma_{\pi}^{+}$ (also stops in flight) 50 μm (unprocessed).

ii) For F_{p}^{+}, $R\Sigma_{p}^{+}$, $R\Sigma^{-}$ and $F\Sigma^{\pm}$ interactions (also fast baryon interactions in flight) 20 μm (unprocessed).

TABLE I.

Event No.	Dip of Σ at decay	Dip of proton at decay	Projected laboratory angle	Laboratory space angle	Range of proton in mm	Range of primary if proton in mm	Energy of Σ at decay from ionisation in MeV	Energy of Σ from dynamics in MeV	Comments
UCL 12905	$26\frac{1}{2}°$ s	53° s	10°	$28 \pm 5°$	26.6	19.2 ± 3.1	99 ± 9	$55 \div 91$ forward $91 \div 148$ backward	Only allowed laboratory angles lie in the range $23 \div 26.4°$ within the quoted errors.
UCL 13610	$31\frac{1}{2}°$ s	$15\frac{1}{2}°$ s	10°	$18\frac{1}{2} \pm 2°$	41.7 ± 2.6	11.8 ± 1.8	73 ± 7	80^{+20}_{-10}	
UCL 11508	38° g	51° g	5°	$14 \pm 5°$	0.2	6.7 ± 1.1	54 ± 5	55 ± 1	
UCL 9914	37° s	69° s	14°	$32 \pm 5°$	8.2	2.0 ± 1.7	26^{+12}_{-18}	15 ± 6	
UCL 14009	9° g	49° s	43°	$49 \pm 1°$	2.3	$5.6^{+1.8}_{-1.1}$	43^{+7}_{-5}	41 ± 2	Σ inelastically scattered before decay
UCL 14210	35° s	4° g	$2\frac{1}{2}°$	$33\frac{1}{2} \pm 3°$	6.2 ± 1	23 ± 5	104^{+13}_{-19}	79 ± 11	
UCL 14109	21° s	$1\frac{1}{2}°$ s	37°	$41 \pm 1°$	6.2	4.1 ± 0.8	41^{+6}_{-4}	44 ± 5	
UCL 13103	37° s	38° s	$23\frac{1}{2}°$	$18\frac{1}{2} \pm 2°$	0.31	6.7 ± 1.8	54 ± 9	64 ± 10	
Br 179/21	40° g	24° s	13°	$19 \pm 2°$	30.27	11.0 ± 2.5	70^{+7}_{-6}	57 ± 10	
Bx 22	43° g	$36\frac{1}{2}°$ g	20°	$17 \pm 3°$	7 ± 2	38 ± 4	144 ± 9	128 ± 20	Stopping proton of 0.66 mm range
Bx 5036	23° s	6° s	17°	$24 \pm 3°$	32 ± 5	10.5 ± 3	69 ± 12	72^{+30}_{-20}	Proton interacts in flight after 13.1 mms.
Mi 610	$22\frac{1}{2}°$ g	28° g	$24\frac{1}{2}°$	$23 \pm \frac{1}{2}°$	33.7	11.3 ± 2	72 ± 8	77 ± 2	
Mi 1179	$12\frac{1}{2}°$ s	12° g	7°	$25\frac{1}{2} \pm 2\frac{1}{2}°$	16.8	2.9 ± 0.9	33 ± 7	34^{+6}_{-3}	
Mi 1823	1° g	19° s	17°	$26 \pm 2°$	18.4	31.6 ± 4	130 ± 10	118 ± 18	
Mi 2427	11° g	27° s	8°	$38\frac{1}{2} \pm 3\frac{1}{2}°$	1.64	8.0 ± 1.2	59 ± 6	59 ± 8	
Mi 3887	18° s	7° g	5	$26 \pm 2\frac{1}{2}°$	33	24.5 ± 4	112 ± 4	$77 \div 105$ forward $105 \div 144$ backward	Only allowed angles lie in range $23.2° \rightarrow 24.6°$ within quoted errors.
Mi 198	1° g	9° g	80°	$80 \pm 1°$	0.67	(0.67)	16	15 ± 1	Velocity of primary at decay not directly measurable, no visible change in ionization as required by decay dynamics. Could be a

TABLE II-*a*). – *No accompanying proton* ⩾ 30 MeV.

No. of prongs	1	2	3	4	5	⩾6	Total
$F\ \Sigma^{\pm}_{\pi}$	7	13 [a]	4	2	3	2 [b]	31
$F\ \Sigma^{+}_{p}$	5	6	1	4	—	—	16
$R\ \Sigma^{+}_{\pi}$	—	1	—	—	—	—	1
$R\ \Sigma^{+}_{p}$	1	2	—	—	—	—	3
$R\ \Sigma^{-}$	—	1	—	—	—	—	1
Previous stack							
$F\ \Sigma^{\pm}_{\pi}$	4	3	4	1	3	1	16
$F\ \Sigma^{+}_{p}$	4	2	—	—	1	—	7
$R\ \Sigma^{+}_{\pi}$	1	—	—	—	—	—	1
$R\ \Sigma^{+}_{p}$	—	—	—	—	—	—	0
$R\ \Sigma^{-}$	—	2	—	1	—	—	3

(*a*) 1 found to be positive by following decay meson.
(*b*) 1 found to be negative by following decay meson.

TABLE II-*b*). – *Associated proton* ⩾ 30 MeV.

No. of prongs	1	2	3	4	5	⩾6	Total
$F\ \Sigma^{\pm}_{\pi}$	—	17 [c]	5 [d]	7	5	3	37
$F\ \Sigma^{+}_{p}$	—	—	—	—	—	—	—
$R\ \Sigma^{+}_{p}$	—	—	—	—	—	—	—
$R\ \Sigma^{+}_{\pi}$	—	—	—	—	—	—	—
$R\ \Sigma^{-}$	—	—	2	2	1	—	5
Previous stack							
$F\ \Sigma^{\pm}_{\pi}$	—	5	4	2	2	—	13
$F\ \Sigma^{+}_{p}$	—	—	1	1	—	—	2
$R\ \Sigma^{+}_{\pi}$	—	—	—	—	—	—	—
$R\ \Sigma^{+}_{\pi}$	—	—	—	—	—	—	—
$R\ \Sigma^{-}$	—	1	—	—	1	—	2

(*c*) 1 found to be negative by following decay meson.
(*d*) 2 found to be negative by following decay meson.

TABLE III. – *Energy dis*

		60÷70	70÷80	80÷90	90÷100	100÷110	11
a) Accompanied by proton of energy ⩾30 MeV	$F\Sigma_{\pi}^{\pm a}$	7	7	7	4	5	
	$R\Sigma^{-}$	3	—	1	—	—	
	$F\Sigma_{p}^{+}$	—	—	—	—	—	
	$R\Sigma_{\pi}^{+}$						
	$R\Sigma_{p}^{+}$						
b) Unaccompanied by proton of energy ⩾30 MeV	$F\Sigma_{\pi}^{\pm b}$	7	6	3	2	2	
	$F\Sigma_{p}^{+}$	1	5	4	2	—	
	$R\Sigma_{p}^{+}$	1	1	1	—	—	
	$R\Sigma_{\pi}^{+}$	1	—	—	—	—	
	$R\Sigma^{-}$	—	1	—	—	—	

(*a*) 3 found to be negative by following decay π-meson to rest.
(*b*) 1 found negative and 1 positive by following decay π-meson to rest.

Since the observational loss of light tracks in this stack is small [1] and the number of stops in flight is consistent with that expected from the observed proton track length, no correction for π meson loss has been made to the number of Σ hyperons.

The decay angle distribution of $F\Sigma_{p}^{+}$ events in the C.M. system was consistent with isotropy, (6 forward, 8 backward, 2 ambiguous) so that no correction has been applied to the observed numbers of such events. However, since confusion often exists between events classed as $F\Sigma_{p}^{+}$ decays and proton scatterings, the details of the 17 $F\Sigma_{p}^{+}$ candidates are presented in Table I. It can be seen that only one event can be interpreted both as a proton single scattering and as an $F\Sigma_{p}^{+}$. Thus, within the criteria adopted in the present work, the ambiguity as to the true number of these decays is less than 10% of the certified $F\Sigma_{p}^{+}$, and was not taken into account in what follows.

The number of observed Σ^{-} hyperon interactions at rest ($R\Sigma_{\sigma}^{-}$), defined as previously [2], needs correcting for $R\Sigma_{\rho}^{-}$ events and 1 prong capture stars where the length of the prong is less than 200 μm. A correction factor of $2.8^{+0.6}_{-0.4}$ obtained from a recent compilation of K^{-}+ H capture data (*) has been applied to these events.

All K^{-} meson capture stars which were found to emit a fast baryon have been fully analysed, looking particularly for the presence of π mesons and strange particles.

(*) 107 events quoted by M. NIKOLIĆ, Y. EISENBERG, W. KOCH, M. SCHNEEBERGER, and H. WINZELER: *Helv. Phys. Acta*, **33**, 237 (1960) and 21 events found in this stack.

bserved Σ hyperons.
ek only

erval MeV								
0÷130	130÷140	140÷150	150÷160	160÷170	170÷180	180÷190	190÷200	>200
3	2	—	—	—	—	—	—	—
—	—	—	—	—	—	—	—	—
—	—	—	—	—	—	—	—	—
3	1	—	1	—	1	1	—	—
—	—	—	—	—	—	—	2	—
—	—	—	—	—	—	—	—	—
—	—	—	—	—	—	—	—	—
—	—	—	—	—	—	—	—	—

3. – Results.

The results presented here have been obtained from 9130 K^- meson interactions at rest. The relevant data from 3020 K^- meson captures analysed in the previous work ([2]) are included separately. The prong distributions of K^- meson stars seen so emit Σ hyperons of energies exceeding 60 MeV are presented in Table II. This table is sub-divided so show whether or not an accompanying proton of energy greater than 30 MeV was emitted.

The energy spectra of observed fast charged Σ hyperons are shown in Table III. The corrected spectra for both Σ^+ and Σ^- hyperons are given in Fig. 1*a* and 1*b*. To obtain these, the numbers of $R\Sigma^-$ have been corrected for observational loss, geometrical corrections have been applied and a value of unity accepted for the branching ratio $\Sigma^+ \to p + \pi^0$: $\Sigma^+ \to n + \pi^+$ ([3]) The final corrected results of the previous work are also included. The total number of Σ hyperons of energies exceeding 60 MeV emitted from 12150 K^- meson absorptions at rest is thus found to be 275, of which 96 are Σ^+ and 179 are Σ^- hyperons.

All baryons other than identified hyperons have been regarded as protons and their spectra are given in Fig. 2, 3 and 4. Fig. 2 is the spectrum of

([3]) D. A. Glaser: *Kiev Conference Report* (1959).

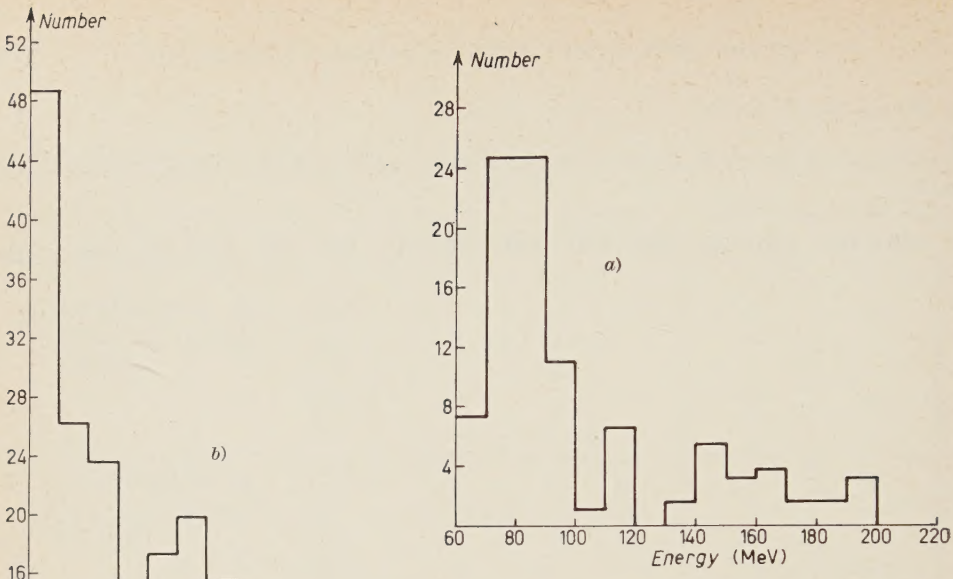

Fig. 1-*a*. – Corrected Σ^+ hyperon spectrum. (96 events).

← Fig. 1-*b*. – Corrected Σ^- hyperon spectrum. (179 events).

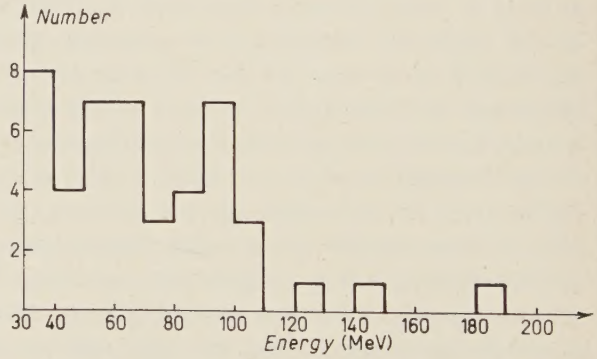

Fig. 2. – Energy spectrum of protons accompanying fast Σ hyperons. (kin. energy $\geqslant$ 30 MeV).

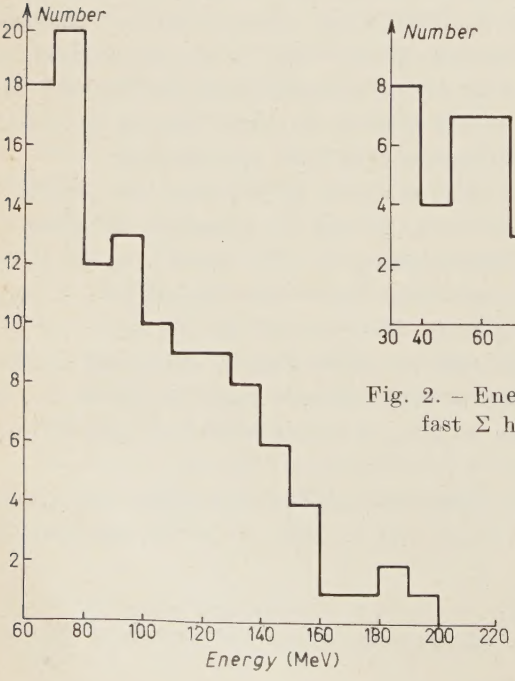

Fig. 3. – Energy spectrum of fast protons emitted without any other accompanying charged particles (kin. energy $\geqslant$ 60 MeV).

protons accompanying fast charged Σ hyperons and is extended down to 30 MeV, Fig. 3 is that of protons unaccompanied by any other charged par-

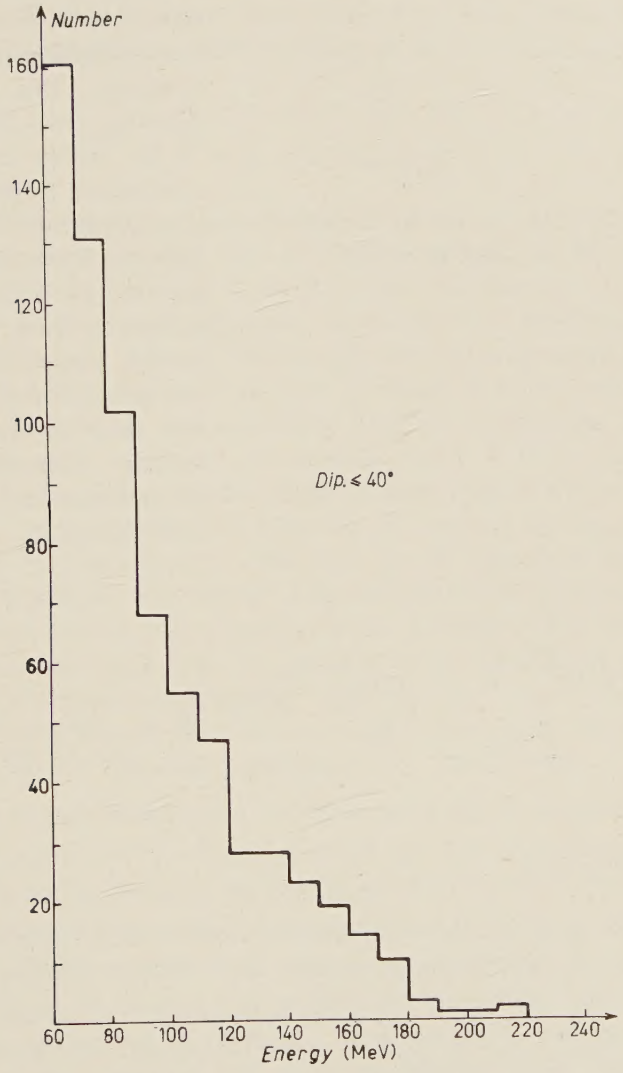

Fig. 4. – Energy spectrum of all fast protons emitted unaccompanied by π mesons, Σ hyperons or hyperfragments (kin. energy ⩾ 60 MeV).

ticles at the parent K^- meson star, whilst Fig. 4 is a composite spectrum of all protons (with kinetic energy ⩾ 60 MeV) except those emitted in asso-

ciation with hyperfragments, charged π mesons or Σ hyperons: in three cases the energy is larger than 200 MeV.

The masses of a sample of particles which came to rest in emulsion after a range exceeding one centimetre have been determined from ionisation and range measurements. Fig. 5 shows the resulting mass distribution.

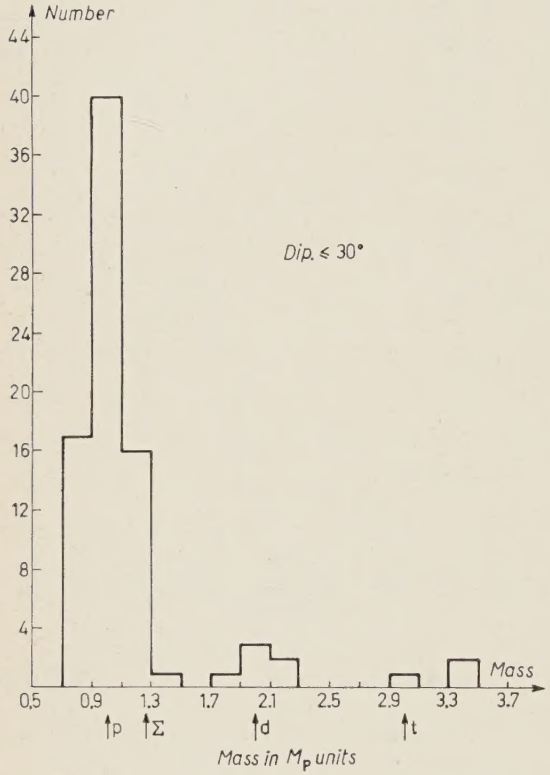

Fig. 5. – Baryon mass spectrum. 83 events.

No further example of an exothermic interaction ([4]) has been found but two Σ^+ hyperon inelastic scatterings have been reported ([5]). A total of 1328 cm of baryon track length in the energy range $(52 \div 220)$ MeV has been followed and the mean free path for interaction (including inelastic scattering) in emulsion is found to be $(33.2^{+5.9}_{-4.3})$ cm (*).

4. – Discussion.

From Table II it can be seen that identified fast Σ^- hyperons are often associated with protons of energy greater than 30 MeV whereas identified Σ^+ are in general not. There are 15 cases of Σ^- hyperons of energies $\geqslant 60$ MeV and of those 10 have a fast proton $\geqslant 30$ MeV in association and none was emitted without other charged particles (**). Further, over a total of 29,

([4]) K$^-$ European Collaboration, Part III: *Nuovo Cimento*, **15**, 873 (1960).

([5]) D. H. Davis, B. D. Jones and J. Zakrzewski: *Nuovo Cimento*, **14**, 265 (1959).

(*) One interacting primary was too short to enable distinction between π meson or baryon to be made. If a baryon, the interaction length would become 32.5 cm.

(**) 3 further Σ^- hyperons of energies just less than 60 MeV were each accompanied by a fast proton.

there are only two examples of a fast Σ^+ hyperon accompanied by a fast proton, but 11 cases where the fast Σ^+ is the only charged secondary. This suggests that the $F\Sigma_{\pi}^{\pm}$ hyperons associated with protons $\geqslant 30$ MeV are mostly negative, whereas those emitted alone are positive.

Assuming the fast hyperons arise from K^- meson interactions with two nucleons, the Σ^- hyperons could be produced in the following two reactions:

$$(1) \qquad K^- + n + n \to \Sigma^- + n$$

$$(2) \qquad K^- + n + p \to \Sigma^- + p\,.$$

The non-observation in this investigation of fast Σ^- emitted without other accompanying prongs (*) could then be interpreted to mean that the transition amplitude leading to (1) is much smaller than that leading to (2). This interpretation has in fact been advanced previously (**). The results could also be explained, however, if the K^- interaction with more than one nucleon occurs predominantly with a cluster of nucleons in which at least one is a proton ([2,6]). In particular the results are consistent with the assumption that the commonest cluster with which K^- interactions occur is the α-particle. Recent observations in the helium bubble chamber have indicated that a considerable fraction of Σ^- hyperons observed following K^- capture at rest originated from multi-nucleon interactions (***). This has to be compared with the observations that less than 1 in 250 K^- interactions (*,*) at rest in the deuterium bubble chamber involve both nucleons in the deuteron. The emission of energetic deuterons and tritons, as observed, is to be expected if the K^- mesons sometimes interact with α-particles.

The direct estimate of the fraction of multi-nucleon K^- meson absorptions is restricted by the following uncertainties:

i) the energy distribution at creation of the Σ hyperons;

ii) the extent of the degradation of the fast Σ hyperon energy distributions by inelastic scattering processes within the parent nuclei;

iii) the absorption probabilities applicable to Σ hyperons;

iv) the fraction of direct Λ^0 hyperon production.

If it is assumed that the multi-nucleon processes do in fact take place with two nucleons and the calculated spectra ([2]) are correct, and that charge inde-

(*) Two events of this type have in fact been found by the Rehovoth group (private communication), but this is not in conflict with the conclusion that they are rare.

(**) See reference ([2]), and also report by E. H. S. Burhop to the Kiev Conference, 1959.

([6]) D. H. Wilkinson: *Phil. Mag.*, **4**, 215 (1959).

(***) Helium Bubble Chamber, K⁻ Collaboration Group, Rochester Conference, 1960.

(*,*) L. W. Alvarez: *Kiev Conference Report*, (1959).

pendence holds, on applying the Σ hyperon absorption probabilities obtained from a study of one nucleon processes (*i.e.* ~ 0.5), 9% of K^- meson interactions at rest occur with two nucleons to produce Σ hyperons. This value must be considered a lower limit of K^- meson multi-nucleon capture processes since resolution of the uncertainties mentioned above seem likely to increase this value. Also the contribution from direct Λ^0 hyperon production has to be added and the presence of three fast protons in the sample with energies exceeding 200 MeV suggests that this process does occur.

An alternative method of estimating the fraction of multi-nucleon K^- meson absorptions is provided by the study of π mesons emitted from K^- meson captures. The $\pi^{\pm}/K^-$ ratio has been found to be 40% [1] and after allowance for π meson absorption [2] and assuming charge independence, this implies that at least 70% of K^- meson captures at rest create π mesons. If any π loss remains and/or the absorption probability assumed for mesons created with Λ^0 hyperons is too low, this figure will increase. Thus the upper limit for multi-nucleon processes which do not produce π mesons deduced from our work is $\sim 30\%$ (*). This is consistent with the result quoted in Part II[2] on incomplete data.

5. – Conclusions.

i) $(2.3 \pm 0.2)\%$ of K^- meson interactions at rest with emulsion nuclei are seen to emit charged Σ hyperons of energies greater than 60 MeV.

ii) In general fast Σ hyperons accompanied by protons $\geqslant 30$ MeV are negative whereas those emitted with no other charged secondaries are positive.

iii) The above results could indicate an intrinsic infrequency of the reaction

$$K^- + n + n \to \Sigma^- + n .$$

They could also be explained however in terms of a K^- meson α-particle interaction model. In support of such a hypothesis is the observation of a substantial admixture of deuterons and tritons amongst the so-called fast protons.

iv) Also the production of Σ^- hyperons occurs with about twice the frequency of Σ^+ hyperons.

v) The upper limit of the frequency of multi-nucleon processes not producing π mesons, as deduced from the $\pi^{\pm}/K^-$ ratio, is $\sim 30\%$. The lower limit obtained from this study of fast Σ hyperons is 9%.

(*) The Berne group, (see footnote, page 4), from a similar argument, quote the frequency of multi-nucleon processes to be $(37 \pm 5)\%$. U. Kundt, K. Lanius and K. Lewin (*Nuovo Cimento*, **14**, 943 (1959)) find from their data $\sim 20\%$, but they use larger absorption probabilities for the π mesons.

vi) The presence of protons with energies greater than 200 MeV strongly indicates direct Λ_0 hyperon production in K^- meson multinucleon interactions.

* * *

We wish to thank Professor E. J. Lofgren and the Bevatron crew for the exposure and Professors E. H. S. Burhop, A. J. Herz and G. P. S. Occhialini and Drs. D. Evans and W. M. Gibson for many helpful discussions. We thank also Dr. R. C. Kumar for his contributions in the early stages of this work.

Acknowledgement is also made to D.S.I.R. for a special development grant to University College London and research studentships to B.D.J. and M.J.B., to the Conselho Nacional de Pesquizas (Brasil) for the award of a fellowship to E.F.-P., to the Indian Ministry of Education and University of Mysore for an overseas Scholarship to B.S., to the Institute for Nuclear Research, Warsaw, for a grant to J.Z., and to the Istituto Nazionale di Fisica Nucleare, Sottosezione di Firenze for a grant to P.G.B.; B.S. and J.Z. also wish to express their gratitude to Professor C. F. Powell for the hospitality extended to them at Bristol.

Finally, we wish to thank the many scanners and microscopists for their diligent work.

RIASSUNTO

Allo scopo di determinare la frequenza e le caratteristiche del processo di cattura « a più nucleoni » dei mesoni K^-, sono stati studiate la frequenza e la distribuzione energetica dei barioni « veloci » (energia cinetica $\geqslant 60$ MeV per iperoni Σ) emessi da un gruppo di 12150 interazioni di mesoni K^- a riposo. Gli iperoni Σ carichi « veloci » sono emessi con la frequenza del $(2.3 \pm 0.2)\%$, i negativi essendo due volte più numerosi dei positivi. La frequenza di produzione di iperoni Σ carichi e neutri nell'ipotesi di processi « a due nucleoni » può essere valutata del 9%: questo è anche un limite inferiore per la frequenza dei processi « a più nucleoni » (nei quali non vengano prodotti mesoni π). Un limite superiore si ottiene dal rapporto $\pi^{\pm}/K^-$, e risulta $\sim 30\%$. La presenza di protoni (non accompagnati da iperframmenti, mesoni $\pi^{\pm}$ o iperoni $\Sigma^{\pm}$) con energia maggiore di 200 MeV indica la possibilità di produzione diretta di iperoni Λ^0 in processi « a più nucleoni ». Si osserva infine che gli iperoni Σ^- « veloci » sono accompagnati in due terzi dei casi da un protone di più di 30 MeV, ed è raro che siano emessi senza essere associati ad altre particelle cariche, mentre gli iperoni $\Sigma^{\pm}$ « veloci » sono raramente accompagnati da protoni veloci, mentre in poco meno del 40% dei casi sono l'unica particella carica emessa. Questo risultato può indicare una intrinseca rarità della reazione $K^- + n + n \to \Sigma^- + n$, ma può essere interpretato anche come conseguenza dell'interazione del mesone K^- con un gruppo di nucleoni, di cui almeno uno è un protone, e in particolare con una particella α. Il fatto che il 10% circa dei barioni veloci sia costituito da deutoni e tritoni è in accordo con questo modello.

Primary Cosmic-Ray α-Particles - I (*).

A. Engler (**), M. F. Kaplon, A. Kernan (***), J. Klarmann
Department of Physics and Astronomy, University of Rochester

C. E. Fichtel (***) and M. W. Friedlander
Department of Physics, Washington University - St. Louis

(ricevuto il 31 Ottobre 1960)

Summary. — The primary cosmic-ray α-particle energy spectrum has been investigated, using photographic emulsions flown from Minneapolis on July 30th, 1957. The total flux observed was (151 ± 9)particles/cm^2 sr s. The differential energy spectrum shows a broad maximum between 400 and 600 MeV/nucleon, and appears different in shape from the spectrum observed at solar minimum. No particles were observed to have kinetic energies below 200 MeV/nucleon, but a substantial flux was observed between 200 and 300 MeV/nucleon. From the centered dipole approximation to the geomagnetic field, one would expect a cut-off energy at this latitude of 292 MeV/nucleon. The results presented here are in disagreement with this figure, but do not allow a choice to be made between cut-off energies predicted from other models.

1. – Introduction.

Studies of the primary cosmic radiation, particularly the α-particle component, have been pursued intensely in recent years with nuclear emulsions and counters. Two effects have become apparent: *a*) the simple centered dipole approximation for the earth's magnetic field affecting the arrival of

(*) The work reported here has been supported by the Air Force Office of Scientific Research, under contracts AF. 49(636)-303 and AF. 18(603)108.

(**) Now at Duke University, Durham, N.C.

(***) Now at University College, Dublin.

(***) Now at Goddard Space Flight Centre, N.A.S.A., Washington, D.C.

cosmic rays is not valid, and *b*) the fluxes and energy spectra are observed to be strongly affected by solar activity and show a definite correlation with the 11 year solar cycle.

The present work, together with that to be reported in later papers (II and III) is the result of collaboration and discussion between the groups at the University of Rochester, Oxford University and Washington University. Here we shall discuss in detail the general approach and experimental procedure employed in these experiments and also the results obtained at one geomagnetic latitude, $\lambda = 55\,^{\circ}\mathrm{N}$, within narrow limits of longitude. The second paper will contain the results obtained from another balloon flight further north, and all the data pertinent to the low energy part of the α-particle energy spectrum will be discussed and summarized; the third paper will be devoted to results obtained at higher energy, on a more southerly balloon flight.

2. – Experimental details.

2·1. *Balloon flight and emulsion stack.* – On July 30th, 1957, a stack of emulsions was launched on a balloon flight from Minneapolis, Minnesota. The trajectory of the flight and the time-altitude curve are given in Fig. 1 and 2. During the flight, these emulsions formed one block, suspended inside

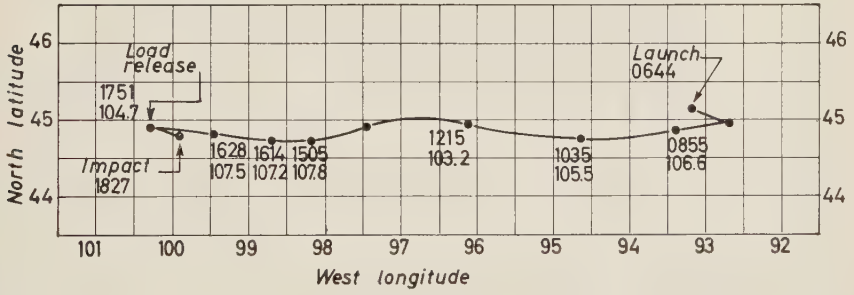

Fig. 1. – Flight trajectory, as determined from theodolite and spotting-plane data. Times are Central Daylight Times, altitudes are in thousands of feet.

a fibreglass gondola. This was launched with the emulsion planes horizontal; 30 minutes after the balloon reached ceiling, the stack was rotated so that the emulsion planes were vertical. After this rotation, a mean pressure altitude of 8.5 mb was maintained for 8 h 51 min. The thickness of the fibreglass and packing material above the emulsions was equivalent to 0.3 g/cm² of air.

The stack of 12 in.×10 in. Ilford G-5 emulsions was divided between the University of Rochester (150 sheets, each 400 μm thick) and Washington Uni-

versity (88 sheets, each 600 μm thick). These emulsions were processed by the usual temperature cycle method.

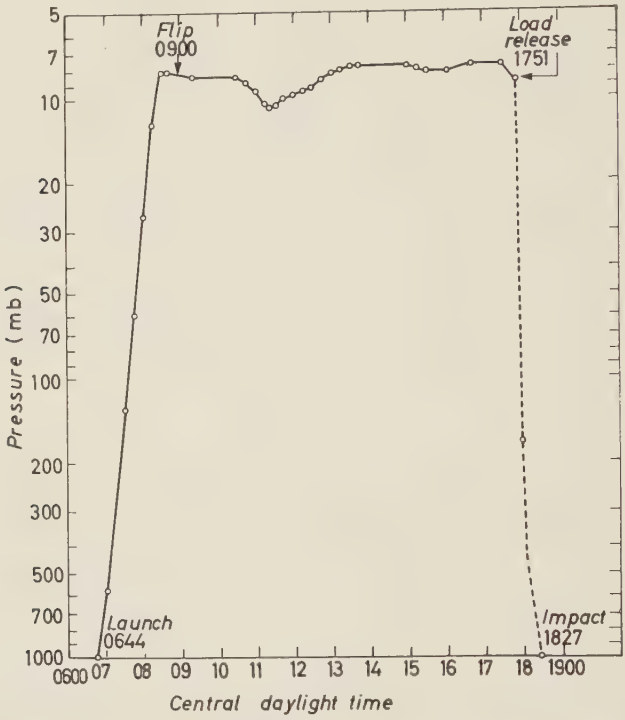

Fig. 2. – Time-altitude curve. At the time indicated by « flip », the emulsions were rotated through 90°, setting their planes vertical.

2·2. *Scanning and efficiency of detection.* – Along the selected scanning lines only those tracks were accepted by the scanners for which:

i) the projected length was at least 5 mm (in the 400 μm emulsions) or 7 mm (in the 600 μm emulsions) or, in the case of interacting particles, the dip angle of the track was equivalent to this length requirement;

ii) the projected angle to the zenith was not more than 30°, and

iii) the grain density was at least $3g_0$ (g_0 is the grain density of tracks of singly charged particles at plateau ionization).

To these tracks, as found by the scanners, more stringent criteria were applied:

i) the projected track lengths had to be greater than 6 mm or 9 mm (depending on the emulsion thickness) or, for interacting particles, the track dip must be equivalent, and

ii) the projected zenith angle had to be less than 20°.

Error in measurement on the part of the scanners will thus be unimportant as the final flux values are based upon the more restricted group of tracks only.

It was found, in the 600 μm emulsions, that these were not completely flat at the top of the stack and that the length per plate of fast α-particles did not become constant until about 2 cm from the top. Accordingly the scanning line was set at 3 cm from the top of the stack. No such effect was observed in the 400 μm emulsions, which were closer to the rigid end plates, and scanning in these plates was along a line 1 cm from the top.

It has previously [1] been pointed out that the usual check for scanning efficiency, namely the length distribution of tracks found, is only an approximately valid procedure and this is particularly true for this experiment. Hence the most sensitive method of obtaining information on the scanning efficiency is by rescanning part of the emulsions by different observers. If the observers are experienced and do not tend to miss tracks in any systematic manner, then rescanning will yield a reliable estimate of the overall scanning efficiency. This has been done and the results indicate that the scan at W.U. was 98% efficient while at U.R. 2 scanners had 100% efficiency and a third one only 85%. The final results include the appropriate corrections for these factors.

3. – Particle identification and energy measurements.

All tracks of particles obeying the scanning criteria were traced back to the top of the stack and, if they originated from an interaction, rejected; otherwise they were followed until they stopped, interacted or left the stack. In 16 plates, corresponding to total horizontal area of 5.1 cm² W.U. found 667 tracks, while in 10 plates of 4.33 cm² horizontal area, U.R. found 648 tracks obeying the scanning criteria.

By inspection, it was possible to reject most of the slow protons, which were recorded in the scanning. On the remaining tracks the following measurements were performed:

i) Estimation of the ionization loss parameter g^* from counts of 400 blobs and 100 gaps (the length was chosen so that $\log B/H \sim 2.5$) on each track. Each plate in which the ionization measurements were done was calibrated by determining g_0 from similar counts on several slow protons and using the known g-R relation for singly charged particles [2]. The standard error in $g^* = g/g_0$ was about 6%.

---

[1] A. Engler, M. F. Kaplon and J. Klarmann: *Nuovo Cimento*, **12**, 310 (1958).
[2] P. H. Fowler and D. H. Perkins: *Phil. Mag.*, **46**, 587 (1955).

ii) Multiple scattering measurements were made on each track on a basic cell size of (200÷500) μm depending upon the value of g^* for the track in question. Sufficient readings were taken so that at least 72 3rd differences were obtained on the third overlap. (On a few tracks this was not possible as the particles either interacted or were sufficiently scattered to shorten their track length per plate.) The statistical error in $p\beta$ was $\leqslant 25\%$. For details of the determination of $p\beta$ including possible systematic errors we refer to Appendix A.

The combined measurements of g^* and $p\beta$ serve to identify a particle and yield an estimate of its velocity or energy.

For kinetic energies up to 600 MeV/nucleon ($g^* \geqslant 1.2$), the most reliable energy estimates come from the g^* measurement and the g^*-range-energy relation (*). The energy estimates up to 600 MeV/nucleon are thus based on g^* measurements and their error, while depending on the actual energy value, are of the order of 10%. In the energy interval (600÷1000) MeV/nucleon the energy estimates were taken from multiple scattering measurement with an error of $\leqslant 25\%$. Beyond, that as pointed out in Appendix A, energy measurements become unreliable in these emulsions. However, for the discussion of flux and the integral energy spectrum, particles with energies in excess of 1 GeV/nucleon can still be considered.

4. – Results and discussion.

4·1. *The flux of α-particles.* – The total number of α-particles found at the scan line was 160 and 126 in the two laboratories (W.U. and U.R. respectively). Correcting for scanning efficiency these become 163 and 132 α-particles. To convert these numbers into a flux at the top of the atmosphere, the intensities observed at the scan line were first extrapolated to the top of the stack by giving each track a weight of $\exp[x/\lambda]$, where x is the distance traversed in emulsion before detection and $\lambda = 20$ cm, the interaction m.f.p. of α-particles. Finally to extrapolate the flux to the top of the atmosphere the appropriate diffusion equations (3) were solved using the « Bristol » m.f.p.'s and fragmentation parameters (4) and taking into account the solid angle of acceptance. (See Appendix B for a brief discussion of the calibration of the original emulsion thickness.) The final results are: U.R. (138 ± 13) par-

(*) Preliminary measurements (C. FICHTEL: *Thesis*, W.U. (1959)) indicate the g^*-R curve for α-particles to be the same as that obtained by FOWLER and PERKINS (2) for singly charged particles, for $g^* \geqslant 1.2$.

(3) Reference (1), eq. (5.*b*).

(4) V. Y. RAJOPADHYE and C. J. WADDINGTON: *Phil. Mag.*, **3**, 19 (1959).

ticles/m² sr s and W.U. (162 ± 13) particles/m² sr s with a weighted mean of (151 ± 9) particles/m² sr s, the error being statistical only. The above figures refer to all particles above a given cut-off energy E_0. Slow particles with $E < E_0$ will be lost if they are brought to rest either in the atmosphere or in the emulsion above the scan line. For W.U. this cut-off is at 145 MeV/nucleon while for U.R. it is 112 MeV/nucleon. We have nevertheless taken the mean of both fluxes, since as is evident from the differential energy spectrum the flux in the interval (110÷145) MeV is negligible; in fact, no particles were observed to have kinetic energies below 200 MeV/nucleon.

Table I summarizes all the flux values from 1950 until 1958 obtained by emulsion and counter techniques. The correlation with solar activity noted

TABLE I. – *Fluxes obtained over Minneapolis, Minn.* $\lambda = 55°$ N.

Date of flight	Residual matter above detector (g/cm²)	Zenith angle cut-off	E_{min} (MeV)	Flux (particles/ /m² sr s)	Refer-ences	Technique
October 4.50	10	—	—	280 ± 8	(5)	counters
October 5.50	14	60°	< 150 MeV	320 ± 36	(6)	emulsions
October 20.52	8	—	?	320 ± 40	(7)	counters
July 7.55	9	—	285	286 ± 24	(8)	counters
August 21.56	?	—	?	262 ± 15	(8)	counters
May 17.57	?	?	225	157 ± 17	(9)	emulsions
July 30.57	8.8	20°	110	151 ± 9	pres.work	emulsions
September 1.57	18	45°	200	136 ± 9	(10)	emulsions
February 16.58	5	—	145	131 ± 8	(11)	counters
July 2.58	5	—	< 145	126 ± 7	(11)	counters

For counters the zenith angle of acceptance is essentially zero.

previously by other authors (9-13) is clearly seen. The value obtained in this work is in excellent agreement with results obtained during the period of solar maximum. At this stage of experimental accuracy it is clearly difficult to

(5) E. P. NEY and D. M. THON: *Phys. Rev.*, **81**, 1069 (1951).
(6) C. J. WADDINGTON: *Phil. Mag.*, **45**, 1312 (1954).
(7) L. R. DAVIS, M. M. CAULK and C. Y. JOHNSON: *Phys. Rev.*, **101**, 800 (1956).
(8) F. B. MCDONALD: *Phys. Rev.*, **107**, 1386 (1957).
(9) S. E. FORBUSH: *Journ. Geophys. Research*, **59**, 525 (1954).
(10) P. S. FREIER, E. P. NEY and C. J. WADDINGTON: *Phys. Rev.*, **114**, 365 (1959).
(11) F. B. MCDONALD: *Phys. Rev.*, **116**, 462 (1959).
(12) P. MEYER and J. A. SIMPSON: *Phys. Rev.*, **99**, 1517 (1955).
(13) P. S. FREIER, E. P. NEY and P. H. FOWLER: *Nature*, **181**, 1319 (1958).

distinguish minor variations of total fluxes. The data obtained during the solar maximum however, seem to indicate a small decrease in the flux of α-particles in 1958 as compared to 1957, which is also reflected in the differential energy spectrum.

4·2. *Differential energy spectrum.* – The differential energy spectrum obtained in the present experiment, is shown on Fig. 3, together with other data

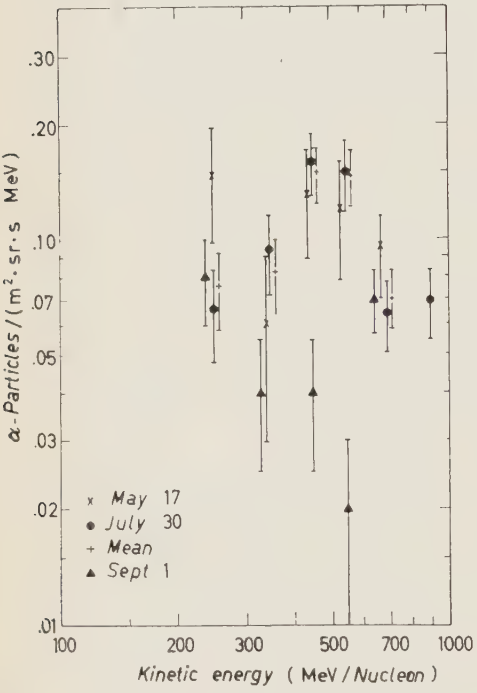

Fig. 3. – Differential energy spectra for α-particles, as observed using emulsions, on three balloon flights during 1957, at 55° N geomagnetic latitude. The mean of the spectra for the May and July flights is also shown.

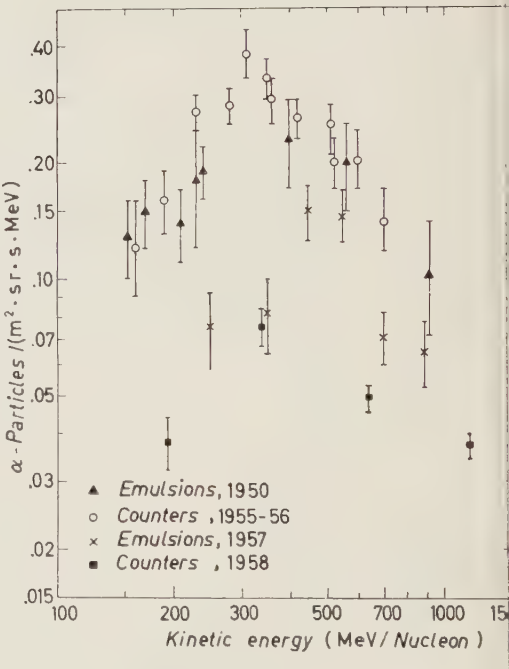

Fig. 4. – Differential energy spectra fo α-particles, as observed at 55° N geomagnet latitude, by *a*) emulsions, in 1950, *b*) counter during 1955-56, *c*) emulsions, in 1957, an *d*) counters, in 1958.

obtained during 1957 over Minnesota. The agreement between the spectra obtained on May 17 and July 30 is fairly good. The spectrum of September 1 shows rather peculiar features which can possibly be attributed to the fact that this particular flight was made in the wake of a large Forbush decrease. Hence, for comparison with data obtained at other epochs of the solar cycle we have decided to take the mean between the May 17 and July 30 data as representative of the year 1957. The mean differential energy spectrum is compared with further data obtained by counters and emulsions in Fig. 4.

Two features are apparent: *a*) a large decrease in the flux over a wide range of energy, and *b*) the broad maximum on the spectrum around 350 MeV/n which existed during the sunspot minimum of the solar cycle, seems to have disappeared, diminished considerably or shifted to higher energy.

The possible mechanisms responsible for such effects will be discussed in a following paper.

4·3. *Geomagnetic cut-off energies.* – Cut-off energies determined from the observation of total fluxes or differential energy spectra may be subject to several sources of error. This has previously been discussed by ENGLER, KAPLON and KLARMANN [1].

The centered dipole approximation leads to a cut-off energy of 292 MeV/nucleon for α-particles incident in the vertical direction at $\lambda = 55°$N. As became apparent several years ago [14,15], this approximation is not valid and several semi-empirical approaches [16,17] have been proposed which yield improved predictions. The most extensive investigation thus far has been made by QUENBY and WEBBER [17] who predict a cut-off of 145 MeV/nucleon at this latitude. MACDONALD [11] has recently measured this cut-off for protons and finds a value of (0.8 ± 0.1) GeV as the cut-off rigidity, corresponding to an α-particle kinetic energy of 80 MeV/nucleon. Our own data do not permit us to decide between these figures.

* * *

The authors wish to thank LINDA MAURER, LYDIA HAWRYLAK, Y. YELLIN, BETTY HERR, LEE WARE and MAFALDA ZWIRN for their scanning of the emulsions. Skyhook flight facilities of the Office of Naval Research are gratefully acknowledged. The flight was made by General Mills Inc. under the supervision of C. P. MERRILL through the arrangements of Cmdr. COCHRAN.

APPENDIX A

Multiple scattering measurements were performed on all tracks according to the method of FOWLER [18]. Overlapping cells were used in eliminating

---

[14] D. C. ROSE, K. B. FENTON, J. KATZMANN and J. A. SIMPSON: *Phys. Rev.*, **102**, 1648 (1956).

[15] P. H. FOWLER and C. J. WADDINGTON: *Phil. Mag.*, **1**, 637 (1956).

[16] P. ROTHWELL and J. J. QUENBY: *Suppl. Nuovo Cimento*, **8**, 249 (1958).

[17] J. J. QUENBY and W. R. WEBBER: *Phil. Mag.*, **4**, 90 (1959).

[18] P. H. FOWLER: *Phil. Mag.*, **41**, 169 (1950).

noise. A 4 $\bar{D}$ replacement cut-off was employed and in addition distortion was eliminated by taking third differences and the relation between second and third differences was taken to be [19]

$$\frac{D_{n,\mathrm{III}}}{D_{n,\mathrm{II}}} = \frac{1}{1.06\sqrt{3/2}},$$

where n indicates the degree of overlap. Measurements were only considered to be significant if either $(D_2/D_1) \geqslant 1.73$ or $(D_3/D_1) \geqslant 2.6$. The error in $\bar{D}$ can be calculated from the relation [20]

$$\Delta\bar{D} = 0.76\,(\varrho/[\varrho - 1])/\sqrt{n},$$

where n is the number of independent cells on the larger cell size and $\varrho = (D_n/D_1)^2$. Since in almost all cases the number of readings taken on a track was such that at least 72 third differences on the third overlap were obtained the error in $\bar{D}$ is $\Delta\bar{D} \leqslant 24\%$.

In addition spurious scattering was taken into account by the method of Fowler and Waddington [15]. It was found that this effect became important in these emulsions for kinetic energies greater than about 1.2 GeV/nucleon while its effect was small below that energy and negligible below about 750 MeV.

Finally to convert the mean angle of scattering into $p\beta$ the values of the scattering constant as calculated by FICHTEL and FRIEDLANDER [21] were used. As a replacement cut-off was employed, the appropriate value of the scattering constant was taken as $0.75(K_0 - K_{c0})$ higher than K_{c0}.

APPENDIX B

The original emulsion thickness was calibrated by measurements on the long range α-particles arising from RaC′ and ThC′ decays. The U.R. emulsions were measured to be (388 ± 2) μm, those of W.U. (580 ± 8) μm. Should these results be in error, and the true thicknesses be closer to the nominal values of 400 μm and 600 μm respectively, then the flux values will be reduced by $\sim 6\%$. The emulsion thickness enters the flux calculations quadratically; firstly in calculating the collecting area, and again in specifying the acceptance

[19] M. DI CORATO, D. HIRSCHBERG and B. LOCATELLI: *Suppl. Nuovo Cimento*, **4**, 448 (1956).

[20] A. ENGLER, P. B. JONES and J. H. MULVEY: *Proc. Roy. Soc.*, A **254**, 425 (1960).

[21] C. FITCHEL and M. W. FRIEDLANDER: *Nuovo Cimento*, **10**, 1032 (1958).

angle via the length per plate. The errors quoted here are standard deviations on the mean values, derived from the distribution of the measured thickness values.

RIASSUNTO (*)

È stato analizzato lo spettro di energia delle particelle α dei raggi cosmici primari usando emulsioni fotografiche lanciate da Minneapolis il 30 Luglio 1953. Il flusso totale osservato fu di (151 ± 9) particelle/m^2 sr s. Lo spettro differenziale dell'energia presenta un largo massimo fra 400 e 600 MeV/nucleone, ed appare di forma diversa da quello osservato nei minimi solari. Non si osservarono particelle aventi energie cinetiche inferiori a 200 MeV/nucleone, ma si osserva un flusso notevole fra 200 e 300 MeV/nucleone. Dalla approssimazione al campo geomagnetico con dipolo centrato, ci si aspetterebbe a quella latitudine una energia di cut-off di 292 MeV/nucleone. I risultati qui presentati, sono in disaccordo con questo valore, ma non permettono di fare una scelta fra le energie di cut-off predette con altri modelli.

(*) *Traduzione a cura della Redazione.*

The Heavy Component of the Primary Cosmic Radiation during Solar Maximum (*).

C. E. Fichtel (**)

Department of Physics, Washington University - St. Louis, Mo.

(ricevuto il 31 Ottobre 1960)

Summary. — The heavy component of the primary cosmic radiation was studied at geomagnetic latitude 55° N at a time of solar maximum. The total flux was found to be down by a factor of about two, compared to the results obtained during solar minimum, but the charge spectrum was found to be the same, to within experimental errors. The extrapolated fluxes at the top of the atmosphere were found to be: (3.08 ± 0.64) part./m² sr s for $3 \leqslant Z \leqslant 5$; (8.26 ± 0.82) part./m² sr s for $6 \leqslant Z \leqslant 9$; and (2.96 ± 0.49) part./m² sr s for $10 \leqslant Z$. When this work was combined with that of other experimentalists obtained at different latitudes and compared to the data obtained at solar minimum, the change in the integral spectrum was found to be in fair agreement with the predictions of an electric deceleration modulating mechanism.

1. – Introduction.

Ever since particles of charge greater than two were discovered in the primary cosmic radiation (1), attempts have been made to learn more about these particles. Only within the last few years, however, have balloon flights been able to reach high enough altitudes above the earth to permit a reasonably unambiguous extrapolation of the observed fluxes at the flight altitude to the

(*) The work reported here has been supported by the Air Force Office of Scientific Research, the Office of Ordnance Research and the National Science Foundation.

(**) Now at Goddard Space Flight Centre, N.A.S.A., Washington, D.C.

(1) P. Freier, E. Lofgren, E. Ney, F. Oppenheimer, H. Bradt and B. Peters: *Phys. Rev.*, **74**, 213 (1948).

top of the atmosphere. Further, there is a large variation of the cosmic ray proton and α fluxes with time, which may be associated with the solar cycle. Therefore, it is not only worth-while to obtain as much accurate, detailed information about the cosmic rays at any one time as possible, it is also valuable to perform many careful experiments at different places and times to learn the exact nature of the variations of the primary cosmic rays.

The experiment described here was aimed at helping to resolve the general problem of the composition and time variation of the heavy component of the primary cosmic radiation. In particular, it was concerned with the measurement of the properties of the primary particles of charge greater than two at a time of solar maximum (July 30, 1957) and at a geomagnetic latitude with a low energy cut-off (Minneapolis, Minnesota).

The details of the charge spectrum were examined, the energy spectrum was obtained, and the absolute flux values of the light ($3 \leqslant Z \leqslant 5$), medium ($6 \leqslant Z \leqslant 9$), and heavy ($Z \geqslant 10$) particles were obtained. Finally, the results of this experiment, combined with the results of other experimentalists obtained at different latitudes during solar maximum, were compared with the early work during solar minimum to observe the nature of the changes and to compare these changes with those of the α-particles.

2. – Preliminary experimental procedures.

The Ilford G-5 nuclear emulsions used in this experiment were the same as those used by the Washington University group in a parallel investigation on α-particles ([2]); the balloon was launched from Minneapolis, Minnesota (geomagnetic latitude 55° N) on July 30, 1957. The flight curve is reproduced in ref. ([2]); the plane of the emulsions was held horizontal until after the balloon has reached its floating altitude, and then rotated through 90°. The effective collection time for the tracks selected was $8^{h}\,51^{m}$ with the average amount of air above the stack being 8.5 g/cm^3. To this must be added approximately 0.3 g/cm^3 for the packing material and the $\frac{1}{4}$ inch fiberglass dome in which the emulsions and rotating mechanism were housed. The trajectory of the balloon was almost straight west from Minneapolis and deviated from the latitude of the launch site by less than one-half of a degree.

In the preliminary scanning of the plates the following criteria were used. In order to be able to estimate the energy of the particles from scattering measurements, a minimum length per plate of any track that was used

([2]) A. Engler, M. F. Kaplon, A. Kernan, J. Klarmann, C. E. Fichtel and M. W. Friedlander: *Nuovo Cimento* (in press).

in the final analysis was set at nine millimeters. In the preliminary scan, the lower limit on the track was set at 7.5 mm per plate. The maximum projected zenith angle that was accepted in the preliminary scan was set at 45°, and the limit was reduced to 40° in the final analysis. As a scanning efficiency check, the observed distributions of the number of particles as a function of the length per plate and projected zenith angle were compared with the expected ones, and found to be in good agreement. The minimum grain density demanded for track selection was set at six times the proton plateau value, hereafter called g_0, so that the detecting efficiency for lithium nuclei would be as high as practicable. The main method used for checking the scanning efficiency for tracks with low grain density was the rescanning of several plates by a person other than the one who originally scanned them. There was evidence that particles whose grain density was in the region of $6g_0$ to $7.5g_0$ were missed, but not in the region above $7.5g_0$. A study of the number of particles as a function of the depth in the emulsion indicated no loss of particles near the surface or the glass.

3. – The basic measurements.

In order to determine the charge of the primary nuclei, it is necessary to know both the energy and the rate of energy loss. The energy was estimated by measuring the mean angle of deflection resulting from Coulomb scattering. The « noise-free » mean angle of deflection was calculated from a combination of the first and second overlapped cells, and also the first and third overlaps, using the Fowler-Weddington [3] scheme, and then taking the weighted average of these two values. Third differences were used to eliminate C-shaped distortion.

As one measure of the rate of energy loss, the Fowler-Perkins [4] blob-gap method was employed. For large grain densities, there is the problem of saturation. There are many theoretical models that attempt to take this effect into account [5-9]. However, to within experimental errors, the grain densities calculated from the Fowler-Perkins expression essentially agree with all of the models. The curves for one of the models, that of Demers [5], is shown

[3] P. H. Fowler and C. J. Waddington: *Phil. Mag.*, **1**, 637 (1956).
[4] P. H. Fowler and D. H. Perkins: *Phil. Mag.*, **46**, 587 (1955).
[5] P. Demers: *Can. Journ. Res.*, A **25**, 223 (1947).
[6] M. Blau: *Phys. Rev.*, **75**, 279 (1949).
[7] W. Happ, T. Hull and A. Morrish: *Can. Journ. Phys.*, **30**, 699 (1952).
[8] A. Herz and G. Davis: *Austral. Journ. Phys.*, **8**, 129 (1955).
[9] J. Blatt: *Austral. Journ. Phys.*, **8**, 248 (1955).

in Fig. 1, where the « ideal grain density » is the grain density that would have occurred if there had been no saturation effect. With respect to the accuracy of the grain density measurement, the standard deviation is given by the expression (4):

$$\frac{\Delta g}{g} = \frac{1}{(\sqrt{N_H})\ln(B/H)} . \tag{1}$$

The δ-ray density was used as a second measure of the rate energy of loss of the heavy primary nuclei. Whereas the grain density method is applicable only in the low charge region, the δ-ray density can be employed with reasonable success over the entire range. In measuring the δ-ray density, enough slow secondary electron tracks were counted so that any two charges were separated by at least 4.0 standard deviations up to charge nine, on the basis of the number of δ-rays counted. Over the region of interest, the δ-ray density can be represented by the equation

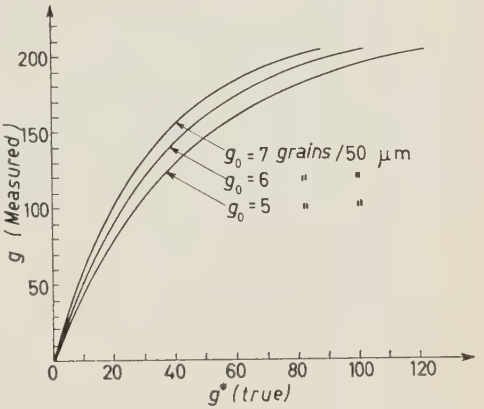

Fig. 1. – The measured grain density as a function of the « ideal grain density relative to the proton plateau » for several values of g_0.

$$N_\delta = b\frac{Z^2}{\beta^2} + c , \tag{2}$$

where N_δ is the number of δ-rays per 100 μm, b and c are constants, Z is the charge of the primary, and β is the velocity of the primary in units of the speed of light. The value of β is obtained from the scattering measurement, and, for most tracks, it is known very well because it varies very slowly with $\overline{\alpha}$, in the region of interest. In the high energy region, the measured value of $\overline{\alpha}$ is known to be affected appreciably by the residual noise, and, in general

$$[\overline{\alpha}\ (\text{measured})]^2 = [\overline{\alpha}\ (\text{true})]^2 + [\overline{\alpha}\ (\text{noise})]^2 .$$

$\overline{\alpha}$ (noise) was estimated from the lower limit of $\overline{\alpha}$ (measured) found for the tracks in this experiment and the deviation of the energy spectrum from the one expected from the measurements at other latitudes. Assuming the error in β to be comparatively small, then, the uncertainty, in the charge determination can be found from eq. (2) to be given by:

$$\frac{\Delta Z}{Z} = \frac{\Delta N_\delta}{N_\delta}\left\{\frac{1+\beta^2 c/bZ}{2}\right\} = \frac{1}{\sqrt{N_c}}\left\{\frac{1+\beta^2 c/bZ}{2}\right\} , \tag{3}$$

where N_c is the number of δ-rays counted.

To be sure that there was no bias in obtaining the necessary number, a criterion for the number of δ-rays to be counted was set in such a way that it did not depend on a subjective opinion in regard to the appearance of the track. To obtain the accuracy desired, all the δ-rays in at least five millimeters were counted unless the total number in that length was less than one-hundred or more than five hundred. If there were less than one-hundred, the count was continued until that number was obtained, and, at the other extreme, no more than five hundred were counted because at about this number they become uncomfortably close together for complete resolution, and the accuracy begins to suffer anyway. In regard to the criteria for accepting a δ-ray in the count, basically, any δ-ray of four or more grains was included. For consistency, all types of configurations of grains that might be encountered were considered, and standard tracks of various δ-ray densities were referred to often. Sets of plates in different processing batches were calibrated separately.

Other methods of estimating the charge in the high Z region which were tried gave an uncertainty in the charge determination that was considerably greater than that of the δ-ray method; so they were not used in determining the charge of the heavy nuclei.

4. – Experimental results.

4·1. *Charge spectrum.* – Fig. 2 shows the charge distribution determined by the δ-ray method. If the experimental resolution is as good as was expected, there should be four standard deviations between charges up to about

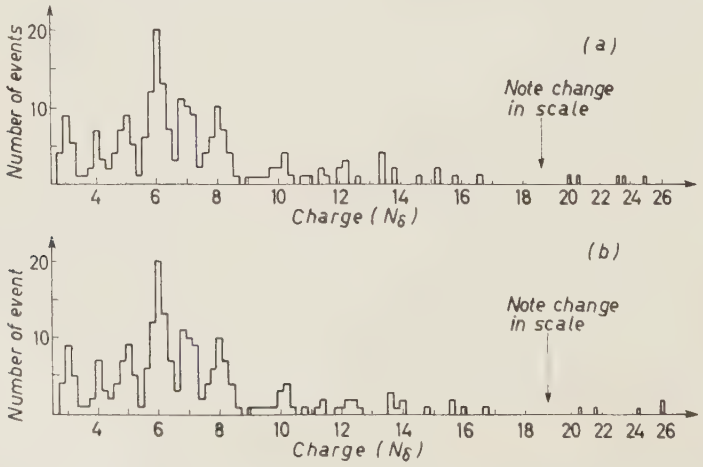

Fig. 2. – *a*) Charge spectrum determined from N_δ without saturation correction. *b*) Charge spectrum determined from N_δ with saturation correction.

charge nine, for all particles, and up to about charge twelve for relativistic particles. On this basis, the percentages of the total number of particles expected in the group listed in Table I were obtained. The agreement between the experimental distribution and the expected distribution shows that the errors are as expected and no larger. Taking the expected error as the true error then, the fraction of particles which have been assigned the wrong charge is about 4.6%, and, in general, the interchange of one or two particles between groups is all that occurs. The two exceptions are the probable net shift of 0.6 oxygen particles to the charge nine group, and similar shifts of carbon nuclei to the charge five and seven groups.

TABLE I. – *Internal check on the charge resolution obtained by the δ-ray method.*

Charge interval	$(Z-.1)$ to $(Z+.1)$	$(Z-.1)$ to $(Z-.3)$ and $(Z+.1)$ to $(Z+.3)$	$(Z-.3)$ to $(Z-.5)$ and $(Z+.3)$ to $(Z+.5)$
Percentage expected on the basis of four standard deviations separating charges	31.0%	46.0%	23.0%
Number found in the 2.5 to 5.5 charge group	25	26	9
Number expected in the 2.5 to 5.5 charge group on the basis of four standard deviations separating charges	19 ± 4	27 ± 5	14 ± 4
Number found in the 5.5 to 9.5 charge group	41	59	28
Number expected in the 5.5 to 9.5 charge group on the basis of four standard deviations separating charges	40 ± 6	59 ± 8	29 ± 5

As a second test of resolution between charges in the group $3 \leqslant Z \leqslant 8$, the charge estimate obtained from the grain density method can be compared to that from the δ-ray method. This comparison is shown in Fig. 3. No point based on a grain density greater than 180 grains per fifty microns is included because the error of these points would be so large as to make them have little meaning. On the basis of the uncertainty in the value of g, calculated from eq. (1), and the variation of g (measured) with g (true) shown in Fig. 1 the uncertainty in the charge determined from the grain density in terms of the percentage that will be incorrectly identified can be calculated. The proba-

bility that a value of the charge will lie within the boxes drawn in Fig. 3 is the product of the probability that it will lie within 0.5 of the true charge by one method times the probability that it will by the other method, plus the very small probability that it will fall into one of the other boxes. Table II demonstrates that the expected accuracy is obtained.

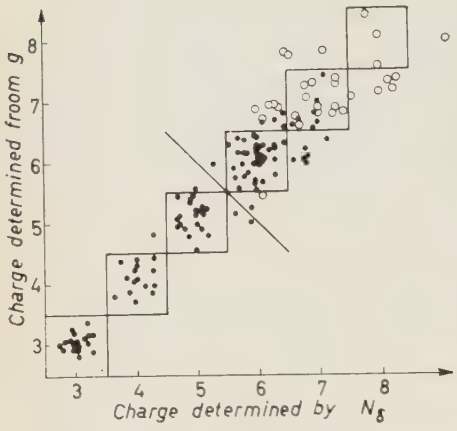

Fig. 3. – Comparison of the charge values determined by the grain density and the δ-ray density methods. The dots in the figure represent tracks whose grain density was less than 160 grains/50 μm and the open circles represent tracks whose grain density was between 160 and 180 grains/50 μm.

TABLE II. – *Cross check on the accuracy of the charge determination by the two methods employed.*

	Number expected	Number found
Particles assigned a charge of less than 5.5 on the basis of the average of both methods and not found in a box in Fig. 3	5 ± 2	4
Particles assigned a charge greater than 5.5 on the basis of the average of both methods, represented by dots, and not found in a box	11 ± 3	12
Particles represented by open circles not in a box	12 ± 3	16

Returning now to the δ-ray method of determining charge, a saturation effect must be expected for the very dense tracks, due primarily to the difficulty of counting electron tracks which are close together and even interwoven. Assuming an exponential saturation factor and keeping only the first order correction term, one has:

$$N_\delta \text{ (measured)} = N_\delta \text{ (saturated)} - d[N \text{ (saturated)}]^2 . \tag{4}$$

If one assumes that the last few tracks are iron nuclei, on the grounds that there is a very large abundance of iron as compared to its near neighbors in the distri-

bution of elements in the universe, and stars which are believed to be likely sources of cosmic rays could have an even greater abundance of iron than average ([10]), d can be obtained from the presumed iron points. The results are shown in Fig. 2*b*. There is no effect on charges less than ten, as there should not be, and very little in general except on the largest charges. The resulting charge distribution, including the very small corrections mentioned above, is shown in Table III.

TABLE III. – *Final charge spectrum at the scan line.*

Charge	3	4	5	6	7	8	9	$10 \leqslant Z \leqslant 25$		26	> 26
								Z even	Z odd		
Number of particles	20	15	25	59	35	32	3	27	8	2	0

In the heaviest group, if the correction for saturation is sufficiently valid so that it will not increase the experimental error appreciably beyond that due to the statistical uncertainty (as it should be up to about charge sixteen at least, since the correction below this point is small), the charge determination would be correct about 94% of the time for the charge ten group and decrease gradually to 70% at about charge 16 to 20, depending on the value of β. Since all but four of the particles in the charge group $10 \leqslant Z \leqslant 25$ have a charge of of sixteen or less, the fact that the even to odd ratio is as large as 27 to 8 is almost certainly significant. This result is in agreement with other experimental results, and consistent with the fact that there is an excess of even charges in the distribution of elements in the universe ([11]), which is larger than that observed here. One would expect the cosmic ray excess to be somewhat smaller because of fragmentation. Even if one makes such an extreme hypothesis as assuming that the presumed iron peak used as a calibration point is really composed of particles of charge 25 or 27, rather than 26, the even to odd ratio is still 24:11 and 25:10, respectively.

With respect to the lower charges, notice that the relative abundances of carbon, nitrogen, and oxygen are quite different from that observed in the distribution of elements in the universe ([11]), but consistent with those observed by other experimentalists during solar minimum under similar conditions, and notice that the number of lithium particles is approximately equal to the number of beryllium or boron.

([10]) G. R. BURBIDGE: *Supp. Nuovo Cimento*, **8**, 403 (1958).
([11]) H. E. SUESS and H. C. UREY: *Rev. Mod. Phys.*, **28**, 53 (1956).

4·2. *Absolute fluxes.* – With respect to absolute fluxes, first, the fluxes at the scan are shown in Table IV. The statistical uncertainty arises primarily from the finite number of particles found and the smaller uncertainty in the plate thickness. Since all particles were followed to the top of the stack and

TABLE IV. – *Heavy particle fluxes in particles/m² sr s.*

Charge group	$3 \leqslant Z \leqslant 5$	$6 \leqslant Z \leqslant 9$	$Z \geqslant 10$	$Z \geqslant 3$
Flux at the scan line	$2.40 \pm .32$	$5.17 \pm .48$	$1.48 \pm .24$	$9.05 \pm .56$
Flux at the top of the stack	$3.02 \pm .44$	$6.59 \pm .61$	$2.00 \pm .32$	$11.61 \pm .84$
Flux at the top of the atmosphere (Energy/nucleon > 360 MeV)	$3.08 \pm .64$	$8.26 \pm .82$	$2.96 \pm .49$	14.30 ± 1.15

any coming from interactions were rejected, the flux values at the top of the stack can be obtained simply by using the mean free paths of the particles in the emulsion. The values of the parameters used in this calculation, as well as those used in the subsequent extrapolation are listed in Table V, and represent a weighted average of the values listed in the indicated references ([12-17]). Present evidence indicates that these parameters are not dependent on the energy in the energy interval of interest, and this hypothesis was assumed.

TABLE V. – *Fragmentation expectations and mean free paths used in this work.*

Fragmentation expectations in emulsion	P_{LL}	P_{ML}	P_{MM}	P_{HL}	P_{HM}	P_{HH}
Light target nuclei	$.12 \pm .04$	$.23 \pm .03$	$.16 \pm .03$	$.18 \pm .04$	$.33 \pm .04$	$.26 \pm .04$
Hydrogen target	$.06 \pm .06$	$.32 \pm .05$	$.14 \pm .04$	$.09 \pm .04$	$.46 \pm .09$	$.32 \pm .08$

Charge group	$3 \leqslant Z \leqslant 5$	$6 \leqslant Z \leqslant 9$	$Z \geqslant 10$
λ in centimeters of emulsion	14.3 ± 1.1	$13.4 \pm .6$	$10.8 \pm .6$
λ in g/cm² for air	32.8	27.0	18.0
λ in g/cm² for hydrogen	8.7	6.0	4.0

([12]) E. LOHRMANN and M. W. TEUCHER: *Phys. Rev.*, **115**, 636 (1959)
([13]) P. FOWLER, R. HILLIER and C. J. WADDINGTON: *Phil. Mag.*, **2**, 293 (1957).
([14]) R. CESTER, A. DE BENEDETTI, C. GARELLI, B. QUASSIATI, L. TALLONE and M. VIGONE: *Nuovo Cimento*, **7**, 371 (1958).
([15]) M. KOSHIBA, G. SCHULTZ and M. SCHEIN: *Nuovo Cimento*, **9**, 1 (1958).
([16]) V. Y. RAJOPADHYE and C. J. WADDINGTON: *Phil. Mag.*, **3**, 19 (1958).
([17]) J. NOON and M. F. KAPLON: *Phys. Rev.*, **97**, 769 (1955).

In extrapolating to the top of the atmosphere, the standard extrapolating equations were used ([18]), and the results are shown in Table IV. One consideration worth mentioning is that some heavy particles will not reach the scan line because their energies are too low. This problem is treated in Section 4·4 with the conclusion that the flux values above 360 MeV/nucleon can be calculated reliably. The errors quoted include the statistical uncertainty, already mentioned, and the uncertainty resulting from the limits on the accuracy of the values of λ_i and P_{ji}, quoted in Table V, only.

From Table IV, the light to medium ratio at the top of the atmosphere was found to be $.37 \pm .08$, and the heavy to medium ratio was found to be $.36 \pm .08$. The light to medium plus heavy ratio is $.35 \pm .06$ at the top of the stack, and $.27 \pm .06$ at the top of the atmosphere.

4·3. *Energy spectrum.* – The energy of any particle was obtained in the stack from the scattering measurement. In obtaining the energy of the particle at the top of the atmosphere, there is one consideration which needs some discussion. This is that, although the rate of energy loss in air is fairly certain and the length of each track in the air is known, some of the particles arriving at the top of the stack are secondaries. The energy per nucleon probably has not changed very much, but the rate of energy loss per nucleon is greater for nuclei of larger charge. About 7% of the particles of charge greater than two arriving at the top of the stack come from interactions of heavier particles in the air above the emulsion, and the average error introduced by assuming no change in the nucleus is about 15 MeV/nucleon for the amount of air above the stack in this experiment. The actual value, of course, depends on the exact charges of the particles and the energy of the particle. Since there is no way of knowing which particles came from interactions in the atmosphere, and making an average correction of the order of 1 MeV/nucleon on each particle would have no meaning, the effect of interactions on the energy spectrum was omitted, as being negligible.

The cut-off due to the material above the scan line is about 300 MeV/nucleon for carbon, 360 MeV/nucleon for oxygen, and 465 MeV/nucleon for charge twelve. The actual cut-off depends slightly on angle. In order to obtain a spectrum for the heavies to as low energies as possible in the region from 360 MeV/nucleon to the cut-off for iron, the measured flux values were corrected for the number of particles that could not reach the scan line because their charge was too great. This correction was made from the knowledge of the charge spectrum and the assumption that the energy spectrum is the same for all charges. This correction can be justified on the grounds that it

([18]) S. HAYAKAWA: *Prog. Theor. Phys.*, **15**, 111 (1956)

is very small in the region that it was used, and that, although the statistics are poor, the assumption that the spectrum is the same for all particles of the same charge to mass ratio seems to be valid. The correction was not attempted below 360 MeV/nucleon because there it becomes too large.

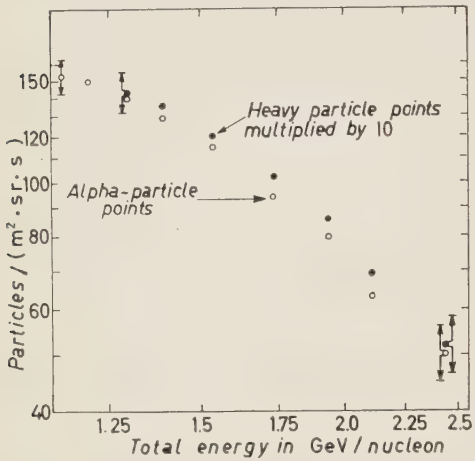

Fig. 4. – Measured integral energy spectra of the α and heavy particles.

It is known that the spurious scattering causes the energy to be underestimated in the high energy region. However, an α-particle spectrum was obtained in plates spread among those in which the heavy particle data were obtained, so it is meaningful to compare the two measured spectra extrapolated to the top of the atmosphere. Fig. 4 shows the integral energy spectrum for both the α-particles and the heavy ones. One can see that the two spectra are very similar and that they can be taken to have the same form to within experimental errors.

5. – Comparison with solar minimum data.

Having the experimental data for $\lambda = 55°$ during solar maximum, the work reported in this paper can be compared with other experiments to obtain a more complete picture of the cosmic rays. In a survey of the experimental data from 1950, approximately when the first meaningful flux experiments were performed, until the spring of 1956, no significant changes in the cosmic rays are detectable. These same years were characterized generally by a relatively low rate of solar activity ([19]). After this period, the solar activity increased and reached a maximum late in the summer of 1957. The α-particle flux, which has been studied much more carefully than the heavy particle one, was observed to fall off sharply at this time, in the companion experiment ([2]) as well as others. Fig. 5 shows the change in the integral energy spectrum for the α's, and Fig. 6 depicts the similar change for the medium and the heavy particles. The points in these figures are based on the weighted average of the experimental points where more than one result is available,

([19]) S. W. Visser: *Nature*, **182**, 253 (1958).

and, in every case, the numbers of the references to the work are listed. Fig. 5 and 6 are based on experiments performed at geomagnetic latitudes of 0°, 41°, and 55°, since most of the data have been obtained at these points. Unfortunately, the only medium and heavy particle experiments before solar maximum at $\lambda = 55°$ to which the work of this paper can be compared were performed on low altitude flights in 1952 and before. However, to within experimental error, the α-particle flux during those years was the same as that at the true solar minimum in 1954. The energy cut-offs for the medium and heavy particles at $\lambda = 55°$ are average material cut-offs.

It is known that if a power law of the form $N(>E) = N_0 E^{-\gamma}$, where E is the total energy per nucleon, is fitted to the α-particle data obtained during solar minimum, one gets a very good fit. For the points in Fig. 5, the value of γ was found to be 1.44. If one assumes that the medium and heavy spectra should be the same because of the same charge to mass ratio of the nuclei,

Point	References
a_1	(22), (23), (24), (25)
a_2	(24), (26), (27), (28), (29)
a_3	(2), (20), (21)
a_4	(20), (21)
a_5	(30), (44)

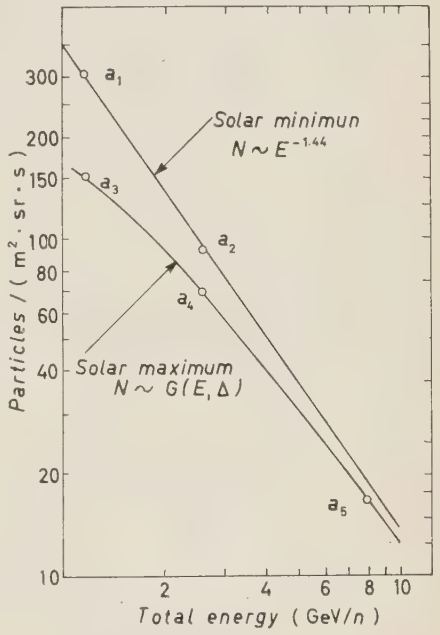

Fig. 5. – Integral energy spectrum for α particles at solar minimum and solar maximum.

(20) P. S. Freier, E. P. Ney and C. J. Waddington: *Phys. Rev.*, **114**, 365 (1959).
(21) F. B. McDonald: Bulletin SUI-59-11, State University of Iowa (1959).
(22) L. Davis, H. Caulk and C. Johnson: *Phys. Rev.*, **91**, 431 (1953).
(23) C. J. Waddington: *Phil. Mag.*, **45**, 1312 (1954).
(24) F. B. McDonald: *Phys. Rev.*, **104**, 1732 (1956).
(25) P. H. Fowler, C. J. Waddington, P. S. Freier, J. Naugle and E. P. Ney: *Phil. Mag.*, 2, 157 (1957)
(26) J. Linsley: *Phys. Rev.*, **101**, 826 (1956).
(27) N. Horwitz: *Phys. Rev.*, **98**, 165 (1955).
(28) J. L. Bohl: Thesis at the University of Minnesota (1954).
(29) A. Engler, M. F. Kaplon and J. Klarmann: *Phys. Rev.*, **112**, 597 (1958).
(30) F. B. McDonald: *Phys. Rev.*, **109**, 1367 (1958).

in almost every case, and tries to fit a curve of the same form and with the same value of γ to the medium and heavy spectrum at solar minimum, good agreement is obtained, with only the value of N_0 being different, as is known. Next the experimental points obtained during solar maximum for the α-particles shown in Fig. 5 are seen to agree very well with the function $G(E, N_0, \Delta, \gamma)$, given by eq. (7) below with $\Delta = 325$ MeV, although there are some discrepancies at the very low energy end ($\leqslant 600$ MeV/nucleon) when one takes a detailed look at the differential energy spectrum. The discrepancy takes the form of having the experimental points of different physicists being scattered on both sides of the mathematical curve. The important consideration is that

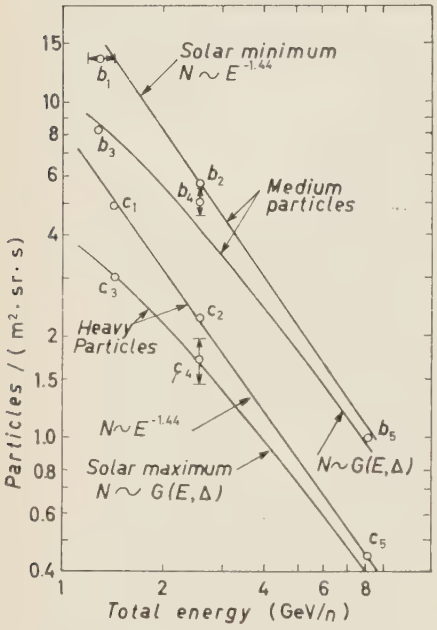

Point	References	Point	References
b_1	(31), (33), (34), (35), (37)	c_1	(31-36)
b_2	(33), (37-42)	c_2	(34), (37-42)
b_3	This work	c_3	This work
b_4	(42)	c_4	(42)
b_5	(43), (44)	c_5	(43), (41)

Fig. 6. – Integral energy spectrum for medium and heavy particles at solar minimum and solar maximum.

(31) H. L. Bradt and B. Peters: *Phys. Rev.*, **80**, 943 (1950).
(32) E. P. Ney and D. M. Thon: *Phys. Rev.*, **84**, 1068 (1951).
(33) P. S. Freier, G. W. Anderson, J. E. Naugle and E. P. Ney: *Phys. Rev.*, **84**, 322 (1951).
(34) M. F. Kaplon, B. Peters, H. Reynolds and D. M. Ritson: *Phys. Rev.*, **85**, 295 (1952).
(35) A. D. Dainton, P. H. Fowler and D. W. Kent: *Phil. Mag.*, **43**, 729 (1952).
(36) G. W. Anderson, P. S. Freier and J. E. Naugle: *Phys. Rev.*, **94**, 1317 (1954).
(37) M. F. Kaplon, J. H. Noon and G. W. Racette: *Phys. Rev.*, **96**, 1408 (1954).
(38) H. Yagoda: *Can. Journ. Phys.*, **34**, 122 (1956).
(39) J. H. Noon, A. J. Herz and B. J. O'Brien: *Nature*, **179**, 91 (1957).
(40) R. E. Danielson and P. S. Freier: *Phys. Rev.*, **109**, 151 (1958).
(41) M. V. K. Appa Rao, S. Biswas, R. R. Daniel, K. A. Neelakantan and B. Peters: *Phys. Rev.*, **110**, 751 (1958).
(42) P. S. Freier, E. P. Ney and C. J. Waddington: *Phys. Rev.*, **113**, 921 (1958).
(43) C. J. Waddington: *Supp. Nuovo Cimento*: **8**, 518 (1958).
(44) W. R. Webber: *Supp. Nuovo Cimento*, **8**, 532 (1958).

the points for the heavy and medium particles are also in good agreement wtih a curve of exactly the same form, that is $G(E, N_0, \Delta, \gamma)$, except for one point of relatively low statistical weight, with Δ and γ being the same for the α-particle spectrum and the N_0 values being taken from the solar minimum results.

There has been much speculation with respect to the cause of this decrease of the cosmic ray intensity. It is beyond the scope of this paper to discuss all of the theories in detail; however, basically, there seem to be two general types of modulating mechanisms which have received some attention. The first involves time varying magnetic fields, but no model based on these fields and assuming the solar minimum spectrum at large distances from the disturbing region has agreed quantitatively with experimental results ([45]). The other is an electric deceleration mechanism, which was first suggested some time ago by NAGASHIMA ([46]). If a differential flux of the form $j(E)$ goes through a decelerating potential V, according to the extended Liouville theorem, the new differential flux, $g(E)$, will be given by the following relation ([46,47]):

$$g(E) = \left\{\frac{E^2 - m^2}{[E + ZeV/A]^2 - m^2}\right\} j\left(E + \left|\frac{ZeV}{A}\right|\right), \tag{5}$$

where E is the total energy per nucleon, A is the atomic number of the primary, and m is the rest mass of a nucleon in units of energy. Taking the solar minimum form for $j(E)$, since the flux at large distances from the solar system is assumed to be the same, yields:

$$g(E) = \left\{\frac{E^2 - m^2}{[E + \Delta]^2 - m^2}\right\} \left\{\frac{-N_0\gamma}{[E + \Delta]^{\gamma+1}}\right\}, \tag{6}$$

where $\Delta = |ZeV/A|$. Expanding and integrating $g(E)$ yields

$$\int_{E'}^{\infty} g(E, N_0, \Delta, \gamma)\, dE \equiv G(E', N_0, \Delta, \gamma) = \Big[(E' + \Delta)^{-\gamma} - \tag{7}$$

$$-2\Delta\left\{\frac{\gamma}{\gamma+1}(E'+\Delta)^{-(\gamma+1)} + \frac{\gamma}{\gamma+3}m^2(E'+\Delta)^{-(\gamma+3)} + \frac{\gamma}{\gamma+5}m^4(E'+\Delta)^{-(\gamma+5)} + \ldots\right\} +$$

$$+\Delta^2\left\{\frac{\gamma}{\gamma+2}(E'+\Delta)^{-(\gamma+2)} + \frac{\gamma}{\gamma+4}m^2(E'+\Delta)^{-(\gamma+4)} + \ldots\right\}\Big] N_0 .$$

([45]) For a summary, see F. MCDONALD and W. WEBBER: *Bulletin* SUI-59-1, State University of Iowa (1959).

([46]) K. NAGASHIMA: *Journ. Geomagn. Geoelectric.*, **5**, 141 (1953).

([47]) L. JÁNOSSY: *Cosmic Rays*, (Oxford 1950) p. 269.

One can see that, since the expression for $g(E)$, involves only Z/A, the spectra for the α, medium, and heavy particles would still have the same form for the electric decelerating mechanism. The experimental results have already been seen to agree with all of these predictions, except at low energies, where it is possible that other effects, perhaps short term ones, are important. This last equation also predicts that the α and proton rigidity spectra should be different by a measurable amount at very low energies. This effect was looked for by McDonald ([21]) and not found.

Time varying magnetic fields could be the real cause of the change, and the lack of agreement may only be due to the inability to find a good model of the physical situation. In any case, these fields could play a role in further changing a spectrum, which is being more seriously modified by some other mechanism.

6. – Conclusion.

During solar maximum, fluxes of medium and heavy particles were found to be approximately half of their respective values at solar minimum at a geomagnetic latitude of 55° N. The results of this work as well as those of other experimentalists at lower latitudes show that the α, medium, and heavy particle energy/nucleon spectra have all changed in the same way, to within experimental errors. As a result, a curve of the same form still fits each spectrum. Thus, there is strong evidence that any modulating mechanism that exists has the same effect on all particles of the same charge to mass ratio. The decrease was found to be in fair, but not perfect, agreement with the effect that one would expect for a decelerating electric field.

Looking more closely at the charge spectrum, there seems to be no significant change from that at solar maximum. Carbon, nitrogen, and oxygen nuclei are still the most abundant at high altitudes, and individually they occur in amounts decreasing with charge. For charges greater than nine, there is still an irregular decrease in abundance with the highest observed charge being in the neighborhood of iron. Apparent sharp charge resolution indicates that there is a large even to odd ratio among the particles of charge equal to or greater than ten. With respect to charge determination, adequate charge resolution, as checked by the tests employed here, seems attainable even in an experiment at high latitudes, where the geomagnetic cut-off energies are not in the relativistic region.

* * *

I am grateful to Dr. M. W. Friedlander for many interesting discussions. I wish to thank the scanners, Miss N. Dryden, Mrs. B. Depew, Mrs. E. Kneer,

and Mrs. L. WARE, for their careful work, and Mr. O. RETZLOFF for the precision work on the microscopes. The Skyhook flight services of the Office of Naval Research are gratefully acknowledged.

RIASSUNTO (*)

Abbiamo studiato la componente pesante della radiazione cosmica primaria alla latitudine geomagnetica 55° N all'epoca del massimo solare. Abbiamo trovato che il flusso totale era diminuito per un fattore di circa due rispetto ai risultati ottenuti durante il minimo, ma lo spettro delle cariche era lo stesso entro i limiti degli errori sperimentali. Abbiamo trovato che i flussi, estrapolati alla sommità dell'atmosfera, sono: (3.08 ± 0.64) part./m^2 sr r per $3 \leqslant Z \leqslant 5$; (8.26 ± 0.82) part./m^2 sr s per $6 \leqslant Z \leqslant 9$, e (2.96 ± 0.49) part./m^2 sr s per $10 \leqslant Z$. Dopo aver combinato i dati di questo lavoro con quelli di altri sperimentatori, ottenuti a latitudini diverse, ed averli confrontati con i dati ottenuti al minimo solare, abbiamo trovato che la variazione dello spettro integrale era in buon accordo con le predizioni di un meccanismo elettrico di modulazione della decelerazione.

(*) *Traduzione a cura della Redazione.*

IL NUOVO CIMENTO Vol. XIX, N. 6 16 Marzo 1961

A Method for Expanding the Phase-Stable Regime in Synchronous Accelerators (*).

L. L. Foldy

Case Institute of Technology - Cleveland, Ohio

(ricevuto il 7 Novembre 1960)

Summary. — Possible advantages resulting from the use of non-sinusoidal radiofrequency accelerating potentials in synchronous accelerators in extending the regime of phase stability and in overcoming space charge effects are pointed out and discussed.

In accelerators employing synchronous acceleration with a *sinusoidal* radio frequency voltage, once the energy gain per turn ΔE_s and the maximum energy deviation ΔE_m of a particle from the synchronous energy during synchrotron oscillations are fixed, the range of useful phase stability is essentially determined. This is illustrated in Fig. 1, where there is plotted the « phase potential » against the phase (1) for various R.F. voltages and fixed energy gain ΔE_s per turn. The ordinate indicated by $\sim (\Delta E_m)^2$ represents the limi-

(*) Work supported in part by the U.S. Atomic Energy Commission. Since the preparation of this manuscript, it has been called to the author's attention that a similar proposal to that contained in this communication (with regard to expansion of the phase stable region) was made by N. M. Blachman in 1949 and is described in an internal memorandum of Brookhaven National Laboratory. We regret that no further publication was made by Dr. Blachman at that time, since we believe that the suggestion has sufficient potential virtues as to deserve wider circulation, and for this reason publish these independently derived results. We have not had an opportunity to see a copy of Dr. Blachman's memorandum but are happy to acknowledge his priority where our results overlap his. To our knowledge, Dr. Blachman did not discuss the pertinence of the proposal to problems of space charge limitation as described herein.

(1) For background theory one may consult the paper by D. Bohm and L. L. Foldy: *Phys. Rev.*, **70**, 249 (1946).

tation on energy excursions about the synchronous energy during synchrotron oscillations. Curve II is that for a voltage such that the limit of phase stability lies at this limit. Curve I corresponds to a lower applied voltage; in this case the phase stable region is contracted. Curve III corresponds to a higher applied voltage; in this case the phase stable region is expanded, but the region of useful phase stability is again contracted owing to the limit on energy excursions.

Now, if the limitation on sinusoidal variation for the R.F. voltage is removed, it becomes theoretically possible to extend the phase stable region to nearly a full 360° even under the limitations mentioned above. What is necessary is simply to shape the voltage signal so as to lead to a « phase potential » of the form schematically indicated by curve IV in Fig. 1. Ideally the barriers at the end should be infinitely thin, and clearly in this case the phase stable region includes all phases except for an infinitesimal region about $\varphi = 180°$. At the same time the « motion curves » in the energy-deviation *vs.* phase plane become rectangles so that the same limits on phase stability exist for all energy deviations within the maximum allowed. Hence, in multiturn injection, the full range of phases are accepted into stable orbits for all deviations of the injection energy from the synchronous energy within the limit ΔE_m.

Of course the ideal shape cannot be achieved in practice for various reasons. The required R.F. signal would have infinite peak voltages, both positive and negative. Furthermore, since the acceleration process is impulsive rather than continuous, the barriers at the ends of the trough in Fig. 1 cannot be infinitely thin; otherwise a particle could « jump » the

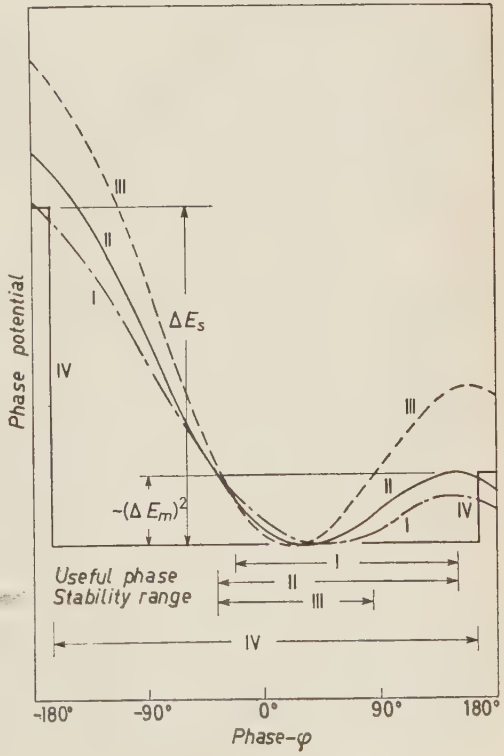

Fig. 1. – Phase potentials for various R.F. accelerating potentials with fixed synchronous energy gain ΔE_s per turn. Curves I, II, and III are for sinusoidal voltages with peak voltages of 1.4 ΔE_s, 2 ΔE_s, and 2.8 ΔE_s, respectively. Curve IV represents schematically the ideal potential. The useful phase stability ranges are indicated at the bottom of the figure.

barrier during the acceleration process ([2]). Nevertheless, substantial gains would be expected if the voltage is shaped even approximately to the ideal shape.

To illustrate this, we have calculated a special case in which the voltage is shaped by adding only some second harmonic to the fundamental R.F. frequency in appropriate phase and amplitude. In Fig. 2 is shown a « phase potential » curve corresponding to a sinusoidal signal

$$V = +1.35 \sin \varphi .$$

ΔE_s is such that tchis orresponds to a rather « conservative » synchronous phase φ_s for which $\sin \varphi_s = 0.36$, and the extent of the phase-stable region is 213°. If instead, keeping ΔE_s fixed, one applies a signal of the form ([3])

$$V = \sin \varphi - \tfrac{2}{3} \sin 2\varphi + \\ + \cos \varphi - \tfrac{2}{3} \cos 2\varphi ,$$

the resultant « phase potential » is given by the curve labeled « shaped voltage » in Fig. 2. The region of phase stability is extended to 268° representing a 25% increase. The phase stable region in the energy-

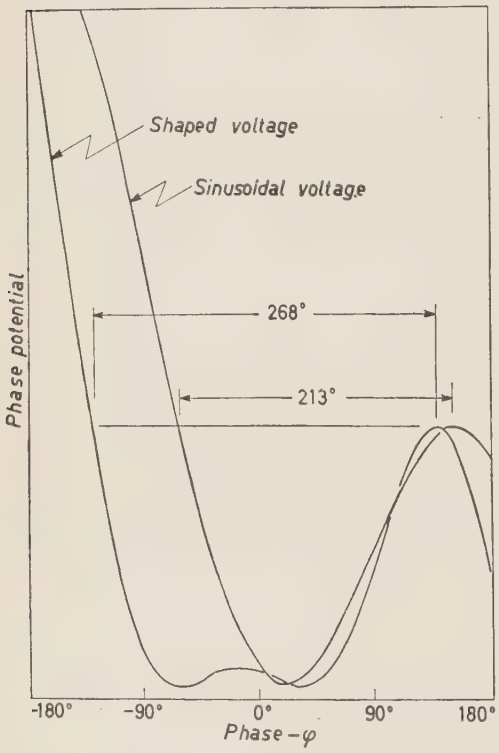

Fig. 2. – Phase potentials for sinusoidal R.F. voltage given in eq. (1) and for a shaped voltage given by eq. (2) with same synchronous energy gain per turn and same maximum phase-stable energy excursion from synchronous energy.

([2]) In the ideal case, phase correcting R.F. voltage is present on the electrodes only for infinitesimal times; hence only particles which pass the electrodes during this interval will have their phase corrected. Clearly the end barriers should be thicker than the change in phase per revolution of a particle whose energy deviation from the synchronous energy is about ΔE_m.

([3]) With a change of the origin from which the phase is measured, this may also be written as $V = 2 \sin \varphi - (2\sqrt{2}/3) \sin (2\varphi - \pi/4)$.

deviation *vs.* phase plane is correspondingly expanded (4) as shown in Fig. 3. The peak voltage of the shaped signal is approximately 2.2 times that of the sinusoidal signal, while the RMS voltage is 1.7 times higher.

The gains which can be achieved through signal shaping will be substantially greater in a case where the corresponding sinusoidal operation is at a higher synchronous phase, such as $\sin \varphi_s = 0.5$, and can be further increased by the use of higher harmonics. In our discussion above we have assumed that the energy gain per turn and the maximum energy excursion is kept fixed and used signal shaping to increase the stability region. Conversely, if the phase-stable region is already adequately wide, the same technique can be employed to reduce the energy excursions and hence the particle channel width, or to increase the energy gain per turn, and hence the number of acceleration cycles per unit time.

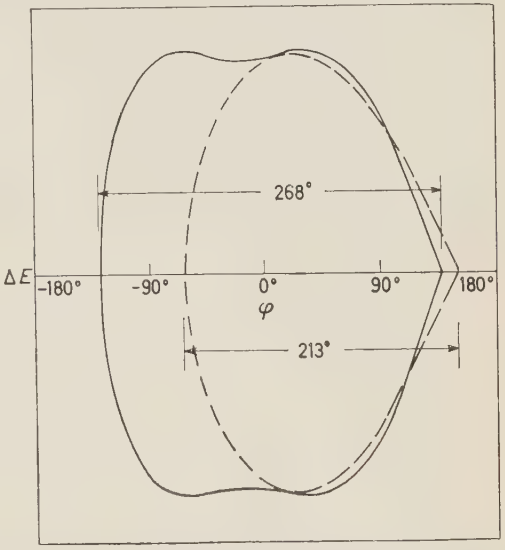

Fig. 3. – Regions of phase stability in plane of energy deviation from synchronous energy *vs.* phase. The dashed curve is for the sinusoidal voltage of Fig. 2 and the full curve for the shaped voltage curve of Fig. 2.

The employment of R.F. voltage shaping can also be beneficial when space charge effects in the circulating beam give rise to a limitation of the beam current, particularly in accelerators in which single-turn injection is under consideration. In such accelerators the fact that the phase-potential is nearly parabolic means that the synchrotron oscillations will have a period nearly independent of amplitude. As a consequence strong « bunching » of particles occurs at an epoch approximately one quarter of a synchrotron oscillation after injection. The fact that R.F. voltage shaping makes the phase potential quite anharmonic (even when only second harmonic addition is employed) means that such bunching effects, while not necessarily completely eliminated, will be strongly inhibited. Even with multiturn injection, the particles injected

(4) Since this manuscript was completed, more detailed calculations have shown that the phase-stable area in the phase plane can be increased by second harmonic addition from 45% to 70% over that obtained with sinusoidal operation under conditions corresponding to those for ordinary operation with a synchronous phase ranging from 20° to 40°, respectively.

in each turn tend to bunch strongly after a quarter of a synchrotron oscillation under a sinusoidal R.F. potential, and again the effect can be reduced by voltage shaping.

While we do not feel competent to discuss the technical feasibility of the suggestions made here, and in particular whether the gains which can be achieved would warrant the extra complication of the R.F. system, we do feel that the use of voltage shaping can give to the machine designer an extra degree of freedom which is worth keeping in mind both from the point of view of efficiency in the original design or as a potential remedy for other problems as they may arise.

The discussion above is applicable to the case of synchrotrons. For synchrocyclotrons, the considerations are of a sufficiently different character that they require a separate analysis which is being carried out and will be reported if the results warrant this.

RIASSUNTO (*)

Si rilevano e si discutono i possibili vantaggi derivanti dall'impiego negli acceleratori sincroni di potenziali d'accelerazione a radiofrequenza non sinusoidali che estendono il regime di stabilità di fase e annullano gli effetti dovuti alla carica spaziale.

(*) *Traduzione a cura della Redazione.*

On the Decay of the ^{95}Tc Isomer (*).

G. Chilosi, R. A. Ricci, G. Varcaccio and G. B. Vingiani

Istituto di Fisica Superiore dell'Università - Napoli
Istituto Nazionale di Fisica Nucleare - Sottosezione di Napoli

(ricevuto il 10 Novembre 1960)

Summary. — The γ-ray spectrum following the radioactive decay of the ^{95}Tc isomer (half life 62^{d}) has been investigated by scintillation techniques. The sources were obtained by Mo(d, 2n) reactions in the synchrocyclotron of the Institute for Nuclear Physics Research in Amsterdam. The measurements were performed with a NaI(Tl) welltype crystal (76 mm $\times$ 76 mm) and the different spectra were displayed in a 200 channel LABEN analyser. γ-γ cascades were investigated with a conventional coincidence set-up and using the summing technique. The direct disintegration of the isomeric state of ^{95}Tc to the stable ^{95}Mo, in competition with the 39 keV isomeric transition to the ^{95}Tc ground-state, is confirmed. Excited levels of 1040, 820, 780 and 203 keV are assigned to the ^{95}Mo structure, de-exciting mostly with the following transitions, in keV: 1040 (5$\pm$1), 838 (38$\pm$4), 820 (13$\pm$2), 780 (17$\pm$2), 580 (50$\pm$5); 203 (100).

1. – Introduction.

^{95}Tc is known to disintegrate into ^{95}Mo by positons and electron captures with two different activities corresponding to the 20 h ground state decay and to the 60 days metastable state decay. The two activities have been reported by several authors (1) who used (α, p), (p, n) and (d, 2n) reactions to produce them.

(*) Comunicato al XLVI Congresso della Società Italiana di Fisica, Napoli (Settembre-Ottobre 1960).

(1) B. N. Cacciapuoti: *Phys. Rev.*, **55**, 110 (1939); J. E. Edwards and M. L. Pool: *Phys. Rev.*, **72**, 384 (1947); D. T. Eggen and M. L. Pool: *Phys. Rev.*, **74**, 57 (1948); E. E. Motta and G. E. Boyd: *Phys. Rev.*, **74**, 344 (1948).

The first type of decay seems to occur only by electron capture ([2]) populating levels in ^{95}Mo at 1070, 930 and 760 keV which de-excite by direct γ-rays to the ^{95}Mo ground-state ([2,3]).

The second type of decay occurs also by two weak positon transitions of 460 and 680 keV ([4]) and seems to populate levels at 1020, 770 and 200 keV in ^{95}Mo as deduced by the associated γ-rays of energy: 1020, 810, 570 and 201 keV ([2,3,5]).

The metastable state decays also to the ^{95}Tc ground state by a 39 keV isomeric transition, for 3% of the total number of disintegrations, as established by MEDICUS and PREISWERK ([6]).

Some ambiguities about the level structure of ^{95}Mo have been solved more recently by UNIK and RASMUSSEN ([7]) who studied the decay of the ^{95}Tc isomer essentially with high resolution spectrometer techniques.

They found γ transitions of energy 204, 584, 763, 768, 784, 788, 822, 837 and 1040 keV and assigned levels at 204, 763, 784, 788, 822 and 1040 keV to ^{95}Mo, populated from the decay of the ^{95}Tc metastable state, while the 768 keV γ-ray was interpreted as the de-excitation of the level at the same energy known from the decay of the ^{95}Tc ground state. However the relative photon intensities were mostly deduced from the relative internal conversion electron intensities and on the basis of theoretical interpretations of the γ transition multipolarities. The level structure of ^{95}Mo, as proposed by UNIK and RASMUSSEN, is mostly based on these deductions.

In order to obtain independent direct information about the de-excitation properties of the ^{95}Mo levels populated from the decay of the ^{95}Tc isomer, the γ-ray spectrum associated with this decay was investigated in a detailed way at this laboratory, using scintillation techniques.

2. – Source production and experimental techniques.

Several sources of ^{95}Tc were produced by bombarding natural Mo with 24 MeV deuterons (20 μAh) in the synchrocyclotron of the Instituut voor Kernphysisch Onderzoek (IKO) in Amsterdam. The irradiated targets were

([2]) H. MEDICUS, P. PREISWERK and P. SCHERRER: *Helv. Phys. Acta*, **23**, 299 (1950).
([3]) G. E. BOYD and B. H. KETELLE: ORNL-1053 (1951); V. S. SHPINEL: *Žur. Èksp. Teor. Fiz.*, **27**, 387 (1954).
([4]) C. LEVI, L. PAPINEAU and N. SAUNIER: *Compt. Rend.*, **245**, 1918 (1957).
([5]) G. E. BOYD and B. H. KETELLE: *Phys. Rev.*, **83**, 216A (1951).
([6]) H. A. MEDICUS and P. PREISWERK: *Phys. Rev.*, **80**, 1101 (1950).
([7]) J. P. UNIK and J. O. RASMUSSEN: *Phys. Rev.*, **115**, 1687 (1959).

melted with sodium hydroxide and sodium nitrate and some Re (2 mg) was added as carrier. The melt was dissolved in 50 cm^3 water, the solution boiled and then neutralized by sulphuric acid. A 2N solution of ammonium acetate (5 ml) was added and the pH was made 8÷9 with sodium-bicarbonate. After addition of tetraphenilarsenic chloride and chloroform (~ 10 ml for each ml of solution), Tc and Re were extracted into the chloroform. The chloroform layer was evaporated under water and the precipitate, then formed, was filtered and dryed. All the chemical separations were performed at IKO in Amsterdam.

Experimental measurements were delayed at least four months to eliminate shorter Tc activities. The whole measured γ-ray spectrum was found to decay with the same half life (62 days) showing other contributions to be negligible.

The various spectra were investigated with a scintillation detector consisting of a NaI(Tl) Harshaw crystal of the well-type (diameter 76 mm, height 76 mm) coupled with a 6363 DuMont photomultiplier. The pulse height distribution was sent to a linear amplifier of Fairstein type and then displayed on a LABEN 200 channel analyzer. For the direct γ-ray spectra, a source-detector distance of ~ 13 cm was used in order to minimize geometrical summing effects.

The summing technique was also used placing the sources inside the well of the crystal in order to get information about γ-γ cascades.

γ-γ coincidences were also performed using a conventional circuit of 1 μs resolving time incorporated in the 200 channel analyzer.

A 25 mm × 25 mm NaI(Tl) Quartz and Silica crystal was used in this case, to select the 200 keV photopeak, connected with a Franklin single channel analyser. The coincident spectrum was detected by the large crystal and displayed on the multichannel analyser.

3. – Experimental results.

The direct γ spectrum is shown in Fig. 1 in two different energy regions. The resolved γ-rays are shown.

The analysis was performed by successively peeling off the pulse height distributions due to the single γ-rays starting from the higher energies. These distributions were constructed by comparison and interpolation with some standard ones, measured in the same geometrical conditions. We have used, for this purpose, the following γ-ray sources: ^{65}Zn (1112 keV), ^{207}Bi (1064 and 570 keV), ^{54}Mn (834 keV), ^{137}Cs (662 keV), ^{89}Sr (513 keV), ^{203}Hg (279 keV) and ^{114}In (191 keV). The complex peak at ~ 820 keV was analysed in three

different peaks whose relative intensities are, of course, only approximate; however this decomposition seems to be unambiguous on the basis of our results.

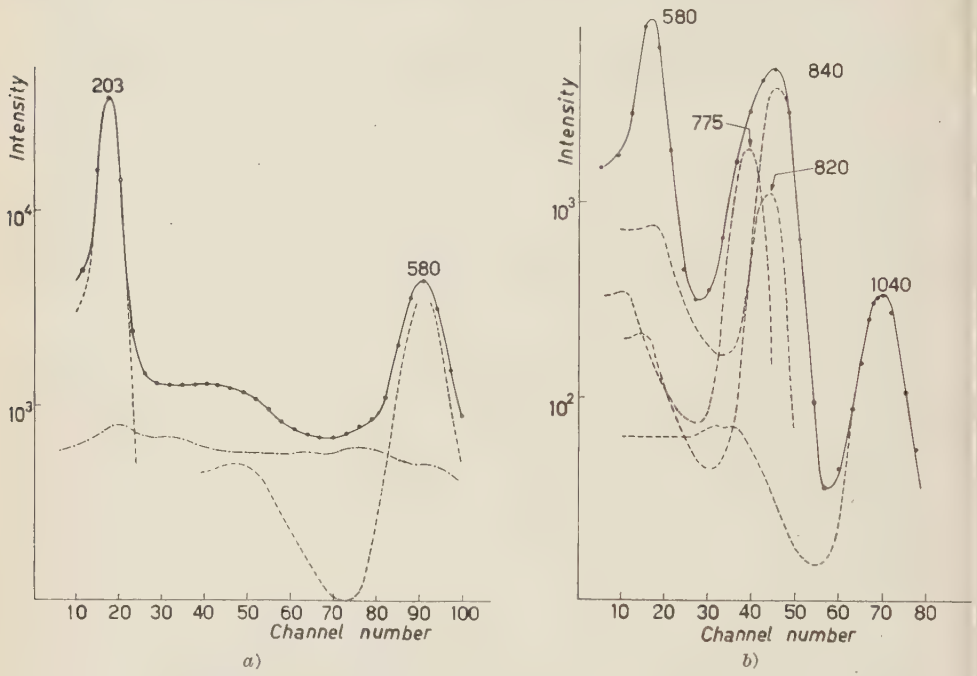

Fig. 1. – γ-ray spectrum associated with the decay of the ^{95}Tc isomer: *a*) low energy region; *b*) high energy region. The pulse height distributions due to monoenergetic γ-rays are drawn as dashed lines. The contribution of the high energy γ-rays is shown in the low energy part of the spectrum *a*) (dotted and dashed line).

The energies and relative intensities of the resolved γ-rays are reported in Table I.

TABLE I. – *γ-rays from the ^{95}Tc isomer (analysis of the direct spectrum).*

^{95}Tc produced by Mo (24 MeV d, 2n) chem; $T_{\frac{1}{2}} = (62 \pm 2)$d	
Energy in keV	Relative intensity
$1\,040 \pm 15$	5 ± 1
840 ± 10	37 ± 7
820 ± 10	12 ± 5
775 ± 8	18 ± 5
580 ± 5	50 ± 5
203 ± 3	100
$\gamma^{\pm}$	$\leqslant 3$

A better determination of the relative intensities of the γ-rays belonging to the 820 keV complex peak was obtained by analysing the results about γ-γ cascades.

Fig. 2 shows the summing spectrum (dashed line) in comparison with the direct spectrum (full line) in the high energy region.

Summing peaks at 1040 and 780 keV are evident: because of the corresponding lowering of the 840 and 580 keV peaks (and of the 203 keV peak, which is not shown) it can be deduced that there exist two cascades: (840+203) keV and (580+203) keV respectively from the corresponding levels at 1040 and 780 keV.

Table II summarizes the situation.

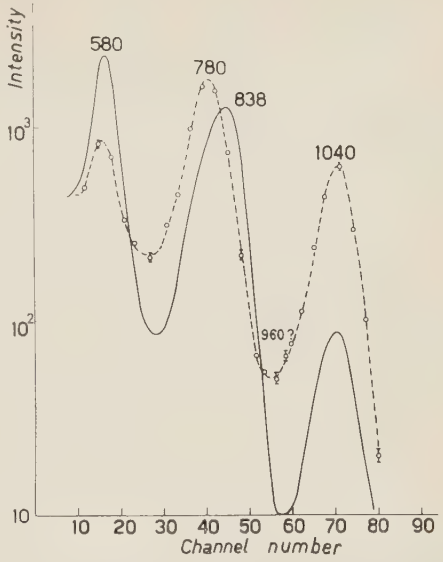

Fig. 2. – Summing spectrum (dashed line) obtained when the source is placed inside the well of the crystal. The direct spectrum (full line), reported for comparison, has been normalized at the 820 keV non coincident γ-ray.

TABLE II. – *Summing peaks and their interpretation.*

Energy in keV	Possible origin
1 040	203 + 838
960?	—
780	203 + 580

The whole γ spectrum in coincidence with the 203 keV γ-ray is reported in Fig. 3. Corrections for chance coincidences have been applied in a normal way.

The direct spectrum is also reported for comparison. Only the 838 keV γ-ray is coincident, of the complex structure at $\sim$ 820 keV. When this is subtracted, a residual structure is obtained, as reported in the insert of Fig. 2, which in turn can be analysed in two different peaks of energies 780 and 820 keV respectively. This is in good agreement with the results of the preliminary analysis performed on the direct γ spectrum.

The more precise analysis enabled us to give more accurate intensity values of the resolved γ-rays. These are reported in Table III, where the energies

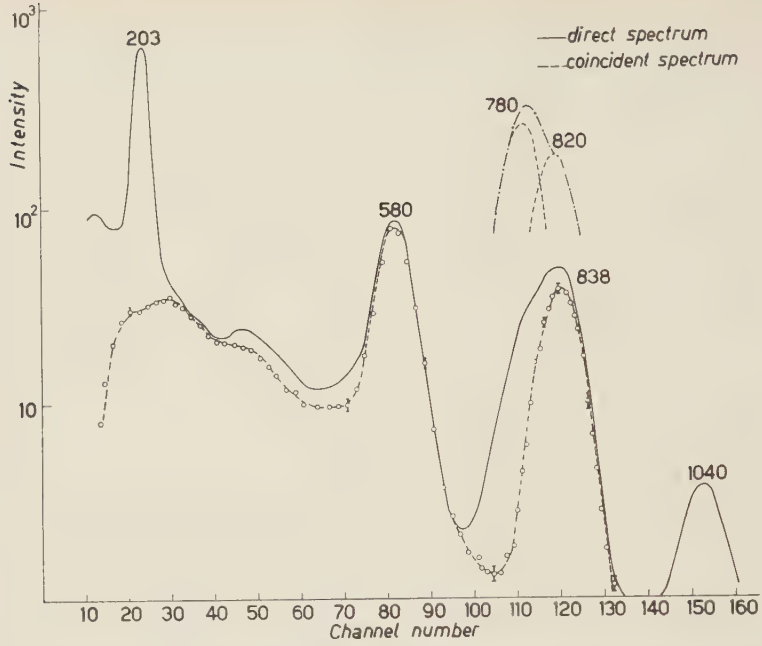

Fig. 3. – γ-ray spectrum in coincidence with the 203 keV photopeak (dashed line). The full line represents the direct γ spectrum reported for comparison. The result of the subtraction of the 838 keV coincident peak from the complex group at $\sim$ 820 keV, present in the direct spectrum, is shown in the insert. The successive analysis in two peaks of 780 adn 820 keV is also indicated.

TABLE III. – *Definitive analysis of the γ-ray spectrum from the ^{95}Tc isomer.*

UNIK and RASMUSSEN (ref. (7))		Present work	
Energy (keV)	Rel. intensity (*)	Energy (keV)	Rel. intensity
1040	5.6 ± 1.1	1040 ± 15	5 ± 1
	42	838 ± 5	38 ± 4
822	7	820 ± 5	13 ± 2
788	16 } 80 ± 8	780 ± 5	17 ± 2
784	< 6		
763	< 3		
584	56 ± 5	580 ± 5	50 ± 5
204	100	203 ± 3	100

(*) The relative photo intensities have been reported by UNIK and RASMUSSEN only for the 1040, 584 and 204 keV γ-rays. For the other transitions they have been deduced from relative conversion electron intensities and theoretical assumptions on multipolarities. We have here normalized these intensities at the 204 keV peak in order to have a comparison with our results.

and the deduced relative intensities of the γ-rays found by UNIK and RASMUSSEN are also shown for comparison.

No evidence for positons was found: the upper limit of their relative intensity is 1.5% of the 203 keV γ-ray, as deduced from the absence, in the limit of the errors, of an annihilation peak. This result should be compared with the value of 0.11% found by LEVI, PAPINEAU and SAUNIER, and the value of 0.56% deduced by UNIK and RASMUSSEN.

The other γ-rays reported by UNIK and RASMUSSEN with energies of 763, 768 and 784 keV were not resolved in our case from the 780 keV peak because of the very close energy values and their low relative intensities. The 768 keV γ-ray has been assigned by UNIK and RASMUSSEN to the ^{95}Tc ground state decay due to the de-excitation of the metastable state by the isomeric transition.

On the other hand it should be mentioned that the presence of a bump at ~ 960 keV in the summing spectrum (Fig. 2) may be due to a weak $[(760 \pm 30) + (203)]$ keV cascade, which cannot be interpreted as originating from the 930 keV level populated by the ^{95}Tc ground-state decay, because of the very low rate of population of this latter .

Moreover no evidence for a ~ 760 keV peak was found in the spectrum coincident with the 203 keV γ-ray. An upper limit of 2% of the 838 keV γ-ray can be set on the basis of the experimental errors: this is not enough to explain the 960 keV bump as a (203+760) keV summing. Probably this is also due to the summing structure of the 1040 keV peak distribution.

4. – Discussion.

The outstanding feature of the ^{95}Tc isomer decay is the population by electron capture, of the two excited levels at 1040 and 780 keV in ^{95}Mo. This can be compared with the population, by the electron capture decay of the ^{95}Tc ground state of the two levels at 930 and 760 keV. No interference between the two sets of levels is present owing to the large difference in the involved spin ($\frac{1}{2}^-$ for the ^{95}Tc metastable state, $\frac{9}{2}^+$ for the ^{95}Tc ground state, as predicted by the shell model).

A direct population of, at least, another level at 820 keV seems to be well established on the basis of our results, in agreement with UNIK and RASMUSSEN.

The population, by electron capture, of these three levels constitutes the essential mode of decay of ^{95}Tc isomer.

Weak transitions to the lower levels (ground-state and first-excited level at 203 keV) can be present on the basis of the γ-ray intensity balance. This situation is summarized in Table IV, where the calculated log *ft* values, for every transition, are reported.

TABLE IV. – log *ft* values of the electron capture transitions.

Energy of the transition in keV	Intensity	Populated level (keV)	log *ft*
660	31 %	1 040	6.8 ± 0.1
880	10 %	820	7.8 ± 0.2
920	49 %	780	7.1 ± 0.1
1 497	~ 8 %	203	~ 8.5
1 700	~ 2 %	0	~ 8.7

The gross structure of the proposed decay scheme is shown in Fig. 4. The agreement with UNIK and RASMUSSEN is very good, except for the relative intensity of the direct γ transition from the 820 keV level.

The relative transition intensities have been normalized to the total number of disintegrations and the small percentage of the positon group has been also considered.

The de-excitation properties of the different levels can be summarized as follows:

a) The 203 keV level certainly corresponds to the lowest excitation of ^{95}Mo. This was already known from the Coulomb excitation work done by MC GOWAN and STELSON [8] who also determined the characteristics of the 203 keV γ transi-

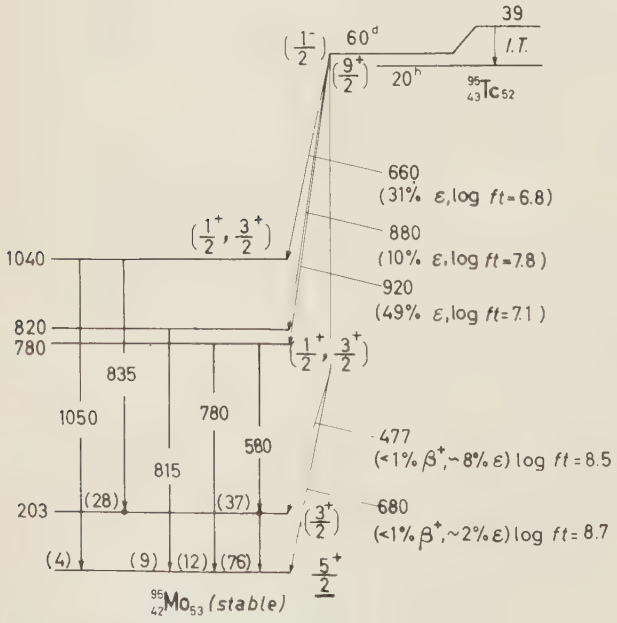

Fig. 4. – Proposed decay scheme for the decay of the ^{95}Tc isomer. Log *ft* values and relative decay intensities have been deduced from the intensity balance of the γ-ray spectrum. The relative photon intensities are reported in units of beta disintegrations. For the 203 keV γ transition the conversion fraction (~ 4%) has been taken into account.

([8]) F. K. MCGOWAN and P. H. STELSON: *Phys. Rev.*, **109**, 901 (1958).

tion by angular distribution and polarization directional correlation. This transition occurs as $M1$ ($\sim 80\%$)+$E2$ ($\sim 20\%$).

The conversion coefficient has been reported to be 3.6% by MEDICUS *et al.* ([2]), while the calculated value deduced from the mixing ratio $E2/M1$ found by MC GOWAN and STELSON is $(4.3 \pm 0.5)\%$.

b) The two levels at 1040 and 780 keV are very similar: both de-excite mostly to the first excited level with a less intense cross-over transition. The log *ft* values of the β decay to these two levels are very close, showing these latter to have very similar configurations. The multipolarities of the γ-rays originating from these levels, namely the 838, 780 and 580 keV γ-rays, have been discussed by UNIK and RASMUSSEN on the basis of the relative conversion electron intensities. A self consistent hypothesis is based on the assignment of $M1$ multipolarity to the 580 keV transition and of $M1$, $E2$ or ($M1 + E2$) multipolarities to the other transitions. The close values of conversion coefficients for $M1$ and $E2$ transitions for energies around 800 keV and for this region of atomic number makes a choice impossible. Perhaps angular correlation measurements involving the 580 and 838 keV γ-rays will give more information.

c) The 820 keV level de-excites only to the ground state by the 820 keV direct transition; this fact, together with the relatively high log *ft* value of the corresponding β branch seems to indicate that this level is quite different from the 1040 and 780 keV level. Moreover the absence of a de-excitation to the 203 keV level could be interpreted as due to a difference in the structure between the 820 keV and the 203 keV level.

Concerning the 820 keV γ transition a multipolarity assignment of $E1$, $M1$ or $E2$ is consistent with the results of UNIK and RASMUSSEN. However, the relative intensity found in our work, together with the electron conversion ratios reported by UNIK and RASMUSSEN and the $M1$ assignment to the 580 keV transition, would indicate the $E1$ multipolarity more plausible.

On the other hand this is inconsistent with the log *ft* value and the shell model predictions, which exclude the presence of an odd parity level at this energy and at the neutron number involved. If the results of UNIK and RASMUSSEN about the electron conversion intensities are correct, we have no explanation for such a situation.

Spin and parities have been assigned on the basis of the preceding arguments, taking into account the log *ft* values and the de-excitation properties.

However some remarks can be made. ^{95}Mo has 3 neutrons outside the 50 closed shell. The ground state spin has been measured and found to be $\frac{5}{2}$ ([9]),

([9]) E. C. WOODWARD: *Phys. Rev.*, **93**, 954 (1954); J. OWEN and I. M. WARD: *Phys. Rev.*, **102**, 591 (1956).

in agreement with the shell model prediction for a $(d_{\frac{5}{2}})^3$ neutron configuration. The first excited level could have spin $\frac{3}{2}^+$, $\frac{5}{2}^+$ or $\frac{7}{2}^+$ as deduced from the $(M1+E2)$ character of the 203 keV γ transition, with preference for $\frac{5}{2}^+$ if the log *ft* value is considered. However, from the measurement of McGowan and Stelson [8] a $\frac{3}{2}^+$ assignment was made. If this is true, the 230 keV level cannot be interpreted as a single particle state, but rather as a three particle state with a $[(d_{\frac{5}{2}})^3]\frac{3}{2}^+$ neutron configuration [7]. This will explain retardation effects in the log *ft* value and in the relatively long half life of the level [8,10,11].

For the other levels the assignment $\frac{1}{2}^+$ or $\frac{3}{2}^+$ to the 1040 and 780 keV levels seems to be very plausible, while the unclarified situation concerning the 820 keV level leaves the spin of this latter indeterminate.

Nothing can be said from this work about other levels in the ^{95}Mo structure. Unik and Rasmussen have reported levels at 763 and 784 keV directly populated by the ^{95}Tc metastable state decay, because of the presence of weak γ-rays with the above energies.

However the possibility that a 760 keV transition comes from a level at ~ 960 keV associated with the decay of the ^{95}Tc isomer ($\sim 1\%$) cannot be excluded, as pointed out in 3).

* * *

We wish to express our gratitude to Prof. G. Cortini for his interest and encouragement and to Dr. R. Van Lieshout for valuable discussions and suggestions. Thanks are due to Miss J. C. Kapteijn (IKO, Amsterdam) for performing the chemical separations and to the cyclotron personnel of IKO (Amsterdam) for the irradiations.

([10]) J. Quidort: *Compt, Rend.*, **246**, 2119 (1958).
([11]) R. E. Holland and F. I. Lynch: *Bull Am. Phys. Soc.*, **4**, 232, (1959).

RIASSUNTO

Si è studiato, con tecniche a scintillazione, lo spettro γ associato al decadimento radioattivo dello stato isomerico del ^{95}Tc, ottenuto per reazione (d, 2n) sul Mo naturale. Le misure si sono effettuate con un cristallo NaI(Tl) a pozzo, ottenendo anche informazioni sulle cascate γ-γ con la tecnica di somma, oltre che con circuiti a coincidenze convenzionali. Gli spettri sono stati analizzati con un selettore di impulsi LABEN a 200 canali. Si conferma il decadimento per cattura elettronica, dell'isomero ^{95}Tc a stati eccitati del ^{95}Mo cui vengono assegnati livelli a 1040, 820, 780 e 203 keV. La diseccitazione di questi livelli avviene essenzialmente per transizioni γ le cui energie (in keV) e intensità relative sono: 1040 (5 ± 1), 838 (38 ± 4), 820 (13 ± 2), 780 (17 ± 2), 580 (50 ± 5), 203 (100).

IL NUOVO CIMENTO Vol. XIX, N. 6 16 Marzo 1961

Angular Distribution of Photofission Fragments from Uranium (*).

H. G. de Carvalho (**), A. G. da Silva (***)

Centro Brasileiro de Pesquisas Fisicas - Rio de Janeiro

J. Goldemberg

Departamento de Fisica, Universidade - São Paulo

(ricevuto l'11 Novembre 1960)

Summary. — The angular distributions of photofission fragments from uranium at X-ray maximum energies of 6.9, 8.1, 9.4, 15.5 and 20 MeV were measured using a 24 MeV betatron. The anisotropy was found to increase with decreasing X-ray energy and to be mainly consistent with $a + b \sin^2 \theta$ electric dipole photon absorption distribution. The quadrupole contribution is shown to be small. The ratio of the anisotropic dipole absorption to the isotropic fission yields at the first three superior energies are 2.80 ± 0.44, 1.18 ± 0.14 and 0.62 ± 0.12. At 15.5 and 20 MeV the distributions are almost isotropic.

1. – Introduction.

The anisotropy of the angular distribution of photofission fragments is a property of the heavy and strongly deformed even-even nuclei. In 1952 Winhold, Demos and Halpern [1], found, by the catch foil technique, that

(*) Presented to the 46-th National Conference of the Italian Physical Society, Naples, September 29, October 5th. This work is supported in part by funds provided by the Conselho Nacional de Pesquisas and by Comissão Nacional de Energia Nuclear (Brazil).

(**) At present on leave of absence from the Centro Brasileiro de Pesquisas Fisicas and Brazilian Nuclear Energy Comission at the Istituto Nazionale di Fisica Nucleare, Sottosezione di Napoli.

(***) On leave of absence from the C.B.P.F. at the high voltage Lab., M.I.T., Mass. (U.S.A.).

[1] E. J. Winhold, P. T. Demos and I. Halpern: *Phys. Rev.*, **87**, 1139 (1952); E. J. Winhold and I. Halpern: *Phys. Rev.*, **103**, 990 (1956).

the angular distribution of photofission fragments from thorium has a maximum at right angles to the beam of X-rays. It was found also that the anisotropy decreased with the increase in maximum energy of the bremsstrahlung radiation and that within the experimental errors the angular distribution appears to be of the form $a+b\sin^2\theta$, resulting from a dipole photon absorption.

KATZ, BAERG and BROWN [2] in 1958, using ionization chambers, measured the angular distribution of photofission fragments from ^{238}U at nine different energies between 6 and 20 MeV and it was found to be consistent with a dipole photon absorption of the form $1+\alpha\sin^2\theta$. However LAZAREVA [3] *et al.* have found by means of the photo-plate technique, that the angular distribution of the fragments of photofission of ^{238}U contains a term in $\sin^2\theta\cos^2\theta$, implying some quadrupole absorption. This is mainly observed at the maximum bremsstrahlung radiation energy of 9.4 MeV in disagreement with Katz's results at the same energy.

In the experiment described in the present paper the angular distribution of photofission fragments from uranium was obtained from careful measurements made at six different angles and at five different energies using the nuclear emulsion technique.

2. – Method.

The measurements were performed on the fission fragment tracks produced by the γ-rays in Ilford 100 and 200 μm K-O nuclear emulsions loaded with natural uranium. By a systematic search the best method for uranium loading of nuclear emulsion resulted to be the following: the solution for loading was prepared mixing equal volumes of a molar solution of sodium citrate with a 0.5 molar solution of uranyl nitrate and adjusting the pH to about 5 pH units with sodium hydroxide. The plates were immersed in this solution for 20 or 60 minutes according to the thickness of emulsion (100 μm or 200 μm) and put to dry at room temperature.

Natural uranium was used as ^{238}U target nuclide. The other isotopes in natural uranium at the X-ray energies used have a photofission contribution of less than 1.8% of the total number of fissions produced. Furthermore

(2) L. KATZ, A. P. BAERG and F. BROWN: *Second United Nations International Conference on Peaceful Uses of Atomic Energy*, Geneve P/200, **15**, 188 (1958).

(3) B. P. BANNIK, N. M. KULIKOVA, L. E. LAZAREVA and V. A. IAKOVLEV: *Sov. Phys. J.E.T.P.*, **6**, 39 (1958); A. I. BRAZ, N. M. KULIKOVA, L. E. LAZAREVA, N. V. NIKITINA and V. A. SEMENOV: *Second United Nations International Conference on the Peaceful Uses of Atomic Energy*, Geneve P/2037, **15**, 184 (1958).

the ^{235}U is an odd-even nuclide, therefore it is expected to give a nearly isotropic angular distribution.

The X-ray dose in roentgens received by the plates was measured using a Victoreen ion chamber placed in a cavity at the center of an 8 cm lucite cube. The energy scale was calibrated detecting the threshold of the following reactions: ^{63}Cu (γ, n) 10.6 MeV and ^{16}O (γ, n) 15.85 MeV, ^{12}C (γ, n) 18.75 MeV. The energy scale is believed to be accurate to ± 0.1 MeV.

The plates (one by three inches) were exposed longitudinally at 0° angle in the axial part of the beam of X-rays at different maximum energies at a distance of 45 cm from the betatron target. Only the central axial part of the plates was used in the scanning work. Due to absorption of X-rays in the plates the X-ray spectrum was somewhat hardened along the plates.

The thicknesses of the loaded emulsions were measured just before the exposure at four points, with a dial micrometer, around a small hole cut in the emulsion, so as to allow the surface of the glass backing to be taken as the zero of the micrometric measurements. The shrinkage factor was obtained by measuring the thickness of the four points in the developed plates with the same dial micrometer adapted to the microscope.

The development method used was the following ([4]). The loaded and exposed plates were washed with cold distilled water (5 °C) for 45 minutes before immersion in the developing bath: boric acid 3.5 g, sodium sulfite 4.5 g, potassium bromide 1.5 g, amidol 0,45 g, distilled water to complete 2 liters of solution.

The developing time was adjusted to the condition of the X-ray dose and uranium loading desensitization, in such a way that only the fission tracks were well developed. This made the scanning of plates considerably easier since no α-particle tracks were visible.

After the developing bath the plates were washed in cold distilled water for 2 hours and fixed with a very cold 30% hypo solution that had been used before so that it contained a few grams of silver in solution. This diminishes the production of background grains during the fixing process.

In order to keep the shrinkage factor low the plates after fixing and washing in cold tap water, were immersed in a 10% glycerine solution and submitted to a slow drying, thus yielding a shrinkage factor of about 1.6, and so increasing the precision of the measurements of depth with the microscope.

The fraction of fission due to fast neutrons from the betatron, slow neutrons and scattered X-rays present in the background of the experimental area, was measured by the recoil proton method with E-1 Ilford nuclear emulsion placed

([4]) H. G. DE CARVALHO and A. G. DA SILVA: *III International Conference on Corpuscular Photography*, (Moscow, July 1960).

in and out of the X-ray beam and KO Ilford uranium impregnated plates placed out of the beam during the exposure time. The fraction was found to be less than 2% of the total number of fissions at the X-ray energies used.

Since the origin point of the tracks could not be determined, the angles θ and $\pi-\theta$ were indistinguishable and the obtained angular distribution is actually $Y(\theta)=I(\theta)+I(\pi-\theta)$.

For the indicated angle intervals in Table I the relative yields per unit solid angle are given by

$$\overline{Y}(\theta)=\int_{\theta_1}^{\theta_2}[I(\theta)+I(\pi-\theta)]\,\mathrm{d}\Omega\Big/\int_{\theta_1}^{\theta_2}\mathrm{d}\Omega\,.$$

The scanning was performed with Leitz Ortholux microscopes with 100× objective and 6× eye-pieces. The dip angles of all tracks were obtained by measuring the horizontal projection and the vertical depth of the tracks. As mentioned above, the shrinkage factor was reduced by adding glycerine and it was measured four times a day to correct for the daily relative humidity variations.

TABLE I. – ^{238}U *angular distributions.*

Maximum X-ray energy E_0 (MeV)	Relative yield for angle interval (per unit of solid angle)						Value of b/a in $Y(\theta)=a+b\sin^2\theta$
	0° ≃ 15° 180° ≃165°	15° ≃ 30° 165° ≃150°	30° ≃ 45° 150° ≃135°	45° ≃ 60° 135° ≃120°	60° ≃ 75° 120° ≃105°	75° ≃90° 105° ≃90°	
6.9	1.00±.21	1.28±.14	1.70±.13	2.45±.13	3.30±.18	3.28±.17	2.80± .44
8.1	1.00±.15	1.22±.09	1.52±.08	1.79±.08	2.06±.10	2.10±.09	1.18± .14
9.4	1.00±.10	1.10±.08	1.33±.10	1.46±.10	1.54±.10	1.55±.10	.62± .12
15.5	1.00±.09		1.01±.09		1.08±.09		0.09±0.14
20	1.00±.10	.98±.10	.96±.10	.98±.10	1.03±.10	1.00±.10	0.08±0.13

The dip angle α of the fragment with the horizontal plane and the angles β of the horizontal projection of the fragment and the direction of the X-ray beam were measured and the actual angles θ of the fragment with the axial direction of the beam were obtained from the relation $\cos\theta=\cos\alpha\cos\beta$.

The fission yield per roentgen and per nucleus decreases sharply with the X-ray energy and at 6.5 MeV it is about 100 times smaller than at 16 MeV,

therefore for the same dose of X-rays near the photofission threshold, where the anisotropy is high, the number of tracks available for measurement is very small. At energies higher than 9 MeV due to the abundance of tracks it is possible to select only the tracks oriented at angles smaller than 15° to the plane of the nuclear emulsion plates. However at energies smaller than 9 MeV due to the paucity of tracks it was decided to apply a different criterion in order to permit the use of a greater number of tracks. If the beam of γ-rays is not polarized the measurements of the differential cross-sections at a particular average angle with the beam direction (but at different angles with the plane of emulsion) must yield the same differential cross-section since there is an axial symmetry around the beam. Therefore measurements of this kind show the overall effect of distortion and microscope scanning losses on the measurement of the angular distribution at a particular angle with the beam direction and at a particular angle with the plane of the emulsion. The analysis of the data made it possible to determine the effect of distortion and scanning losses and to set a proper cut-off at angles greater than the 15° used previously (at energies greater than 9 MeV) so as to accept the maximum number of tracks.

3. – Experimental results and discussion.

The angular distribution of fission fragments from the photofission reaction produced by dipole and quadrupole γ-ray absorption has the following general form:

$$I(\theta) = a + b(\sin\theta + d\sin\theta\cos\theta)^2 .$$

With the method used in the present work it is impossible to distinguish the heavy fragment from the light one, thus the measured distribution is $Y(\theta) = I(\theta) + I(\pi - \theta)$ and, as a result, the term with forward backward asymmetry, due to electric dipole-electric quadrupole interference is cancelled out.

The following expression remains:

$$Y(\theta) = a + b\sin^2\theta + c\sin^2\theta\cos^2\theta ,$$

or

$$W(\theta) = 1 + \frac{a}{b}\sin^2\theta + \frac{c}{a}\sin^2\theta\cos\theta^2 .$$

The coefficient « a » determines the isotropic part of the angular distribution, the coefficients « b » and « c » the anisotropic part related to dipole and quadrupole absorption of the γ-rays respectively.

Two different methods, yielding practically the same results, were used

in the computation of the coefficients a, b and c from the experimental data: the least square method, and a cosine Fourier series, which is very appropriate to this particular case of angular distributions (dipole and quadrupole photon absorption), and very easy to calculate. This latter method also permits the computation of the errors of the coefficients a, b and c from the statistical errors of the angular distribution measurements.

The measurements were made at six intervals of solid angles defined by the angles θ with the γ-rays beam direction *i.e.* 0, 15, 30, 45, 60 and 90. For the computations of the coefficients it is necessary to determine an average angle $\overline{\theta}$ for each solid angle interval. This may be done taking the arithmetical mean: $\overline{\theta} = (\theta_1 + \theta_2)/2$ or averaging θ in the solid angle interval used:

$$\overline{\theta} = \int_{\theta_1}^{\theta_2} \theta \sin\theta \, d\theta \Big/ \int_{\theta_1}^{\theta_2} \sin\theta \, d\theta \, .$$

The last method was used in computing the coefficients by means of the least square method, because it introduced corrections to the first solid angle intervals. Using the Fourier cosine series

$$Y(\overline{\theta}) = a_1 - (b/2)\cos 2\theta - (c/8)\cos 4\theta \, ,$$

where $a_1 = a + (b/2) + (c/8)$, $\overline{\theta}$ was taken as the arithmetical mean, so as to yield in the interval 0 to 180°, twelve equal angle intervals each of $(\pi/12)$.

The coefficients a_1, b and c were obtained by the usual Fourier series method as follows:

$$a_1 = (1/6)\sum y_0 \, , \qquad b = (2/3)\sum y_0 \cos 2\theta \, , \qquad c = (8/3)\sum y_0 \cos 4\theta \, ,$$

where y_0 is the measured angular distribution. Since each measured point has a statistical error $\pm\varepsilon$, the mean square errors of the coefficients are calculated straightforwardly from the statistical errors $\pm\varepsilon$ as follows:

$$\Delta a_1 = \pm(1/6)\sqrt{\sum \varepsilon^2}, \qquad \Delta b = \pm(2/3)\sqrt{\sum \varepsilon^2 \cos^2 2\theta}$$

and

$$\Delta c = \pm(8/3)\sqrt{\sum \varepsilon^2 \cos^2 4\theta} \, .$$

Therefore this method yields errors in a form more reliable than the one usually obtained from the least squares method, in which the probable errors computed for the constants result from the closeness of the fit and is not related to the statistical error of the measurements. This point is emphasized here to illustrate the effect of the statistical errors on the computation of the quadrupole term coefficient in which the error is about four times greater than on the dipole term coefficient.

The angular distributions obtained with the statistical errors at all energies measured are given in Table I.

The calculated coefficients are given in Table II.

TABLE II.

Maximum X-ray energy (MeV)	$\frac{b}{a}$	$\frac{c}{a}$
6.9	2.80 ± 0.44	0.34 ± 0.85
8.1	1.18 ± 0.14	0.52 ± 0.52
9.4	0.62 ± 0.12	0.60 ± 0.56
15.5	0.09 ± 0.14	—
20.0	0.08 ± 0.13	

3·1. *Dipole photon absorption.* – The ideas put forward by A. BOHR [5] on the unified model of the nucleus allow an explanation of the observed anisotropy in fission fragment emission in terms of the excitation spectrum at fission barrier. For excitation energies only slightly in excess of the lowest fission barrier the nucleus when passing over the barrier is « cold », meaning that a great deal of the excitation energy is spent in potential energy of deformation in reaching the barrier. This implies that the level spectrum at the saddle point should be rather simple if the excitation energy is only slightly greater than the barrier height. It is assumed also that the spectrum of the nucleus at the barrier should resemble the spectrum of the nucleus in the ground state.

In Bohr's model one assumes that the nucleus retains axial symmetry throughout the fission process and that the fission fragments are emitted in the direction of the symmetry axis of the nucleus, therefore the orientation of the symmetry axis corresponds to the angular distribution of the fragments. The distribution is given by the square of the symmetric top wave function for a compound state of angular momentum I, and z component along the beam M, which pass the barrier in a state of excitation with component K of angular momentum along the symmetry axis.

---

[5] A. BOHR: *Proceedings of the First United National International Conference on the Peaceful Uses of Atomic Energy*, Geneve 1955, Report no. 911, vol. 2 (New York, 1956), pp. 151.

The anisotropy of photofission of even-even nuclei (spin zero) resulting from a dipole absorption is explained as follows: when the photon is absorbed in the electric dipole mode, the compound state has $I = 1$, $M = \pm 1$. The low-lying states are characterized by pairing of nucleons to states with $K = 0$. For photofission resulting from the low-lying 1^- states with $K = 0$ at the barrier, the angular distribution would be proportional to a positive $\sin^2\theta$ term, with emission of fragments dominantly in the 90° directions with the beam. The dipole absorption corresponding to the $K = 1$ states would give an anisotropy of the opposite character, peaked at 0° corresponding to a negative $\sin^2\theta$ term.

Near the threshold the lowest-lying saddle point is the only one available and the resulting anisotropy is peaked at 90°, but at a few MeV above the threshold both states $K = 0$ and $K = 1$ are available and the anisotropy from both states tends to cancel yielding a more isotropic distribution. At higher energies there will be many more channels corresponding to other different states and the average angular distribution will then be isotropic.

As illustrated in Fig. 1 the ratio (b/a) measured at five different energies is in a very good agreement with the results of KATZ and LAZAREVA. The

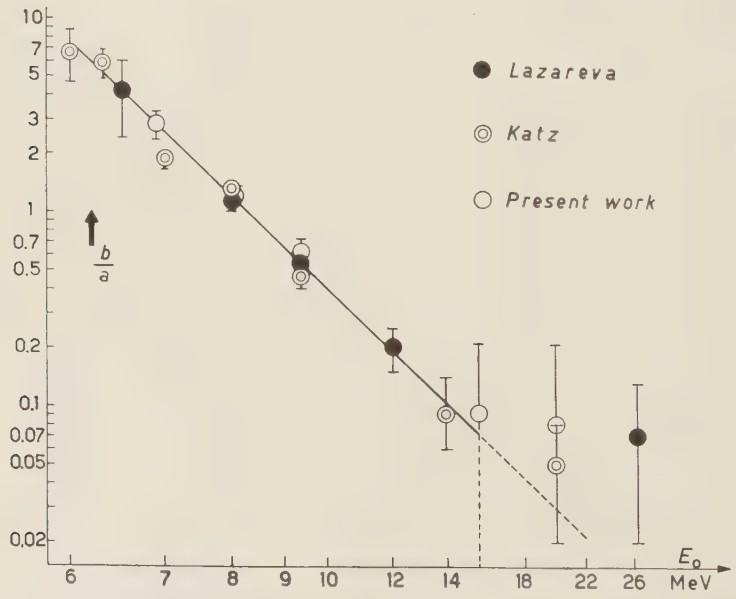

Fig. 1. – Variation with the maximum bremsstrahlung energy E_0 (in MeV) of ratio b/a, between the coefficients « a » related to the isotropic part of the angular distribution and « b » the anisotropic part related to the dipole photon absorption. The solid line represents the empirical equation $\log(b/a) = (1.676 \pm 0.24) - (2.66 \pm 0.10)\log(E_0 - 4)$ obtained from a least square fitting of the results of KATZ, LAZAREVA and the present work.

ratios b/a are represented in a Katz plot corresponding to the following empirical formula:

$$\log (b/a) = (1.676 \pm 0.024) - (2.66 \pm 0.10) \log (E_0 - 4) ,$$

calculated by the least square method from the overall data available. (Where E_0 is the peak bremsstrahlung energy in MeV.) This is represented in Fig. 1 by the solid straight line.

3·2. *Quadrupole photon absorption.* — For quadrupole absorption of a photon the compound state will have quantum number $I = 2$, $M = \pm 1$ and the lowest corresponding excitation at the barrier would be a 2^+ state with $K = 0$, the second member of the even parity rotational band.

If at the barrier this state lies sufficiently low compared with the 1^- state, then there might exist a range of photon energies over which the smaller probability of quadrupole absorption is counterbalanced by smaller probability of fission through the 1^- state. The resulting fission fragment angular distribution would have a component proportional to a $\sin^2 2\theta$ term with a maximum at 45°, and the same happens for the $K = 2$ state. However the $K = 1$ state has a negative $\sin^2 2\theta$ acting to cancel out the $K = 0$ and $K = 2$ quadrupole angular distributions.

If appropriate proportions of quadrupole are invoked and appropriate K values are assumed it is possible to explain the variation of quadrupole absorption with energy.

As mentioned above, at 9.4 MeV, the angular distributions obtained by KATZ with the ionization chamber and by LAZAREVA with the nuclear emulsion technique differ very much regarding the quadrupole coefficient c/a. The results from KATZ, LAZAREVA and the present work, normalized at an angle of 7.5°, are represented in Fig. 2 for comparison. It may be observed that the Katz measurements at 0°, 45° and 90° fit a pure dipole curve (2) with $b/a = 0.46$ but the Lazareva experimental points correspond to a fitting $b/a = 0.5$ and $c/a = 0.9$; the present results correspond to $b/a = 0.6$ and $c/a = 0.6$. Curve (1) represents a Fourier best fitting of Lazareva and the present results together corresponding to $b/a = 0.47$ and $c/a = 0.80$. In conclusion it appears that there is a measurable quadrupole photon absorption at 9.4 MeV with a c/a of about 0.8 ± 0.4.

As was pointed out by Lazareva, c/b gives a certain estimate of the relation between the cross-sections for electrical dipole and electrical quadrupole photon absorption but due to the high statistical errors (see Table II) and other sources of errors not considered (beam collimation, small errors due to distortion, and so on), the measurements of quadrupole coefficients, in the range of energy investigated, are at present very poor indeed and do not allow

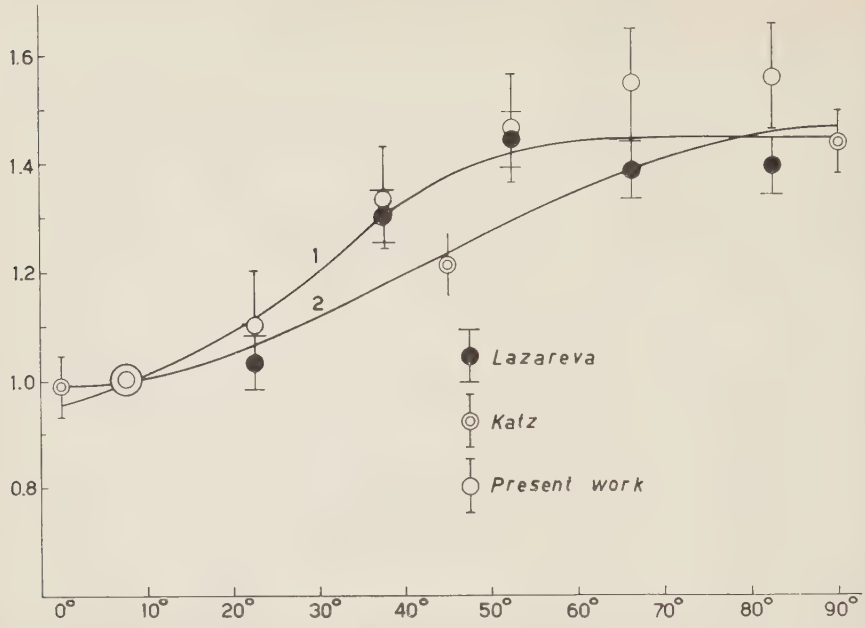

Fig. 2. – Angular distribution for 9.4 MeV bremsstrahlung showing the data of KATZ, LAZAREVA and the present work, normalized to 7.5°. Curve 1 corresponds to the best fitting of the data of LAZAREVA and the present work together $(1+0.47 \sin^2\theta+0.80 \sin^2\theta \cos^2\theta)$, curve 2 is a fitting of KATZ's results with a pure dipole photon absorption curve $(1+0.46 \sin^2\theta)$.

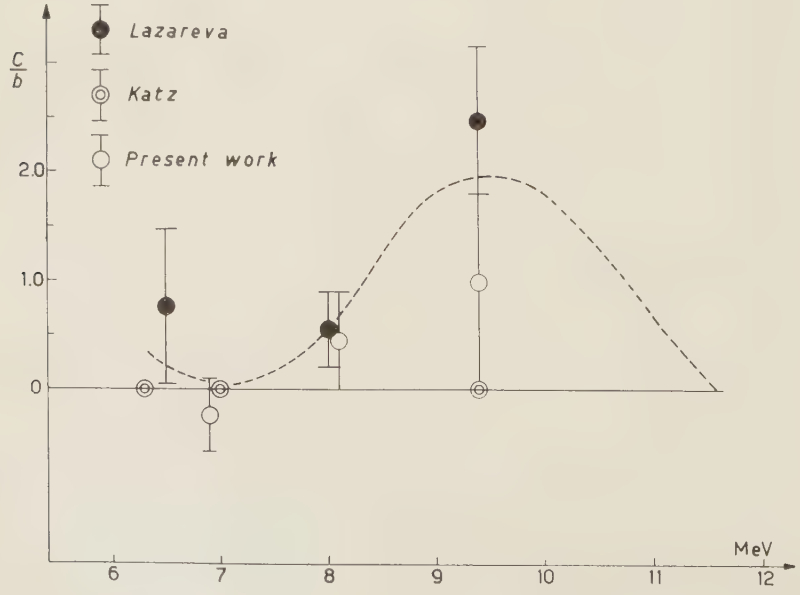

Fig. 3. – Variation of the ratio c/b with the peak bremsstrahlung energy.

us to draw definite conclusions. However, assuming that the measurements of LAZAREVA and of the present work are correct, the general trend of variation of c/b with energy is illustrated in Fig. 3.

In order to obtain a better quadrupole coefficient measurement it is necessary to perform more accurate experiments using an indicator of the origin of fission tracks like a 1 μm diameter grain of U_3O_8, so as to distinguish the light fragment from the heavy one and thus to obtain the angular distribution in the interval 0 to 180° and from that to compute the interference term, which is removed when it is impossible to distinguish the heavy fragment from the light one.

* * *

The authors would like to thank the betatron group at the Physics Department of the University of S. Paulo and Misses L. TAVORA, D. MARTINS, S. GAERTNER, T. VILLAR, N. MIRANDA, M. SETTE and E. LUIZ PINTO from the C.B.P.F. for the careful scanning of plates and measurements of angles, and Prof. G. CORTINI for helpful discussions.

RIASSUNTO (*)

Usando un betatrone da 24 MeV si sono misurate le distribuzioni angolari dei frammenti di fotofissione dell'uranio ad energie massime dei raggi X di 6.9, 8.1, 9.4, 15.5 e 20 MeV. Si è riscontrato che l'anisotropia cresce al decrescere dell'energia dei raggi X e si accorda sostanzialmente con una distribuzione dell'assorbimento dei fotoni di dipolo elettrico secondo la legge $a+b\sin^2\theta$. Si mostra che il contributo di quadrupolo è piccolo. I rapporti fra l'assorbimento anisotropo di dipolo e le rese dalla fissione isotropa per i primi tre valori suddetti dell'energia sono 2.80 ± 0.44, 1.18 ± 0.14 e 0.62 ± 0.12. A 15.5 e 20 MeV le distribuzioni sono pressochè isotrope.

(*) *Traduzione a cura della Redazione.*

IL NUOVO CIMENTO Vol. XIX, N. 6 16 Marzo 1961

The Relativistic Increase of the Specific Primary Ionization in Helium.

C. Ballario (*), A. De Marco, R. D. Fortune and C. Verkerk

CERN - Geneva

(ricevuto il 14 Novembre 1960)

Summary. — The relativistic increase of the specific primary ionization produced by electrons in a helium-alcohol mixture, has been determined from measurements of mean length made on photographs of post-expansion tracks in a Wilson cloud chamber. The results show a logarithmic increase of the relative ionization as a function of p/mc from $p/mc \sim 5$ up to $p/mc \sim 300$ and there is some evidence of the density effect at $p/mc \sim 678$ where the primary ionization relative to minimum is 1.50 ± 0.03. The extent of the logarithmic increase and the ratio of the plateau to the minimum ionization are significantly greater than those calculated for pure helium from the theory of Budini and Taffara. Measurements of the specific primary ionization by the technique of gap counting are shown to be uncorrelated with variations in the relative condensation efficiency (θ) in the range $0.2 \leqslant \theta \leqslant 0.6$. This enables precise measurements of ionization to be made which do not necessitate critical adjustments of expansion conditions in the cloud chamber.

1. – Introduction.

Very few results have been published on the relativistic increase of the specific primary ionization in gases. Hazen [1], using a helium-filled magnetic cloud chamber, made droplet density measurements on post-expansion cosmic ray tracks, but he did not find any evidence for a relativistic increase. He concluded that either the momentum of the particles was over-estimated or the primary ionization did not increase as rapidly with velocity as predicted

(*) Now at the University of Rome.

(1) W. E. Hazen: *Phys. Rev.*, **63**, 107 (1943).

theoretically. This appears to be the only cloud chamber measurement so far published on this subject. In the field of counter experiments, somewhat better agreement between theory and experiment has been obtained. HEREFORD [2] made measurements of the primary ionization using low-efficiency hydrogen counters and his results indicate a relativistic increase: his measurements, however, extend only as far as $p/mc \sim 14$. Other workers [3], also using hydrogen counters, measured the mean primary ionization of the sea level cosmic radiation and found a value of the same order as that predicted from Wilson's [4] meson spectrum and the theory of Halpern and Hall [5].

There do not appear to be any published experiments using relativistic particles of well-defined momentum.

From the theoretical point of view, most of the work up to the present has been done on the derivation of formulae for the average collision energy loss. A theory giving explicitly the relativistic increase and density effect for the specific primary ionization has only recently been developed by BUDINI and TAFFARA [6] from a more simplified approach by FERMI [7]. The theory of Budini and Taffara, however, can be numerically calculated only for the simplest gases (H_2, He) for which the electronic ionization potentials, oscillator strengths and photo-electric cross-sections are known.

The interest of precise measurements of the primary ionization of relativistic particles lies not only in the comparison with theory but in the application of the relativistic increase to the identification of particles from independent measurements of momentum and ionization. FRETTER *et al.* [8] and LAGARRIGUE *et al.* [9] have measured the relativistic increase of the probable ionization in various gases and gas mixtures, with this application in mind. Their experiments were conducted with cosmic ray particles and they each used drop-counting technique on the photographs of diffuse pre-expansion tracks formed in a magnetic cloud chamber.

For work with particle accelerators, the possibility of freely controlling the time of arrival of the particles relative to the chamber expansion permits the use of post-expansion tracks, and hence the measurement of primary

---

(2) F. L. HEREFORD: *Phys. Rev.*, **74**, 574 (1948).

(3) For references up to 1955 see the review article by B. T. PRICE: *Prog. Phys.*, **18**, 52 (1955).

(4) J. G. WILSON: *Nature*, **158**, 414 (1946).

(5) O. HALPERN and H. HALL: *Phys. Rev.*, **57**, 459 (1948); **73**, 477 (1948).

(6) P. BUDINI and L. TAFFARA: *Nuovo Cimento* **4**, 23 (1956).

(7) E. FERMI: *Phys. Rev.*, **56**, 1242 (1939); **57**, 485 (1940).

(8) R. G. KEPLER, C. A. D'ANDLAU, W. B. FRETTER and L. F. HANSEN: *Nuovo Cimento*, **7**, 71 (1958).

(9) A. ROUSSET, A. LAGARRIGUE, P. MUSSET, P. RANÇON and X. SAUTERON: *Nuovo Cimento*, **14**, 365 (1959).

ionization, in experiments where a counter-control is not essential. This appears to offer the following advantages.

i) Measurements of the primary ionization should be much less affected by fluctuations in the negative ion condensation efficiency ([10]) and should also be much less affected by the Landau fluctuations ([11]).

ii) Measurements of momentum from track curvature should be more precise with the narrower track and the track distortions due to gas movements should be smaller ([12]), since the time interval between the passage of the particle and the moment of photography is shorter.

The aim of the present work is firstly, to determine whether the primary ionization in helium shows a relativistic increase comparable in slope and plateau to that predicted by the Budini theory, and secondly, to determine to what extent the measurements of primary ionization on post-expansion tracks are affected by variations in the condensation efficiency.

The primary ionization measurements were made on stereoscopic photographs of post-expansion tracks in a cloud chamber filled with helium. Each photograph contained tracks of particles of high and well-defined momentum, reference tracks of minimum ionizing electrons and diffused field-separated tracks with which to measure the condensation efficiency. For relativistic particles we have used negative electrons from the materialization of γ-rays from the decay of neutral pions produced in an aluminium target by nuclear interactions of protons of the external beam of the CERN 600 MeV Synchrocyclotron. For reference particles we have used electrons from a Strontium 90 radioactive source.

2. – Apparatus.

2·1. *General.* – Fig. 1 shows the position of the cloud chamber with respect to the external proton beam, target, bending magnets, accelerator shielding wall and radioactive source. Negative pions, muons and electrons of momentum selected by the magnet $M1$ and the collimating hole in the shielding wall were deviated in the experimental hall by the magnet $M2$, and entered the cloud chamber through an aluminium window 0.3 mm thick. With this thickness, only 6% of the high-energy electrons lose more than 5% of their energy by radiation, the ionization losses being negligible.

The momentum of the particles of the accelerator beam was chosen so that the ionization of the mesons was either very near minimum ($250 \leqslant p_\pi \leqslant 370$ MeV/c) or more than three times minimum ($p_\pi \leqslant 80$ MeV/c): it

([10]) W. E. HAZEN: *Phys. Rev.*, **65**, 259 (1944) and ref. ([8]).
([11]) L. LANDAU: *Journ. Phys. USSR*, **8**, 201 (1944).
([12]) P. M. S. BLACKETT: *Supp. Nuovo Cimento*, **11**, 264 (1954).

was thus possible to distinguish the electron tracks from the meson tracks in the photographs, by the difference in their ionization.

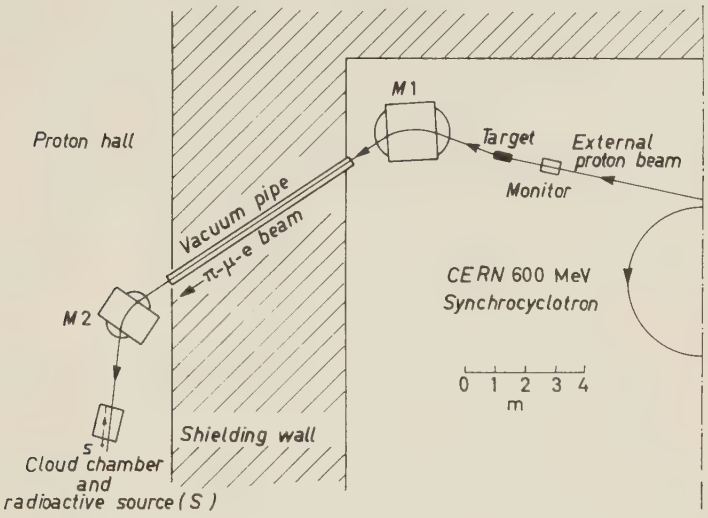

Fig. 1. – General layout of apparatus.

A counter telescope, set up in the position later occupied by the cloud chamber, was used to make preliminary measurements on the accelerator beam. From differential range measurements on the meson content of the beam at different momenta, the relation between the currents in $M1$ and $M2$ and the beam momentum was deduced. From the results of these preliminary measurements we also concluded that the spread in momentum at any particular momentum in the range (15÷350) MeV/c was about $\pm 3\%$, and that at a momentum of 250 MeV/c about 40% of the particles were electrons.

As reference particles, electrons in the momentum range $1.6 \leqslant p \leqslant 2.0$ MeV/c were obtained from a 25 millicurie Strontium 90 radioactive source and a small momentum-selecting magnet. A shutter was made which could open or close the source in 0.8 ms and give reproducible exposure down to 4 ms duration. This device was used to inject two pulses of electrons of duration 10 ms into the cloud chamber through a «mylar» window of thickness 2 mg/cm²: the first pulse arrived 15 ms after the expansion trigger and the second 150 ms after. The positive and the negative ions of tracks from the first pulse were separated by means of a suitably timed electric field, so that the relative condensation efficiency (*) could be determined in each expansion.

(*) The relative condensation efficiency is defined as the ratio of the number of droplets forming on the negative ion column to the number of droplets forming on the positive ion column.

2·2. *Cloud chamber and photography.* – A large cloud chamber of internal dimensions (130 × 100 × 80) cm, formerly used in cosmic-ray work, was employed with the piston in the horizontal position (Fig. 2). The chamber was filled with 99.9% pure helium and the vapour of 95% ethyl alcohol to a total pressure of 775 + 39 = 814 mm Hg when the piston was in the expanded posi-

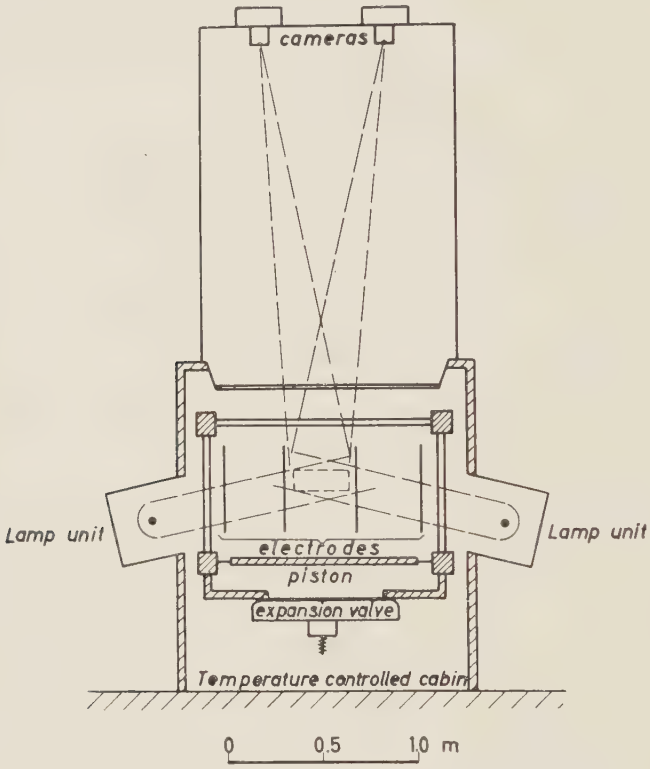

Fig. 2. – View of cloud chamber apparatus in the direction of the cyclotron beam.

tion. The chamber was operated in a thermally insulated cabin in which the air temperature was controlled to (20 ± 1.5) °C. The temperature of the cloud chamber itself was recorded continuously with a precision of 0.1 °C from thermo-couples placed on the piston and in the frame of the observation window.

An electric clearing field of 130 V per cm was applied for 130 ms preceding the expansion which lasted 50 ms. Fig. 3 shows the relative timing of the electric field, the electrons from the radioactive source, the accelerator pulses and the expansion and lamp triggers. The expansion was followed after a delay of 0.5 s by a moderately fast recompression of duration 0.8 s. The cycling time of the chamber was about 15 min and was determined primarily

by the time required for vapour lost in the fast expansion to redistribuite itself. The time required for the re-establishment of vapour equilibrium was observed by means of the thermo-couples on the piston which registered temperature changes due to alcohol evaporation from the velvet.

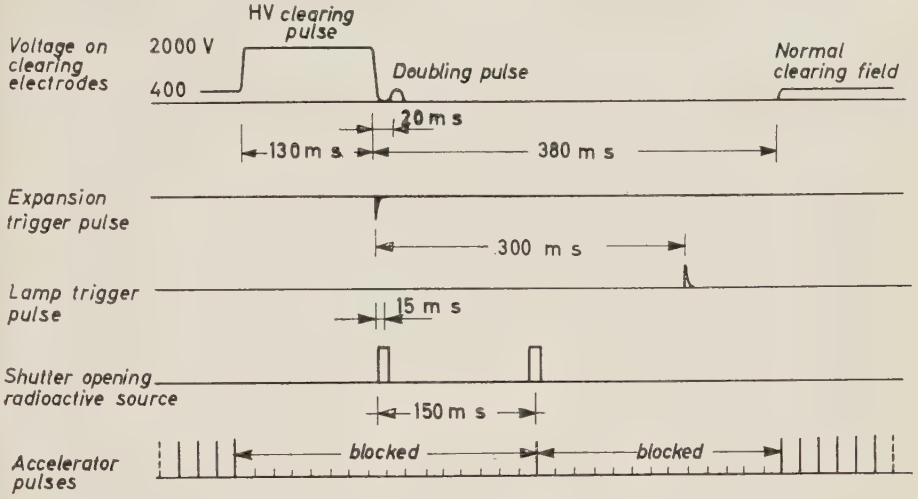

Fig. 3. – Timing diagram.

The central region of the chamber, a volume $(90 \times 30 \times 15)$ cm, was illuminated by two 4 000 joule xenon discharge lamps which directed parallel beams at 10° to the horizontal. In this way a factor of about two was gained in the light scattered by the droplets, over that scattered at the normal 90° illumination angle. The lamps were triggered 300 ms after the expansion trigger and the flash duration was about 2 ms. The illuminated region was photographed stereoscopically from a distance of 240 cm, the mean demagnification being 10 and stereo angle 14°.

With a lens aperture f:20, high contrast droplet images of diameter ~ 20 μm were obtained over a focal depth of 15 cm. Field curvature of the lenses was compensated by bending the film pressure plates ([13]). This enabled the entire illuminated volume to be in focus and greatly facilitated the subsequent measurements on the droplet images. The film used was Kodak 35 mm Plus-X, processed in developer D19B for 5 min at 18° C.

3. – Measurements.

3·1. *Selection of tracks.* – With the apparatus described, we have taken 300 photographs in 200 of which *a*) there was at least one track of an accel-

([13]) R. D. Fortune: *Thesis*, CERN (July, 1960).

erated beam particle, *b*) there was at least one track of a minimum ionizing electron and *c*) the relative condensation efficiency was in the range $0.2 < \theta < 0.6$.

The selection of these photographs was made in a preliminary scanning where beam particles and reference tracks were identified by their approximate orientation, with respect to the position of each particle source and by their multiple scattering. After the primary ionization of the tracks in these photographs had been measured and their orientation calculated from measurements on the separate stereoscopic views, a final check on their identity was made by confirming that their extrapolated directions passed through their respective source apertures, the mylar window for the radioactive source particles, and a 12×12 cm square aperture at the exit of $M2$ for the accelerator beam particles. A small number ($\sim 5\%$) of « doubtful » particles, which appeared to pass through both apertures or which passed near but did not cross either of the apertures, were excluded. After these discriminations, 296 useful tracks of high-energy particles remained, covering the momentum range (14.1÷347) MeV/c.

3·2. *Measurements on the photographs.* – The appearance of a post-expansion track is shown in the photograph, Fig. 4. The structure of the track shows that despite the fact that supersaturation was well established when the particle traversed the cloud chamber, the primary and the secondary ions, resulting from a single primary collision, were generally far enough apart to form more than one droplet. The droplet density did not therefore correspond to the specific primary ionization we wished to measure. Moreover, the droplet density would be affected by fluctuations in the relative condensation efficiency. We therefore decided to measure the distribution of gaps between the centres of successive droplet images along the track and look for the Poissonian component corresponding to the distribution of gaps between primary events, rather than try to formulate rules for the recognition of primary groups.

The measurements were made on a stereoscopic microscope which magnified the film image $40\times$. Gap measurements were made using a logarithmically spaced reticule in one of the microscope oculars. The reticule was of the same type ([14]) as that used in emulsion gap counting, the smallest interval corresponding to 60 μm on the film. To determine the track length, the microscope was equipped to make co-ordinate measurements with a precision of 1 ± 5 μm. Parts of the track in which it was impossible to measure due to a high local background (such as an old diffuse track or crossing) were omitted. The mean useful length of track thus obtained was ~ 50 cm.

([14]) C. O'Ceallaigh: *CERN*, BS-11 (1954).

Fig. 4. – Cloud chamber tracks (scale full size). On the left is a diffuse doubled track of a minimum ionizing electron from the ^{90}Sr radioactive source; on the right, a post-expansion track of an electron of energy 34.7 MeV passing through the chamber 150 ms after the expansion.

3·3. *Analysis of measurements.* – The integral distribution of gaps for 25 tracks of particles from the radioactive source is shown in Fig. 5. Apart from the first point $N_{>0}$, the points follow very well the distribution law

$$N_{>l} = N \exp[-jl]. \tag{1}$$

The deviation of the point $N_{>0}$ is attributed to the diffusion of secondary ions during the formation of the track. By comparing eq. (1) with the distribution law for gaps between randomly spaced primary events of mean density I per cm

$$n_{>l} = n \exp[-Il] \tag{2}$$

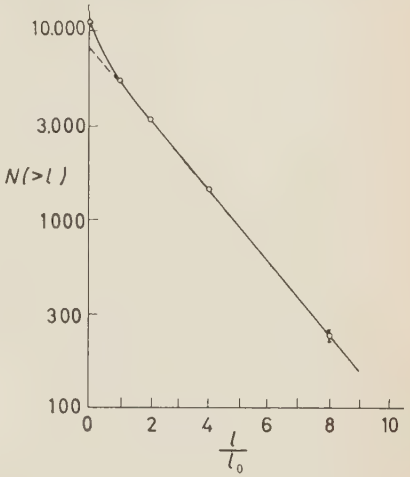

Fig. 5. – Combined integral distribution of gaps for 25 tracks of electrons from the radioactive source.

j, the slope of the experimental distribution (excluding the point $N_{>0}$) may be identified with the specific primary ionization I. The best value of j for each track and the statistical error on it, Δj, are determined by the maximum likelihood method. To determine the relative ionization of the particles from the synchro-cyclotron, the minimum ionization for each photograph is calculated by taking the weighted mean $\bar{j}_{\min}$ of the j's of electron tracks in that photograph, coming from the radioactive source. The relative ionization is then given by

$$j_{\text{rel}} = j/\bar{j}_{\min} \tag{3}$$

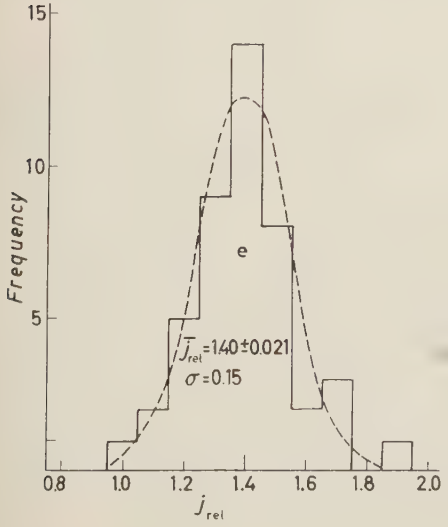

Fig. 6. – Relative primary ionization for electrons of momentum 75.2 MeV/c $(p/mc)_e = 147$.

4. – Results.

4·1. *Relative ionization of cyclotron particles.* – Fig. 6, 7 and 8 give the distributions of the relative ionization due to synchro-cyclotron particles of momentum 75, 235 and 347 MeV/c respectively.

At 75 MeV/c the distribution agrees well with tye Gaussian law and the internal and the external errors are not significantly different. This is also the case for other measurements at 14.1, 23.5 and 47.0 MeV/c. For particles

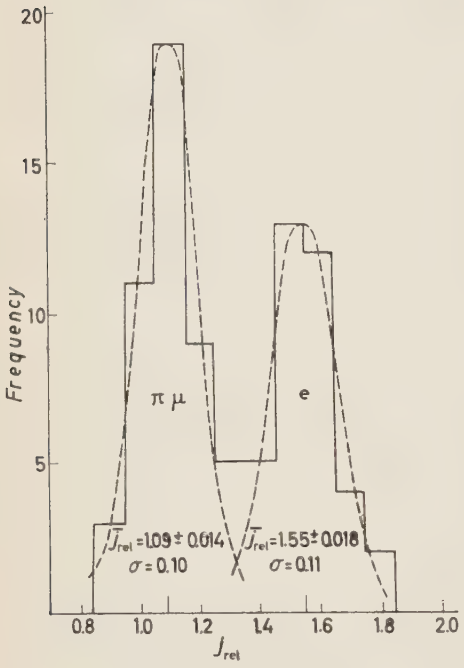

Fig. 7. – Relative primary ionization for particles of momentum 235 MeV/c $(p/mc)_{\pi\mu} = 1.81$ $(p/mc)_e = 460$.

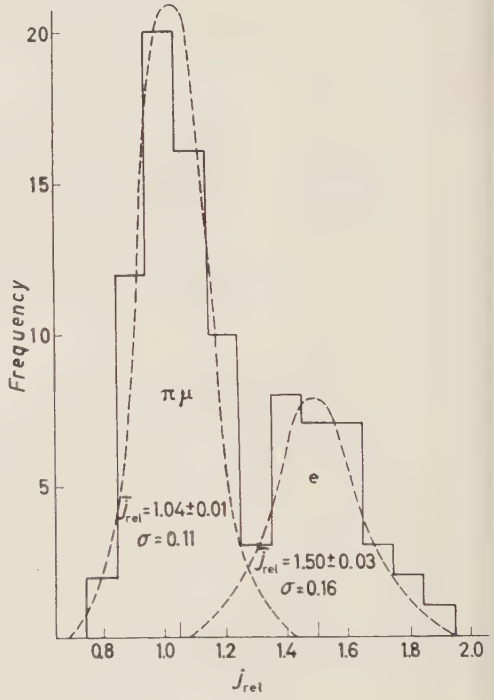

Fig. 8. – Relative primary ionization for particles of momentum 347 MeV/c $(p/mc)_{\pi\mu} = 2.67$ $(p/mc)_e = 678$.

of momentum 235 and 347 MeV/c, the distributions show two peaks, one near the minimum ionization which we have attributed to the mesons, and the other at about 1.5 times the minimum due to electrons of the same momentum. A χ^2 test applied to test the assumption that the total distribution in each case is a composition of two Gaussian distributions, indicates a very good fit ($P_{\chi^2} \sim 85\%$). The percentage of mesons in the 235 MeV/c beam, calculated from the ratio of the Gaussian surfaces, agrees well with the value found from the preliminary counter measurement (60%). This supports our assumption that the peak near minimum ionization is due to the mesons in the accelerator beam, and the second peak is due only to electrons of the same momentum. The mean relative ionization of the electrons at momenta 235 and 347 MeV/c is taken as the mode of the second Gaussian curve, and the error on the mean is calculated as the standard deviation divided by the square root of the

number of electrons. Table I gives the mean relative ionization of the electrons, the error on the mean, the number of tracks and the total track length measured at each momentum.

TABLE I.

P(MeV/c)	14.1	23.5	47.0	75.2	235	347
$\bar{j}_{rel}$	1.18	1.25	1.37	1.40	1.55	1.50
$\Delta\bar{j}_{rel}$	0.042	0.021	0.031	0.021	0.018	0.029
N	8	41	20	45	38	28
L(cm)	439	2371	1050	2428	2112	1495

4·2. *Effect of variations in condensation efficiency.* – The relative condensation efficiency at each expansion was measured by counting the density of droplets in the negative ion column (d_-) and in the positive ion column (d_+) of the field separated tracks. A correlation plot of the ratio d_-/d_+ as a function of the absolute primary ionization (j) of the tracks from the radioactive source, is shown in Fig. 9. This shows no significant correlation between these quantities.

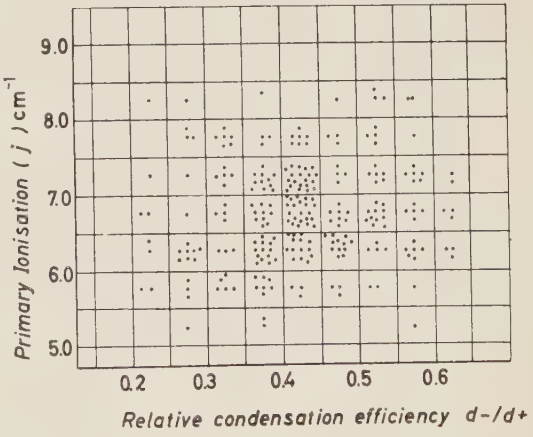

Fig. 9. – Correlation between the relative condensation efficiency in the cloud chamber and the corresponding measurements of the primary ionization (j cm^{-1}) of electrons from the radioactive source.

4·3. *Minimum ionization.* – The mean specific primary ionization of 286 electrons from the radioactive source is 6.70 per cm, the external and internal errors being 0.57 (8.5%) and 0.49 (7.3%) respectively (standard deviations). The 8.5% error includes variations in the ionization due to temperature changes during the experiment. The vapour pressure of the alcohol at 20 °C is about 40 mm Hg and changes by about 2 mm per °C change in the temperature of the liquid phase. Since the contribution of the alcohol vapour to the total

ionization is of the order of 30% ([15]), the error due to the temperature variation between 18.5 and 21.5 °C is considerable.

In order to see the effect of improving the thermal control of the cloud chamber, we have measured the absolute ionization of 65 electrons from the radioactive source, forming tracks in consecutive expansions in which the temperature of the piston was controlled to (18.8 ± 0.2) °C. Under these conditions, the external error reduces to 7.8% and the internal error is 7.3%.

5. – Discussion.

5·1. *Theory and experiment.* – The experimental points plotted as a function of p/mc are given in Fig. 10. The full line is calculated using the Budini and Taffara formula for pure helium at a pressure of 775 mm Hg and

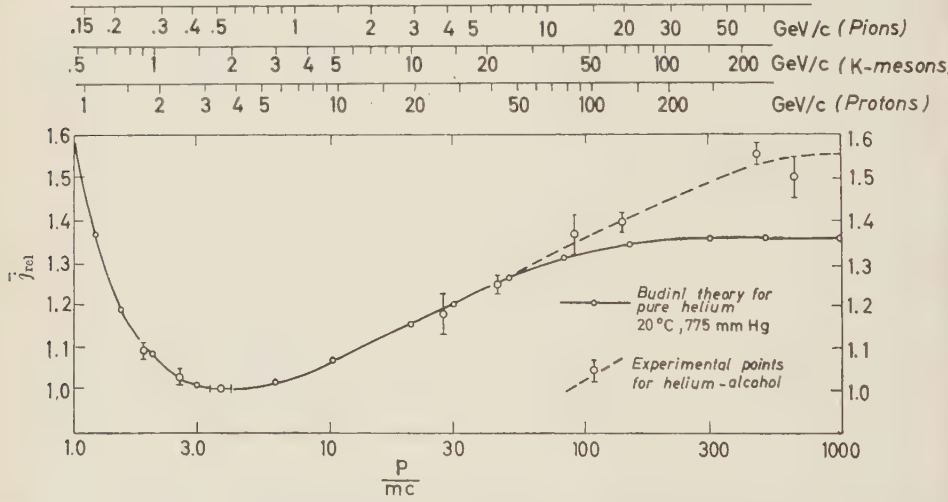

Fig. 10. – Relative primary ionization in a mixture of helium and alcohol vapour at 20 °C and total pressure 814 mm Hg.

temperature 20 °C. In making these calculations we have taken an ionization potential $I_0 = 24.59$ eV, the oscillator strengths and frequencies from LANDOLT and BÖRNSTEIN ([16]), and the photoelectric cross-sections from the experimental results of LEE and WEISSELER ([17]).

([15]) C. FROST and C. E. NIELSEN: *Phys. Rev.* **91**, 864 (1955); R. VAN DER WALLE: *Compt. Rend.*, **248**, 3292 (1959).

([16]) H. LANDOLT and R. BÖRNSTEIN: *Tables*, Vol. 1, part 1, p. 262.

([17]) P. LEE and G. L. WEISSELER: *Phys. Rev.* **99**, 540 (1955).

In comparing our experimental points with the theoretical curve, we see that there is good agreement for the meson points near minimum ionization and for the electron points up to $p/mc = 50$. The electron points for p/mc greater than 50, however, show that the extent of the logarithmic increase and the ratio of the plateau to minimum ionization are significantly greater than those given by the theory for pure helium.

After consideration of the results of the counter measurements and of the distributions of the ionization measurements, we may exclude the possibility that the divergence can be explained either by mis-identification of particles of momenta 235 and 347 MeV/c, or by errors in the fitting of the Gaussian curve (see Section 4·1.).

The divergence may perhaps be due to the influence of the alcohol vapour. The addition of vapour to the gas, however, should increase the polarization or density effect and therefore reduce the height of the primary ionization plateau relative to minimum. We conclude that if the Budini and Taffara theory gives the correct results for pure helium, processes other than a direct ionization of the helium and alcohol molecules by the primary particles, must be invoked to explain the discrepancy.

5·2. *Measurement errors.* – We have seen in Section 4·2 that the measurement of the primary ionization by the method of gap-counting, is not affected by fluctuations in the relative condensation efficiency over the range 0.2 to 0.6. Moreover, if the temperature control of the cloud chamber is sufficiently good ($\pm$ 0.1 °C), the errors in the measurements appear to be almost entirely statistical (Section 4·3). If this is so, we should be able to avoid the use of reference tracks in every expansion and thereby reduce the errors still further.

It is already possible, with the precision obtained in this experiment, to distinguish to 1.5 standard deviations individual pions and protons in a beam of well-defined momentum. By using a heavier gas and longer tracks to improve the statistics, we may obtain sufficient precision to distinguish individual protons and K-mesons.

* * *

We wish to thank Professors L. Lederman and J. A. Newth for their encouragement in the initial stages of this work; Dr. T. Fazzini for his help with the counter measurements; Dr. J. P. Astbury for his aid with the analysis, and the CERN Synchro-cyclotron group for the particle beam facilities. We record our gratitude to Mr. R. Bouchet and Mr. H. Maurer for their resource and initiative in maintaining the operation of the cloud chamber apparatus, and to Mrs. K. Erikson, Mrs. F. Verkerk and Mrs. B. Vosicki who made the microscope measurements on the photographs. We are indebted

to Professors G. BERNARDINI and P. PREISWERK and to Dr. J. P. ASTBURY for reading the manuscript and giving helpful criticism, and also to Professor L. BUDINI for most helpful discussions.

RIASSUNTO

È stata studiata, attraverso misure di lunghezza media del gap eseguite su fotografie di tracce post-espansione in camera di Wilson, la salita relativistica della ionizzazione primaria prodotta da elettroni in una miscela di elio ed alcool. I risultati ottenuti mettono in luce una salita logaritmica della ionizzazione primaria al variare di p/mc tra $p/mc \sim 5$ e $p/mc \sim 300$. Si è trovata una indicazione dell'effetto di densità per $p/mc \sim 678$; il rapporto tra la ionizzazione primaria a questo valore di p/mc e la ionizzazione primaria al minimo risulta essere 1.50 ± 0.03. L'intervallo di p/mc che caratterizza la salita relativistica ed il rapporto sopra indicato sono, in modo significativo, maggiori di quelli che si calcolano per elio puro con la teoria di Budini e Taffara. Si è visto inoltre che le misure di ionizzazione specifica primaria eseguite con il metodo del gap-counting non presentano alcuna correlazione con la variazione della efficienza di condensazione (θ) nell'intervallo $0.2 \leqslant \theta \leqslant 0.6$. Questo fatto ci permette di eseguire misure precise di ionizzazione senza dover ricorrere ad un aggiustamento critico delle condizioni di espansione della camera di Wilson.

IL NUOVO CIMENTO Vol. XIX, N. 6 16 Marzo 1961

Properties of Neutral Strange Particles Produced in a Xenon Bubble Chamber (*).

J. L. Brown (**), H. C. Bryant (***), R. A. Burnstein (*.*), D. A. Glaser (*.*), R. Hartung (†), J. A. Kadyk (**), J. D. Van Putten, D. Sinclair, G. H. Trilling (*.*) and J. C. Van der Velde

University of Michigan - Ann Arbor, Mich.

(ricevuto il 22 Novembre 1960)

Summary. — By means of direct observations of the neutral decay modes $\Lambda \to n + \pi^0$ and $K_1^0 \to \pi^0 + \pi^0$ of Λ's and K^0's produced in a 21 liter liquid xenon bubble chamber exposed to 1.0 GeV and 1.1 GeV π^- beams at the Bevatron, we measured the branching ratios

$$B_\Lambda \equiv \frac{(\Lambda \to \pi^0 + n)}{(\Lambda \to \pi^0 + n) + (\Lambda \to \pi^- + p)} = 0.35 \pm 0.05 ,$$

$$B_K \equiv \frac{(K_1^0 \to \pi^0 + \pi^0)}{(K_1^0 \to \pi^0 + \pi^0) + (K_1^0 \to \pi^- + \pi^+)} = 0.30 \pm 0.035 ,$$

in agreement with predictions of the $|\Delta I| = \frac{1}{2}$ rule. The fraction of all K^0's which did not decay into $\pi^+ + \pi^-$ or $\pi^0 + \pi^0$ in a time of the order of 10^{-10} s is $X_K = 0.47 \pm 0.03$, as expected from the particle mixture description of the K^0. Λ's produced in xenon exhibit an « up-down » asymmetry associated with a polarization of the Λ normal to the production plane, although this polarization is not as great as that observed for Λ's produced by similar beams in hydrogen. No significant forward-backward decay asymmetry of the Λ with respect to its own line of flight is found. Strange particle production cross-sections in xenon are reported.

(*) Work supported in part by United States Atomic Energy Commission.

(**) Now at Lawrence Radiation Laboratory, Berkeley, Cal.
(***) Now at University of New Mexico, Albuquerque, New Mex.
(*.*) Now at University of Maryland, College Park, Md.
(*.*) Now at University of California, Berkeley, Cal.
(†) Now at University of Wisconsin, Madison, Wis.

1. – Introduction.

Most experimental studies of the production and decay of strange particles in bubble chambers and nuclear emulsions depend on the observation of tracks of charged particles, since γ-rays, neutral pions, and neutrons are not detected efficiently by the usual techniques. Decays involving uncharged products must be studied indirectly by assuming that a momentum and energy imbalance among the charged products is due to neutral products or that totally unseen decays occur according to decay schemes expected on theoretical grounds. In the case of the neutral decays $\Lambda \to n + \pi^0$ and $K_1^0 \to \pi^0 + \pi^0$, nearly all the information concerning the rates of the decays is deduced from the apparent « disappearance » of Λ's and K^0's, which are expected to be produced if these strange particles are always made in associated pairs. Direct observation of these modes is desirable to find out if they are indeed the correct decay schemes of the usually unseen Λ's and K^0's, if their rates account for the « missing » decays, and if the branching ratios between neutral and charged modes agree with the predictions of the $|\Delta \boldsymbol{I}| = \frac{1}{2}$ rule and the particle mixture description of the K^0. Measurement of the asymmetry of the Λ-decay in its neutral mode is also interesting, although excellent results of a counter experiment on this asymmetry have already been reported [1].

In order to make these observations of neutral Λ and K^0-decay modes, we have constructed and operated a bubble chamber filled with liquid xenon because this liquid has a density of 2.2 g/cm^3 and a radiation length of 3.9 cm. In the present experiment, the average detection efficiency for γ-rays is 70%. Preliminary results from 160 000 pictures taken with this chamber exposed to 1.0 GeV and 1.1 GeV π^- beams at the Berkeley Bevatron have already been presented [2]; here we report the final results together with a brief description of how they were obtained.

The chamber and experimental beam arrangement are described in Section **2**; the data reduction system is outlined briefly in Section **3**. Results concerning branching ratios of the Λ and K^0, decay asymmetries of the Λ, and production cross-sections are given in detail in Section **4**. Our conclusions are summarized in Section **5**.

(1) R. L. COOL, B. CORK, J. W. CRONIN and W. A. WENZEL: *Phys. Rev.*, **114**, 912 (1959).

(2) J. L. BROWN, H. C. BRYANT, R. A. BURNSTEIN, R. W. HARTUNG, D. A. GLASER, J. A. KADYK, D. SINCLAIR, G. H. TRILLING, J. C. VANDER VELDE and J. D. VAN PUTTEN *Phys. Rev. Lett.*, **3**, 51, 563 (1959).

2. – Experimental apparatus.

2·1. *Bubble chamber.* – The sensitive volume of the xenon chamber (see Fig. 1) used in this experiment was a cylinder with its axis horizontal, 30 cm in diameter, 25 cm in depth, and with a volume of 21 liters. The chamber body, machined from an aluminum forging, had two vertical windows made

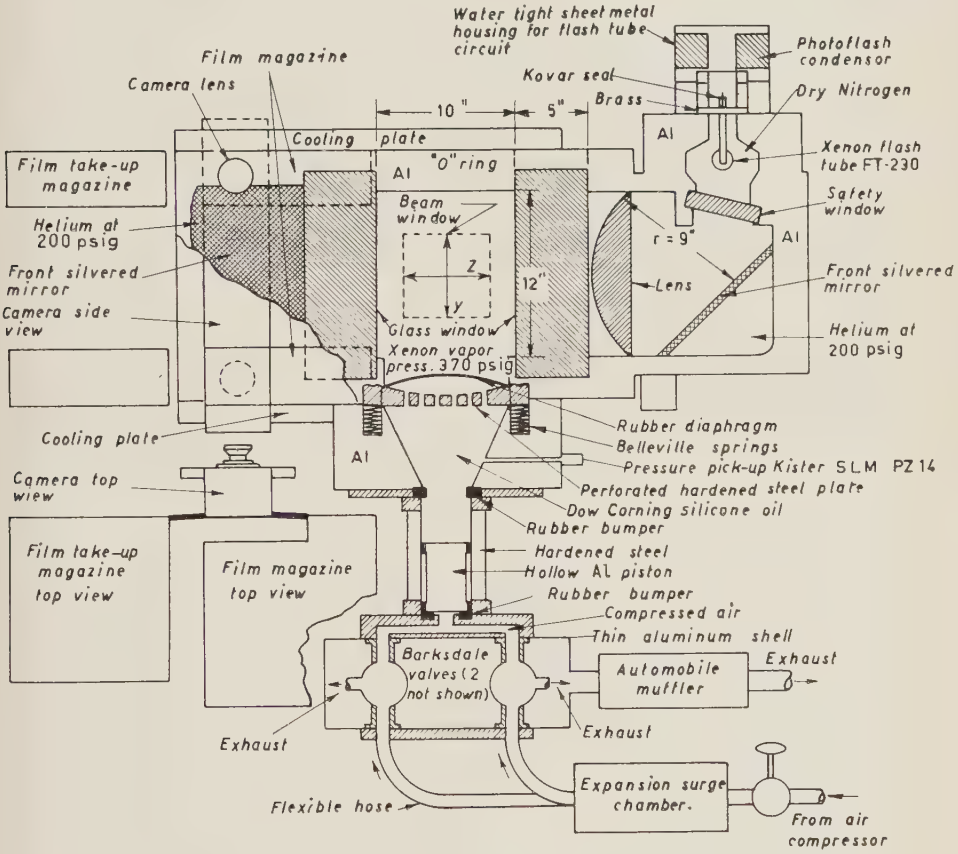

Fig. 1. – Schematic drawing of xenon chamber.

of 5 in. thick glass. These windows were completely enclosed with metal shields, which were filled with helium gas at 200 psig. The pressurized shields served to reduce the stress on the windows; they also prevented the escape of the xenon and provided a protection from flying glass in case of a window failure. The optical system viewed the chamber through mirrors and small shatter-proof peepholes in the metal shields.

The chamber was cooled to its operating temperature of — 21.5 °C by

means of liquid (50% ethylene glycol, 50% water) circulated around the chamber body and window shields at a rate of roughly 18 gallons/minute. This liquid was cooled by a commercial refrigerating unit with 9 kW of cooling capacity. The temperature was regulated to ± 0.1 °C by means of electronically controlled heaters in the liquid flow line.

The expansion system was coupled to the liquid xenon through a three-ply nylon-reinforced circular rubber diaphragm 9 in. in diameter. The diaphragm, supported by a perforated metal back plate, was actuated by low viscosity silicone oil, which in turn was actuated by a 4 in.-diameter piston driven by compressed air. The compressed air was controlled by four $\frac{3}{4}$ in. Barksdale valves. The expansion system had the property, characteristic of the rest of the chamber design, that the liquid xenon was isolated from the atmosphere by two independent seals. With the expansion system described above, expansion and recompression times of 15 ms and sensitive times of 5 ms were obtained.

The optical system used dark field illumination. Light from a single FT-230 flash lamp was focussed into a parallel beam by a single large condensing lens. Two camera lenses (Schneider Super-Angulon, 65 mm focal length, $f/45$) were placed just outside this parallel beam of light to produce a stereo angle of 35°. The images, demagnified by a factor of 7, were recorded on 70 mm Linagraph Pan film.

As discovered previously ([3]), it was necessary to add a small amount of contaminant to the xenon before it would function satisfactorily as a bubble chamber liquid; in our case 0.5% of ethylene by weight was added. This mixture operated at a temperature of -21.5 °C with a vapor pressure of 370 psig and a liquid density of 2.2 g/cm^3. The radiation length ([4]) was 3.9 cm; because of this short radiation length, multiple Coulomb scattering was relatively large. Consequently, the present chamber does not have a magnetic field, since a field of the order of 125 000 gauss is needed to permit momentum measurements with useful accuracy.

2·2. *Experimental arrangement.* – The high energy π^- beam used in this experiment was an extension of the beam used in a counter experiment by COOL *et al.* ([1]). The beam emerging from their hydrogen target was refocussed by a quadrupole triplet and bent through a sweeping magnet into a bubble chamber. In operation almost all of the Bevatron circulating beam struck an internal target over an extended period of about 50 ms and was used in the counter experiment. After the counter « spill » was over, the chamber was expanded and the remainder ($\sim 10^{-4}$) of the original beam was thrown

([3]) J. L. BROWN, D. A. GLASER and M. L. PERL: *Phys. Rev.*, **102**, 586 (1956).
([4]) B. ROSSI: *High Energy Particles* (New York, 1952), p. 50.

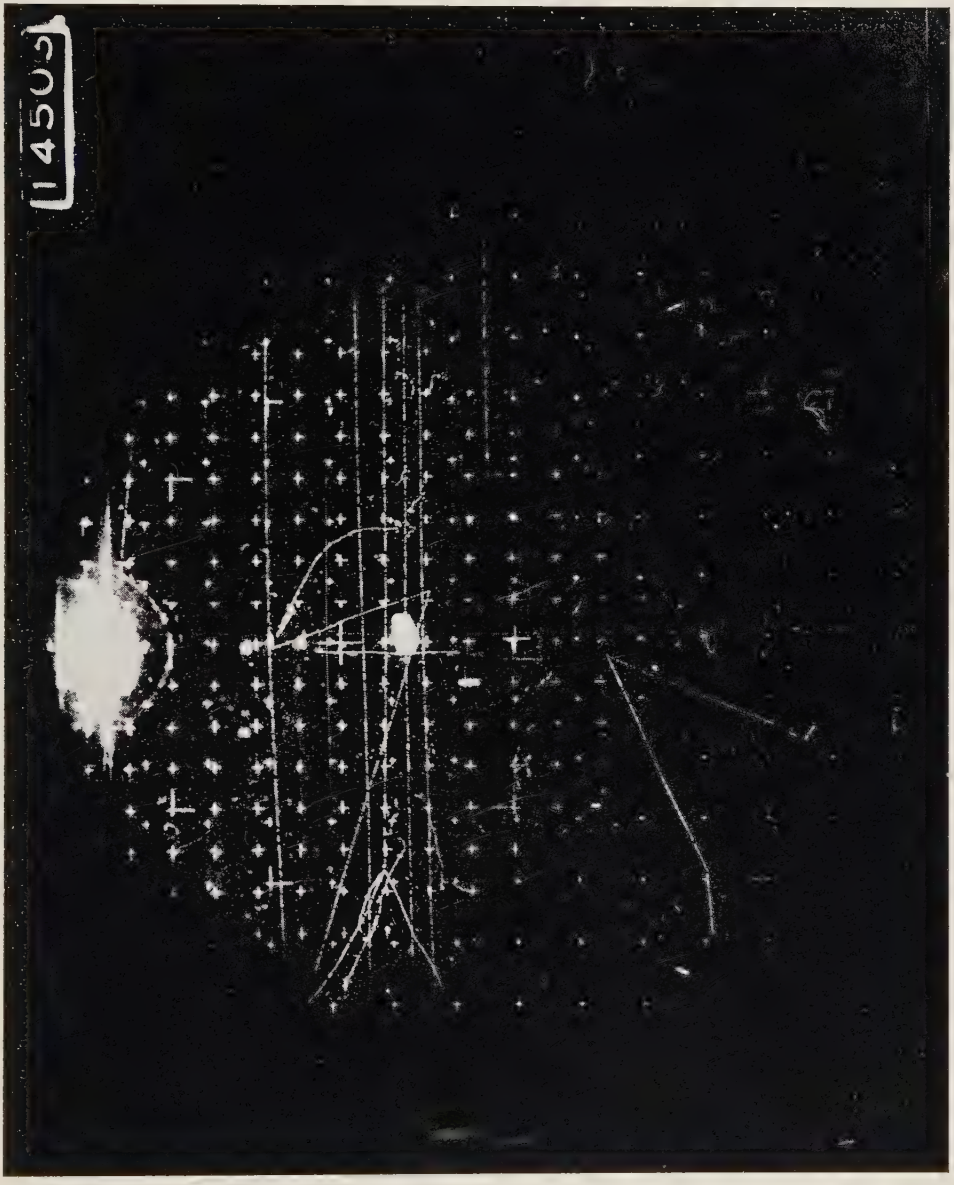

Fig. 2. – Example of $\pi^- + Xe \to \Lambda_- + K_1^{\pm}$.

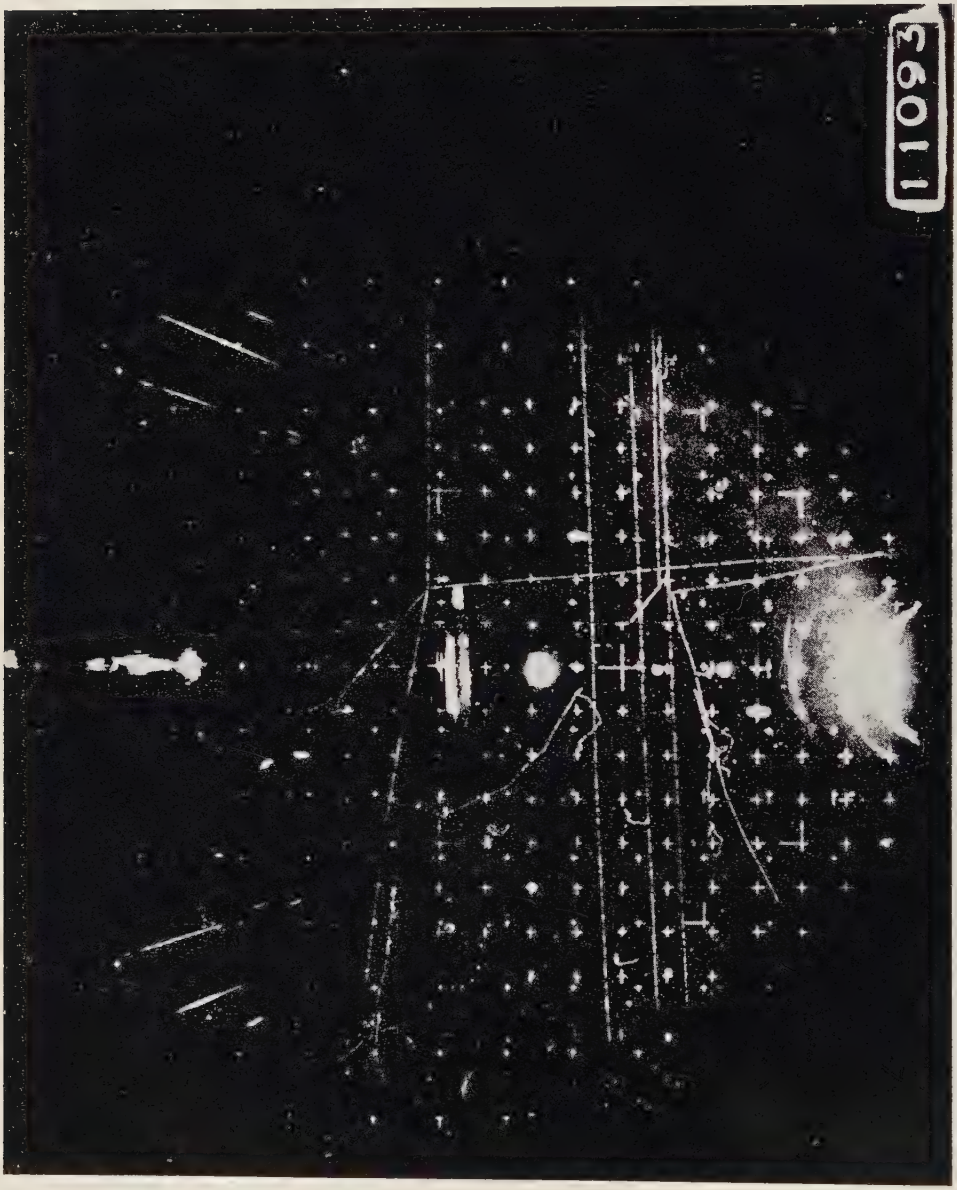

Fig. 3. — Example of $\pi^- + Xe \to \Lambda + K^+$; both γ-rays convert.

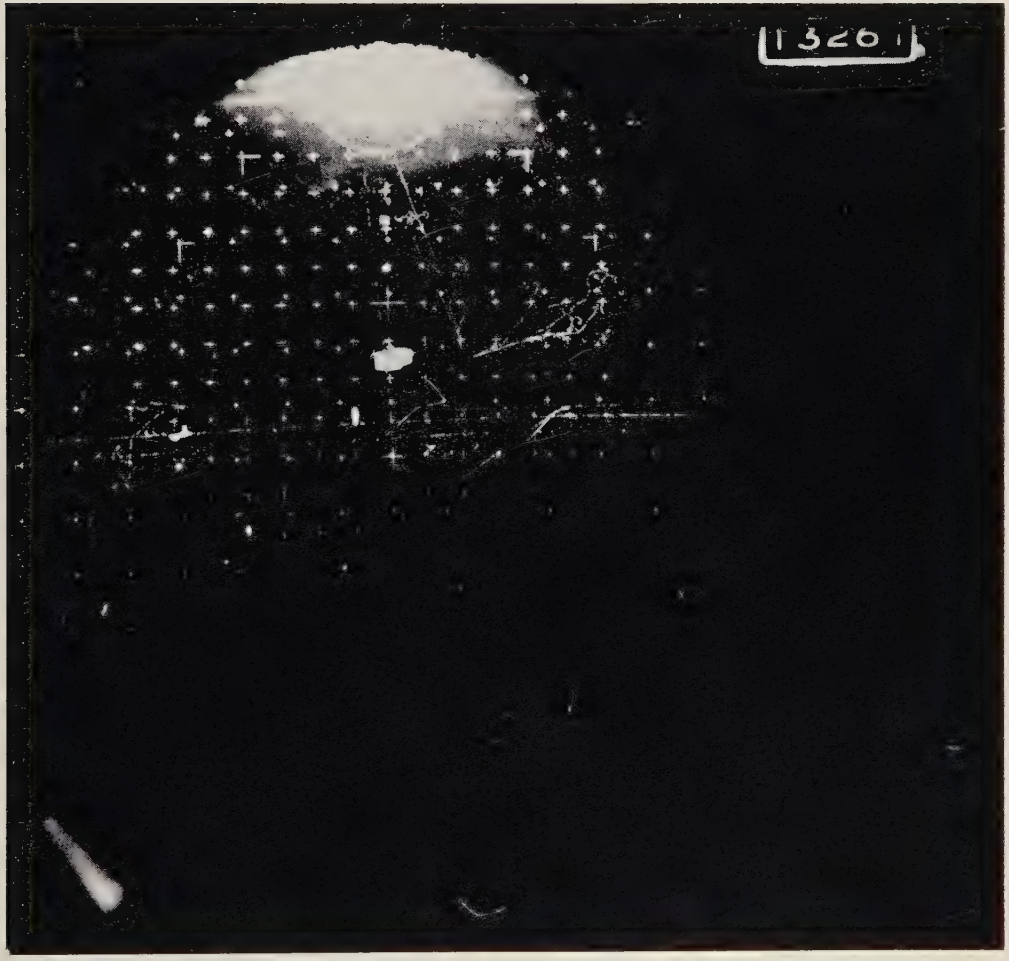

Fig. 4. – Example of $\pi^- + Xe \to \Lambda + K_1^0$; three of the four γ-rays convert.

onto the internal target using the rapid beam ejector. Because of the low circulating beam intensity when the chamber was sensitive, elaborate shielding precautions did not have to be taken.

3. – Data reduction.

Of the 160 000 pictures taken in this experiment, half were taken at a nominal beam energy of 1.0 GeV, and half at a nominal beam energy of 1.1 GeV. The two halves of the experiment were processed in slightly different ways, experience from the first (lower energy) half being used to expedite analysis of the second half.

3·1. *Processing of the first half of the data.* – The pictures (see Fig. 2-4 for examples) were scanned by physicists on projectors which simultaneously provided life-size images of each of the two stereo views on an opaque white screen. These two images could be moved with respect to each other so that various grid marks on one view could be brought into coincidence with the corresponding ones on the other view. This procedure permitted rough depth measurements in the course of the scan, which aided in the interpretation of the events. Any example of a possible strange particle with or without a visible point of production was recorded. Only events in which one or more V^0 decays occurred were processed further.

Measurement was performed on projectors with translucent screens; magnifications of approximately $1\times$ and $3\times$ life size were available, the higher magnification being used for the actual settings. Co-ordinate measurements were recorded automatically on IBM cards; auxiliary information such as frame number was entered manually. Computations were performed initially on an IBM 650, and later on an IBM 704. Calculations made included:

a) Real-space co-ordinates of measured points,

b) Direction cosines of tracks,

c) Angles between relevant tracks, planes, etc., and

d) Expected errors in *c*) due to errors in *a*).

With the output listed above, various kinematic hypotheses were tested with the aid of appropriate graphs. Auxiliary quantities such as momentum and center-of-mass decay angle were also determined from prepared graphs. Once an event was identified, the picture was rescanned to check the plausibility of the assignment, and to search for any associated strange particles missed in the first scan. On the basis of first scan, second scan, and analysis records, the events were subjected to various criteria for use in the various samples, as described in more detail in Section **4**.

3·2. *Processing of the second half of the data.* – Technicians scanned the second half of the pictures, using more rigid criteria. These had the effect of removing many of the background events, while including essentially all the real events. K_1 events without an accompanying Λ_0 or Λ_- decay (*) were omitted. Measurement, analysis, an rescan were performed by physicists. Criteria for various samples were simplified to save processing time.

4. – Results.

4·1. *Branching ratios of the various* Λ *and* K^0 *decay modes.*

4·1.1. Theoretical predictions. – The Λ is known to decay via the mode

$$\Lambda \to \pi^- + p \equiv \Lambda_- \,. \tag{4.1}$$

It has been assumed that the Λ also has another two-body decay mode:

$$\Lambda \to \pi^0 + n \equiv \Lambda_0 \,. \tag{4.2}$$

If one also assumes that the total isotopic spin in the decay of the Λ changes by $\frac{1}{2}$ only ($|\Delta \boldsymbol{I}| = \frac{1}{2}$), then one can predict the branching ratio

$$B_\Lambda = \frac{N(\Lambda_0)}{N(\Lambda_0) + N(\Lambda_-)} = \frac{1}{3} \,, \tag{4.3}$$

neglecting small corrections such as phase space differences. One can further define another quantity:

$$X_\Lambda = 1 - \frac{N(\Lambda_0) + N(\Lambda_-)}{N(\text{all } \Lambda)} \,; \tag{4.4}$$

X_Λ will be greater than zero if there exist Λ-decay modes other than (4.1) and (4.2), *e.g.* β-decay, or if hyperfragments are formed.

The decay of the K^0 can be described by similar parameters, although the

(*) We use the following notation for the various decay modes:

Λ_-: $\Lambda \to \pi^- + p$, $\qquad$ $K_{1\pm}$: $K_1 \to \pi^+ + \pi^-$,

Λ_0: $\Lambda \to \pi^0 + n$, $\qquad$ K_{1^0}: $K_1 \to \pi^0 + \pi^0$.

We will also use the notation $N(\Lambda_-)$, for example, to stand for the number of events decaying via the Λ_- mode.

theory used to predict these parameters is more involved. To simplify the discussion we assume the rigorous validity of time reversal invariance in K^0-decay. Then the proper states for description of K^0 (and $\bar{K}^0$) decay are the eigenstates of the CP operator (C = charge conjugation operator, P= parity operator) denoted by K_1^0 and K_2^0, and the following holds:

$$X_K = 1 - \frac{N(K_1^0)}{N\,(\text{all } K^0)} = \frac{1}{2}. \tag{4.5}$$

The K_1^0 state with eigenvalue $CP = +1$ will consist almost entirely of decay into two pions:

$$K_1^0 \to \pi^+ + \pi^- \equiv K_{1\pm}^0\,, \tag{4.6}$$

$$K_1^0 \to \pi^0 + \pi^0 \equiv K_{1^0}^0\,, \tag{4.7}$$

with other modes much less probable.

It has been pointed out by Lee, Oehme, and Yang [5] and by Weinberg [6] that even without the assumption of time reversal invariance, the known large ratio of K_2^0 to K_1^0 lifetimes and the absence of 2π decay modes in K_2^0 decay imply that the previous predictions are essentially unaltered.

Making the same $|\Delta I| = \frac{1}{2}$ assumption as we did for Λ decay, one can predict (neglecting small corrections),

$$B_K = \frac{N(K_{1^0}^0)}{N(K_{1^0}^0) + N(K_{1\pm}^0)} = \frac{1}{3}. \tag{4.8}$$

This assumption prohibits the decay

$$K^+ \to \pi^+ + \pi^0\,, \tag{4.9}$$

which, although known to be inhibited by a factor of about 500 in relation to the K_1^0 decay modes, is not completely forbidden. Electromagnetic corrections to $|\Delta I| = \frac{1}{2}$ calculations will permit (4.9) to occur, but at a rate which is probably $\sim 10^{-2}$ too small [7]. Reaction (4.9) will also be permitted theoretically if the strict $|\Delta I| = \frac{1}{2}$ rule is relaxed, and $|\Delta I| = \frac{3}{2}$ and $\frac{5}{2}$ transitions are permitted.

If one admits enough $|\Delta I| = \frac{3}{2}$ transition (and no $|\Delta I| = \frac{5}{2}$) to account for the observed rate of (4.9), one predicts a range of allowed values for B_K

$$0.28 < B_K < 0.38\,. \tag{4.10}$$

---

[5] T. D. Lee, R. Oehme and C. N. Yang: *Phys. Rev.*, **106**, 340 (1957).
[6] S. Weinberg: *Phys. Rev.*, **110**, 782 (1957).
[7] R. H. Dalitz: *Proc. Phys. Soc.*, A **69**, 527 (1956).

4·1.2. Results. – Events for calculation of the various branching ratios were chosen by the « signature » method [8]. Roughly speaking, Λ_0 and Λ_- events used in calculating B_Λ and X_Λ were required to be accompanied by an easily recognized $K_{1^\pm}$ decay. Under these conditions it was felt that the detection efficiency for Λ_- and Λ_0 decays would be high (since only those pictures with a $K_{1^\pm}$ decay had to be studied carefully) and relatively unbiased (since the detection efficiency of the $K_{1^\pm}$ was largely independent of the decay mode of the Λ). Specific criteria, listed in the Appendix, were applied to insure that the sample of Λ decays used contained no biases whose effects could not be calculated. These criteria rejected about half the events found on the initial scan. In an analogous way, K_{1^0} and $K_{1^\pm}$ events used in calculating B_K and X_K were required to be accompanied by an easily scanned Λ_- decay.

Once a Λ signature, say, was found, the picture was carefully scanned for any evidence of either a Λ_0 or Λ_- decay. An event was assumed to be a Λ_- if it satisfied certain kinematic criteria (*) (*e.g.* coplanarity of Λ_- decay plane with origin of signature). It was assumed to be a Λ_0 if there were two γ-ray pairs whose lines of flight intersected at a point inside the chamber where there was no visible interaction. Similar rules were used to define K^0 signatures and to identify K_1 events. A K_{1^0} event was defined as the intersection of the lines of flight of 2, 3, or 4 γ-ray pairs in association with a K^0 signature. The experimentally observed numbers of events are listed in Table I. Corrections to these numbers must be made to take account of the fact that some γ's do not convert inside the chamber, some decays take place outside the allowed fiducial volume, and finally, that some biases are introduced by the selection criteria. The last two of these corrections were made by using the observed momentum and angular distributions of the strange particles and their known life-times. The γ-ray conversion probabilities were computed by a Monte Carlo calculation in which the observed energy and angular distributions of the charged decay modes of Λ and K^0 were used to calculate the corresponding distributions for the γ-rays. From these and from the calculated pair production mean free paths, the conversion efficiencies were determined. All corrections are listed in Table I. Using the corrected numer of events, we find

$$X_\Lambda = 0.13 \pm 0.07 \text{ (**)} \qquad X_K = 0.47 \pm 0.03$$

$$B_\Lambda = 0.35 \pm 0.05 \qquad B_K = 0.30 \pm 0.035 .$$

(8) F. Eisler, R. Plano, N. Samios, M. Schwartz and J. Steinberger: *Nuovo Cimento*, **5**, 1700 (1957).

(*) Specific criteria are listed in the Appendix.

(**) Using only events from the first half of the experiment.

The values of $B_\Lambda B_K$, and X_K are in good agreement with theoretical predictions. The value of X_Λ, which does not differ significantly from zero, does not preclude the formation of a small percentage of hyperfragments.

TABLE I*a*. – Λ *decays*.

Uncorrected $N(\Lambda_-)$	96
1) Correction factor for decays too close to origin	1.21 ± 0.01
2) Correction factor for cut-off on length of Λ_- secondaries	1.07 ± 0.01
3) Correction factor for relative scanning efficiencies of Λ_- and Λ_0 modes	0.96 ± 0.07
Corrected $N(\Lambda_-)$ (error includes uncertainties in corrections and statistical error due to number of events)	119.6 ±15.1
Uncorrected $N(\Lambda_0)$	35
1) Correction factor for γ's escaping from chamber	2.02 ± 0.04
2) Correction factor for cases in which one of the two observed electron pairs is from a $\Sigma^0 \to \Lambda + \gamma$ decay	0.93 ± 0.04
3) Background correction factor	0.99 ± 0.01
Corrected $N(\Lambda_0)$	65.1 ±11.4

TABLE I*b*. – K^0 *decays*.

	First half	Second half
Uncorrected $N(K_{1\pm})$	69	51
Correction factor for decays outside fiducial volume or too close to origin (*)	1.00	1.20±0.04
Corrected $N(K_{1\pm})$	69 ±8.3	61.2 ±8.8
Uncorrected $N(K_{1^0})$	21	28
Correction factor for failure to convert 2, 3, or 4 γ's inside fiducial volume (*)	1.09±0.05	1.20±0.05
Corrected $N(K_{1^0})$	22.9 ±5.1	33.6 ±6.5

(*) The numbers relevant to the first and second halves of the experiment are given in this table because somewhat different criteria were used in the selection of the samples. These differences in criteria are reflected in differences in the correction factors for the two halves of the experiment.

4·2. *Identification of neutral decay modes.* – In addition to calculating the branching ratios mentioned above, we can use our data to verify the existence

of the decay modes:

$$\Lambda \to \pi^0 + \mathrm{n}$$

$$\mathrm{K}_1^0 \to \pi^0 + \pi^0 .$$

Previous evidence for these modes has been rather indirect ([8,9]).

4·2.1. Decay length distribution. – The Λ_0 and K_{1^0} modes must have the same lifetime and momentum distribution as their charged decay mode counterparts. Hence the average distance travelled before decay, $\bar{L}$, must be the same for the Λ_- (or K_{1^+}) as for the Λ_0 (or K_{1^0}) after corrections for biases. The experimental numbers are

$$(4.11) \qquad \begin{cases} \bar{L}(\Lambda_-) = 3.09 \pm 0.30 \text{ cm} , \\ \bar{L}(\Lambda_0) = 2.39 \pm 0.51 \text{ cm} , \\ \bar{L}(\mathrm{K}_{1^\pm}) = 1.70 \pm 0.22 \text{ cm} , \\ \bar{L}(\mathrm{K}_{1^0}) = 2.25 \pm 0.34 \text{ cm} . \end{cases}$$

These numbers are to be compared with an average potential path of about 13 cm. If the events we identify as Λ_0 and K_{1^0} decays were accidental coincidences of background γ-ray pairs, one might expect $\bar{L}$ for these decays to be around half the average potential path, *i.e.* about 6 cm, rather than the experimentally observed 2-3 cm.

4·2.2. Kinematic checks. – As has been mentioned, a Λ event is presumed to have occurred when, in the presence of a Λ signature, two γ-ray pairs are seen which could have come from a common point inside the chamber. If these two γ-rays are assumed to have come from the following sequence:

$$\Lambda_0 \to \mathrm{X}^0 + \mathrm{n} ,$$

$$\mathrm{X}^0 \to 2\gamma ,$$

one can estimate, statistically, the mass of X^0 from knowledge of the γ-ray directions and the Λ momentum distribution. When this is done, one finds

$$(4.12) \qquad m(\mathrm{X}^0) = (127 \pm 6) \text{ MeV} ,$$

to be compared with $m(\pi^0) = 135$ MeV.

(9) S. L. Ridgway, D. Berley and G. B. Collins: *Phys. Rev.*, **104**, 513 (1956).

4·2.3. Background checks. – There exists a third way of demonstrating that few events were incorrectly identified as Λ_0 or K_{1^0} decays. Spurious Λ_0 and K_{1^0} events arise from the intersection of γ-rays not produced by a strange particle decay associated with a particular signature. The rate of finding such spurious events can be estimated by observing the number of 2, 3, or 4 γ events occurring in pictures with a $\Lambda_- - K_{1^\pm}$ event, where it is known that such γ event must be spurious in the sense defined above. In 120 $\Lambda_- - K_{1^\pm}$ events, one such spurious 2γ event was found (which could have been interpreted as an example of $\pi^- + p \to \Lambda_- + K^0_{1^\pm} + \pi^0$).

4·3. *Asymmetry parameters in Λ-decay.* – As is well known now, parity is not conserved in the reaction $\Lambda_- \to \pi^- + p$ ([10,11]). One manifestation of this is the distribution of the π^- directions in the Λ center of mass system, given by

$$W(\theta)d\cos\theta = \tfrac{1}{2}[1 + \alpha_- \overline{P}\cos\theta]d(\cos\theta)\,, \tag{4.13}$$

where θ is the angle between the π^- momentum vector and some direction $\hat{n}$ with respect to which the average Λ polarization $\overline{P}$ is measured. α_- is a parameter which measures the degree of parity non-conservation and is known to be greater than 0.73 ± 0.14 ([12]).

It is of some interest to known whether the decay asymmetry is still present when Λ's are produced in complex nuclei. Previous results ([13]) have not, in general, indicated such an asymmetry. Using 221 events in which the Λ_- was associated with a $K_{1^\pm}$ decay (*i.e.* « double V's »), we found

$$\alpha_- \overline{P} = +\,0.32 \pm 0.11\,. \tag{4.14}$$

The direction of Λ polarization, $\hat{n}$, was chosen to be

$$\hat{n} = \frac{\boldsymbol{P}_{\text{beam}} \times \boldsymbol{P}_\Lambda}{|\boldsymbol{P}_{\text{beam}} \times \boldsymbol{P}_\Lambda|}\,. \tag{4.15}$$

([10]) F. S. Crawford jr., M. Cresti, M. L. Good, K. Gottstein, E. M. Lyman, F. T. Solmitz, M. L. Stevenson and H. K. Ticho: *Phys. Rev.*, **108**, 1102 (1957).

([11]) F. Eisler, R. Plano, A. Prodell, N. Samios, M. Schwartz, J. Steinberger, P. Bassi, V. Borelli, G. Puppi, G. Tanaka, P. Waloschek, V. Zoboli, M. Conversi, P. Franzini, I. Mannelli, R. Santangelo, V. Silvestrini, D. A. Glaser, C. Graves and M. L. Perl: *Phys. Rev.*, **108**, 1353 (1957).

([12]) F. S. Crawford, jr., M. Cresti, M. L. Good, K. Gottstein, E. M. Lyman, F. T. Solmitz, M. L. Stevenson and H. K. Ticho: 1958 *Annual International Conference on High Energy Physics at CERN* (Geneva, 1958), p. 323.

([13]) T. Bowen, J. Hardy, jr., G. T. Reynolds, C. R. Sun, G. Tagliaferri, A. E. Werbuck and W. H. Moore: *Phys. Rev.*, **119**, 2030 (1960).

The same calculation applied to 233 Λ_- events *not* accompanied by a visible K_1 decay gave the result

$$\alpha_- \overline{P} = + 0.05 \pm 0.11 . \tag{4.16}$$

On the hypothesis that (4.14) and (4.16) represent really different numbers, the two samples were investigated to see where such a difference could have arisen. No biases, calculational errors, or differences in production mechanisms could be found which would explain the discrepancy. If, on the other hand, one accepts the hypothesis that the two results are statistical fluctuations from an average value, then this average value is

$$\alpha_- \overline{P} = 0.18 \pm 0.08 . \tag{4.17}$$

The chance of getting two measurements (4.14) and (4.16) differing this much or more from the mean (4.17) is about 8%.

Presumably a distribution of the form (4.13) holds true for the decay $\Lambda \to \pi^0 + n$ also, except that the previous asymmetry parameter α_- should be replaced by α_0. The $|\Delta \boldsymbol{I}| = \frac{1}{2}$ rule predicts $\alpha_- = \alpha_0$. The average polarization, $\overline{P}$, is expected to be the same. An experimental difficulty in determining α_0 is that the direction of the π^0 in the Λ center of mass cannot be measured, *i.e.* θ cannot be determined. One can show, however, that $\alpha_0 \overline{P}$ can be determined from the distribution in the Λ center of mass of the bisector of the angle between the two γ-rays, and that the answer is very insensitive to the momentum assumed for the Λ. Using this method on 71 events, one finds

$$\alpha_0 \overline{P} = + 0.37 \pm 0.28 . \tag{4.18}$$

4·4. *Production cross-sections.* – Reactions involving strange particles which were observed and for which cross-sections were calculated in this experiment included

$$\begin{aligned} \pi^- + \mathrm{Xe} &\to \Lambda + \mathrm{K}^0 \\ &\to \Sigma^0 + \mathrm{K}^0 \\ &\to \Sigma^- + \mathrm{K}^0 \\ &\to \Lambda + \mathrm{K}^+ \ (*). \end{aligned}$$

Because xenon is a complex nucleus, Fermi momentum and secondary inter-

(*) This last reaction can result only from two or more successive reactions in the same nucleus.

actions make difficult the interpretation of the basic production reactions. Cross-sections for the various observed reactions can still be computed, however; results are listed in Table II. The nominal beam energies are reduced slightly to allow for energy loss in the xenon.

TABLE II. – *Production cross-sections.*

Reaction products	π^- interaction energy (*)	
	0.96 GeV	1.05 GeV
$\Lambda + K^0$	7.0 ± 1.0 mb/nucleus	13.0 ± 2.0
$\Lambda + K^+$	1.4 ± 0.3	2.0 ± 0.5
$\Sigma^- + K^{-0}$	0.2 ± 0.1	not measured
$\Sigma^0 + K^0$	0.7 ± 0.4	0.9 ± 0.4

(*) These are nominal beam energies corrected for ionization loss to the center of the chamber,

4·5. *Forward-backward ratio in Λ-decay.* – The Λ-decay asymmetry discussed in Section **4·3** was measured by assuming the Λ polarization to be perpendicular to the production plane (the plane containing $\boldsymbol{P}_{\text{beam}}$ and $\boldsymbol{P}_\Lambda$); indeed, this must be the direction of the Λ polarization if parity is conserved in the Λ production reaction. If, however, parity is not conserved in the strong interaction producting the Λ, then the Λ can have a net polarization *in* the production plane. This could be exhibited experimentally by a fore-aft asymmetry, in the Λ center of mass, of the decay proton with respect to the Λ momentum. Various indications of this have been reported in the past [14]. Unlike the usual « up-down » asymmetry, detection of a forward-backward asymmetry is beset with experimental biases. Specifically, in the present experiment, there are strong biases against seeing Λ_- decays whose center of mass decay angles are near 0° and 180°, these biases not necessarily being equal. These two regions correspond to low pion and proton laboratory energies with correspondingly short ranges. To avoid these biases as much as possible, we have used only those Λ_-'s accompanied by a Λ signature (see Appendix). Taking the 94 events in the above category and making a small correction for the remaining bias, we find the fraction, f, of protons going forward in the Λ center of mass to be

$$f = 0.57 \pm 0.05 .$$

In view of the fact that our bias corrections may have been underestimated, we consider that this result is completely consistent with $\frac{1}{2}$, the value expected if parity is conserved in the Λ production reaction. It should be noted that

what little asymmetry the above result seems to suggest is in the opposite direction from that reported in other experiments ([14]). However, in all the experiments, including this one, the asymmetries are in the directions expected if the biases have been somewhat underestimated. We thus conclude that we have no evidence for any fore-aft asymmetry in Λ_- decay.

5. – Conclusions.

By directly observing (via γ-ray pairs) the neutral decay modes of the Λ and K^0, we are able to verify the predictions of the $|\Delta I| = \frac{1}{2}$ rule for the branching ratios of Λ and K^0 decays. Our value of α_0/α_- for Λ decay, while of little statistical weight compared to the result of reference ([4]), is also consistent with the value predicted by the $|\Delta I| = \frac{1}{2}$ rule. The direct observation of both the charged and neutral decay modes of the K_1 enables us to verify the prediction of the K_1-K_2 particle mixture theory for X_K, the fraction of all K^0's decaying via the K_2 mode.

We have measured the total cross-sections for various strange-particle-producing reactions in xenon. These numbers, when compared with corresponding numbers for free nucleon targets, show the effect of various secondary interactions. Λ_-'s produced in xenon by $(1.0 \div 1.1)$ GeV negative pions seem to show a net polarization perpendicular to the production plane, as evidenced by « up-down » decay asymmetries. We find no significant evidence for longitudinal Λ polarization in the production plane.

Appendix

Event criteria (*).

1. *General criteria.*

Any event used must be on a picture of acceptable photographic quality with fewer than 16 beam tracks and low background.

2. *Criteria for events used in Λ branching ratios.*

A) The Λ signature. – A « Λ signature » consists of a beam π interaction (or « origin ») and a *V*-shaped track which is kinematically consistent

([14]) R. A. Salmeron and A. Zichichi: *Nuovo Cimento*, **11**, 461 (1959).

(*) These criteria strictly apply only to the second half of the experiment; slightly different rules were applied to events in the first half.

with being a decay ($K_{1\pm} \to \pi^+ + \pi^-$) of a K^0 produced at the beam interaction and which satisfies the following:

1) There must be no prongs from the origin which either decay or leave the chamber (this eliminates Σ^--K^0 events).

2) The flight path of the *V* must be $\geqslant 0.5$ cm (this eliminates « close » $K_{1\pm}$'s which are hard to see and interpret).

3) The apex of the *V* must lie in a fiducial volume whose boundaries are 2 cm inside the front and back windows and 4 cm inside the walls of the chamber.

4) The *V* must be coplanar with the origin within 5°.

B) Λ_- events. – 1) A second *V*-shaped track must be associated with the Λ signature.

2) This *V* must be kinematically consistent with a decay ($\Lambda \to p + \pi^-$) of a Λ produced at the same beam interaction.

3) The flight path of the *V* must be $\geqslant 0.5$ cm;

4) The apex of the *V* must lie inside the fiducial volume described in 2-*A*-3

5) Each leg of the *V* must be more than 2 mm long.

C) Λ_0 events. – 1) Associated with the Λ signature there must be two γ-ray pairs whose lines of flight intersect within measuring error.

2) The pairs must not appear to come from a beam interaction except that their intersection point may be close to the origin of the $K_{1\pm}$.

3) There must be at least 3 cm of ionizing track length in each pair (this energy cut-off has a negligible effect on the Λ_0 detection efficiency).

4) The apexes of the pairs must lie inside the fiducial volume described in 2-*A*-3.

3. *Criteria for events used in* K^0 *branching ratios.*

A) The K^0 signature. – A « K^0 signature » consists of a beam interaction and a *V*-shaped track which is kinematically consistent with being a decay ($\Lambda \to p + \pi^-$) of a Λ produced at the beam interaction and which satisfies the following:

1) There must be no prongs from the origin which either decay or leave the chamber (this eliminates Λ-K^+ events).

2) The flight path of the *V* must be $\geqslant 0.5$ cm (this eliminates « close » Λ_-'s which are hard to see and interpret).

3) The apex of the *V* must lie in a fiducial volume whose boundaries are 2 cm inside the front and back windows and 4 cm inside the walls of the chamber.

4) The *V* must be coplanar with the origin.

5) Both secondary legs of the *V* must be longer than 0.5 cm, and one must be longer than 2.0 cm (this eliminates unidentifiable events and insures high scanning efficiency for K^0 signatures independent of the K_1 decay mode).

B) $K_{1^{\pm}}$ events. – 1) A second *V*-shaped track must be associated with the K^0 signature.

2) This *V* must be kinematically consistent with a decay ($K^0 \to \pi^+ + \pi^-$) of a K^0 produced at the same beam interaction.

3) The flight path of the *V* must be greater than 0.2 cm.

4) The apex of the *V* must lie inside the fiducial volume described in 2-*A*-3.

C) K_{1^0} events. – 1) Associated with the K^0 signature there must be 2, 3, or 4 γ-ray pairs whose lines of flight intersect inside the fiducial volume of 2-*A*-3 within measuring error.

2) The apexes of the pairs must lie inside the fiducial volume of 2-*A*-3.

3) There must be at least two of the γ-ray pairs which could not have come from an interaction inside the chamber except possibly the Λ origin.

RIASSUNTO (*)

Per mezzo della osservazione diretta dei processi neutri di decadimento $\Lambda \to n + \pi^0$ e $K_1^0 \to \pi^0 + \pi^0$ dei Λ e K^0 prodotti in una camera a bolle a xenon da 21 litri esposta ai fasci di π^- da 1.0 ed 1.1 GeV del bevatrone, abbiamo misurato i rapporti di branching

$$B_\Lambda \equiv \frac{(\Lambda \to \pi^0 + n)}{(\Lambda \to \pi^0 + n) + (\Lambda \to \pi^- + p)} = 0.35 \pm 0.05 ,$$

$$B_K \equiv \frac{(K_1^0 \to \pi^0 + \pi^0)}{(K_1^0 \to \pi^0 + \pi^0) + (K_1^0 \to \pi^- + \pi^+)} = 0.30 \pm 0.035 ,$$

che sono in accordo con le predizioni della legge $|\Delta \boldsymbol{I}| = \frac{1}{2}$. La frazione di K^0 che non decadono in $\pi^+ + \pi^-$ oppure $\pi^0 + \pi^0$ in un intervallo dell'ordine di 10^{-10} s è $X_K = 0.47 \pm 0.03$ quale ci si attende dalla descrizione della miscela di particelle del K^0. I Λ prodotti nello xenon presentano una asimmetria alto-basso associata ad una polarizzazione normale al piano di produzione, per quanto questa polarizzazione non sia elevata come quella osservata in Λ prodotti da fasci analoghi nell'idrogeno. Non si riscontra alcuna significativa asimmetria di decadimento avanti-indietro del Λ rispetto alla sua propria traiettoria. Si riportano le sezioni trasversali per la produzione di particelle strane.

(*) *Traduzione a cura della Redazione.*

IL NUOVO CIMENTO Vol. XIX, N. 6 16 Marzo 1961

Interactions of 1.15 GeV/c K^--Mesons in Emulsion – II.

A. Marzari Chiesa, B. Quassiati and G. Rinaudo

Istituto Nazionale di Fisica Nucleare - Torino

(ricevuto il 23 Novembre 1960)

Summary. — In the present paper we report some results on the interactions of high energy K^--mesons in emulsion. The results concern the energy spectrum and angular distribution of the re-emitted K^-, the π-meson production, the mean life time of $\Sigma^\pm$, Σ^+ and Σ^- hyperons, the nuclear scatterings of $\Sigma^\pm$ and the up-down asymmetry in the decay of the Σ^+ hyperon.

1. – Introduction.

In Part I of this work (1) some results were given on the interactions of 1.15 GeV/c K^--mesons in emulsion. The analysis was made on 1675 stars found by area and track scanning. In particular the emission of charged hyperons, their energy spectrum and angular distribution, the ratio Σ^- emitted/Σ^+ emitted and the probability of K^- inelastic re-emission have been studied.

In the present paper we give further results concerning the life-time and the nuclear scattering of Σ-hyperons, the re-emission and the energy spectrum of K^--mesons and the production of π-mesons.

An attempt was made in order to find the Ξ^--hyperon. In addition to the 1675 stars that have been completely analysed, we have followed from 1270 other stars the tracks with $\beta \leqslant 0.7$ emitted within an angle of 45° around the K^- direction. This work has been done in order to check the reaction:

(1) C. M. Garelli, B. Quassiati and M. Vigone: *Nuovo Cimento*, **17**, 786 (1960).

$K^- + \mathcal{N} \to \Xi^- + K^0$, in fact the maximum emission angle of the Ξ^--hyperon in the laboratory system is about 45° (*).

When possible, the data of these 1270 stars were added to the previous ones in order to improve the statistics.

2. – Identification of K^--mesons and $\pi^\pm$-mesons.

The work was performed on 1506 stars found by area scanning. In these stars all the tracks were followed until they decay or interact, come to rest or leave the stack. The identification of the tracks up to a $\beta \leqslant 0.7$ is always sure. The results concerning the π and K^--mesons emitted with $\beta \leqslant 0.7$ are the following:

28 K^--mesons

125 π^--mesons

31 π^+-mesons

5 $\pi^\pm$-mesons

The tracks with $\beta > 0.7$ consist of π and K^--mesons, since the contamination of fast protons in negligible.

In order to distinguish the π-mesons from the K^--mesons, ionization and scattering measurements were performed on the tracks with a range per plate ~ 3 mm. The $p\beta$ value was determined by the second and third differences and a general agreement between these values was found. In few cases showing a discrepancy probably due to distortion in the plate, the $p\beta$ value derived from the third differences was taken. As it is shown in Fig. 1 the identifi-

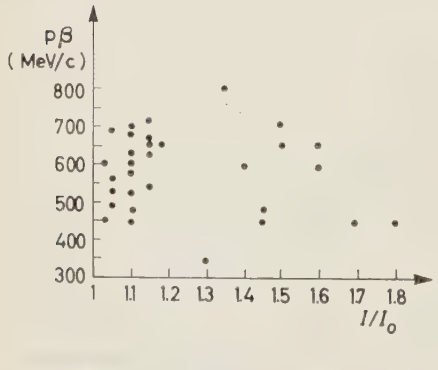

Fig. 1. – Plot of the $p\beta$ values *vs.* ionization for the measured tracks of $p\beta > 300$ MeV/c.

(*) No sure example of Ξ hyperon was found but in 8 cases out of 2945 stars it was not possible to distinguish between Σ^- and Ξ^--decays. The value of the cross section for Ξ^- production by K^- given by ALVAREZ (2) is 0.02 mb per nucleon: according to this figure the number of Ξ^--hyperons produced in the 2945 interactions studied by us in the emulsion would be of the order of one or two, so that our result is not inconsistent with the very low value of the cross-section for Ξ^- production.

(2) C. W. ALVAREZ: *Report at the Kiev high Energy Nuclear Physics Conference* (1959).

cation of pions and K⁻-mesons was possible also at high energies. The statistical error is of 10% in the determination the $p\beta$ value and 8% in the ionization value. The ionization measurements have been made on several plates.

The informations obtained from this sample of relativistic tracks are biased by the limitations on the dip angle imposed by measurements, since the number and the energy of pions and K⁻-mesons are a function of the emission angle.

To test this dependence we have plotted the energy *vs.* the emission angle for the K⁻-mesons and pions separately, as it is shown in Fig. 2 and 3.

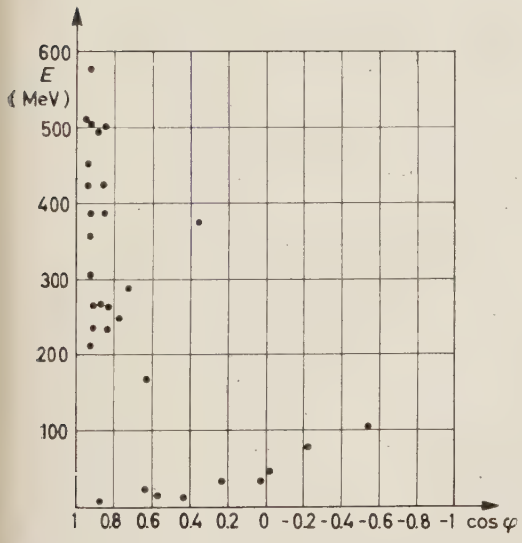

Fig. 2. – Plot of the energy *vs.* cos φ for K⁻-mesons.

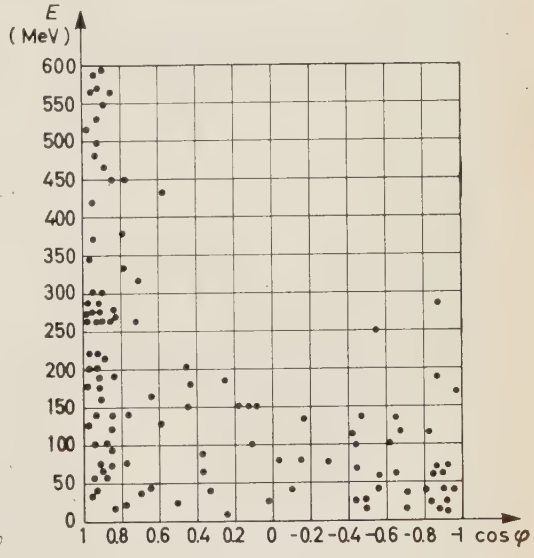

Fig. 3. – Plot of the energy *vs.* cos φ for $\pi^{\pm}$-mesons.

In order to obtain an energy spectrum and an angular distribution not affected by a geometrical loss, we have calculated the fraction of particles emitted in an angle between φ_0 and $\varphi_0 + \mathrm{d}\varphi$ with the primary direction, which has a range per plate $\geqslant 3$ mm.

This fraction ω is determined by the ratio:

$$\omega = \frac{4 \int_{79^\circ}^{90^\circ} \sin i \, \mathrm{d}i \int_{\arccos(\cos\varphi_0/\sin i)}^{\arccos(\cos(\varphi_0+\mathrm{d}\varphi)/\sin i)} \mathrm{d}\vartheta}{2\pi \int_{\varphi_0}^{\varphi_0+\mathrm{d}\varphi} \sin\varphi \, \mathrm{d}\varphi},$$

where ϑ is the projected angle and $((\pi/2) - i)$ is the dip angle. The values

of the correction factor $1/\omega$ calculated for $\cos\varphi$ intervals $= 0.2$ ($\varphi =$ emission angle) are given in Table I.

TABLE I.

$\cos\varphi_1 \div \cos\varphi_2$	$0.98 \div 0.8$ $-0.8 \div -0.98$	$0.8 \div 0.6$ $-0.6 \div -0.8$	$0.6 \div 0.4$ $-0.4 \div -0.6$	$0.4 \div 0.2$ $-0.2 \div -0.4$	$0.2 \div 0$ $0 \div -0.2$
$1/\omega$	3.5	6.3	7.7	8.6	8.9

The plots of Fig. 2 and Fig. 3 have been separated in intervals of 100 and 50 MeV respectively.

In each energy interval the number of particles has been multiplied, according to the emission angle, by the relative correction factor $1/\omega$ given in Table I.

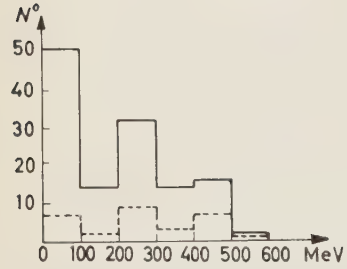

Fig. 4. The dashed line histogram refers to the energy distribution of K^--mesons with a range per plate ≥ 3 mm; the full line to the corrected one.

In Fig. 4 and 5 the energy spectra for the K^--mesons and pions are shown. As one can see, the modification due to the geometrical correction is very important.

To test the reliability of this correction method we have compared the experimental angular distribution of all tracks with the calculated one. The calculated distribution was obtained by adding the plots 2 and 3, and by multiplying the number of particles falling in each interval of $\cos\varphi$ by the relative correction factor. To give the experimental distribution we measured the emission angle of π-mesons and K^--mesons with $\beta < 0.7$ and of all relativistic tracks, even if their identification was not possible. The agreement between these two distributions is quite satisfactory, as it is shown in Fig. 6.

Another test of the validity of this correction is obtained by looking at the pions energy distribution in the low energy region. In fact, up to $\beta = 0.7$ all π-mesons could be identified; we know therefore the true ex-

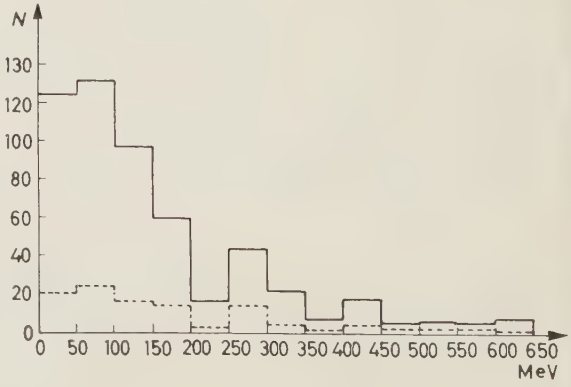

Fig. 5.

perimental number of π-mesons having energy $\leqslant 55$ MeV which is found to be 126 (only stars with one pion were considered). This number agrees quite well with the value of 130 deduced from the method of geometrical correction used above.

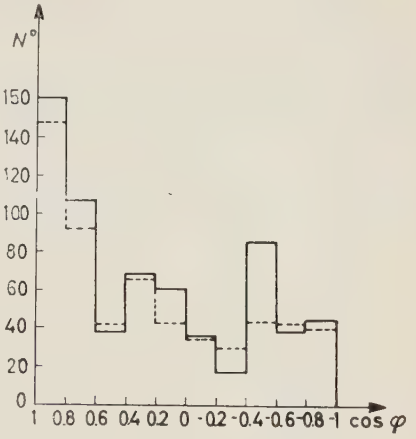

Fig. 6. – The full line histogram refers to the angular distribution of π-mesons and K⁻-mesons deduced by the geometrical corrections. The dashed line histogram gives the experimental distribution.

3. – K⁻ inelastic re-emission.

The number of K⁻ re-emitted derived by the method developed in Section 2 is 130 ± 40. If we take into account that in our beam 10% of the star-producing particles are π⁻-mesons, the number of K⁻-mesons re-emitted corresponds to a re-emission of $(11.5 \pm 3)\%$, where the error is statistical. The energy spectrum shown in Fig. 4 seems to indicate a large amount of cases in the low energy region. This effect may be partly due to large statistical fluctuations and partly to bias of the area scanning method; in fact the events in which the K⁻-mesons are re-emitted without a large energy loss and nucleus excitation have been probably missed. The value of re-emission given above is then an underestimated one.

An alternative evaluation of K⁻ re-emission can be derived by the following considerations, similar to those made in Section 8 of the previous work (Part I).

The tracks of the particles of 2 776 stars, emitted with $\beta > 0.7$ have been followed only if they have an angle $\leqslant 45°$ with the primary direction. The number of tracks thus selected is 380; the total track length followed is 3 320 cm. A total number of 118 secondary interactions has been found and 7 of these have been certainly recognized as K⁻ interactions producing $\Sigma^{\pm}$-hyperons. If we assume the cross-section for interactions of π-mesons and K⁻-mesons to be nearly equal in the energy interval considered, and the probability for the K⁻-mesons to produce a star from which a recognized Σ-hyperon is emitted, to be $\sim 10\%$, we can estimate that 70 of the secondary interactions observed are due to K⁻-mesons and the remaining 48 to π-mesons.

This means that in the considered cone of 45° around the primary direction there are 225 K⁻ from 2 770 stars (10% of which are produced by π⁻-mesons).

If we assume that the angular distribution of K^- re-emitted in the C.M. system is isotropic, one can see that the number of particles which in the laboratory system fall in a cone of 45° around the primary direction, corresponds to 45% of the total number. It follows that the K^- inelastic re-emission occurs in hte $(20 \pm 7)\%$ of the cases.

The angular distribution of K^--mesons deduced from the plot of Fig. 2 with the method explained in Section 2, of correcting for geometrical loss, is shown in Fig. 7.

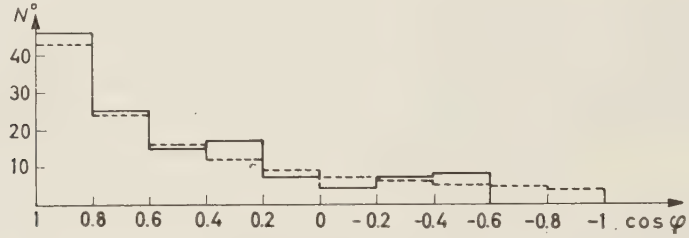

Fig. 7. – The dashed line histogram shows the angular distribution of K^--mesons expected in the laboratory system if the K^--mesons are produced isotropically in the C.M. system. The full line histogram shows the experimental distribution.

It seems to correspond rather well to an isotropic distribution in the C.M. system, but we cannot rely upon such an agreement because of the too big statistical fluctuations, and of the above mentioned observational loss of K^- in the forward direction.

On the other hand, the distribution expected in the laboratory system if the K^--mesons are produced isotropically in the C.M. system is calculated under the hypothesis of a reaction $K^- + \mathcal{N} \to K^- + \mathcal{N}$ without K^- scattering inside the nucleus and without associated pion production. This further hypothesis is in disagreement with the fact that in $(16 \pm 7)\%$ of the cases we observe a K^--meson emitted from the nucleus with a charged pion. This percentage of 16%, furthermore, can rise to much higher values if one takes into account the absorption of π-mesons inside the nucleus and the fact that the neutral pions are not detectable.

4. – Pion production.

An attempt was made in order to give an evaluation of the π-meson absorption in the nucleus. This value can be derived from the ratio

$$\frac{\Sigma^+ \text{ alone}}{\Sigma^+ + \pi^-} = \frac{20}{33},$$

that corresponds to an absorption of $(60^{+30}_{-20})\%$. This result is in agreement with that found by several authors ([3-6]).

The total number of $\pi^{\pm}$ emitted from the analysed stars is 730, 530 in stars with only one visible pion and the others in 100 stars with two pions. The cases where the star had two unmeasurable prongs of $\beta > 0.7$ were assumed to be cases of two pions production, the K^- re-emission with one pion production being very unimportant. Taking into account an absorption of 50%, we found that the number of $\pi^{\pm}$ produced is 1260. If the ratio of π^0 prod./$\pi^{\pm}$ prod. is $\frac{1}{2}$ (according to charge independence), the total number of neutral and charged pions raises to 1890. In the hypothesis that the K^- re-emission occurs with π production only in 16% of the cases, the number of pions per star is 1890/1397 = 1.35. Thus the double pion production results to about 35%.

Such a high value of the double pion production does not allow any conclusion on the energy spectrum shown in Fig. 5, because the large amount in the low energy region can be due either to inelastic scatterings in the nucleus or to double pion production.

In Table II the ratio π^-/π^+ as a function of the energy is given. Only the cases of stars with one visible pion have been considered.

TABLE II.

E	$(0 \div 55)$ MeV	> 55 MeV
π^-/π^+	$4.6^{+2.1}_{-1.2}$	$2.6^{+3.4}_{-1.3}$

Although there is a large contamination from double pion production and large statistical fluctuations, our results indicate that the π^-/π^+ ratio decreases with increasing energy, as found by other authors ([4-6]).

5. – Lifetime of Σ hyperons.

In the course of this work a total number of 192 $\Sigma^{\pm}$ hyperon decays in flight and at rest were observed. Between them, we have identified:

45 $\Sigma^- \to \pi^-$ in flight

23 $\Sigma^+ \to \pi^+$ in flight and at rest.

([3]) C. DILWORTH: *Report on the Seventh Annual Rochester Conference* (1957).

([4]) Y. EISEMBERG, W. KOCH, E. LORHMANN, M. NIKOLIĆ, M. SCHNEEBERGER and H. WINZELER: *Nuovo Cimento*, **9**, 745 (1958).

([5]) Y. EISEMBERG, W. KOCH, M. NIKOLIĆ, M. SCHNEEBERGER and H. WINZELER: *Nuovo Cimento*, **11**, 351 (1959).

([6]) S. C. FREDEN, F. C. GILBERT and R. S. WHITE: *Phys. Rev.*, **118**, 564 (1960).

Following the Bartlett's method (7), in order to estimate the mean lifetime τ of the Σ-hyperon from the decays in flight, we have plotted, *vs.* $1/\tau$, the function $S(\tau)$ given by the expression

$$S(\tau) = \frac{\sum_{i=1}^{n}\left(\frac{t_i}{\tau} - 1 + \frac{T_i}{\tau}\frac{\exp[-T_i/\tau]}{1-\exp[-T_i/\tau]}\right)}{\left[\sum_{i=1}^{n}\left(1-\left(\frac{T_i}{\tau}\right)^2\frac{\exp[-T_i/\tau]}{(1-\exp[-T_i/\tau])^2}\right)\right]^{\frac{1}{2}}},$$

where: t_i is the time of flight of the i-th particle before decay and T_i is the total time available for the i-th particle for decaying within the emulsion.

For the best estimate of the Σ-hyperon lifetime from decays in flight and at rest we have followed the modified Bartlett's method given by CASTAGNOLI *et al.* (8). In this case the $S(\tau)$ function becomes:

$$S(\tau) = \frac{\sum_{i=1}^{n_a}\frac{t_i^0}{\tau} + \sum_{k=1}^{n_b}\left(\frac{t_k}{\tau}-1\right) + \sum_{l=1}^{n_c}\left(\frac{t_l}{\tau}-1+\frac{T_l/\tau}{\exp[T_l/\tau]-1}\right)}{\left\{n_b + \sum_{l=1}^{n_c}\left[1-\left(\frac{T}{\tau}\right)^2\frac{\exp[-T_l/\tau]}{(1-\exp[-T/\tau])^2}\right]\right\}^{\frac{1}{2}}},$$

where: n_a is the number of particles which are brought to rest in emulsion and then decay and t_i^0 is their time of flight;

n_b is the number of particles which decay in flight when they have such a small velocity that they would have been brought to rest in the emulsion;

t_k is their time of flight before decay;

n_c is the number of particles which decay in flight and are not included in n_b; t_l is their time of flight before decay and T_l is the time for which the l-th particle would have travelled in the emulsion had it not decayed.

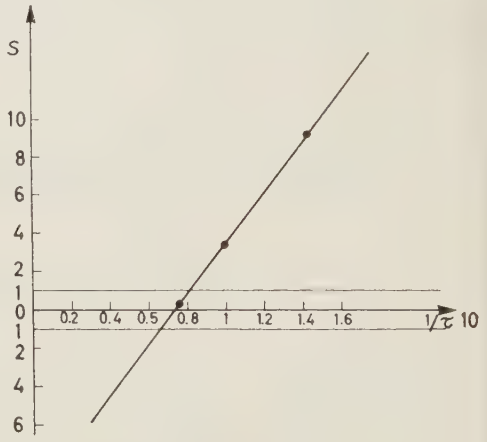

Fig. 8. – Plot of $S(\tau)$ for $\Sigma^{\pm} \to \pi^{\pm} + n$ decays in flight.

(7) M. S. BARTLETT: *Phil. Mag.*, **44**, 249 (1953).

(8) C. CASTAGNOLI, G. CORTINI and C. FRANZINETTI: *Nuovo Cimento*, **12**, 297 (1954).

The best estimate of τ is the value which makes $S(\tau)=0$ and the standard deviation is given by the variance ± 1 of $S(\tau)$. In Fig. 8 and 9 the plots of $S(\tau)$ *vs.* $1/\tau$ for each sample of Σ-hyperons are shown and the results are given in Table III.

TABLE III.

Type of event	$\Sigma^{\pm}\to\pi^{\pm}$ in flight	$\Sigma^-\to\pi^-$ in flight	$\Sigma^+\to\pi^+$ in flight	$\Sigma^+\to\pi^+$ in flight and at rest
Observed number of decays	189	45	20	23
Meanlife. 10^{10}	$1.35^{+0.14}_{-0.13}$	$1.35^{+0.32}_{-0.17}$	$0.81^{+0.32}_{-0.17}$	$0.76^{+0.22}_{-0.14}$

The β value of the Σ-hyperons was determined by careful ionization measurements and was checked by the decay kinematics. All the secondary π-mesons were followed in order to establish a better value of their energy and, when possible, their charge. In this manner the contaminations in the decays in flight from the decays at rest and from the scatterings are negligible.

We did not consider the mean lifetime value of Σ^+ derived from $\Sigma^+\to p+\pi^0$ because our sample is very biased by the loss of the decays in flight.

As it appears in Table III, the mean life of the Σ^--hyperon can be considered to be almost double of that of the Σ^+, and there is no indication for an anomalous behaviour in the $\Sigma^{\pm}$-decay in flight processes. The high value of $\Sigma^{\pm}$ lifetime is probably due to the high percentage of Σ^- with respect to Σ^+ as already indicated in Part I of this work ([1]). These results agree very well with the data of the bubble chamber ([9-11]);

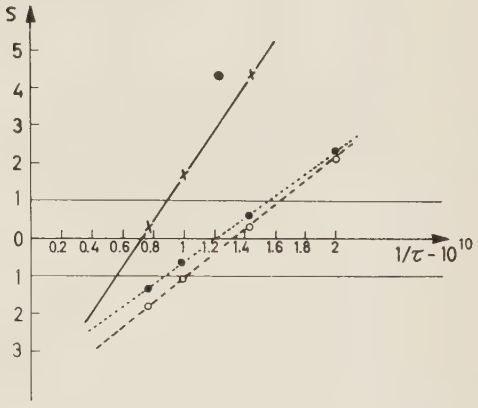

Fig. 9. – The full line represents the plot of $S(\tau)$ for $\Sigma^-\to\pi^-+n$ decays in flight; the dotted line for $\Sigma^+\to\pi^++n$ decays in flight and the dashed line for $\Sigma^+\to\pi^++n$ decays in flight and at rest.

([9]) CERN Conference of high energy nuclear physics (Geneva, 1958).

([10]) D. A. GLASER: *Report on Strange Particle Decays at the Kiev high Energy Nuclear Physics Conference* (1959).

([11]) F. EISLER, R. PLANO, A. PRODELL, N. SAMIOS, M. SCHWARTZ, J. STEINBERGER, P. BASSI, N. BORELLI, G. PUPPI, A. TANAKA, P. WALOSCHEK, N. ZOBOLI, M. CONVERSI, P. FRANZINI, I. MANNELLI, R. SANTANGELO, N. SILVESTRINI: *Nevis Report* 69 (1958).

on the contrary the mean life of Σ^--hyperon is higher than the value found by several authors in nuclear emulsions ([9-12]).

6. – Nuclear scattering of $\Sigma^\pm$ hyperons.

We have followed 323.7 cm of $\Sigma^\pm$-hyperon tracks looking for single scatterings. We have considered Σ^+-hyperon paths in the energy range $(50 \div 450)$MeV and we have excluded the tracks with a dip $\geqslant 50°$. During the course of the scanning all scatterings with a projected angle $\geqslant 2°$ in the emulsion plane were recorded and their spatial angles were then measured.

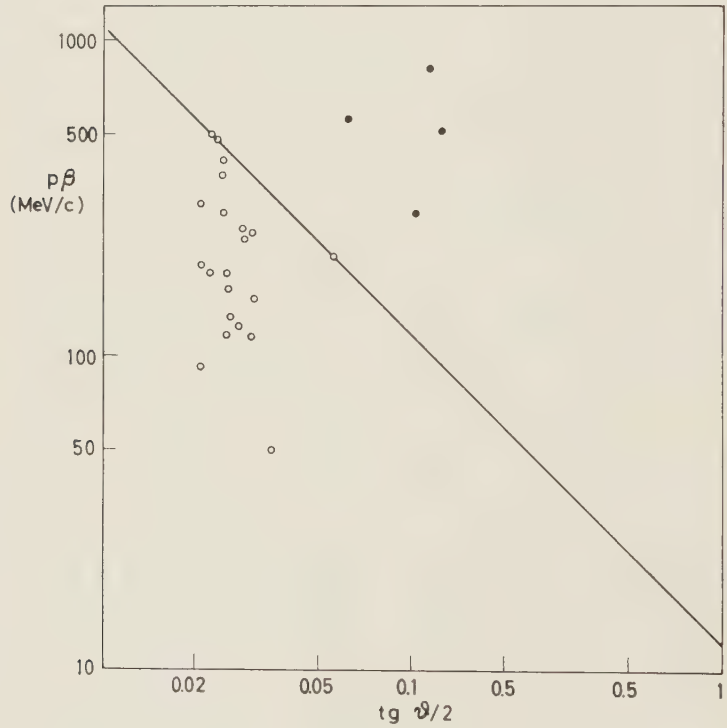

Fig. 10.

In order to separate nuclear from Coulomb scatterings we have plotted in Fig. 10 $\mathrm{tg}\,\vartheta/2$ (ϑ being the spatial scattering angle) as a function of $p\beta$.

([12]) K$^-$-Collaboration: *Nuovo Cimento*, **15**, 873 (1960).

The full line refers to the Coulomb cut-off angle. The four dots represent those scatterings exceeding by more than 20% the Coulomb cut-off angle and provide a lower limit for the cross-section of nuclear scattering. In two of these events no visible energy loss was observed, while the others reveal a blob at the vertex.

The value of the cross-section is the following:

$$\sigma_{(\text{nuclear scattering})} = (19 \pm 10) \text{ mb per nucleon} .$$

If we take as nuclear scatterings also the 3 cases falling on the line of Coulomb cut-off in Fig. 10 the nuclear scattering cross-section becomes

$$\sigma_{(\text{nuclear scattering})} = (33 \pm 13) \text{ mb per nucleon} .$$

7. – Up-down asymmetry in Σ hyperon decay.

As it was found by COOL *et al.* [13] the decay channel $\Sigma^+ \to p + \pi^0$ is a good analyser to test the non-conservation of parity in the Σ^+-hyperon decay. We have looked in our Σ-decays for such violation, by measuring the up-down asymmetry of the decay proton.

The result is the following:

$$\alpha \bar{P} = \frac{3}{N} \sum_i \cos \delta_i^* \pm \sqrt{\frac{3}{N}} = -0.14 \pm 0.31 ,$$

where δ^* is the angle in the C.M. system between the proton and the normal to the production plane, containing the momenta P_K of the K^--meson and P_Σ of the Σ^+-hyperon, and N is the total number, 30, of events.

Even with the large statistical error, our value of $\bar{P}\alpha$ is much lower than the one found by COOL *et al.* This result can be an indication that in the mechanism of production $K^- + \mathcal{N} \to \Sigma^+ + \pi$ the Σ-hyperon is not polarized, as was suggested by ALVAREZ [2]. On the other hand, it is to be taken into account the possibility of Σ-hyperon suffering collisions, inside or outside the nucleus, which will tend to alter the plane of production.

---

[13] R. L. COOL, B. CORK, J. W. CRONIN and W. A. WENZEL: *Phys. Rev.*, **114**, 912 (1959).

* * *

We are very indebted to Dr. R. CESTER, Prof. C. M. GARELLI and Dr. M. VIGONE for the many useful discussions and for their constant interest and encouragement.

RIASSUNTO

In questo lavoro sono dati alcuni risultati sulle interazioni di K^- di alta energia con i nuclei dell'emulsione. In particolare vengono dati lo spettro angolare e di energia dei K^- riemessi; alcuni dati sulla produzione di pioni da parte dei K^-; la vita media degli iperoni $\Sigma^=$, Σ^+ e Σ^-; la sezione d'urto per lo scattering nucleare degli iperoni $\Sigma^\pm$ e l'asimmetria, rispetto al piano di produzione del Σ^+, dei protoni derivanti dal decadimento: $\Sigma^+ \to p + \pi^0$.

IL NUOVO CIMENTO Vol. XIX, N. 6 16 Marzo 1961

Analyticity in the Coupling Constant and Bound States in Potential Theory (*).

B. Bosco (**)

Brookhaven National Laboratory - Upton, N. Y.

J. Sucher (***)

University of Maryland - College Park, Md.

(ricevuto il 28 Novembre 1960)

Summary. — A method for determining the wave function in potential scattering from the S-matrix, using unitarity and analyticity, is extended to the case where bound states are present by using analytic continuation in the coupling constant. A numerical example is given, illustrating the passage of a pole from the second Riemann sheet of the energy to the first sheet.

1. – Introduction.

It is well known that a knowledge of a phase shift as a function of the energy, together with a knowledge of the discrete spectrum, determines completely the potential, and hence the wave function solutions of the Schrödinger equation. This so-called inversion problem was solved by Gel'fand and Levitan [1], who gave a general procedure for finding the potential and also the

(*) Supported in part by the United States Atomic Energy Commission and by the United States Air Force.

(**) Permanent Address: Istituto di Fisica dell'Università, Torino, Italy. Present Address: Institute of Theoretical Physics, Stanford University, Stanford, California.

(***) Permanent and Present Address: Department of Physics, University of Maryland, College Park, Maryland.

(1) I. M. Gel'fand and B. M. Levitan: *Dokl. Akad. Nauk S.S.S.R.*, **77**, 557 (1951); *Izvest. Akad. Nauk S.S.S.R.*, **45**, 309 (1951) and Ref. (6).

radial wave function by quadratures involving a kernel function $K_l(r, r')$ which is determined as the solution of a linear integral equation.

It has been pointed out [2] that in the case where the S-matrix is given as an analytic function of a coupling constant and there are no bound states, the wave function can be determined directly, using the analytic properties of the wave function, in the spirit of the Gell-Mann program.

In this note it is shown that this procedure may be extended very simply to the case where bound states are present. This is done in Section 2. The result is discussed in Section 3, and the connection between the two cases is illustrated by an explicit example, for which the motion of a pole of the wave function on the second Riemann sheet to the first sheet is traced as the coupling constant is increased.

2. – Determination of the wave function in the presence of bound states.

We first review briefly the procedure of (B). Let $\Phi(k, r; g)$ be the S-state solution of the radial Schrödinger equation, satisfying the boundary condition,

$$\begin{cases} \Phi(k, 0; g) = 0 , \\ \Phi'(k, 0; g) = 1 . \end{cases} \tag{1}$$

Here k^2 is the energy [3], the prime denotes differentiation with respect to the radial variable, and g is the coupling constant, the potential having the form $gU(r)$. Then Poincaré's theorem implies that Φ is an entire function of k and also of g [4]. Similarly, let $\varphi^{\text{out}}(k, r; g)$ be a solution of the same equation, satisfying, for large r,

$$\varphi^{\text{out}}(k, r; g) \sim (\exp[-ikr] - S \exp[ikr])/(-2ik) , \tag{2}$$

where $S = S(k; g)$ is the S-wave scattering matrix. The connection between φ^{out} and Φ is given by [2]

$$\varphi^{\text{out}}(k, r; g) = \Phi(k, r; g)/f(-k; g) . \tag{3}$$

Here $f(k; g)$ is the well known Jost function, which is regular for $\operatorname{Im} k < 0$ and, important for our purpose, has zeros on the negative imaginary k axis which correspond to bound states.

[2] B. Bosco: *Nuovo Cimento*, **17**, 558 (1960), hereafter referred to as (B).

[3] We use a system of units such that $\hbar = 2m = 1$.

[4] For a statement of Poincaré's theorems, see *e.g.*, R. G. Newton: *Journ. Math. Phys.*, **1**, 319 (1960).

In (B) essential use was made of the fact that in the absence of bound states, both φ^{out} and S are analytic functions of g for values of g less than the critical value g_c for which a bound state first appears (5). It then followed that φ^{out} could be determined, as a power series in g, order by order, by making use, at each order in g, of the analyticity in k, the unitarity of S and the asymptotic behaviour of φ^{out} with respect to large values of k.

This procedure can be simply extended to cover the case of bound states, as follows. First we observe that when $g > g_c$, φ^{out} is not expressible as a power series in g, uniformly in k, so that the direct procedure of (B) fails. However, we note that, as stated above, Φ is an *entire* function of g and therefore a power series for Φ obtained for $g < g_c$ continues to converge for $g > g_c$ and so defines Φ for all values of g. But for $g < g_c$ a power series for Φ can obviously be obtained from the relation $\Phi = \varphi^{\text{out}} \times f$ since f is known (6) and φ^{out} has been determined by using the method of (B). Eq. (3) then determines φ^{out} for $g > g_c$.

3. – Discussion.

It should be noted that by this method, apparently, the wave functions and consequently the potential are determined from a knowledge of only the continuous spectrum, in contrast with the well-known result (7) that only the complete spectrum determines the potential uniquely. There is, however, no contradiction with this fact, since in our case the S-matrix is given as a function of a coupling constant g, and this knowledge of the dependence on g is equivalent to the knowledge of the bound states.

In particular, it is the knowledge of the analytic behavior of $S(k; g)$ as a function of g (certainly a strong requirement) that can replace the explicit information concerning bound states. It should be remarked that our procedure breaks down if, as is the case for example for potentials of the Bargmann type, there is no domain of the coupling constant or, more generally coupling parameter, for which no bound states are present.

It is clear from eq. (3) that if $g > g_c$, φ^{out} has singularities, as a function of k, at values of k corresponding to the position of the bound states. It is instructive to consider the appearance of these singularities in the dispersion relation for the wave function, as g increases from $g < g_c$ to $g > g_c$.

---

(5) R. Jost and A. Pais: *Phys. Rev.*, **82**, 840 (1951). A potential can give rise to bound-states only if $\int_0^\infty r\,|V(r)|\,\mathrm{d}r \geqslant 1$.

(6) See for example R. Jost and W. Kohn: *Dan. Mat. Fys. Medd.*, **27**, 9 (1953), Footnote (6).

(7) See Ref. (6).

The dispersion relation for the wave function is, in the absence of bound states,

$$\text{(4)} \qquad \mathrm{Re}\,[\varphi^{\mathrm{out}}(E;r)\exp[i\sqrt{E}\,r]] = \frac{P}{\pi}\int_0^\infty \frac{\mathrm{Im}\,[\varphi^{\mathrm{out}}(E',r)\exp[i\sqrt{E'}\,r]}{E'-E}\,\mathrm{d}E'.$$

This equation results on applying Cauchy's theorem to the function $\varphi_1 = \varphi^{\mathrm{out}}(E,r)\exp[i\sqrt{E}\,r]$, analytic in the cut E-plane; the contour is shown in Fig. 1*a*. φ_1 has poles on the negative E axis, but these are on the second Riemann sheet. As g increases beyond g_c these poles pass successively from the second sheet, through 0, to the negative E axis on the first sheet. The contour must therefore be deformed, as shown in Fig. 1*b*, to include these poles. On shrinking the contour, and separating real and imaginary parts, the net effect is to add to the right-hand side of eq. (4) a term of the form [8]

$$\sum_\varrho N_\varrho \frac{\exp[-\chi_\varrho]\psi_\varrho(r)}{\chi_\varrho^2 + E}.$$

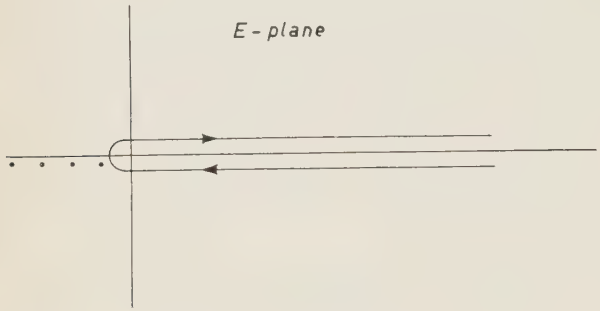

Fig. 1*a*. – Integration contour for $g < g_c$. The dots indicate poles on the second sheet of E, on the real negative axis.

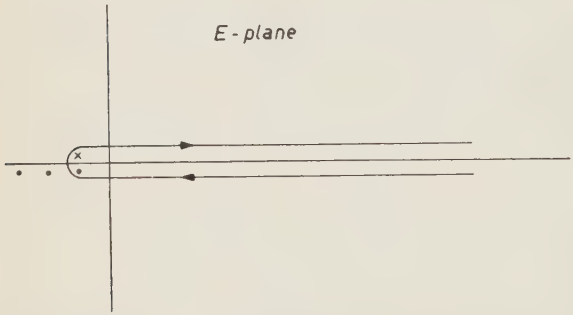

Fig. 1*b*. – For $g > g_c$, a pole on the second sheet has moved to the first sheet, and the contour must be modified to include this pole.

The motion of the poles from the second sheet to the first sheet may be illustrated by an example for which the Schrödinger equation is explicitly solvable. We consider the case of an exponential potential, $V = -g\exp[-r/a]$. In this case [9],

$$\text{(5)} \qquad f(k;g) = \exp[-iak\log(a^2g)]\times\Gamma(1+2iak)\times J_{2iak}(2ag^{\frac{1}{2}}),$$

[8] For details, see Appendix B of (B).

[9] R. JOST: *Helv. Phys. Acta*, **20**, 256 (1947); H. A. BETHE and R. BACHER: *Rev. Mod. Phys.*, **8**, 111 (1936); S. T. MA: *Phys. Rev.*, **69**, 668 (1946).

and the poles are determined by those values of $k = -i\chi$ (with χ real) for which $f(k; g) = 0$, or

$$J_{2a\chi}(2ag^{\frac{1}{2}}) = 0 \,. \tag{6}$$

$\chi > 0$ corresponds to a bound state, while $\chi < 0$ corresponds to a pole in the second sheet of E. Of course, for fixed g eq. (6) has many solutions. In Fig. 2, the behavior of a particular root is shown, as ga^2 increases from 0.

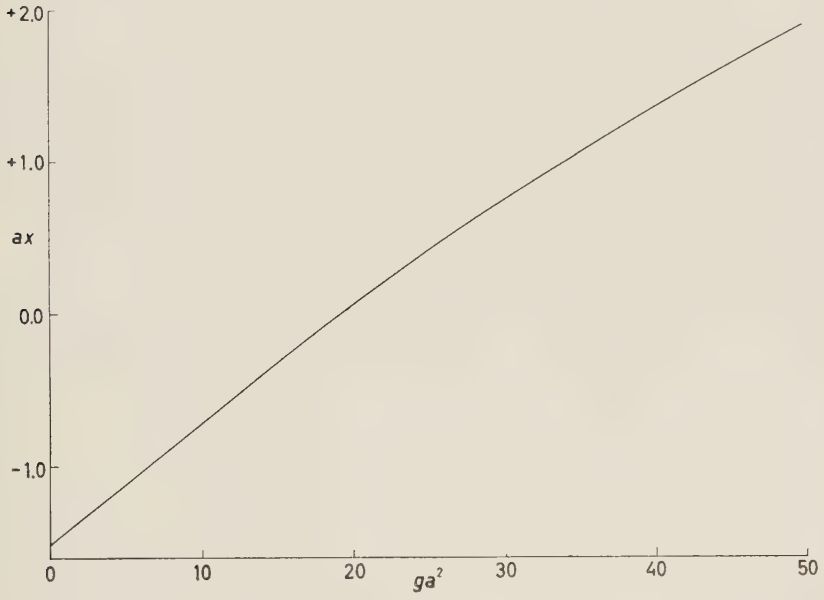

Fig. 2. – Motion of a pole from the second sheet of the energy plane ($\chi < 0$) to the first sheet ($\chi > 0$) as a function of ag^2, for an exponential potential, $V = -g \exp[-r/a]$.

In conclusion, we remark that it would be interesting to test the procedure described here as a calculational tool, for determining the wave function for $g > g_c$ from approximate calculations for $g < g_c$.

* * *

We are indebted to Dr. R. Blankenbecler for an essential suggestion and would like to thank him as well as Professors G. C. Wick and R. Oehme for enlightening discussions.

One of us (B.B.) wishes to express his gratitude to Professor Wick for

giving him the opportunity to spend the summer at the Brookhaven National Laboratory; he must also acknowledge a Fulbright Travel Grant. We both would like to thank the Department of Physics at Brookhaven National Laboratory for its hospitality.

RIASSUNTO

Un metodo precedentemente proposto per la determinazione della funzione d'onda nella teoria dello scattering da potenziale usando l'analiticità e l'unitarietà è esteso al caso in cui sono presenti stati legati, facendo uso della continuazione analitica nella costante d'accoppiamento. È dato un esempio esplicito ad illustrazione dello spostamento di un polo dal secondo foglietto di Riemann dell'energia al primo.

Millimetre Wave Spectrum and Dipole Moment of Vinyl Fluoride (*).

A. M. Mirri, A. Guarnieri and P. Favero

Istituto di Chimica Fisica dell'Università - Padova

(ricevuto il 1° Dicembre 1960)

Summary. — By analysing the millimetre wave spectrum of vinyl fluoride in the range from 100 to 160 GHz its rotational constant A has been determined and found to be 64 582.7 MHz. The centrifugal distortion constants are also given. Measurements of Stark effect on four low J «a» type transitions give for the total dipole moment the value $\mu = (1.42_7 \pm 0.010) D$.

1. – Introduction.

Although the molecular structure of vinyl fluoride has been determined from its centimetre wave spectrum (1), its dipole moment is not known.

In the present work the dipole moment of vinyl fluoride has been determined from the Stark effect splittings of some rotational transitions in the centimetre region. However, it has been necessary to get a value of the rotational constant A which could not be obtained from the data of the previous investigations.

For this purpose some rotational transitions in the millimetre wave region, from 100 to 160 GHz, have been measured using the planarity relation to get an approximate value of A for their location.

(*) This research was supported by the Consiglio Nazionale delle Ricerche, Roma.

(1) H. W. Morgan and J. H. Goldstein: *Journ. Chem. Phys.*, **30**, 1025 (1959); B. Bak, D. Christensen, L. Hansen-Nygaard and J. Rastrup-Andersen: *Spectrochim. Acta*, **13**, 120 (1958).

2. – Experimental.

The millimetre wave spectrometer was of the video type already described [2]. In the harmonic generator a specially treated Silicon crystal kindly supplied us by C. A. BURRUS, of Bell Telephone Laboratories, was used. Stark patterns were studied by means of a conventional four metres X band Stark cell, using 6 kHz square wave field modulation and De-Re-De Amplifier [3]. The cell was calibrated by observations on the $0 \rightarrow 1$ transition of OCS and using for the dipole moment of OCS the value $\mu = (0.7124 \pm 0.0002)D$ [4]. The limiting accuracy of the peak to peak voltmeter was found to be of the order of 0.5%. Frequency measurements were made at the fundamental frequency by means of a frequency standard calibrated on some ammonia lines. The maximum estimated error is ± 0.05 MHz at the fundamental frequency. The vinyl fluoride sample, kindly supplied us by Sicedison S.p.A., Milano, was 99% pure and was used without further purification.

3. – Determination of the rotational constant A.

Following the procedure outlined in a previous investigation [5], two series of « a » type transitions have been measured to get a first approximation value of the constant A; that is the transitions $J = 5 \rightarrow 6$ with $\Delta K_1 = 0$, and $\Delta K_{-1} = 1$ and $J = 7 \rightarrow 8$ of the same type, that are listed in Table I.

Because of the fact that even large changes in the A value slightly affect the frequency of such transitions (an uncertainty of 10 MHz in A corresponds to about 0.3 MHz in the line frequency) it has been necessary to analyse the centrifugal distortion effect which is very relevant in this respect. The centrifugal distortion analysis has been carried out by using the formula given by J. G. BAKER [6] and following the method already described by one of us [5]. With the A constant obtained in this way it was easy to locate two « b » type transitions and give a final value with an accuracy of ± 0.5 MHz.

In Table II are listed the rotational and centrifugal distortion constants together with the inertial defect which is much greater than that predicted by MORGAN and GOLDSTEIN [1].

[2] C. KING and W. GORDY: *Phys. Rev.*, **93**, 407 (1954).

[3] M. W. STRANDBERG, H. R. JOHNSON and J. R. ESHBACH: *Rev. Sci. Instr.*, **75** 776 (1954).

[4] S. A. MARSHALL and J. WEBER: *Phys. Rev.*, **105**, 1502 (1957).

[5] A. M. MIRRI: *Nuovo Cimento*, **18**, 849 (1960).

[6] J. G. BAKER: *Bull. Am. Phys. Soc.*, **5**, 241 (1960); P. FAVERO, A. M. MIRRI and J. G. BAKER: *Nuovo Cimento*, **17**, 740 (1960).

TABLE I. – *Transitions of vinyl fluoride.*

Assignment	Frequency calculated	Frequency observed	Centrifugal shift
	« *a* » type transitions		
$5_{05} \rightarrow 6_{06}$	117 431.51 MHz	117 431.32 MHz	— 6.94 MHz
$5_{14} \rightarrow 6_{15}$	122 813.47	122 813.35	— 7.95
$5_{15} \rightarrow 6_{16}$	113 727.40	113 727.20	— 5.12
$5_{23} \rightarrow 6_{24}$	119 474.77	119 474.65	— 4.52
$5_{24} \rightarrow 6_{25}$	118 384.11	118 383.85	— 3.74
$5_{32} \rightarrow 6_{33}$	118 716.13	118 715.90	+ 0.51
$5_{33} \rightarrow 6_{34}$	118 693.08	118 693.10	+ 0.50
$5_{41} \rightarrow 6_{42}$	118 644.51	118 644.25	+ 6.85
$5_{42} \rightarrow 6_{43}$	118 644.34	118 644.35	+ 6.85
$5_{5} \rightarrow 6_{5}$	118 624.06	118 623.85	+ 14.97
$3_{13} \rightarrow 3_{12}$	9 111.13	9 111.32	
$5_{15} \rightarrow 5_{14}$	22 765.82	22 765.84	— 2.46
$7_{07} \rightarrow 8_{08}$	155 476.98	155 476.98	— 15.46
$7_{16} \rightarrow 8_{17}$	163 410.26	163 410.32	— 19.37
$7_{17} \rightarrow 8_{18}$	151 370.69	151 370.98	— 12.79
$7_{25} \rightarrow 8_{26}$	160 185.18	160 185.15	— 14.78
$7_{26} \rightarrow 8_{27}$	157 641.79	157 641.90	— 12.90
$7_{34} \rightarrow 8_{35}$	158 464.66	158 464.81	— 7.43
$7_{35} \rightarrow 8_{36}$	158 361.69	158 362.00	— 7.38
$7_{43} \rightarrow 8_{44}$	158 264.12	158 264.18	+ 1.21
$7_{44} \rightarrow 8_{45}$	158 262.50	158 262.74	+ 1.20
$7_{5} \rightarrow 8_{5}$	158 206.76	158 206.80	+ 12.07
$7_{6} \rightarrow 8_{6}$	158 184.74	158 184.68	+ 25.43
$7_{7} \rightarrow 8_{7}$	158 179.44	158 179.25	+ 40.99
	« *b* » type transitions		
$4_{04} \rightarrow 5_{15}$	142 347.22	142 347.30	— 0.63
$5_{05} \rightarrow 6_{16}$	157 931.81	157 931.82	— 1.58

TABLE II. – *Constants of vinyl fluoride.*

A	64 582.7	MHz
B	10 636.83	MHz (*)
C	9 118.18	MHz (*)
$I_c - I_a - I_b$	0.088	a.m.u. A^2
D_J	0.008 6	MHz
D_{JK}	— 0.074 6	MHz
δ_J	— 0.001 7	MHz
D_K	2.27	MHz
R_5	0.002 9	MHz
R_6	— 0.000 15	MHz

(*) MORGAN and GOLDSTEIN [1].

4. – Stark effect and dipole moment.

Because of the planarity of the molecule ([1]), the dipole moment has components only in the directions of the a- and b-axes. Although both « a » and « b » type transitions were observed, only some low J « a » type lines could be used for Stark measurements. In fact the low J « b » type transitions were either too weak or too near other lines.

Measurements of the Stark components of the $0_{00} \rightarrow 1_{01}$, $1_{01} \rightarrow 2_{02}$, $3_{13} \rightarrow 3_{12}$ transitions have been fitted to the equation of GOLDEN and WILSON ([7]):

$$\Delta W = (A + M^2 B) E^2 ,$$

with A and B functions of the molecular transition probabilities and rotational energy differences. Tables of the former are available ([8]), but instead of using an interpolation method, it was more satisfactory to calculate the required values from symmetric top transition probabilities and the asymmetric top transformation appropriate to the observed rotational constants.

This calculations give the following results:

$$0_{00} \rightarrow 1_{01}\,(M = 0)\,\Delta\nu/E^2 = 6.149\,2\,\mu_a^2 + 0.534\,9\,\mu_b^2 ,$$

$$1_{01} \rightarrow 2_{02}\,(M = 0)\,\Delta\nu/E^2 = 17.567\,2\,\mu_a^2 + 9.574\,5\,\mu_b^2 ,$$

$$1_{01} \rightarrow 2_{02}\,(M = 1)\,\Delta\nu/E^2 = 14.280\,9\,\mu_a^2 - 0.695\,6\,\mu_b^2 ,$$

$$3_{13} \rightarrow 3_{12}\,(M = 2)\,\Delta\nu/E^2 = 13.914\,8\,\mu_a^2 + 10.220\,1\,\mu_b^2 ,$$

where $\Delta\nu$ is the difference in MHz between the undisplaced line at zero field and the Stark component at a field E in (esu/cm); μ_a and μ_b are the components of the dipole moment in Debye units along the principal axes of inertia.

The above equations, if experimental values for $\Delta\nu/E^2$ are inserted, are a set of relations between μ_a and μ_b that give a well determined area of intersection when plotted in a diagram. Such a diagram is shown in Fig. 1 where the maximum errors are also represented.

The values of the dipole moment components obtained by this method are $\mu_a = (1.280 \pm 0.006)D$ and $\mu_b = 0.62_9 \pm 0.030)D$; the value for the total dipole moment is $\mu = (1.42_7 \pm 0.010)D$.

([7]) S. GOLDEN and E. B. WILSON: *Journ. Chem. Phys.*, **16**, 669 (1948).
([8]) R. H. SCHWENDEMAN and V. W. LAURIE: *Tables of Line Strengths* (London).

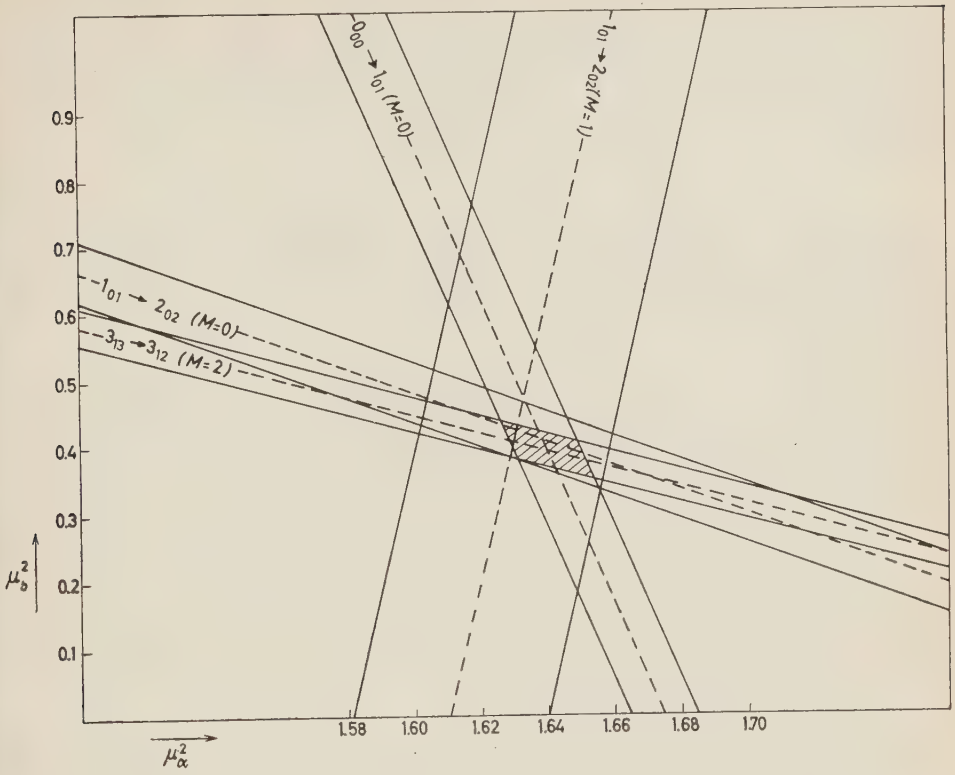

Fig. 1.

The observed and calculated values of $\Delta\nu/E^2$ are listed in Table III.

TABLE III. – *Stark effect measurements.*

Transition	M value	$\Delta\nu/E^2$ MHz/(e.s.u.·cm)^2	
		Observed	Calculated
$0_{00} \rightarrow 1_{01}$	0	10.308 ± 0.062	10.300
$1_{01} \rightarrow 2_{02}$	0	32.772 ± 0.426	32.602
$1_{01} \rightarrow 2_{02}$	1	23.015 ± 0.414	23.145
$3_{13} \rightarrow 3_{12}$	2	26.896 ± 0.269	26.868

If the structure given by MORGAN and GOLDSTEIN [1] is chosen, the total dipole moment μ is found to be almost parallel to the C-F bond. Assuming for the C-H bond moment a value of $0.3D$, the C-F bond moment has a value of $1.1D$ which is much lower than that assumed by KRAITCHMAN and DAILEY

in ethyl fluoride ([9]). This would agree with the presence in the C-F bond of a certain amount of double bond character which is further evidenced by a shorter bond length (the C-F bond length in vinyl fluoride is 1.344 A and in ethyl fluoride is 1.375 A). An analogous situation is found in the formyl fluoride molecule ([10]).

* * *

The authors would like to express their thanks to Prof. L. GRIFONE for his assistance in setting up the electronic and microwave apparatus and Dr. G. ZULIANI for his technical assistance.

([9]) J. KRAITCHMAN and B. P. DAILEY: *Journ. Chem. Phys.*, **23**, 184 (1955).
([10]) P. FAVERO and J. C. BAKER: *Nuovo Cimento*, **17**, 734 (1960).

RIASSUNTO

L'analisi dello spettro millimetrico del fluoruro di vinile, nell'intervallo fra 100 e 160 GHz, ha fornito per la costante rotazionale A un valore di (64 582.7 $\pm$ 0.5) MHz. Sono state determinate anche le costanti di distorsione centrifuga. Le misure di effetto Stark su quattro transizioni a basso J di tipo « a », hanno dato, per il momento dipolare totale del fluoruro di vinile il valore $(1.42_7 + 0.010)D$.

On the μ-Mesonic Atoms.

Y. Eisenberg and D. Kessler (*)

The Weizmann Institute of Science - Rehovoth

(ricevuto il 5 Dicembre 1960)

Summary. — In an attempt to get a deeper insight into the problem of the « missing X-rays » in the capture of μ-mesons in the light elements, a complete cascade calculation of the μ-meson transitions in the mesonic atom was conducted. The results indicate again that the calculated K X-ray yields below $Z=6$ and the L X-ray yields below $Z=14$ are much above the experimental values. As was noted before by other authors, the deficiency of X-rays increases linearly with decreasing quantum energy between about 90 keV and 20 keV. The experimental yields agree with the calculations above 90 keV, and are lower than the calculated values, by a factor of about 5, at 20 keV. Good agreement between the calculations and experiment is obtained, however, for the (approximately energy-independent) ratios of the higher to basic X-ray yields, provided that a proper choice of the initial meson distribution is made. A comparison between the calculated Auger electron yields and the experimental results for μ^--capture in nuclear emulsions seems to indicate that the « mixed » Auger-radiative transitions introduced by Ruderman are indeed effective (apparently close to 100%) in the de-excitation of the metastable $2s$ level in CNO. If this mixed transitions play the same role also in the lightest elements (Li, Be, B), the problem of the « missing » X-rays becomes more serious than before. The expected Auger electron spectrum for μ^--capture in the heavy elements (AgBr) of nuclear emulsion has also been calculated.

1. – Introduction.

The problem of the « missing X-rays » [1] in mesonic atoms has been the subject of several recent investigations [2-7]. Briefly stated, the problem is the

(*) Also from the Israeli A.E.C. Establishment, Rehovoth.

[1] M. B. Stearns and M. Stearns: *Phys. Rev.*, **105**, 1573 (1957).
[2] T. B. Day and P. Morrison: *Phys. Rev.*, **107**, 912 (1957).
[3] J. Berstein and T. Y. Wu: *Phys. Rev. Lett.*, **2**, 404 (1959).
[4] T. B. Day and J. Sucher: AFOSR TN-59-771 (1959), unpublished.
[5] N. A. Krall and E. Gerjuoy: *Phys. Rev. Lett.*, **3**, 142 (1959).
[6] R. A. Ferrell: *Phys. Rev. Lett.*, **4**, 425 (1960).
[7] M. A. Ruderman: *Phys. Rev.*, **118**, 1632 (1960).

following: when a negative μ-meson, for example, is stopped in matter, it will be captured in an atom and form a « mesonic » atom. In a relatively short time ($\sim 10^{-12}$ s) the meson will cascade down to its grond state in the mesonic atom, from which it will either decay or be captured by the nucleus (the characteristic time involved in the latter processes is $\sim 10^{-6}$ s). While the penetration of the μ-meson through the electronic cloud is very complicated and has so far not been described in detail, upon reaching the $n = 14$ level, the meson is already below the K electron shell, and is expected to behave as a heavy electron in a hydrogen-like central field of charge $+Ze$. In particular, it should cascade down to the ground state, emitting X-rays or Auger electrons in each quantum jump.

Several investigators studied various aspects of this phenomenon, both for μ-mesons and for π-mesons ([8]). In particular, STEARNS and STEARNS ([1]) measured systematically the mesonic K X-ray and L X-ray yields for most of the elements ranging from Li ($Z = 3$) until K ($Z = 19$). They pointed out that since the radiative rate is proportional to Z^4, and the calculated ([9]) Auger transition rate is, in a first approximation, Z-independent, the observed X-ray yields as a function of Z should behave like: $y \simeq Z^4/(C+Z^4)$. Indeed the experimental curve of y *vs.* Z could be fitted to the above formula, both for the K and L X-ray yields. However, the experimental constant C turns out to be 300 times bigger then the calculated one for the K X-rays, and 30 times the calculated value for the L X-rays. The actual drop of the experimental X-ray yields (see ref. ([1]) or Table IV of this work) in the lightest elements was by a factor of ~ 5.

Several explanations ([2,5]) for this deficiency of X-rays have been offered. However, until now, no satisfactory explanation for these « missing » X-rays exists ([7]). In fact, in a sense, the problem seems to be now more acute then ever. This will be discussed in more detail later, but very briefly one can state that there seems to be no possibility of explaining the « missing X-rays » by any kind of single electron emission because these electrons were looked for ([10,11]), and were not found!

The present investigation was started over a year ago, for a somewhat different reason: mainly in order to predict an exact Auger electron spectrum associated with the absorption of negative particles (μ^-, π^-, K^-, etc.) in nuclear emulsions, so that captures in the light emulsion elements (CNO) could be

([8]) For a comprehensive review, see D. WEST: *Reports on Progress of Physics*, **71**, 271 (1958).

([9]) G. R. BURBIDGE and A. H. DE BORDE: *Phys. Rev.*, **89**, 189 (1953); A. H. DE BORDE: *Proc. Phys. Soc.*, A **67**, 57 (1954).

([10]) W. F. FRY: *Nuovo Cimento*, **10**, 490 (1953).

([11]) A. PEVSNER, R. STRAND, L. MADANSKY and T. TOOHIG: *Johns Hopkins University Reports*, AFOSR TN-60-463 (1960), unpublished.

distinguished from captures in the heavy elements (AgBr). It was soon realized that such a calculation could not be trusted, unless the μ-meson puzzle is somewhat better understood. The purpose of the present work was then:

a) To supplement the work of BURBIDGE and DE BORDE, and DE BORDE [9] in calculating all the possible Auger and radiative transition rates for the elements of interest in the μ-meson experiments.

b) To perform an exact cascade calculation, using the above transition rates, for various possible initial distributions and, if not to explain the « missing » X-rays, at least to pin down the discrepancy between theory and experiment more precisely. Furthermore, to see if some aspects of the phenomena (for instance the relative yields of the higher transitions to the basic α lines which, so far, have never been discussed) agree with the calculations.

c) Finally, to determine if the calculated Auger energy spectrum for emulsion could be trusted, and to what extent.

The present paper will deal only with μ-mesons. In a forthcoming paper the results for π^- and K^- mesons will be given.

2. – Radiative transitions and Auger effect.

The radiative transition rates were calculated by standard procedures (see Appendix). These rates are proportional to the square of the matrix element and the cube of the energy difference between the initial (n_1, l_1) and final (n_2, l_2) states. The matrix elements are larger for small Δn, whereas the energy dependent factor favors quantum jumps with large Δn. In most cases the last factor predominates, so that radiative transitions to the lowest possible state n_2 are usually preferred. An inversion of this behaviour occurs only for high n_1 and l_1; however, in this region the radiative transitions are unimportant anyway compared with the Auger transitions, as we shall see below. Moreover, the $(n_1, l_1) \to (n_2, l_1-1)$ transitions are larger than the $(n_1, l_1) \to (n_2, l_1+1)$ transitions by about two to thee orders of magnitude. Therefore the most important radiative transition is: $(n_1, l_1) \to (n_2 = l_1, l_2 = l_1-1)$, with the obvious exception of higher s-states which make transition mainly to $2p$.

The Auger effect obeys the same selection rules as radiation, except that $\Delta l = 0$ transitions are not absolutely forbidden. The Auger transition probabilities for the P-transitions ($\Delta l = \pm 1$), which usually are the dominant ones and for the S-transitions ($\Delta l = 0$), are given in the Appendix.

The qualitative behaviour of Auger transitions is different from that described above for the radiative ones, because of the weak energy-dependence of the transition probabilities. Thus transitions with $\Delta n = -1$, $\Delta l = -1$

are favored, the dominant transition being therefore $(n_1, l_1) \to (n_2 = n_1 - 1, l_2 = l_1 - 1)$. When this transition is energetically impossible for K electron emission (large n_1), there is competition between Auger effect with L electron emission ($\Delta n = -1$), and Auger effect with K electron emission and higher Δn.

For the lightest elements, the Auger effect is the dominant process down to $n_1 = 3$, whereas in heavier elements like potassium the radiative competition manifests itself strongly already in the $10p$ state (about 40%), becoming gradually more important for lower n and higher l.

In our calculation of the Auger process, we have always supposed the K electron shell to be filled, since, in general, replenishing of K shell vacancies from the L shell or band electrons, is faster than the Auger transition [7,12]. Even if this were not strictly true for the lightest elements, this would not modify our cascade calculations in any important way. In the region where the Auger effect dominates (for high n), the relative transition probabilities to lower states are not changed, even if the absolute time of each step is dominated by the time required to replenish the K electron shell. Such an effect can only be important in the region of smaller n where radiation effectively competes with the Auger effect. But this is just the region where the transition rates are smallest, about 10^{13} s^{-1}, the Auger effect being nearly exhausted and radiation not yet having come into full play, leaving enough time for replenishing of holes in the K shell.

3. – Cascade calculations.

Calculations were made for elements with $Z = 3$, 4, 6, 8, 10, 14, 19 and 40. All cascades were started from the level with principal quantum number $n = 14$. The μ-meson was assumed to be in a Hydrogen-like field for all $n \leqslant 14$.

Four different populations of the $n = 14$ level were tried:

C^{I}: Only the $14s$ state is populated, all other states of the $n = 14$ level are empty.

C^{II}: Equal population of all initial states.

C^{III}: Statistical population, each initial state having a weight $2l+1$.

C^{IV}: A modified statistical population, more peaked towards the high l values: each initial state having a weight of $(2l+1) \cdot \exp[al]$. The constant a has been chosen equal to 0.2, because it gave the best agreement with

[12] E. H. S. Burhop: *The Auger Effect*, Chapter VII (Cambridge, 1952).

experiment for the ratio of higher to basic K and L X-ray yields (see Section 4).

It was clear from the start that significant results could be expected from these calculations only if the two following conditions are fulfilled:

1) The type of initial distribution assumed for the $n = 14$ level should not change drastically in the first few steps of the cascade. This comes from the fact that the choice of the $n = 14$ level as the initial stage of the cascade calculation, or in fact of any other single level, is rather artificial. We would like, therefore, to see the chosen initial distribution as a characteristic of the whole group of the higher levels.

2) The results should not be too sensitive to the chosen initial distribution, since we do not have a physical theory which predicts the way in which the « initial » levels are populated, except for a slight intuitive preference for the statistical distribution. If the results of the cascade calculation were strongly dependent on the assumed « initial distribution », a theory of the whole process of meson capture would be necessary. Such a theory is hardly justified at the present stage.

TABLE I. – *Population of states in Carbon for a statistical initial distribution* (C^{III}).

n \ l	0	1	2	3	4	5	6	7	8	9	10	11	12	13
14	10	30	50	70	90	110	130	150	170	190	210	230	250	270
13	11	32	51	66	81	97	114	134	155	183	212	244	270	
12	10	28	39	47	57	67	82	98	123	157	209	278		
11	18	45	59	77	92	107	126	150	188	243	334			
10	22	53	72	84	96	114	140	182	249	388				
9	39	100	127	142	164	194	242	313	454					
8	60	139	166	182	208	255	326	474						
7	84	193	220	232	268	335	492							
6	123	272	283	294	352	514								
5	181	375	363	378	538									
4	245	493	437	570										
3	183	580	614											
2	156	941												
1	1960													

TABLE II. – *Population of states in Silicon for a statistical initial distribution* (C^{III}).

n \ l	0	1	2	3	4	5	6	7	8	9	10	11	12	13
14	10	30	50	70	90	110	130	150	170	190	210	230	250	270
13	11	33	50	66	82	97	115	134	156	183	212	242	270	
12	14	37	56	69	84	98	117	140	172	210	248	279		
11	14	39	51	65	77	89	107	134	171	224	295			
10	23	56	75	91	104	123	152	193	255	355				
9	26	69	85	100	116	143	187	259	416					
8	47	118	149	170	198	249	330	490						
7	58	163	194	218	264	349	513							
6	74	199	230	279	360	538								
5	53	205	271	367	563									
4	31	174	322	602										
3	25	211	725											
2	95	1194												
1	1960													

It turns out indeed that both of the above conditions are rather well satisfied (see the following discussion and Section **4**).

Examples of two cascades with statistical initial distribution (C^{III}) for $Z = 6$ and 14, are given in Tables I and II. These were obtained by using the radiative and Auger transition probabilities described in the previous section. In the tables we give the number of mesons passing through each (n, l) level, out of the given initial population. The Auger effect dominates ($> 50\%$) above the solid line drawn in Tables I and II, and the radiative transitions dominate ($> 50\%$) below this line. Above the upper broken line the Auger probability is over 75%, and below the lower broken line, the radiative transition is already $> 75\%$. It is interesting to note that the transition region is always rather narrow, and that therefore very quickly each cascade changes from a pratically pure Auger-type into a pure radiative cascade. This feature is quite characteristic for all the elements that we have tried. One should also note that the cascades conserve approximately the type of distribution assumed for the initial state, although there occurs some enrichment in the p and circular ($l = n - 1$) orbits. The reason for this is obvious: The p states are fed from the d as well as from the s states, whereas all other states are filled mainly from the next higher orbit only. The circular orbits, on the other hand, become

gradually enriched because once the system has reached a circular orbit, it will remain in circular orbits through the whole cascade. Also, the s-states are rather depleted in the first stages of the cascade, because the Auger transitions from the p states show less preference for the $l \to l-1$ transition than the states with higher l.

In the cascade of type C^{I} where only the $14s$ state is filled initially, one soon gets some kind of qualitative equilibrium between the s, p and d states, with a maximum at p. The population of the f states is only a few percent and higher states remain practically empty. Therefore the results of this cascade will be characteristic not so much of the assumed initial distribution, but of the equilibrium distribution reached at the later stages. This example is quite instructive. The circular orbits remain practically empty except $2p$. Therefore if some mechanism existed which would lead to preferential capture in high n orbits of low angular momentum one would expect the L_α X-rays to be extremely weak and the ratio of higher X-rays to K_α very high, in contradiction to experiment. This distribution can also be ruled out because of the relatively high observed yield of π-mesic X-rays ([8]).

4. – Results.

The calculated value for K and L X-ray yields and for the ratios K_α/(all K) and L_α/(all L) are summarized in Table III. In order to compare these results with experiment we have calculated the « normalized » values with respect to the experimental yields of Oxygen for the K-lines and Silicon for the L-lines. This was done because the absolute experimental intensities reported by Stearns and Stearns ([1]) have large errors and only the « relative » values with respect to Oxygen and Silicon are accurate.

Inspection of Tables III and IV shows that the calculated K X-ray yields are practically insensitive to the initial distributions. Discrepancy between theory and experiment is serious for all the elements of $Z \leqslant 6$.

As for the L X-rays, the un-normalized yields (Table III) tend to increase systematically from C^{I} to C^{IV}. However, the normalized predicted yields of C^{II} to C^{IV}, are practically identical (Table IV). The normalized results of C^{I} are not to be taken seriously because of the large normalization factor (2.6) which had to be applied. It is clear from Table IV that for the L X-rays also, the experimental yields below $Z = 14$, are much smaller then the calculated ones. Thus, the complete cascade calculation does not help much in explaining the « missing » X-rays.

It was noted by previous authors ([6,7]) that the K and L X-rays yields are linear functions of energy up to about 100 keV, which was considered ([6]) as an indication that the discrepancy is independent of the target and therefore

TABLE III. – *Calculated X-ray yields.*

Type of cascade	Z	All K-lines	$\frac{K_\alpha}{\text{all } K}$	All L-lines	$\frac{L_\alpha}{\text{all } L}$
	4	.85	.44	.23	.80
C^{I}	6	.89	.28	.28	.61
	8	.90	.22	.30	.36
	14	.90	.21	.29	.18
	3	.80	.57	.16	.89
	4	.87	.54	.26	.85
	6	.91	.42	.36	.72
C^{II}	8	.92	.40	.41	.59
	10	.92	.42	.45	.48
	14	.93	.49	.52	.48
	19	.94	.54	.56	.50
	3	.81	.62	.16	.90
	4	.88	.59	.27	.87
	6	.92	.52	.42	.78
C^{III}	8	.93	.52	.50	.67
	10	.94	.55	.56	.59
	14	.95	.64	.65	.60
	19	.96	.70	.71	.62
	3	.85	.71	.18	.93
	4	.89	.62	.28	.89
	6	.94	.66	.51	.85
C^{IV}	8	.95	.67	.61	.78
	10	.96	.70	.68	.70
	14	.97	.79	.78	.73
	19	.98	.83	.83	.74

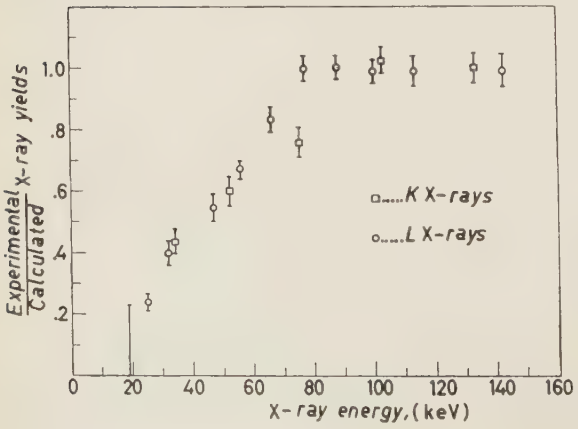

Fig. 1. – Ratio of experimental to calculated X-ray yields as function of energy.

experimental. In order to see this more clearly, we have plotted in Fig. 1 the actual discrepancies (experimental divided by predicted yields) as function of energy. As « predicted » yields, we have taken the normalized results of C^{III}.

TABLE IV. – *Normalized X-ray yields and comparison with experiment.*

	K X-ray yields normalized to $_8$O					*L* X-ray yields normalized to $_{14}$Si				
Z	*E* (keV)	Exp [1] (*)	Calculated			*E* (keV)	Exp [1] (*)	Calculated		
			C^{I}	C^{II}	C^{III}	C^{IV}			C^{I}	C^{II}	C^{III}	C^{IV}
3	18.7	< .16		.69	.69	.72	3.5			.22	.19	.17
4	33.3	.33	.76	.76	.75	.75	6.3		.60	.38	.31	.27
6	75.0	.60	.79	.79	.79	.79	14.2		.73	.52	.48	.49
8	133	.80	.80	.80	.80	.80	25	.14	.80	.59	.57	.59
10	210	.77 (**)		.81	.81	.81	39	.30 (**)		.65	.63	.65
14	410	1.01	.90	.81	.81	.82	77	.75	.75	.75	.75	.75
19	730	.91		.82	.82	.83	142	.81		.82	.82	.80

(*) The experimental errors on the relative yields are about 8%.
(**) Experimental value interpolated between those of $_9$F and $_{11}$Na.

This graph is quite similar to that of FERRELL [6] and shows that the discrepancy seems to be a linearly decreasing function of energy, from a factor of about 5 at 20 keV to one at about 90 keV.

As the discrepancy of the absolute yields seems to depend on energy, it will now be interesting to compare the experimental data with the predicted relative K_α and L_α yields which should be approximately energy independent. Indeed, it seems that here the discrepancy is not serious at all (Table V). The experimental values of K_α/(all *K*) are scattered between .70 and .80 without

TABLE V. – *Relative yields of K_α and L_α and comparison with experiment.*

	K_α/(all *K*)					L_α/(all *L*)				
Z	Exp [1] (*)	Calculated				Exp [1] (*)	Calculated			
		C^{I}	C^{II}	C^{III}	C^{IV}		C^{I}	C^{II}	C^{III}	C^{IV}
3			.57	.62	.71			.89	.90	.93
4	.78	.44	.54	.59	.62		.80	.85	.87	.89
6	.80	.28	.42	.52	.66		.61	.72	.78	.85
8	.79	.22	.40	.52	.67	.72	.36	.59	.67	.78
10	.82 (**)		.42	.55	.70	.80 (**)		.48	.59	.70
14	.74	.21	.49	.64	.79	.69	.18	.48	.60	.73
19	.73		.54	.73	.83	.70		.50	.62	.74

(*) Experimental accuracy about (10÷20)%.
(**) Interpolated between the values of $_9$F and $_{11}$Na.

any special trend, probably because of the large errors involved in the analysis of the spectra ($(10 \div 20)\%$, see ref. [1]). The predicted data of C^{II} and C^{III} show some systematic trend, but both are $\sim 20\%$ below the experimental values. The result of C^{IV}, with a proper choice of the parameter a ($a = 0.2$) give better agreement with the experimental data (Table V). A very similar situation exists also for the L_γ/(all L) ratio. It seems, therefore, that an improved experimental determination of the ratio of the basic to higher transitions for various elements, might be very useful in determining the initial distribution of the captured μ-mesons.

It must be pointed out, that the agreement between theory and experiment in the determination of energy independent quantities, like the K_α/(all K) and L_γ/(all L) yields, support in a sense the view point of FERRELL [6] that the discrepancy in the X-ray yields comes from a loss of soft X-rays. On the other hand, it is hard to imagine that this could happen in such careful experiments. Thus, to our minds, the problem is still an unsolved one and needs both experimental and theoretical attention.

5. – Discussion.

We would like to discuss now the results of the cascade calculations in view of the recent proposal [7] that the de-excitation of the $2s$ level is not a pure Auger S transition.

As far as the K X-rays are concerned, the main deviation from 100% yield is due to those μ-mesons which happen to arrive in the meta-stable $2s$ state and make the Auger S-transition to the ground state. In our preceding calculation we have always supposed that this is the only way by which the meta-stable state can de-excite itself. It was however pointed out by RUDERMAN [7] that owing to a certain admixture of $2p$ to the $2s$ state, some fraction of the meta-stable states will undergo a mixed Auger-radiative transition, where an X-ray will take most of the available energy (and therefore become experimentally indistinguishable from the ordinary K_α rays), and the electron takes up one unit of angular momentum. Both the Auger S and the « mixed » transitions have been shown by RUDERMAN [7] to be of the same order of magnitude, but precise branching ratios are difficult to calculate. It is however possible to get some insight into this problem by experiment owing to the fact that the Auger S-transition, if it predominates over the « mixed » transitions, should produce the bulk of the observed Auger electrons in the light elements, especially above 30 keV. This is clearly shown in Table VI where we give the yields of Auger electrons for the light elements of nuclear emulsion. The results stem from the calculation with the initial statistical distribution C^{III}, but different initial distributions give essentially the same results.

TABLE VI. – *Percentage yield of Auger-electrons (Kinetic energy $T \geqslant 15$ keV) in the light elements of nuclear emulsion.*

Carbon			Nitrogen			Oxygen		
$n_1 \to n_2$	T (keV)	% yield	$n_1 \to n_2$	T (keV)	% yield	$n_1 \to n_2$	T (keV)	% yield
ordinary Auger transitions.								
$4 \to 2$	19	1.02	$3 \to 2$	19	8.32	$3 \to 2$	24	4.39
$5 \to 2$	21	0.20	$4 \to 2$	25	0.77	$4 \to 2$	33	0.49
$2 \to 1$	75	0.06	$5 \to 2$	28	0.13	$5 \to 2$	37	0.11
$3 \to 1$	89	0.02	$6 \to 2$	30	0.02	$6 \to 2$	39	0.02
$4 \to 1$	94	0.01	$7 \to 2$	31	0.01	$7 \to 2$	41	0.01
			$2 \to 1$	103	0.04	$2 \to 1$	134	0.02
			$3 \to 1$	122	0.01			
			$4 \to 1$	128	0.01			
Auger S-transitions, assuming no competition of the « mixed » transitions.								
$2s \to 1s$	75	7.93	$2s \to 1s$	103	7.24	$2s \to 1s$	134	6.62

PEVSNER *et al.* [11] have looked for Auger-electrons in the light elements of nuclear emulsion in the energy range $(30 \div 200)$ keV. In this experiment the light elements were identified by observation of the decay electrons of the μ-meson in the ground state. The observed decays were distributed according to the relative abundance of the elements in nuclear emulsion and corrected both for absorption in CNO and for decay in AgBr. Columns III to VI of Table VII show the corresponding calculated value of Auger-electron yields,

TABLE VII. – *Expected number of Auger electrons for the experiment of Pevsner et al.* [11], *assuming the two extreme cases of de-excitation of the meta-stable 2s state.*

Element	Number of observed μ-decays	Statistical distrib. C^{III}		« Modified statistical » C^{IV}	
		100 % « mixed »	100 % Auger S	100 % « mixed »	100 % Auger S
C	535	0.47	42.8	0.53	32.0
N	113	0.10	8.3	0.07	6.0
O	298	1.95	21.7	1.80	15.7
Total	946	2.52	72.8	2.40	53.7

for the two extreme cases: either 100 % « mixed » $2s$-$1s$ or 100 % pure Auger S-transition. The experimental number of Auger-electrons in the experiment of PEVSNER *et al.* [11] is about 2 (5 electrons in the above energy range ob-

served, 3 of them attributed to μ-capture in heavy elements). Since it is hard to imagine that the results given by PEVSNER *et al.* could be low by a large factor due to experimental difficulties, one must conclude that the « mixed » transitions are dominant.

In order to check this point further, we have also calculated, again assuming a statistical ($\sim 2l+1$) distribution, the expected spectrum of Auger electrons associated with the absorption of μ-mesons in the heavy emulsion nuclei (AgBr). In this spectrum the de-excitation mode of the $2s$-state does not play any role at all. The results are given in Fig. 2. In the spectrum each electron was counted independently. So, for example, if 2 electrons are emitted from a single mesonic atom, both should be counted. One should note that the results of PEVSNER *et al.* [11] do not agree with the calculated spectrum: the calculated yield of electrons between 30 keV and 200 keV is $\sim 20\%$, whereas the experimental value given by PEVSNER *et al.* [11] for the above yields, associated with non-decaying μ-mesons, is only $\sim 4\%$. Earlier experimenters [10], however, did observe yields which are much closer to the predicted values of Fig. 2, and also did not find electrons over 30 keV associated with μ-absorption in CNO, in agreement with the results of PEVSNER *et al.* for the captures in the light elements.

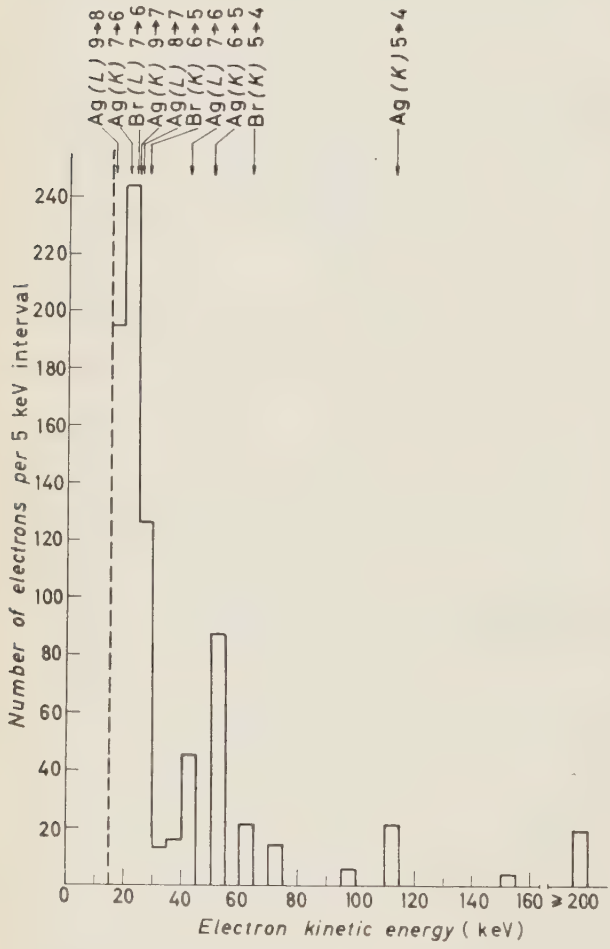

Fig. 2. – Calculated Auger electron spectrum (above 15 keV) for 1000 μ-captures in AgBr.

Thus, if we accept the apparently unavoidable conclusion that the « mixed » transition is the main process for de-excitation of the $2s$ state, and if we as-

sume with RUDERMAN that the resulting X-rays are experimentally indistinguishable from the K_α lines, the situation becomes even worse as far as the K X-ray yields are concerned. These yields are then expected to be close to 100% for all elements!

6. – Conclusions.

1) The results of the straightforward cascade calculation on μ-mesonic atoms agree in a qualitative way with the experimental observation of Auger-electron yields associated with the capture of negative μ-mesons in the heavy elements of nuclear emulsion (AgBr). A better experimental determination of the yields and energy spectrum of the Auger electrons is required for a more quantitative comparison.

2) In order to obtain satisfactory agreement between the calculation and experiment for the light elements of nuclear emulsion (CNO), one is compelled to assume that the « mixed » transition proposed by RUDERMAN is close to 100% effective in the de-excitation of the meta-stable $2s$-state.

3) If these « mixed » transitions play the same role also in the lightest elements (Li, Be, B), then the problem of the « missing X-rays » becomes even more serious. The expected K X-ray yields will then be close to 100% in all. elements. Also in this case there seems to be not much hope in explaining the « missing X-rays » with the help of the meta-stable $2s$-state nor, in fact, by any other process involving the conversion of the γ-ray energy into a single electron.

4) As for the L X-rays, the cascade calculations predict a regular decrease of the yield with Z, but not sufficient to explain the experimental data (see Table IV).

5) As was pointed out before [6,7], the efficiencies of K and L X-rays seem to be an increasing function of energy between about 20 and 90 keV (see Fig. 1). Above 90 keV the expected and experimental yields agree and are close to 100%.

6) On the other hand, the relative yields $K_\alpha/(\text{all } K)$ and $L_\alpha/(\text{all } L)$ which are approximately energy independent, can be explained by the calculations, assuming a suitable and not unreasonable population of mesons entering the high quantum states.

* * *

The help of Mr. M. SCHATZ and U. KARSHON in the numerical computations is greatly appreciated.

We are also thankful to many of our collegues for interesting discussions.

Appendix.

A.1. – Radiative transitions.

The evaluation of the radiative transition probability is straightforward [13]. The result is:

$$(1) \qquad P_E(n_1, l_1 \to n_2, l_2) = \frac{64\pi^4 R_\mu^3}{3h} e^2 a_\mu^2 Z^4 \left[\frac{1}{n_2^2} - \frac{1}{n_1^2}\right]^3 \frac{\mathrm{Max}\,(l_1, l_2)}{2l_1 + 1} I^2 ,$$

where: R is the Rydberg constant $R_\mu = \alpha a_\mu^{-1}/4\pi$,

a_μ is the radius of the first Bohr orbit $a_\mu = \hbar^2/m_\mu e^2 = a_0(m_e/m_\mu)$,

m_μ is the μ-meson mass,

Z is the charge of the nucleus and

I is the dipole matrix element $I = \int_0^\infty r R(n_1, l_1) R(n_2, l_2)\,\mathrm{d}r$, where $R(n, l)$ are the normalized radial functions given by (ref. [13], p. 117). One gets therefore

$$(2) \qquad I(n_1, l_1 \to n_2, l_2) =$$

$$= \sqrt{\frac{2^{2l_1+2l_2+4} n_1^{2l_2+4} n_2^{2l_1+4} (n_1 - l_1 - 1)!(n_2 - l_2 - 1)!(n_1 + l_1)!(n_2 + l_2)!}{(n_1 + n_2)^{2l_1+2l_2+8}}} \cdot$$

$$\cdot \int_0^\infty \mathrm{d}\varrho\, \varrho^{l_1+l_2+3} \exp[-\varrho] \sum_{\gamma_1=0}^{n_1+l_1-1} \frac{\left(-\frac{2n_2}{n_1+n_2}\varrho\right)^{\gamma_1}}{\gamma_1!(n_1 - l_1 - 1 - \gamma_1)!(2l_1 + 1 + \gamma_1)!} \cdot$$

$$\cdot \sum_{\gamma_2=0}^{n_1-l_1-1} \frac{\left(-\frac{2n_1}{n_1+n_2}\varrho\right)^{\gamma_2}}{\gamma_2!(n_2 - l_2 - 1 - \gamma_2)!(2l_2 + 1 + \gamma_2)!} .$$

This has been calculated exactly with the help of the formula

$$\int_0^\infty \mathrm{d}\varrho\, \varrho^k \exp[-\varrho] = k!$$

The term $\mathrm{Max}\,(l_1, l_2)/(2l_1 + 1)$ arises from averaging on initial and summing over final magnetic quantum numbers.

---

[13] See, for example E. U. Condon and G. H. Shortley: *The Theory of Atomic Spectra* (Cambridge, 1957).

A.2. – Auger P-transitions.

The P-Auger transition probabilities ($l_1 - l_2 = \pm 1$) have been calculated by BURBIDGE and de BORDE, and de BORDE [9], both for the ejection of K- and L-shell electrons. These can be expressed best with the help of the dipole matrix element, I, defined above (2). The result is

$$(3) \qquad P_A^P(K) = \frac{\pi\alpha c}{a_0}\frac{2^5}{\mu^2}\left(\frac{Z^*}{Z}\right)^2 \frac{\mathrm{Max}\,(l_1, l_2)}{3(2l_1+1)}\frac{y^2}{1+y^2}\frac{\exp\left[y(4\,\mathrm{tg}^{-1}\,y-\pi)\right]}{\sinh(\pi y)}\cdot I^2\,.$$

$$(4) \qquad P_A^P(L) = \frac{\pi\alpha c}{a_0}\frac{2^4}{\mu^2}\left(\frac{Z^*}{Z}\right)^2 \frac{\mathrm{Max}\,(l_1, l_2)}{3(2l_1+1)}\frac{y^2(4+5y^2)(4+3y^2)}{(4+y^2)^3}\cdot$$
$$\cdot\frac{\exp\left[y(4\,\mathrm{tg}^{-1}(y/2)-\pi)\right]}{\sinh(\pi y)}\cdot I^2\,,$$

where

$$y = \frac{Z^*\alpha}{\sqrt{(T/m_e c^2)^2 + (2T/m_e c^2)}}\,,$$

$$\mu = m_\mu/m_e\,,$$

and T is the kinetic energy of the emitted Auger-electron.

A.3. – Auger S-transitions.

The most general formula for the S-transition rate ($n_1 l \to n_2 l$) has been calculated. The only approximation which was made was to describe the final free electron by a plane wave function. The result is

$$(5) \qquad P_A^S(K) = \frac{\alpha c}{a_0}\frac{1}{\mu^4}\left(\frac{Z^*}{Z}\right)^4 \frac{1}{y}\frac{2^{4l+7}}{3^2}(n_1+l)!(n_1-l-1)!\,(n_2+l)!(n_2-l-1)!\cdot$$
$$\cdot\frac{n_1^{2l+6}n_2^{2l+6}}{(n_1+n_2)^{4l+10}}\cdot Q^2\,,$$

where Q is given by the double sum

$$Q = \sum_{\lambda=0}^{n_1-l-1}\sum_{\varkappa=0}^{n_2-l-1}(-1)^{\lambda+\varkappa+1}2^{\lambda+\varkappa}\frac{1}{n_1^\lambda n_2^\varkappa}\frac{(\lambda+\varkappa+2l+2)!}{(1/n_1+1/n_2)^{\lambda+\varkappa}}\cdot$$
$$\cdot\frac{(\lambda+\varkappa)(\lambda+\varkappa+4l+7)}{\lambda!(n_1-l-1-\lambda)!\,(2l+1+\lambda)!\varkappa!(n_2-l-1-\varkappa)!\,(2l+1+\varkappa)!}\,.$$

The special case of the Auger S-transition rate for $n_2 = n_1 - 1$ and $l = n_1 - 2$ was calculated by BURBIDGE and de BORDE [9]. When applied to this particular transition, our result is practically identical with theirs whenever the plane wave approximation holds.

Note added in proof.

In connection with the interpretation of the energy-dependence of the X-ray deficiency (see end of Sect. 4), we wish to point out that cascade calculations recently completed for π-mesonic atoms indicate that the discrepancy is not a unique function of the quantum energy. The experimental π-mesonic X-ray yields agree with the calculated ones already above ~ 40 keV, in contrast with the μ-mesonic yields (Fig. 1). Thus it seems that the X-ray deficiency can hardly be due to an experimental loss of soft quanta. A full account of the calculations on π-mesonic atoms will be published soon.

RIASSUNTO (*)

Nel tentativo di ottenere una visione più approfondita del problema dei « raggi X perduti » nella cattura di mesoni μ negli elementi leggeri, si è eseguito un completo calcolo della cascata delle transizioni dei mesoni μ nell'atomo mesonico. I risultati indicano ancora una volta che le produzioni di raggi X dallo strato K al di sotto di $Z=6$ e le produzioni di raggi X dello strato L al di sotto di $Z=14$ sono molto superiori ai valori sperimentali. Come è stato notato da altri autori, la deficienza di raggi X aumenta linearmente al decrescere dell'energia quantica fra circa 90 keV e 20 keV. I valori sperimentali della produzione, sopra i 90 keV concordano con i valori calcolati, e a 20 keV risultano inferiori per un fattore di circa 5. Tuttavia si ottiene un buon accordo fra calcolo ed esperimento per i rapporti (approssimativamente indipendenti dall'energia) fra la produzione di raggi X più duri e quella di raggi X basici, purchè si faccia una opportuna scelta della distribuzione iniziale dei mesoni. Un confronto fra la produzione calcolata di elettroni di Auger ed i risultati sperimentali per le catture μ^- nelle emulsioni nucleari sembra indicare che le transizioni radiative « miste » di Auger introdotte da Ruderman sono realmente efficienti (apparentemente quasi al 100% nella diseccitazione del livello metastabile $2s$ in CNO. Se le transizioni miste hanno lo stesso effetto anche negli elementi più leggeri (Li, Be, B), il problema dei raggi X « perduti » diventa più complicato di prima. Si è anche calcolato lo spettro previsto degli elettroni di Auger per la cattura μ^- negli elementi pesanti (AgBr) delle emulsioni nucleari.

(*) *Traduzione a cura della Redazione.*

IL NUOVO CIMENTO Vol. XIX, N. 6 16 Marzo 1961

Effects of Centre-of-Mass Motion in the Nuclear Shell Model on Scattering Problems.

F. C. Barker

Research School of Physical Sciences, Australian National University - Canberra

L. J. Tassie (*)

Australian National University - Canberra
Weizmann Institute of Science - Rehovoth

(ricevuto il 9 Dicembre 1960)

Summary. — The nuclear shell model does not describe correctly the motion of the centre of mass of the nucleus. The correction due to this is considered for scattering problems, and especially for the scattering of high-energy electrons. We include the interaction of the electrons with the nuclear current and magnetization densities as well as with the charge density. The correction is obtained only for the harmonic-oscillator shell model.

1. – Introduction.

The nuclear shell model has been used in many treatments of the scattering of particles by nuclei. However, the shell-model Hamiltonian is not translationally invariant and thus does not give a correct description of the motion of the centre of mass of the nucleus. If the momentum transfer involved in a collision is sufficiently large, incorrect treatment of the centre-of-mass motion may give rise to considerable errors in the calculated cross-section. In Section 2, this effect is considered for the simplest case of the scattering of a particle by a nucleus described by the harmonic-oscillator shell model. The scattering of electrons by the nuclear charge density has been treated pre-

(*) Now at Argonne National Laboratory.

viously (1). In Section **3** this treatment is extended to include the interaction of the electron with the current density and magnetization density of the nucleus. The effects of the finite electromagnetic size of the nucleon are also included.

The Born approximation is used throughout. As the centre-of-mass correction is large only for large momentum transfer, and thus only for high energies of the incident particles, there is some justification for this approximation. However, for the scattering of electrons by the spherically symmetrical part of the nuclear charge density, accurate calculations can be carried out by using the nuclear charge distribution of reference (1).

2. – Scattering by harmonic-oscillator nucleus.

The wave function of a nucleus enclosed in a box of volume V but otherwise free is

$$\Psi(\boldsymbol{r}_1 \ldots \boldsymbol{r}_A) = \frac{1}{\sqrt{AV}} \exp\left[i\boldsymbol{K}\cdot\boldsymbol{R}\right] \Phi(\boldsymbol{r}'_1, \ldots \boldsymbol{r}'_{A-1}) , \tag{1}$$

where $\boldsymbol{R} = (1/A) \sum_{j=1}^{A} \boldsymbol{r}_j$ is the centre-of-mass co-ordinate, $\boldsymbol{r}_j$ $(j = 1, ..., A)$ are the position co-ordinates of the A nucleons, and $\boldsymbol{r}'_i = \boldsymbol{r}_j - \boldsymbol{R}$ $(j = 1, ..., A-1)$ are the relative co-ordinates. The momentum of the nucleus is $\hbar\boldsymbol{K}$. The normalization is

$$\int\ldots\int |\Psi(\boldsymbol{r}_j)|^2 \, \mathrm{d}\boldsymbol{r}_1 \ldots \mathrm{d}\boldsymbol{r}_A = 1 , \tag{2}$$

$$\int\ldots\int |\Phi(\boldsymbol{r}'_j)|^2 \, \mathrm{d}\boldsymbol{r}'_1 \ldots \mathrm{d}\boldsymbol{r}'_{A-1} = 1 . \tag{3}$$

The harmonic-oscillator shell-model wave function can be written (2)

$$\Psi_{\mathrm{SM}}(\boldsymbol{r}_1, ..., \boldsymbol{r}_A) = \mathscr{R}(\boldsymbol{R}) \, \Phi_{\mathrm{SM}}(\boldsymbol{r}'_1, ..., \boldsymbol{r}'_{A-1}) , \tag{4}$$

with Ψ_{SM} and Φ_{SM} normalized as in eq. (2) and (3) so that

$$\int |\mathscr{R}(\boldsymbol{R})|^2 \, \mathrm{d}\boldsymbol{R} = \frac{1}{A} . \tag{5}$$

(1) L. J. TASSIE and F. C. BARKER: *Phys. Rev.*, **111**, 940 (1958).
(2) J. P. ELLIOTT and T. H. R. SKYRME: *Proc. Roy. Soc.* (*London*), A **232**, 561 (1955).

It is assumed that the shell model provides a good description of the internal structure of the nucleus; *i.e.*, that

$$\Phi(\boldsymbol{r}'_k) = \Phi_{\mathrm{SM}}(\boldsymbol{r}'_k)\,. \tag{6}$$

We consider the nuclear scattering of a particle, distinguishable from the nucleons in the nucleus and interacting with them by a non-exchange, velocity-independent potential

$$V' = \sum_{k=1}^{A} v(|\boldsymbol{r} - \boldsymbol{r}_k|) \tag{7}$$

depending only on the position co-ordinates of the particles. In Born approximation, the matrix element for this scattering from state i to state f, with momentum transfer $\hbar\boldsymbol{q} = \hbar\boldsymbol{K}_f - \hbar\boldsymbol{K}_i = \hbar\boldsymbol{k}_i - \hbar\boldsymbol{k}_f$, where $\hbar\boldsymbol{k}$ is the momentum of the scattered particle, is

$$\left.\begin{aligned} M &= \int\!\dots\!\int \exp\,[-i\boldsymbol{k}_f\cdot\boldsymbol{r}]\Psi_f^*(\boldsymbol{r}_j)\sum_{k=1}^{A} v(|\boldsymbol{r}-\boldsymbol{r}_k|)\,\exp\,[i\boldsymbol{k}_i\cdot\boldsymbol{r}]\cdot \\ &\qquad\qquad \cdot\Psi_i(\boldsymbol{r}_j)\,\mathrm{d}\boldsymbol{r}\,\mathrm{d}\boldsymbol{r}_1\dots\mathrm{d}\boldsymbol{r}_A\,, \\ &= \int \exp\,[i\boldsymbol{q}\cdot\boldsymbol{r}]v(r)\,\mathrm{d}\boldsymbol{r}\cdot F(q)\,, \end{aligned}\right\} \tag{8}$$

where

$$F(q) = \int\!\dots\!\int \Psi_f^*(\boldsymbol{r}_j)\sum_{k=1}^{A}\exp\,[i\boldsymbol{q}\cdot\boldsymbol{r}_k]\Psi_i(\boldsymbol{r}_j)\,\mathrm{d}\boldsymbol{r}_1\dots\mathrm{d}\boldsymbol{r}_A \tag{9}$$

is the nuclear form factor. After substituting from (1) and writing

$$\sum_{k=1}^{A}\exp\,[i\boldsymbol{q}\cdot\boldsymbol{r}_k] = \exp\,[i\boldsymbol{q}\cdot\boldsymbol{R}]\sum_{k=1}^{A}\exp\,[i\boldsymbol{q}\cdot\boldsymbol{r}'_k]\,, \tag{10}$$

where

$$\boldsymbol{r}'_A = -\sum_{k=1}^{A-1}\boldsymbol{r}'_k\,, \tag{11}$$

eq. (9) becomes

$$\begin{aligned} F(q) = \int \frac{1}{V}\exp\,[i\boldsymbol{K}_f\cdot\boldsymbol{R}]\exp\,[i\boldsymbol{q}\cdot\boldsymbol{R}]\exp\,[i\boldsymbol{K}_i\cdot\boldsymbol{R}]\mathrm{d}\boldsymbol{R}\cdot \\ \cdot\int\!\dots\!\int\Phi_f^*(\boldsymbol{r}'_j)\sum_{k=1}^{A}\exp\,[i\boldsymbol{q}\cdot\boldsymbol{r}'_k]\Phi_i(\boldsymbol{r}'_j)\,\mathrm{d}\boldsymbol{r}'_1\dots\mathrm{d}\boldsymbol{r}'_{A-1} = \\ = \int\!\dots\!\int\Phi_f^*\sum_{k=1}^{A}\exp\,[i\boldsymbol{q}\cdot\boldsymbol{r}'_k]\Phi_i\,\mathrm{d}\boldsymbol{r}'_1\dots\mathrm{d}\boldsymbol{r}'_{A-1}\,. \end{aligned} \tag{12}$$

In the usual shell-model treatment, $F_{SM}(q)$ is obtained by replacing Ψ by Ψ_{SM} in eq. (9). MARIS and TYRÉN [3] have treated high-energy nucleon scattering in this way. By using (2) and (6), this gives

$$F_{SM}(q) = A\int \mathscr{R}_f^*(\boldsymbol{R}) \exp[i\boldsymbol{q}\cdot\boldsymbol{R}]\mathscr{R}_i(\boldsymbol{R})\,\mathrm{d}\boldsymbol{R}\cdot \cdot\int\ldots\int \Phi_f^*(\boldsymbol{r}_j')\sum_{k=1}^{A}\exp[i\boldsymbol{q}\cdot\boldsymbol{r}_k']\Phi_i(\boldsymbol{r}_j')\,\mathrm{d}\boldsymbol{r}_1'\ldots\mathrm{d}\boldsymbol{r}_{A-1}'\,. \tag{13}$$

By comparison of eq. (13) and (12)

$$F(q) = F_{SM}(q)/F_R(q)\,, \tag{14}$$

where

$$F_R(q) = A\int \mathscr{R}_f^*(\boldsymbol{R})\exp[i\boldsymbol{q}\cdot\boldsymbol{R}]\mathscr{R}_i(\boldsymbol{R})\,\mathrm{d}\boldsymbol{R}\,. \tag{15}$$

If the shell-model states are non spurious in the sense of ELLIOT and SKYRME [2], then the centre of mass moves in the lowest state, and

$$\mathscr{R}_i(\boldsymbol{R}) = \mathscr{R}_f(\boldsymbol{R}) = \left(\frac{A}{\pi^3 a^6}\right)^{\frac{1}{4}}\exp\left[\frac{-AR^2}{2a^2}\right]. \tag{16}$$

The energy separation of adjacent single-nucleon states is $\hbar\omega = \hbar^2/Ma^2$. Then

$$F(q) = \exp\left(\frac{q^2a^2}{4A}\right)F_{SM}(q)\,. \tag{17}$$

3. – Scattering of electrons.

For the nuclear scattering of electrons with momentum transfer $\hbar\boldsymbol{q}$, the matrix element of the interaction can be written [4]

$$H' = \int\left(\varrho\Phi - \frac{1}{c}\boldsymbol{j}\cdot\boldsymbol{A} - \boldsymbol{M}\cdot\boldsymbol{H}\right)\mathrm{d}\boldsymbol{r}\,, \tag{18}$$

where Φ, $\boldsymbol{A}$, $\boldsymbol{H}$ are the Møller fields

$$\Phi(\boldsymbol{r}) = \Phi(0)\exp[i\boldsymbol{q}\cdot\boldsymbol{r}]\,,\quad \boldsymbol{A}(\boldsymbol{r}) = \boldsymbol{A}(0)\exp[i\boldsymbol{q}\cdot\boldsymbol{r}]\,,\quad \boldsymbol{H}(\boldsymbol{r}) = \boldsymbol{H}(0)\exp[i\boldsymbol{q}\cdot\boldsymbol{r}], \tag{19}$$

---

[3] TH. A. J. MARIS and H. TYRÉN: *Nucl. Phys.*, **3**, 35 (1957).
[4] L. I. SCHIFF: *Phys. Rev.*, **96**, 765 (1954).

and ϱ, $\boldsymbol{j}$, $\boldsymbol{M}$ are respectively the nuclear charge, current, and magnetization densities,

$$\varrho(\boldsymbol{r}) = e\int\ldots\int\Psi_f^* \sum \varepsilon_k g_1(|\boldsymbol{r}-\boldsymbol{r}_k|)\Psi_i \,\mathrm{d}\boldsymbol{r}_1 \ldots \mathrm{d}\boldsymbol{r}_A\,, \tag{20}$$

$$\boldsymbol{j}(\boldsymbol{r}) = \frac{\hbar e}{2Mi}\int\ldots\int\sum \varepsilon_k g_1(|\boldsymbol{r}-\boldsymbol{r}_k|)\,\{\Psi_f^*\nabla_k\Psi_i - \Psi_i\nabla_k\Psi_f^*\}\,\mathrm{d}\boldsymbol{r}_1 \ldots \mathrm{d}\boldsymbol{r}_A\,, \tag{21}$$

$$\boldsymbol{M}(\boldsymbol{r}) = \frac{e\hbar}{2Mc}\int\ldots\int\Psi_f^* \sum g_2(|\boldsymbol{r}-\boldsymbol{r}_k'|)\,\mu_k\boldsymbol{\sigma}_k\Psi_i \,\mathrm{d}\boldsymbol{r}_1 \ldots \mathrm{d}\boldsymbol{r}_A\,. \tag{22}$$

The functions g_1, g_2 describe respectively the charge and magnetization density distributions of the nucleons [5,6]

$$\int g_1(\chi)\,\mathrm{d}\boldsymbol{\chi} = \int g_2(\chi)\,\mathrm{d}\boldsymbol{\chi} = 1\,,$$

and $\varepsilon_k = 0$, 1 and $\mu_k = -1.91$, $+2.79$ for neutron and proton, respectively. It is assumed that the neutron charge density is identically zero [5].

SCHIFF [4] has shown that there are two contributions to the scattering: i) with $\Delta M = 0$; ii) with $\Delta M = \pm 1$. ΔM is the change in the nuclear spin component along the direction of $\boldsymbol{q}$. The first type is referred to as charge scattering and the second as scattering by the nuclear current and magnetization density. These terms are used because, *in the Coulomb gauge*, the $\Delta M = 0$ scattering is given by the first term of eq. (18) and the $\Delta M = \pm 1$ scattering by the other two terms. The treatment of Section **2** can be applied directly to the scattering with $\Delta M = 0$, but further consideration is needed for the $\Delta M = \pm 1$ scattering because of the gradient operators occurring in $\boldsymbol{j}$.

The second term of (18) can be written

$$-\frac{1}{e}\int \boldsymbol{j}\cdot\boldsymbol{A}\,\mathrm{d}\boldsymbol{r} = -\frac{\hbar e}{2Mci}\,\boldsymbol{A}(0)\cdot\boldsymbol{F}_1(q)\int\ldots\int\sum_{k=1}^{A}\varepsilon_k \exp\,[i\boldsymbol{q}\cdot\boldsymbol{r}_k]\cdot \tag{23}$$
$$\cdot\{\Psi_f^*\nabla_k\Psi_i - \Psi_i\nabla_k\Psi_f^*\}\,\mathrm{d}\boldsymbol{r}_1 \ldots \mathrm{d}\boldsymbol{r}_A\,,$$

where

$$F_1(q) = \int \exp\,[i\boldsymbol{q}\cdot\boldsymbol{x}]g_1(x)\,\mathrm{d}\boldsymbol{x}\,, \tag{24}$$

---

[5] R. HOFSTADTER, F. BUMILLER and M. R. YEARIAN: *Rev. Mod. Phys.*, **30**, 482 (1958).

[6] R. HOFSTADTER, F. BUMILLER and M. CROISSIAUX: *Phys. Rev. Lett.*, **5**, 263 (1960).

is the charge form factor of the proton. Using

$$\nabla_k = \frac{1}{A}\nabla_R + \nabla'_k - \frac{1}{A}\sum_{j=1}^{A-1}\nabla'_j\,, \qquad (\nabla'_A \equiv 0)\,, \tag{25}$$

and proceeding as in Section **2**, we find

$$-\frac{1}{c}\int \boldsymbol{j}\cdot\mathrm{A}\,\mathrm{d}\boldsymbol{r} = \tag{26}$$

$$= -\frac{he}{2Mci}F_1(q)\,\boldsymbol{A}(0)\int\ldots\int\sum_{k=1}^{A}\varepsilon_k \exp\left[i\boldsymbol{q}\cdot\boldsymbol{r}'_k\right]\left\{\frac{i}{A}\,(\boldsymbol{K}_i+\boldsymbol{K}_f)\,\Phi_f^*\Phi_i + \right.$$

$$\left. + \Phi_f^*\left(\nabla'_k - \frac{1}{A}\sum_{j=1}^{A-1}\nabla'_j\right)\Phi_i - \Phi_i\left(\nabla'_k - \frac{1}{A}\sum_{j=1}^{A-1}\nabla'_j\right)\Phi_f^*\right\}\mathrm{d}\boldsymbol{r}'_1\ldots\mathrm{d}\boldsymbol{r}'_{A-1}\,.$$

The gauge can be chosen so that

$$(\boldsymbol{K}_i + \boldsymbol{K}_f)\cdot\boldsymbol{A} = 0\,. \tag{27}$$

In laboratory co-ordinates, $\boldsymbol{K}_i = 0$, and (27) is then the condition for the Coulomb gauge

$$\boldsymbol{q}\cdot\boldsymbol{A} = 0\,.$$

The term depending on the recoil momentum of the nucleus then vanishes.

The other two terms of eq. (18) can be treated similarly to give

$$H' = F_1(q)\int\left(\varrho_{\mathrm{int}}\Phi - \frac{1}{c}\,\boldsymbol{j}_{\mathrm{int}}\cdot\boldsymbol{A} - \frac{F_2(q)}{F_1(q)}\,\boldsymbol{M}_{\mathrm{int}}\cdot\boldsymbol{H}\right)\mathrm{d}\boldsymbol{r}\,, \tag{28}$$

where

$$\varrho_{\mathrm{int}}(\boldsymbol{r}) = e\int\ldots\int\Phi_f^*\sum_{k=1}^{A}\varepsilon_k\,\delta(\boldsymbol{r}-\boldsymbol{r}'_k)\,\Phi_i\,\mathrm{d}\boldsymbol{r}'_1\ldots\mathrm{d}\boldsymbol{r}'_{A-1}\,, \tag{29}$$

$$\boldsymbol{j}_{\mathrm{int}}(\boldsymbol{r}) = \frac{\hbar e}{2Mi}\int\ldots\int\sum_{k=1}^{A}\varepsilon_k\,\delta(\boldsymbol{r}-\boldsymbol{r}'_k)\cdot \tag{30}$$

$$\cdot\left\{\Phi_f^*\left(\nabla'_k - \frac{1}{A}\sum_{j=1}^{A-1}\nabla'_j\right) - \Phi_i\left(\nabla'_k - \frac{1}{A}\sum_{j=1}^{A-1}\nabla'_j\right)\right\}\mathrm{d}\boldsymbol{r}'_1\ldots\mathrm{d}\boldsymbol{r}'_{A-1}\,,$$

$$\boldsymbol{M}_{\mathrm{int}}(\boldsymbol{r}) = \frac{e\hbar}{2Mc}\int\ldots\int\Phi_f^*\sum_{k=1}^{A}\delta(\boldsymbol{r}-\boldsymbol{r}_k)\,\mu_k\boldsymbol{\sigma}_k\,\Phi_i\,\mathrm{d}\boldsymbol{r}'_1\ldots\mathrm{d}\boldsymbol{r}'_{A-1}\,. \tag{31}$$

We now obtain H'_{SM} by using harmonic-oscillator shell-model wave functions and neglecting the finite size of the nucleons, *i.e.*, in eq. (20), (21) and (22),

Ψ in replaced by Ψ_{SM} and $g(|\boldsymbol{r}-\boldsymbol{r}_k|)$ is replaced by $\delta(\boldsymbol{r}-\boldsymbol{r}_k)$. For non-spurious shell-model states there is no current associated with the centre-of-mass motion, and proceeding as in Section **2**, we find

$$H'_{\text{SM}} = F_R(q)\int\left(\varrho_{\text{int}}\Phi - \frac{1}{c}\boldsymbol{j}_{\text{int}}\cdot\boldsymbol{A} - \boldsymbol{M}_{\text{int}}\cdot\boldsymbol{H}\right)\mathrm{d}\boldsymbol{r}\ . \tag{32}$$

Experiments indicate [5] that $F_1(q) = F_2(q)$ for $q^2 < 7\cdot10^{26}\ \text{cm}^{-2}$, and comparison of (32) and (28) then shows that

$$F(q) = \frac{F_1(q)}{F_R(q)}\,F_{\text{SM}}(q). \tag{33}$$

Most experiments on complex nuclei have been in this region.

For $q^2 \geqslant 7\cdot10^{26}\ \text{cm}^{-2}$, recent experiments [6] have indicated that $F_1(q) \neq F_2(q)$ and the simple result (33) is no longer valid. Also, for such large momentum transfers, it is not yet known if the charge scattering by the neutron is still negligible.

4. – Non-separable shell model.

For shell-model potentials other than the harmonic oscillator, the shell-model wave function is not separable in centre-of-mass and internal co-ordinates. Thus the method used here for correcting for the motion of the centre-of-mass cannot be used for other shell-model potentials.

RIASSUNTO (*)

Il modello nucleare a strati non descrive correttamente il moto del centro di massa del nucleo. La correzione dovuta a questo fatto viene presa in considerazione nei problemi di scattering, e specialmente per lo scattering degli elettroni di alta energia. In questi comprendiamo l'interazione degli elettroni con le densità di corrente e di magnetizzazione nucleari ed anche con la densità di carica. La correzione viene ottenuta solo per il modello ad oscillatore armonico a strati.

(*) *Traduzione a cura della Redazione.*

Frequency of the Decay Mode $\Sigma^+ \to p + \gamma$ (*).

J. Schneps (**)

Tufts University - Medford, Mass.
Istituto di Fisica dell'Università - Padova

Y. W. Kang

Tufts University - Medford, Mass.

(ricevuto il 9 Dicembre 1960)

Summary. — We have searched for events which could be attributed to the rare mode of decay $\Sigma^+ \to p + \gamma$. These events in nuclear emulsion will give a proton of unique range 3045 μm. We have found four events consistent with this interpretation in a sample which contained 264 normal decays $\Sigma^+ \to p + \pi^0$. Taking into account background which could come from Σ^- one-prong stars or decays in flight of very slow Σ^+ in the normal way, we estimate the frequency of $\Sigma^+ \to p + \gamma$ to be about 1% that of $\Sigma^+ \to p + \pi^0$.

It is expected that the Σ^+ hyperon, in addition to the usual modes of decay, $\Sigma^+ \to p + \pi^0$ and $\Sigma^+ \to n + \pi^+$, should also decay according to the more rare mode $\Sigma^+ \to p + \gamma$ [1-4]. A Σ^+ hyperon decaying in standard nuclear emulsion via this mode will give rise to a proton of unique range, 3045 μm [5], whereas the range of a proton from the decay $\Sigma^+ \to p + \pi^0$ is 1677 μm.

We have scanned a stack containing about 15000 stars produced by K^--

(*) Supported in part by the United States Atomic Energy Commission.

(**) Part of this work was done while the author was a National Science Foundation Fellow at the University of Padova.

(1) M. Kawaguchi and K. Nishijima: *Prog. Theor. Phys.*, **15**, 182 (1956).
(2) C. Iso and M. Kawaguchi: *Prog. Theor. Phys.*, **16**, 177 (1956).
(3) R. E. Behrends: *Phys. Rev.*, **111**, 1691 (1958).
(4) P. Prakash and A. H. Zimerman: *Nuovo Cimento*, **11** 869 (1959).
(5) W. H. Barkas: *Nuovo Cimento*, **8**, 201 (1958).

mesons at rest for events of the type $\Sigma^+ \to p+\gamma$. All tracks (except minimum tracks) from the K^- stars were followed out and events which appeared to be a decay from rest of a Σ into a proton were recorded. Included in these events were normal $\Sigma^+ \to p+\pi^0$ decays, $\Sigma^+ \to p+\gamma$ decays if they exist, and a background. The background consists mainly of Σ^- one-prong stars and also may include some decays in flight of very slow Σ^+ into $p+\pi^0$. This background can give events in which the proton has a range of about 3 000 μm and therefore simulate $\Sigma^+ \to p+\gamma$ events. In order to determine the ratio $\Sigma^+ \to p+\gamma / \Sigma^+ \to p+\pi^0$ the size of this background must be known. For the purpose of minimizing the number of Σ^- one-prong stars in the background each event was carefully scrutinized for evidence of a short recoil or an Auger electron. Further, a constant sagitta scattering measurement was made on all clean events with range over 2 000 μm, to eliminate when possible those cases where the one prong might be a deuteron or triton. Of course all events which could be interpreted as decays in flight were also excluded. This leaves in the background clean Σ^- one-prong (proton) stars and decays in flight of very slow Σ^+ into $p+\pi^0$ which could not be distinguished from decays at rest (*).

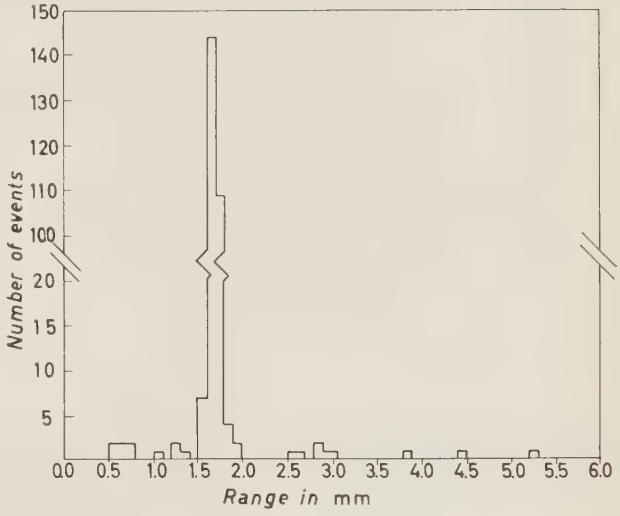

Fig. 1. – Range distribution of protons from one-prong Σ events.

In Fig. 1 is shown a histogram of the range distribution of protons from one-prong events from $R=500\,\mu$m to $R=6000\,\mu$m, using 100 μm intervals. There is seen to be a clustering in the neighborhood of 3 000 μm where there are 4 events which have ranges consistent with a $\Sigma^+ \to p+\gamma$ decay. The ranges of these 4 events in microns are 2 859, 2 983, 2 865, 3 077, and each of them has a measurement error of the order of 2%. The mean value is $2\,946 \pm 52$ where the standard deviation of the mean is quoted.

If we assume the background to be uniform between $R = 2\,000$ and $R = 4\,000$ μm then the average number of background events per 100 μm

(*) For example, a Σ^+ of residual range only $(10 \div 20)$ μm, decaying into $p+\pi^0$, could give a proton of 3 000 μm range.

interval is 0.35 if all events are considered to be background and 0.15 if the 4 events are considered to be $\Sigma^+ \to p + \gamma$. The r.m.s. deviation of the range distribution for our $\Sigma^+ \to p + \pi^0$ events is about 3% due to straggling and errors of measurement. Assuming the same value to hold for protons from $\Sigma^+ \to p + \gamma$ decays, then one standard deviation is about 100 μm. We consider events within two standard deviations of the expected mean range to be consistetn with a $\Sigma^+ \to p + \gamma$ decay, *i.e.*, we consider the region $R = (3045 \pm 200)$ μm.

From the estimate of background made above we would expect to find from 0.6 to 1.4 background events in this region whereas we find a total of 4. This indicates that most likely three of the events are $\Sigma^+ \to p + \gamma$. The total number of $\Sigma^+ \to p + \pi^0$ decays is 264. Therefore the estimated ratio of $p + \gamma$ decays to $p + \pi^0$ decays is 3/264 or about 1%. This is about ½% of all Σ^+-decays. Of course, since the statistics are poor, we cannot give too great a weight to this result. However, it is strengthened by the fact that it is consistent with a result recently reported by QUARENI *et al.* [6], who also estimated 1%. GLASSER *et al.* [7] and FREDEN *et al.* [8] who studied much smaller samples found no evidence for the $\Sigma^+ \to p + \gamma$ decay.

* * *

The authors wish to thank Dr. S. GLASHOW who first brought this question to their attention. One of them (J.S.) wishes to thank Professor N. DALLAPORTA, Professor M. CEOLIN and members of the emulsion group at the University of Padova for their hospitality and help during his stay there. We also are very grateful to Prof. E. J. LOFGREN for making the exposure at the Bevatron possible.

---

[6] G. QUARENI, A. QUARENI VIGNUDELLI, G. DASCOLA and S. MORA: *Nuovo Cimento*, **14**, 1179 (1959).

[7] R. G. GLASSER, N. SEEMAN and G. A. SNOW: *NRL Quarterly on Nuclear Science and Technology* (April 1960).

[8] S. C. FREDEN, H. N. KORNBLUM and R. S. WHITE: *Nuovo Cimento*, **16**, 611 (1960).

RIASSUNTO (*)

Abbiamo fatto ricerca di eventi che potessero essere attribuiti al raro modo di decadimento $\Sigma^+ \to p + \gamma$. Questi eventi daranno in emulsioni nucleari un protone con un range unico di 3045 μm. Abbiamo trovato quattro eventi corrispondenti a questa interpretazione in un campione che conteneva 264 decadimenti normali $\Sigma^+ \to p + \pi^0$. Tenendo conto del fondo che può provenire da stelle Σ^- ad un solo ramo o da normali decadimenti in volo di Σ^+ molto lenti, stimiamo che la frequenza del decadimento $\Sigma^+ \to p + \gamma$ sia circa 1% di quella del $\Sigma^+ \to p + \pi^0$.

(*) *Traduzione a cura della Redazione.*

Proposal for the Determination of the Mesonic Mean Square Radius of Nucleons from « Knock-On » Pion Production.

G. Domokos

Central Research Institute for Physics - Budapest

(ricevuto il 19 Dicembre 1960)

Summary. — A method is proposed to determine the mesonic m.s. radius of nucleons from the differential cross-section of « knock-on » pion production. The essence of the method consists in extrapolating the differential cross-section as a function in the nucleon recoil momentum to unphysical values. The size of the unphysical region decreases with increasing primary energy. Possible limitations of the method are discussed briefly.

1. – Introduction.

Recent experimental data seem to indicate that pion production through pion-pion interaction and one-pion exchange with the nucleon form a considerable fraction of inelastic pion-nucleon events at an incident pion energy of several GeV/s (1). Proposals concerning the determination the of pion-pion coupling constant from this process have been made by Goebel (2). In the present note we propose to use the same process for the determination of the pion-nucleon vertex function, or rather, the mesonic m.s. radius of the nucleon. In fact, as it will be seen—from a certain point of view—, the above-mentioned process shows a striking similarity to the electron-nucleon scattering which in turn has been made use of by Hofstadter and coworkers to determine the electromagnetic structure of the nucleon.

(1) V. Petrzilka: *Report at the 10-th International Conference on High Energy Physics* (Rochester, 1960); G. Domokos, A. Frenkel and P. Surányi: *Proceedings of the Conference on High Energy Physics* (Weimar, September 1960), to be published.

(2) Ch. Goebel: *Phys. Rev. Lett.*, **1**, 337 (1958).

In what follows, we use a—perhaps oversimplified—model in our calculations which, nevertheless, seems to be an appropriate one from our point of view, *scil.* the simplifications introduced do not influence the information to be obtained on nucleon structure.

2. – The differential cross-section of knock-on pion production.

Neglecting isotopic variables, we deal with the interaction of a fermion field of spin one half (nucleons) with a pseudoscalar boson field (pions). A direct self-interaction of the pion field is allowed with a four-pion basic vertex.

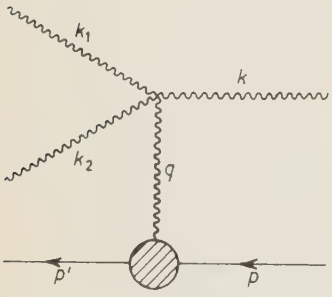

Fig. 1. – Feynman diagram of pion production by means of pion-pion interaction and one-meson exchange with the nucleon (« knock-on » pion production).

In ref. [1] there were given simple criteria which enable one to select those events from a certain experimental material, where the incident pion « collides with one virtual pion » in the proper field of the target nucleon. The Feynman diagram corresponding to this process is shown in the figure. Denote by k, k_1, k_2 the four-momenta of the incident and two outgoing pions respectively, by p and p' those of the incident and outgoing nucleon and by q the four-momentum of the virtual pion. M and μ stand for the masses of the nucleon and pion respectively.

From momentum conservation we have [3]

$$q^2 = 2M(M - \sqrt{\boldsymbol{q}^2 + M^2}) < 0 \,. \tag{2.1}$$

For not too high values of $\boldsymbol{q}^2$ one has approximately:

$$q^2 \approx -\boldsymbol{q}^2 \,. \tag{2.2}$$

In consequence of the fact that q is always space-like, we can use an « uncorrected » propagator for the virtual pion. This may be seen as follows.

The meson propagator, as a function of complex q^2, possesses the well-known spectral representation:

$$\Delta'_c(q^2) = \frac{1}{\mu^2 - q^2} + (\mu^2 - q^2)\int_{9\mu^2}^{\infty} \mathrm{d}\varkappa^2 \, \frac{\varrho(\varkappa^2)}{(\mu^2 - \varkappa^2)(\varkappa^2 - q^2)} \,. \tag{2.3}$$

(3) We use a metric tensor: $g^{00} = 1$, $g^{ik} = -ik$. $\boldsymbol{q}$ is simply the recoil momentum of the nucleon in the L.S.

Because of condition (2.1), q^2 cannot get into the neighbourhood of the branch point, so the pole will be the nearest singularity.

Further, one can estimate the contribution of the three-pion state to $\Delta_c'(q^2)$ with the help of a perturbation calculation of $\varrho(\varkappa^2)$. Assuming a four-pion contact interaction with coupling constant λ, one finds in the neighbourhood of $q^2 = 0$ (this will be the region of interest)

$$\Delta_c'(q^2) \approx \frac{1}{\mu^2 - q^2}\left(1 + \frac{\lambda^2}{4\pi}\frac{0.1}{32\pi^3}\right). \tag{2.4}$$

Even if one assumes $\lambda^2/4\pi \approx 10$, the correction will be small and a multiplicative factor only.

We notice further that as the nucleons emerging from the pion-nucleon vertex are free ones so that they satisfy the free Dirac equation, the only invariant formed from p_μ, $p_{\mu'}$ and γ_μ, which is not reduced to M or M^2, is (pp'). So, if one assumes a spectral representation to hold in q^2, one may write the pion-nucleon vertex function as follows:

$$\Gamma(q^2) = \frac{g}{(4\pi)^{\frac{1}{2}}}\gamma^5\left[1 - q^2\int_{9\mu^2}^{\infty} \mathrm{d}\nu^2\, \frac{\sigma(\nu^2)}{\nu^2(\nu^2 - q^2)}\right]. \tag{2.5}$$

From this expression we find

$$\Gamma(q^2) = \frac{g}{(4\pi)^{\frac{1}{2}}}\gamma^5\left(1 + \frac{1}{6}\langle r^2\rangle q^2 + \ldots\right), \tag{2.6}$$

where $\langle r^2\rangle$, the m.s. radius is expressed with help of the spectral density as follows:

$$\frac{1}{6}\langle r^2\rangle = \int_{9\mu^2}^{\infty}\frac{\mathrm{d}\nu^2}{\nu^4}\,\sigma(\nu^2)\,. \tag{2.7}$$

Assuming again a constant $\pi\pi$-interaction with coupling constant λ, after a straightforward calculation one finds the differential cross-section in L. S.:

$$\frac{\mathrm{d}^3\sigma}{\mathrm{d}k_1^0\,\mathrm{d}\Omega_1\,\mathrm{d}\Omega_2} = \frac{\sigma_0}{M}\,f(\boldsymbol{q}^2)\,\frac{k_1 k_2}{k}\left(1 - \frac{1}{3}\langle r^2\rangle \boldsymbol{q}^2 + \ldots\right), \tag{2.8}$$

where the function $f(\boldsymbol{q}^2)$ arises from kinematic factors and from the meson

propagator and is of the form

$$f(\boldsymbol{q}^2) = \left(\frac{M}{\mu}\right)^4 \frac{M^4(M+\sqrt{\boldsymbol{q}^2+M^2})}{\sqrt{\boldsymbol{q}^2+M^2}[2M^2-\mu^2-2M\sqrt{\boldsymbol{q}^2+M^2}]^2}, \tag{2.9}$$

$$\sigma_0 = M^{-2}(8\pi)^{-1}\frac{g^2}{4\pi}\frac{\lambda^2}{4\pi}\,\mathrm{mb} = 0.26\,\lambda^2/4\pi\,\mathrm{mb} \qquad \text{(we assume } g^2/4\pi = 16\text{)}.$$

In order to determine λ^2 and $\langle r^2\rangle$, one has to measure the differential cross-section as a function of $\boldsymbol{q}^2$, the nucleon recoil momentum and extrapolate it to the unphysical values $\boldsymbol{q}^2 = 0$. If one plots the function

$$\varphi(\boldsymbol{q}^2) \equiv \frac{k}{k_1 k_2}\cdot(f(\boldsymbol{q}^2))^{-1}\frac{\mathrm{d}^3\sigma}{\mathrm{d}k_1^0\,\mathrm{d}\Omega_1\,\mathrm{d}\Omega_2}, \tag{2.10}$$

one should obtain a straight line in $\boldsymbol{q}^2$. (High values of $\boldsymbol{q}^2$ are rather improbable, as $f(\boldsymbol{q}^2)$ strongly decreases.) The intersection with the ordinate axis gives one λ^2, while the slope is proportional to $\langle r^2\rangle$, as it can be seen from the corresponding formulas.

3. – Discussion.

As we have mentioned in the previous section, one has to extrapolate the function $\varphi(\boldsymbol{q}^2)$ through an unphysical region to $\boldsymbol{q}^2 = 0$. The unphysical region is the smaller the higher the incident pion energy is; this suggests that one should use high energy pion beams to perform the measurement of the nucleon size. As far as one can select the events of interest correctly, no disturbing effects are expected to occur. In our case the situation is different from the nucleon-nucleon elastic scattering, where a diffraction scattering may suppress completely the one-meson contribution [4].

As we have seen in Section 2, the propagator correction is expected to be rather small; besides as one can easily see from (2.4) and the figure, in the neighbourhood of $\boldsymbol{q}^2 = 0$ it influences the measured value of λ^2 only and not $\langle r^2\rangle$. A correction to $\langle r^2\rangle$ may arise if the « contact approximation » of the pion-pion vertex is not valid. Perturbation theory suggests that the pion-pion vertex possesses a spectral representation in $\boldsymbol{q}^2$ (the other pion variables being on the mass shell) similar to (2.5). In that case the coefficient of $\frac{1}{3}q^2$ in (2.8)

[4] Cf. G. F. Chew: *Phys. Rev.*, **112**, 1380 (1958), especially Sec. IV.

would change to $\langle r^2 \rangle + a^2$, where a^2 is the « m.s. radius » associated with the four-pion vertex. On the basis of a perturbation calculation the value of a^2, however, is expected to be small.

We have not dealt with the complications arising from the isotopic structure of the amplitude, as with our present knowledge about the structure of the four-pion vertex, the discussion of this point seems to us premature.

Summarizing, we believe that the method outlined here offers a direct possibility for the determination of the « mesonic size » of nucleons.

* * *

The author is indebted to Messrs. A. FRENKEL and P. SURÁNYI for interesting discussions on the subject.

RIASSUNTO (*)

Si propone un metodo per determinare dalla sezione d'urto differenziale nella produzione di pioni di « knock-on » il raggio quadratico medio mesonico dei nucleoni. Il metodo consiste essenzialmente nell'estrapolare sino a valori non fisici la sezione d'urto differenziale espressa in funzione del momento di rinculo del nucleone. L'estensione della regione non fisica decresce al crescere dell'energia primaria. Si discutono brevemente alcune possibili limitazioni del metodo.

(*) *Traduzione a cura della Redazione.*

IL NUOVO CIMENTO Vol. XIX, N. 6 16 Marzo 1961

Towards a Two-Field Theory of Elementary Particles.

R. E. Marshak (*) and S. Okubo (**)

CERN - Geneva

(ricevuto il 23 Dicembre 1960)

Summary. — It is shown why the symmetry principle between the baryon triplet (Anp) and lepton triplet (μ e ν) suggests a two-field theory of elementary particles. One massless spinor field is used to describe the nucleons and light leptons and a second spinor field with finite bare mass the « strange » particles Λ and μ. The two-field model resembles the theories of Heisenberg and Nambu in several respects but there are also important differences which are spelled out.

1. – Introduction.

The number of particles (π, K, $\mathcal{N}$, Λ, Σ, Ξ) which participate in the strong interactions is certainly much larger than the number of invariance principles which characterize these interactions. If we leave aside for the moment the discrete transformations P, C, T (which are associated with the improper Lorentz group), we find that the strong interactions are invariant under two independent gauge transformations (baryon and strangeness) and the isospin rotation group; this follows from the well-known fact that the charge number is related to the baryon and strangeness numbers and the third component of the isospin through the Gell-Mann–Nishijima equation:

$$Q = I_3 + \frac{S+B}{2}. \tag{1}$$

Hence, insofar as the integral degrees of freedom are concerned, all the strongly

(*) Guest Professor under the Ford Foundation and Guggenheim Fellow, on leave from the University of Rochester for the academic year 1960/61.

(**) Supported by National Science Foundation, U.S.A.

interacting particles can be represented by three fields: two fields comprising an isospinor and one field with unit baryon number (if the isospinor is K) or unit strangeness (if the isospinor is $\mathcal{N}$ or Ξ). While SAKATA's [1] choice of the baryon triplet (Λ, n, p) as the three fundamental fields is evidently not unique, it has several advantages as we shall see below.

Although a three-field theory such as Sakata's satisfies all the group-theoretic requirements [2] of the strong interactions, there still remain the particles which do not interact strongly at all, namely the leptons. At first sight, the number of additional fundamental fields required to describe the leptons is also three in number: in order to take account of the charge and lepton gauge transformations as well as the « strange » difference between the muon and the electron; it is natural to choose the observed lepton triplet (μ^-, e^-, ν) as the three fundamental lepton fields. If we introduce formally an isospin space and strangeness gauge transformation for the leptons, the analogue of the Gell-Mann–Nishijima equation becomes:

$$Q = I_3 + \frac{S - L}{2} \tag{1a}$$

where μ^- is an $S = -1$ isoscalar and (e^-, ν) is an $S = 0$ isospinor. The correspondence between Sakata's baryon triplet (Λ, n, p) and the lepton triplet (μ^-, e^-, ν) is now apparent; indeed, eq. (1) and (1*a*) can be consolidated into the single relation [3,4]:

$$Q = I_3 + \frac{S + B - L}{2}. \tag{1b}$$

Furthermore, the implications of the symmetry principle $\Lambda \leftrightarrow \mu^-$, $n \leftrightarrow e^-$, $p \leftrightarrow \nu$ (hereinafter called the BL symmetry principle) for the weak interactions have been discussed in detail [3]. It is also possible to extend the BL symmetry principle to electromagnetic interactions (*e.g.* the absence of a *fast* $\Lambda \to n + \gamma$ decay implies the similar absence of a *fast* $\mu^- \to e^- + \gamma$ decay).

The Nagoya group [5] has attempted to construct a four-field theory for

---

[1] S. SAKATA: *Prog. Theor. Phys.*, **16**, 686 (1956); This type of theory is similar to that of E. FERMI and C. N. YANG: *Phys. Rev.*, **76**, 1739 (1949); cfr. also M. M. LÉVY and R. E. MARSHAK: *Suppl. Nuovo Cimento*, **11**, 366 (1954).

[2] W. E. THIRRING: *Nucl. Phys.*, **10**, 97 (1959); see also Y. YAMAGUCHI: *Prog. Theor. Phys. Suppl.*, **11**, 1, 37 (1959); and M. IKEDA, S. OGAWA and Y. OHNUKI: *Prog. Theor. Phys.*, **22**, 715 (1959); and **23**, 1073 (1960).

[3] A. GAMBA, R. E. MARSHAK and S. OKUBO: *Proc. Nat. Acad. Sci.*, **45**, 881 (1959).

[4] V. I. GOLDANSKI: *Nucl. Phys.*, **6**, 531 (1958); O. KLEIN: *Arkiv. Swed. Acad. Sci.*, **16**, 191 (1959); I. SAAVEDRA: *Nucl. Phys.*, **10**, 6 (1959).

[5] Z. MAKI, M. NAKAGAWA, Y. OHNUKI and S. SAKATA: *Prog. Theor. Phys.*, **23**, 1174 (1960); Y. KATAYAMA and M. TAKETANI: preprint (Kyoto); M. E. MAYER: *Nuovo Cimento*, **17**, 802 (1960).

baryons and leptons on the basis of the BL symmetry principle. They assume that the four fundamental fields are the lepton triplet (μ^-, e^-, ν) plus a positively charged boson B^+ which is supposed to be « strongly » coupled to the leptons. Each member of the baryon triplet (Λ, n, p) is hypothesized to be a composite of B^+ and the corresponding lepton, *i.e.* (Λ, n, p) = $B^+(\mu^-, e^-, \nu)$. Unfortunately, the Nagoya model cannot prevent a process like $n(= B^+e^-) + \bar{p}(= B^-\bar{\nu}) \to e^- + \bar{\nu}$ from being a « strong » reaction without postulating an additional selection rule. This is not surprising since this type of theory implicitly assumes the identity of the isospin space and the strangeness gauge transformation for the baryon and lepton triplets for *all* interactions.

It would thus appear that, within the framework of the standard perturbation-theoretic treatment of interacting fields, a minimum of six fields is required to explain the group properties of the strongly interacting particles and leptons despite the BL symmetry principle. The possibility of developing a theory of elementary particles with fewer than six fields is therefore intimately connected with the invalidity of the perturbation expansion and the breakdown of the « adiabatic theorem » resulting from the infinite number of degrees of freedom in quantum field theory. These points are briefly discussed in Section **2** as the rationale for theories of the type proposed by HEISENBERG ([6]) and NAMBU ([7]). In Section **3**, we summarize and compare the essential ideas and difficulties of Heisenberg's one-field theory and Nambu's « superconductivity » theory of elementary particles; the emphasis is on the significance of the invariance principles employed by the respective authors and not on the detailed quantitative predictions of baryon and meson masses. In Section **4**, we outline our own suggestions for a possible two-field theory of elementary particles; while we take over some concepts from both the Heisenberg and Nambu theories, we ground our theory firmly in the BL symmetry between the baryon and lepton triplets. Some of the problems faced by our theory are also spelled out.

2. – Non-perturbative solutions in quantum field theory.

In quantum field theory it is customary to decompose the total Hamiltonian into two parts; the free part H_0 and the interaction part H_1:

$$H = H_0 + H_1 . \tag{2}$$

([6]) H. P. DÜRR, W. HEISENBERG, H. MITTER, S. SCHLIEDER and K. YAMAZAKI: *Zeits. Naturfor.*, **14** a, 441 (1959); hereinafter we shall call this the Heisenberg theory.

([7]) Y. NAMBU and G. JONA-LASINIO: preprint (University of Chicago); this will be referred to as the Nambu theory. Cfr. also J. GOLDSTONE: CERN preprint.

The diagonalization of H_0 is straightforward and yields the continuous energy spectrum. However, the same is not true for H, where, in general, diagonalization is impossible except for a few rather trivial examples. Nevertheless, one expects a sort of correspondence between H_0 and H which is expressed by the so-called « adiabatic theorem ». This theorem asserts that, except for possible bound states, the eigenfunctions of H can be obtained from those of H_0 by adiabatically switching on the interaction. In other words, new types of states other than those corresponding to states of H_0 should not arise except for possible bound states. The adiabatic theorem obviously holds within the framework of perturbation theory.

The HEISENBERG ([6]) and NAMBU ([7]) programmes for constructing a theory of elementary particles depend for their success upon the existence of non-perturbative solutions of the field equations and the breakdown of the adiabatic theorem. It is therefore of great importance that HAAG has proved ([8]) (Haag's theorem) that the adiabatic theorem need not hold in quantum field theory. Haag's theorem essentially states that the Hilbert space constructed from the eigenfunctions of H (so that H is a proper operator in this space) is completely inequivalent to those of H_0, or, more precisely, that the domain of H is completely disjoint from that of H_0 in some wider space (except, of course, for a null element). This fact, related as it is to the unbounded character of the interaction Hamiltonian H_1, is sufficient to invalidate the perturbation expansion and the adiabatic theorem. If H_1 were a completely continuous transformation (*i.e.* if any element f_n of the Hilbert space satisfied the condition $f_n \to f$ weakly (f is also an element of the Hilbert space) then $H_1 f_n \to H_1 f$ strongly), then the limit (roughly speaking, continuous) spectrum of H would have to agree with that of H_0 (Weyl's theorem ([9])). If this were the case, then it would be impossible to construct theories of the Fermi-Yang or Sakata type ([1]) since the continuous spectrum of the pion is lower than that of the nucleon. Thus the possibility of composite models probably depends upon the unbounded character of H_1 and the Haag theorem.

The above situation is connected with the appearance of the inequivalent representations ([10]) of the commutation rings when we have an infinite number of degrees of freedom. Suppose that we have N anti-commuting operators $a_1, ..., a_N$ and its adjoints satisfying the following commutation relations:

$$\{a_i, a_j^*\}_+ = \delta_{ij}\,, \quad \{a_i, a_j\}_+ = 0\,, \quad \{a_i^*, a_j^*\}_+ = 0 \qquad (i, j = 1, ..., N). \tag{3}$$

([8]) R. HAAG: *Kgl. Danske Videns. Selb. Mat. Fys. Medd.*, **29**, 12 (1955); P. W. HALL and A. S. WIGHTMAN: *Kgl. Danske Videns. Selb. Mat. Fys. Medd.*, **31**, 5 (1957).

([9]) See *e.g.* F. RIESZ and B. SZ. NAGY: *Functional Analysis*, 2nd. Edition (New York, 1953), pp. 367.

([10]) R. HAAG: see ref. ([8]); L. GÅRDING and A. S. WIGHTMAN: *Proc. Nat. Acad. Sci.* **40**, 617, 622 (1 54); A. S. WIGHTMAN and S. SCHWEBER; *Phys. Rev.*, **98**, 812 (1955).

When N is finite, there is only one essentially independent irreducible representation of this anticommutating ring. It is the usual representation, whose bases are the direct product $\Phi_1 \otimes \Phi_2 \otimes \ldots \otimes \Phi_N$, where Φ_i takes on only two possible values in conformity with the Pauli principle. However, when N becomes infinite, a new situation arises and we can have an infinite number of representations; *i.e.* we can have an infinite number of Hilbert spaces, which are orthogonal to each other ([11]). In some simple soluble examples ([11]), there is a one to one correspondence between the total Hamiltonian H and one of these inequivalent representations; more precisely, H is a proper operator in a subspace of only one of these Hilbert spaces. However, there is in principle no reason why H may not be a proper operator in several such Hilbert spaces which are orthogonal to each other. It is this possibility which permits one to entertain the hope that one field may be employed to describe several particles and, indeed, this is the foundation of our own theory (see Section **4**). The important point is that we must find the Hilbert space, or spaces, in which H is a proper operator (strictly speaking, only in a dense subset of these Hilbert spaces, since H is an unbounded operator). Unfortunately, this is practically impossible to accomplish at the present time since we cannot solve the problem exactly (even if there were no difficulty with the divergences). The best that we can hope to achieve is to find in a self-consistent fashion an approximate Hilbert space or spaces.

We shall illustrate the above remarks by sketching a modified version of Nambu's ([7]) procedure. Suppose, we start with the following Lagrangian:

$$\text{(4)} \qquad \begin{cases} \mathscr{L}_0 = -\,\bar{\psi}\left(\gamma\,\dfrac{\partial}{\partial x}\right)\psi\,, \\ \mathscr{L}_1 = g\,(\bar{\psi}\psi)(\bar{\psi}\psi)\,, \end{cases}$$

where ψ is an ordinary Dirac four-component spinor. Eq. (4) is different from Nambu's, since it does not include the pseudoscalar term. Now let us suppose that the correct Hilbert space $\mathscr{H}_m$ of this theory is built up from the following asymptotic field φ_m with the mass m:

$$\text{(5)} \qquad \left(\gamma\,\frac{\partial}{\partial x} + m\right)\varphi_m = 0\,.$$

In this way, we have an infinite number of Hilbert spaces $\mathscr{H}_m$ corresponding to different masses m. The problem is to find the correct (or approximately correct) Hilbert space corresponding to mass m. In the first approximation in the coupling constant g, $\mathscr{L}_1$ can be replaced by (we neglect the pairing

([11]) R. Haag: see ref. ([8]); L. Van Hove: *Physica*, **18**, 145 (1952); Y. Nambu and G. Jona-Lasinio: ref. ([7]).

of ψ and $\bar{\psi}$ belonging to other combinations, *e.g.* $\bar{\psi}\psi\widehat{\bar{\psi}\psi}$):

$$\mathscr{L}_1 \simeq 2g\langle\bar{\psi}\psi\rangle_0(\bar{\psi}\psi)\,, \tag{6}$$

where $\langle\bar{\psi}\psi\rangle_0$ denotes the vacuum expectation value with respect to the Hilbert space $\mathscr{H}_m$. Hence, we can determine the mass m in a self-consistent fashion and, in first approximation, by the formula:

$$m = -2g\langle\bar{\psi}\psi\rangle_0\,. \tag{7}$$

Furthermore, in the low mass approximation, we have:

$$\langle\bar{\psi}\psi\rangle_0 \simeq -Z_2\,\mathrm{Tr}\,S_F(0, m)\,, \tag{8}$$

where Z_2 is a renormalization constant and consequently:

$$m = 2g'\,\mathrm{Tr}\,S_F(0, m)\,. \tag{9}$$

Eq. (9) is the equation given by NAMBU, where g' is the renormalized coupling constant.

We now note that two asymptotic fields $\varphi_{\pm m}$ can be associated with ψ by following Touschek's « ansatz » [12]. Our equation of motion is:

$$\gamma\frac{\partial}{\partial x}\psi - g\left[(\bar{\psi}\psi)\psi + \psi(\bar{\psi}\psi)\right] = 0\,. \tag{10}$$

Let us put:

$$\begin{cases} \psi_1 = \psi\,, \\ \psi_2 = g[(\bar{\psi}\psi)\psi + \psi(\bar{\psi}\psi)]\,. \end{cases} \tag{11}$$

Then the equation of motion is:

$$\gamma\frac{\partial}{\partial x}\psi_1 - \psi_2 = 0\,. \tag{10a}$$

Now suppose that ψ_1 and ψ_2 go asymptotically to φ_1 and φ_2 respectively and

[12] A. TOUSCHEK: *Nuovo Cimento*, **13**, 394 (1959); in this paper TOUSCHEK also shows that, under certain conditions, a doubling of states is necessary for a finite mass particle independent of the approximation when one starts with a two-component field.

that moreover:

$$\gamma \frac{\partial}{\partial x} \psi_1 \xrightarrow[\text{(weakly)}]{} \gamma \frac{\partial}{\partial x} \varphi_1 ,$$

then we have:

$$\gamma \frac{\partial}{\partial x} \varphi_1 - \varphi_2 = 0 , \tag{12}$$

where φ_1 and φ_2 are assumed to satisfy the free field equations:

$$(\Box - m^2)\varphi_1 = 0 , \qquad (\Box - m^2)\varphi_2 = 0 . \tag{13}$$

(We must modify this equation, when there exists a finite bare mass m_0; however, the final formula is similar to eq. (15)). If we operate with $\gamma(\partial/\partial x)$ on eq. (12), we get:

$$\gamma \frac{\partial}{\partial x} \varphi_2 - m^2 \varphi_1 = 0 . \tag{14}$$

Then, if we define:

$$\begin{cases} \varphi_m = \varphi_2 - m\varphi_1 , \\ \varphi_{-m} = \varphi_2 + m\varphi_1 , \end{cases} \tag{15}$$

we obtain

$$\begin{cases} \left(\gamma \frac{\partial}{\partial x} + m\right) \varphi_m = 0 , \\ \left(\gamma \frac{\partial}{\partial x} - m\right) \varphi_{-m} = 0 . \end{cases} \tag{16}$$

Thus, we may interprete φ_m and φ_{-m} as the asymptotic fields corresponding to the two solutions m and $-m$ (except for a trivial numerical factor). Furthermore, we can show that the two Hilbert spaces $\mathscr{H}_m$ and $\mathscr{H}_{-m}$ are orthogonal (7) and that all matrix elements of $\varphi_{\pm m}$ with respect to $\mathscr{H}_{\mp m}$ must be zero. We can check this in the same approximation in which we derived the mass m, since:

$$\begin{aligned} (\Phi^*_{(\mp m)}, \varphi_{\pm m} \Phi'_{(\mp m)}) &\simeq (\Phi^*_{(\mp m)}, (\psi_2 \mp m\psi_1)\Phi'_{(\mp m)}) \simeq \\ &\simeq [-2g' \operatorname{Tr} S_F(0, \mp m) \mp m](\Phi^*_{(\mp m)}, \psi\Phi'_{(\mp m)}) \equiv 0 , \end{aligned} \tag{17}$$

by virtue of eq. (9). In the above, $\Phi_{(\mp m)}$ and $\Phi'_{(\mp m)}$ are any arbitrary vectors belonging to $\mathscr{H}_{\mp m}$. Of course, these are not rigorous statements but illustrate the type of non-perturbative self-consistent result which is possible.

We have interpreted the two Nambu solutions $\pm m$ as corresponding to

two independent fields whose asymptotic fields are given by φ_{+m} and φ_{-m}. However, this interpretation has several difficulties. One difficulty is that we cannot do the same for the $m = 0$ solution of eq. (9). For $m = 0$, the corresponding asymptotic field φ_0 is given by $\psi \to \varphi_0$ by the same reasoning; however, we already have

$$\psi = \frac{1}{2m}(\psi_2 + m\psi_1) - \frac{1}{2m}(\psi_2 - m\psi_1) \to \frac{1}{2m}(\varphi_m - \varphi_{-m}) ,$$

which cannot be reconciled with $\psi \to \varphi_0$. To avoid this dilemma we may suppose that a single ψ may give rise to more than one asymptotic field. Then, the consequence is essentially the same as doubling the Hilbert space and extending the meaning of ψ to the larger space. We assume this to be the case in the future, whenever a similar situation arises. The second difficulty is that instead of the Lagrangian (4) we may take:

$$\mathscr{L}_1 = g[(\bar{\psi}\psi)(\bar{\psi}\psi) - (\bar{\psi}\gamma_5\psi)(\bar{\psi}\gamma_5\psi)] \tag{18}$$

which is the one adopted by NAMBU (7). If we proceed in the same way as before, the second term $\bar{\psi}\gamma_5\psi$ does not yield any contribution to eq. (9) since $\mathrm{Tr}\,\langle\bar{\psi}\gamma_5\psi\rangle_0 = 0$. Hence the conclusions should be the same as in the previous case. However, in contrast to (4), the Lagrangian (18) possesses the property of chirality invariance, namely it is invariant under the transformation:

$$\psi \to \exp[i\alpha\gamma_5]\cdot\psi . \tag{19}$$

Then, as was noted by NAMBU, this transformation is not a proper operator in a given Hilbert space $\mathscr{H}_m$. When we define $\varphi_m^{(\alpha)}$ by:

$$\left(\gamma\frac{\partial}{\partial x} + m\cdot\exp[2i\alpha\gamma_5]\right)\varphi_m^{(\alpha)} = 0 , \tag{20}$$

we can construct the Hilbert space $\mathscr{H}_m^{(\alpha)}$ from $\varphi_m^{(\alpha)}$. Then, the chirality transformation (19) brings $\mathscr{H}_m$ into $\mathscr{H}_m^{(\alpha)}$ so that now we have an infinite number of spaces $\mathscr{H}_m^{(\alpha)}$ instead of only two, $\mathscr{H}_m$ and $\mathscr{H}_{-m}$. The question now arises as to whether we should interpret this result as implying an infinite mass degeneracy or whether we should regard the total Hamiltonian as being a proper operator in only a small number of orthogonal Hilbert spaces, say $\mathscr{H}_0$, $\mathscr{H}_m$ and possibly $\mathscr{H}_{-m}$. We prefer the latter interpretation since the argument which led to the asymptotic fields $\varphi_{\pm m}$, cannot be extended to the present case. Thus, we take the view that also for eq. (18) only two independent fields $\varphi_{\pm m}$ exist and that the chirality transformation (19) is not defined in our space (since it can be shown that an operator U satisfying the relation $U^{-1}\psi U = \exp[i\alpha\gamma_5]\cdot\psi$ does not exist in our space).

3. – Comparison of the Heisenberg and Nambu theories.

Both the Heisenberg and Nambu theories derive their significance from the possible existence of non-perturbative solutions of the postulated non-linear field equation. In each case, the author deduces a finite « baryon » mass from the self-interaction of a massless field. Within the framework of perturbation theory, the possibility of a finite mass would be excluded. NAMBU argues from the physical fact of superconductivity for the existence of a solutions of his field equation which is a non-analytic function of the coupling constant ([13]) but Heisenberg's theory is equally dependent on the existence of such solutions. Indeed, from the point of view of the baryon mass calculation, the Heisenberg equation ([6]):

$$\gamma \frac{\partial}{\partial x} \psi \pm g\gamma_5\gamma_\mu\psi\bar{\psi}\gamma_5\gamma_\mu\psi = 0 , \tag{21}$$

differs in a non-essential way from Nambu's equation:

$$\gamma \frac{\partial}{\partial x} \psi - g\{\psi(\bar{\psi}\psi) + (\bar{\psi}\psi)\psi - \gamma_5\psi(\bar{\psi}\gamma_5\psi) - (\bar{\psi}\gamma_5\psi)\gamma_5\psi\} = 0 . \tag{22}$$

Heisenberg's method of approximation for dealing with eq. (21) differs in certain details from Nambu's approximation for his eq. (22) but the resulting equation for the mass has the same structure:

$$m = mf(m^2l^2) , \tag{23}$$

where l is a length characteristic of the approximation (in Heisenberg's case $l = \sqrt{g}$ whereas in Nambu's case $l =$ cut-off length - see below). Eq. (23) possesses a solution $m = 0$—which is expected within the usual perturbation-theoretic framework and which is discarded ([14]) by both HEISENBERG and

([13]) However, it must be continuous with respect to the coupling constant, in view of the theorem of Rellich (see: F. RIESZ and B. Sz. NAGY: loc. cit., pp. 169); this remark applies to the continuous spectrum of all theories.

([14]) The reasons are different for the two authors; NAMBU discards the $m=0$ solution since he believes that it is unstable on two counts: 1) the analogy with superconductivity (where the superconducting state is stable and the normal state is not) and 2) on the basis of a calculation of the difference between the divergent zero-point energies. However, neither argument is conclusive: 1) the normal state becomes as stable as the superconducting state in the limit of infinite volume of the superconductor which corresponds more closely to the elementary particle case with its infinite number of degrees of freedom and hence there is no reason why two solutions should not be

NAMBU—and a solution $m \neq 0$ defined by:

$$f(m^2 l^2) = 1 \,. \tag{24}$$

If either eq. (21) or (22) were solved by means of perturbation theory, solution (24) would not be found.

It is of some interest to compare the approximation methods of Heisenberg and Nambu in order to assess more fully the role of l in eqs. (24). This comparison becomes more perspicuous if we employ a common notation; following HEISENBERG, we define the wave function:

$$\chi(x) = \langle 0 \,|\, \psi(x) \,|\, p \rangle \,, \tag{25}$$

where $|p\rangle$ is a state with momentum p, $\langle 0|$ is the vacuum state, and we assume that somehow a Hilbert space can be defined. Then, eq. (21) and (22) can be written in the form:

$$\gamma_{\alpha\beta} \frac{\partial}{\partial x} \chi_\beta(x) = - g \sum O_{\alpha\beta} \chi(x_\beta, x_\lambda \,|\, x'_\lambda) O_{\lambda\lambda'} \,, \tag{26}$$

where $O = \gamma_5 \gamma_\mu$ (eq. (21)) and $O = 1$, $i\gamma_5$ (eq. (22)) and

$$\chi(x_\alpha, y_\beta \,|\, z_\gamma) = \langle 0 \,|\, (\psi_\alpha(x) \psi_\beta(y) \, \bar{\psi}_\gamma(z))_+ \,|\, p \rangle \tag{27}$$

with $\chi(x, x \,|\, x)$ a suitable limit of $\chi(x, y \,|\, z)$. Furthermore, we define the τ-functions by

$$\tau(x) \equiv \chi(x) = \langle 0 \,|\, \psi(x) \,|\, p \rangle \,, \tag{28}$$

$$\tau(x, y \,|\, z) \equiv \chi(x, y \,|\, z) - F(y - z) \tau(x) + F(x - z) \tau(y) \,, \quad \text{etc.} \tag{29}$$

where

$$F(x - y) = \langle 0 \,|\, (\psi(x) \, \bar{\psi}(y))_+ \,|\, 0 \rangle \,. \tag{30}$$

It follows that the τ-functions are the connected parts of the $\chi(x, y \,|\, z)$ in the usual Feynman diagram technique.

HEISENBERG and, in essence, NAMBU now have recourse to the Tamm-

---

equally stable in two orthogonal Hilbert spaces and 2) the meaning of the divergent zero-point energy is unclear at the present stage of quantum field theory. On the other hand, Heisenberg effectively discards the $m = 0$ solution since he wishes to describe the leptons by means of the « scale » transformation. Besides, in the Heisenberg theory, the propagator function is chosen in such a way that it is zero for $m = 0$ and therefore it is self-consistent to discard the $m = 0$ solution.

Dancoff approximation but at a different stage and with a different hypothesis concerning the propagator function $F(x-y)$. NAMBU simply sets $\tau(x, x|x) \equiv 0$ so that;

$$\chi(x_\alpha x_\beta | x_\gamma) \simeq F_{\gamma\beta}(0)\tau_\alpha(x) - F_{\alpha\gamma}(0)\tau_\beta(x) . \tag{31}$$

Thus, one obtains:

$$\gamma \frac{\hat{c}}{\partial x}\tau(x) = -\, 2g(\mathrm{Tr}\, F(0))\,\tau(x) . \tag{32}$$

If one now writes $\tau(x) = \exp[ipx]\cdot\tau(0)$ and $F(0) \simeq Z_2 S_F(0, m)$, eq. (32) becomes:

$$(i\gamma p)\tau(0) = -\, 2g'\ \mathrm{Tr}\, S_F(0, m)\cdot\tau(0) . \tag{33}$$

Setting $(i\gamma p)\tau(0) = -\, m\tau(0)$, eq. (33) yields eq. (9). In the Heisenberg case, by assumption, the interaction term is taken as a « Wick product » and thus one must set $F(0) = 0$; therefore if one stops with $\tau(x, y|z) = 0$ one only obtains the $m = 0$ solution. Hence, Heisenberg goes to the next Tamm-Dancoff approximation, *i.e.* he sets $\tau(x_1 x_2 x_3 | x_4 x_5) \equiv 0$. In effect, NAMBU computes the mass on the basis of the bubble diagram (Fig. 1*a*), whereas HEISENBERG uses the more complicated diagram (Fig. 1*b*).

a) Nambu theory *b*) Heisenberg theory

Fig. 1. - Diagrams used to obtain finite mass solutions.

In addition, HEISENBERG and NAMBU choose different forms of the Green's function (30). NAMBU approximates $F(x-y)$ by

$$F(x-y) \simeq Z_2 \cdot \frac{i}{(2\pi)^4}\int \mathrm{d}^4p\, \frac{i\gamma p - m}{p^2 + m^2}\, C(p^2, \Lambda^2)\exp[ip(x-y)] , \tag{34}$$

where $C(p^2, \Lambda^2)$ is a convergence factor (Λ^{-1} is the cut-off momentum) which must be inserted in order to produce a finite answer. This choice of propagator violates chirality invariance because of its dependence on m. The finite mass which follows from eq. (9) then turns out to be proportional to Λ^{-1}, *i.e.* $l = \Lambda$ in eq. (23). HEISENBERG attempts to maintain a chirality invariant propagator and convergence at the same time. This is achieved by writing down an expression for the propagator which implies an indefinite metric, namely:

$$F(x-y) \simeq \frac{+\,i}{(2\pi)^4}\int \mathrm{d}^4p(i\gamma p)\left[\frac{1}{p^2+m^2} - \frac{1}{p^2} + \frac{m^2}{(p^2)^2}\right]\exp[ip(x-y)] . \tag{34a}$$

In this unorthodox fashion, HEISENBERG can produce a finite mass which is expressed in terms of the fundamental length of the theory, *i.e.* $l = \sqrt{g}$ in eq. (23). These different choices of F reflect the different assumptions which are made by HEISENBERG and by NAMBU concerning the underlying Hilbert space.

There are some more fundamental differences between the Heisenberg and Nambu theories which are related to the interpretation of the field operator ψ. To make the point more clearly, consider the 2-component Weyl field φ:

$$\left(\sigma \frac{\partial}{\partial x}\right)\varphi = 0 \,. \tag{35}$$

It is well known that there is a one-to-one formal correspondence between the Weyl field φ and the Majorana field ψ defined by:

$$\psi = \begin{pmatrix} \varphi \\ \sigma_2 \varphi^* \end{pmatrix}. \tag{36}$$

This follows from the fact that if we use the representation for the Dirac matrices in which γ_5 is diagonal, then:

$$\gamma \frac{\partial}{\partial x}\psi = 0 \,, \qquad C^{-1}\overline{\psi} = \psi \,, \tag{37}$$

i.e. ψ is a Majorana field. This one-to-one correspondence between φ and ψ illustrates the importance of the physical interpretation of the field operator since a Weyl field does not admit the space-reflection operator whereas, for a Majorana field, particle and antiparticle are the same while space-reflection is an allowed operation. In this connection, it is convenient to distinguish between variational variables and canonical variables ([15]). Variational variables are the ones used in the variational principle for the Lagrangian with the proviso that one may adopt any arbitrary combinations as the variational variables. Thus, in the above simple example, φ or ψ can be a variational variable, but if we wish to interpret φ as a real Weyl field, then φ is canonical but not ψ. On the other hand, if we wish to interpret ψ as a real Majorana field, then ψ is canonical but not φ. The choice of canonical variable is not trivial; *e.g.* it has been shown in one simple soluble theory ([16]) that one

([15]) Such a distinction has already been made for different purposes by Y. TAKAHASHI: *Nuovo Cimento*, **1**, 414 (1955).

([16]) S. OKUBO: CERN preprint.

special choice of the canonical variable requires an indefinite metric and gives rise to divergences whereas another choice does not.

Let us now return to Heisenberg's equation:

$$\gamma \frac{\partial}{\partial x}\psi \pm g\gamma_5\gamma_\mu\psi\bar{\psi}\gamma_5\gamma_\mu\psi = 0\,. \tag{38}$$

Heisenberg uses the chirality transformation:

$$\psi \to \exp[i\alpha\gamma_5]\cdot\psi \tag{39}$$

as the generator for the fermion number N whereas Nambu uses the usual gauge transformation:

$$\psi \to \exp[i\alpha]\cdot\psi \tag{40}$$

as the generator for N. In the Heisenberg theory, the transformation (40) is a generator for the third component I_3 of the isospin rotation. Indeed, (40) is a special case of the more general so-called « Pauli-Gürsey » transformation ([17])

$$\psi \to \alpha\psi + \beta\gamma_5 C^{-1}\bar{\psi}\,, \qquad |\alpha|^2 + |\beta|^2 = 1 \tag{41}$$

which is isomorphic to the isospin rotation group.

Dürr ([18]) has shown that the transformations (39) and (41) can be written quite simply if we employ the 2-component spinors φ_1 and φ_2 (instead of the four-component ψ) defined as follows:

$$\begin{cases} \varphi_1 = \frac{1}{2}(1 + \gamma_5)\psi\,, \\ \varphi_2 = \frac{1}{2}(1 + \gamma_5)C^{-1}\bar{\psi}\,. \end{cases} \tag{42}$$

Then, eq. (38) reduces to (see Appendix):

$$\gamma \frac{\partial}{\partial x}\varphi = \pm g\sigma_\mu\varphi\varphi^*\sigma_\mu\varphi\,, \tag{43}$$

with $\varphi = \begin{pmatrix}\varphi_1 \\ \varphi_2\end{pmatrix}$. In the new notation, the chirality transformation (39) is con-

([17]) W. Pauli: *Nuovo Cimento*, **6**, 204 (1957); however, the possible existence of such a transformation was already noted by S. Kamefuchi and S. Tanaka: *Prog. Theor. Phys.*, **14**, 225 (1955).

([18]) H. P. Dürr: preprint (Münich).

verted into the usual fermion gauge transformation:

$$\varphi_{1,2} \to \exp[i\alpha]\varphi_{1,2} \tag{44}$$

and the Pauli-Gürsey transformation (41) reduces to the usual isospin rotation:

$$\begin{cases} \varphi_1 \to \alpha\varphi_1 + \beta\varphi_2 , \\ \varphi_2 \to -\beta^*\varphi_1 + \alpha^*\varphi_2 . \end{cases} \tag{45}$$

Finally, the propagator (34*a*) takes on the simple form:

$$\langle 0 | (\varphi(x)\varphi^*(y))_+ | 0 \rangle = \tag{45a}$$
$$= \frac{-1}{(2\pi)^4} \int \mathrm{d}^4 p (\sigma^+ \cdot p) \left[\frac{1}{p^2 + m^2} - \frac{1}{p^2} + \frac{m^2}{(p^2)^2} \right] \exp[ip(x-y)] .$$

The same decomposition defined by (42) does not lead to any simplification of propagator, etc., in Nambu's theory because of the different choice of canonical variable. That is to say, NAMBU takes the four-component « Dirac » field ψ as the canonical variable whereas HEISENBERG takes the two 2-component « Weyl » fields φ_1 and φ_2 as the canonical variables. This is the reason why in the Heisenberg theory the usual parity operation is no longer valid whereas in the Nambu theory, parity is still defined. The distinction between variational and canonical variables also explains another important point of difference between the Heisenberg and Nambu theories. On the basis of chirality invariance, NAMBU derives a conservation law for the axial vector current and thereby proves the existence of a zero mass pseudoscalar boson (identified as the pion) using some reasonable dispersion-theoretic arguments. However, the same deduction does not hold in Heisenberg's theory [19] since the chirality transformation is utilised to define the fermion number; in fact, the pion in Heisenberg's theory is of non-vanishing mass. This is not surprising, since the choice of the canonical variables is entirely different in the two theories.

The different choice of canonical variables—as well as of the fundamental non-linear equation—in the Heisenberg and Nambu theories flows from a different motivation in each case. HEISENBERG wishes to construct a theory of elementary particles based on *one* massless four-component field operator satisfying a non-linear equation whose invariance properties will automatically give rise to the known additive quantum numbers, isospins and multiplicative quantum numbers of all the elementary particles. (We shall not comment

[19] Actually, in this case, the conservation of the current implies the separate C and P invariance of the matrix elements: W. E. THIRRING: *Nucl. Phys.*, **14**, 565 (1960).

on his hope to derive the properties and relative strengths of the strong, electromagnetic and weak interactions as well as the masses and properties of the particles). He has shown how to derive the fermion (additive quantum) number from chirality invariance and the isospin from « Pauli-Gürsey » invariance. However, the discrimination between the baryon and lepton numbers requires the introduction of the ill-defined « scale » transformation and the strangeness number necessitates the postulation of a vacuum with infinite isospin ([20]). HEISENBERG must introduce an additional hypothesis (he introduces the $l \to -l$ transformation) in order to cope with the multiplicative quantum numbers P and C. It is safe to say that Heisenberg's goal of a one-field theory is extremely ambitious and will be extraordinarily difficult to carry out.

NAMBU seems to be more modest in his objectives. He appears to be willing to introduce the baryon gauge transformation, isospin rotation and strangeness gauge transformation *ad hoc* (by working with three Dirac fields) and he makes no attempt at the present time to deal with the leptons. His chief interest is in pushing the analogy between the chirality invariance of his non-linear field equation, the finite mass solution and the zero-mass pseudoscalar boson on the one hand and (ordinary) gauge invariance, the energy gap and the collective oscillations in superconductivity on the other. NAMBU has suggested introducing a non-zero bare mass ($m_0 \neq 0$) into his equation in order to obtain a finite mass for the pion (but as we shall see, we propose to introduce $m_0 \neq 0$ for a completely different purpose).

4. – Two-field theory.

We believe that the BL symmetry principle stated in the introduction suggests a two-field theory which, while utilizing several key concepts of the Heisenberg and Nambu theories, may possess certain advantages over both. There are also serious problems which will be mentioned at the end.

Let us first consider the isodoublets (n, p) and (e^-, ν); the isosinglets Λ and μ^- will be treated later. It is reasonable to assume that the mass differences between (n, p) and (e^-, ν) are due to electromagnetic effects and hence, if the electromagnetic interaction is neglected, that the nucleons possess equal mass M and the light leptons zero mass. Suppose we start with the Heisenberg

([20]) Recently, HEISENBERG (private communication) has given an argument justifying this approach by using the analogy with superconductivity and ferromagnetism in still another fashion; he argues that the non-zero isospin of the vacuum is only true locally (the over-all vacuum benig symmetrical) just as the breakdown of the usual gauge invariance is only true locally (the gauge invariance returning for large distances).

Lagrangian:

$$(46)\qquad \begin{cases} \mathscr{L} = \mathscr{L}_0 + \mathscr{L}_1 , \\ \mathscr{L}_0 = -\frac{1}{4}\left[\bar{\psi}\gamma \frac{\partial}{\partial x}\psi - \frac{\partial \bar{\psi}}{\partial x}\gamma\psi + \psi\gamma^x \frac{\partial \bar{\psi}}{\partial x} - \frac{\partial \psi}{\partial x}\gamma^x\bar{\psi}\right], \\ \mathscr{L}_1 = g\,{:}(\bar{\psi}\gamma_5\gamma_\mu\psi)(\bar{\psi}\gamma_5\gamma_\mu\psi){:} \end{cases}$$

We note that the four-fermion interaction:

$$(47)\qquad (\bar{\psi}Q\psi - \psi Q^x\bar{\psi})(\bar{\psi}Q\psi - \psi Q^x\bar{\psi})$$

is invariant under both the chirality transformation (39) and Pauli-Gürsey transformation (41) if (see Appendix):

$$Q = A \text{ or } T \quad \text{for Pauli-Gürsey transformation}$$

if

$$Q = A \text{ or } V \quad \text{for chirality transformation.}$$

Thus only $Q =$ axial vector satisfies the invariance under both transformations, which is, of course, the basis of Heisenberg's claim that his non-linear equation is unique (as long as one limits oneself to the simplest type of non-linear spinor equation). It should be emphasized that zero bare mass ($m_0 = 0$) is essential for the validity of both chirality and Pauli-Gürsey invariance.

We now adopt Heisenberg's viewpoint, *i.e.* we think of the two 2-component Weyl fields φ_1 and φ_2 defined by (42) as the canonical variables. Then as has been noted, the field φ describes an isospinor. Thus, as in the Heisenberg theory, we identify the non-perturbative finite mass solution with the nucleon (n, p). Furthermore, to define the parity, we propose to combine the $m = \pm M$ solutions into a four-component Dirac particle with mass M (this bears only a formal resemblance to the $l \to -l$ transformation). In contrast to the Heisenberg theory, we do not discard the $m = 0$ solution but instead identify the associated isospinor with the light lepton (e^-, ν). It follows that the light lepton must be described by a two-component spinor. While this appears satisfactory for the neutrino, it is certainly not true for the non-neutral member of the light lepton doublet, namely the electron. To explain this deficiency, we hypothesize that the other two components of the four-component Dirac spinor actually describing the electron, are generated by the electromagnetic interaction; *i.e.*, we may expect that the non-perturbative finite mass solution for the electron (due to the chirality-invariant electromagnetic interaction) also involves a doubling ([12]) of the number of compo-

nents in the same sense as the baryon case above. In this context the electromagnetic field could be considered as a separate fundamental field.

The next step is to assume the existence of an equation like (23) and to argue, with NAMBU, that the $m = 0$ and $m \neq 0$ solutions refer to inequivalent representations of the anti-commuting ring and that therefore the light lepton and nucleon Hilbert spaces are orthogonal to each other. Consequently, the field operator q or (q_1, q_2) possesses no non-zero transition matrix elements from one Hilbert space to the other. Thus we can double the space and extend the meaning of the field operator q to the product space of the light lepton and nucleon Hilbert spaces instead of the direct sum of the spaces.

The orthogonality of the two spaces implies that nucleons never transform into the light leptons, *i.e.* a kind of the super-selection rule operates, as has been already pointed out by NAMBU. We also note that in this approximation, there is no β-decay interaction since $n+\bar{p} \to e+\bar{\nu}$ is forbidden. It is even tempting to attribute the weak β-decay to a breakdown of the orthogonality of the lepton and baryon Hilbert spaces resulting from the non-zero mass of the electron (by breakdown is meant that the field operators possess non-vanishing matrix elements between the two spaces). Such an explanation would have the virtue that it would at the same time provide a natural basis for the apparent dominance of the charged currents over the neutral currents in weak interactions. The two members of the current contributing to the weak interaction differ in charge because they must differ in mass in order to break the orthogonality of the Hilbert spaces. The electromagnetic interaction is the mechanism whereby the weak interactions become possible. From this viewpoint intermediate charged bosons are unnecessary.

Thus, in the proposed picture, we can readily explain the isospinor character of (n, p) and (e^-, ν) and also we have a super-selection rule which distinguishes between the baryon and lepton numbers. There is, however, a fundamental difficulty: there is no guarantee that the four-lepton interaction is appreciably weaker than the four-baryon interaction. The tremendous difference in observed strengths between the four-lepton and four-baryon interactions must be ascribed, from our viewpoint, to the strikingly different character of the $m = 0$ and $m = \pm M$ solutions ([21]). Since the non-perturbative finite mass solution is a reflection of the non-analytic dependence on the coupling constant, we argue that the effective coupling is an extremely sensitive function of the physical fermion mass and is responsible for the relative strengths of the four-baryon and four-lepton interactions; for example, we

([21]) L. VAN HOVE'S work *Physica*, **25**, 365 (1959) in this connection is unfortunately not relevant since he could only show that in a certain model a strong interaction not satisfying a prescribed invariance principle can be converted into a strong interaction obeying the invariance principle *plus* a weak interaction.

may conjecture that, in analogy with superconductivity, the effective coupling constant is of the form $g \exp[-1/m^2 g]$ or $mf(m^2, g)$. (In superconductivity, the energy gap E is related to the phonon-electron coupling constant g by means of $E \approx \exp[-(W/g^2)]$, where W is the density of states per unit energy at the Fermi surface.) We had hoped to demonstrate the possibility of this behaviour using the Thirring « one-dimensoinal » four-fermion model ([22]); unfortunately, the coupling constant in this model must be dimensionless and the possibility of a non-perturbative finite mass solution is necessarily excluded. A crucial test of our type of theory will be to exhibit the possibility of a non-analytic dependence of the effective strength of the coupling on the physical masses of the four-fermions participating in the interaction.

We now turn to the μ and Λ. The muon possesses a huge mass (on the scale of the electron mass) and it is extremely unlikely that this mass has an electromagnetic origin ([23]). We postulate that the « strange » mass of the muon is due to the existence of a bare mass $m_0 \neq 0$ in the Lagrangian from the beginning and we add a second field ψ' with $m_0 \neq 0$ to the Lagrangian, namely:

$$\mathscr{L}_{m_0} = -\frac{m_0}{2}(\bar{\psi}'\psi' - \psi'\bar{\psi}') \,. \tag{48}$$

We now suppose that there is a non-linear interaction between the ψ and ψ' fields and that the μ and Λ masses arise from a displacement of the $m = 0$ and $m = M$ solutions for ψ alone ([24]). However, in order not to affect the existence of the $m = 0$ solution (see eq. (23)) to describe the light leptons, it is sufficient for the total Lagrangian for the two fields ψ and ψ' to be invariant under the restricted chirality transformation:

$$\psi \to \gamma_5 \psi \,, \qquad \psi' \to \psi' \,. \tag{49}$$

In a sense, the (finite) m_0 plays the role of a strangeness quantum number. This is to be compared with Nambu's proposal of a finite m_0 to enable him to obtain a finite pion mass. From our viewpoint, we interpret the chirality

([22]) W. E. Thirring: *Ann. Phys.*, **3**, 91 (1958); *Nuovo Cimento*, **9**, 1007 (1958); V. Glaser: *Nuovo Cimento*, **9**, 990 (1958).

([23]) See, however, the work by J. Leal Ferreira and Y. Katayama: *Prog. Theor. Phys.*, **23**, 776 (1960).

([24]) H. Kita and E. Predazzi: *Nuovo Cimento*, **17**, 908 (1960); have used a similar method for explaining the mass difference between the muon and electron. They utilize a strong cut-off dependence to obtain the large muon mass from zero bare mass in a way which we consider unreasonable.

transformation in the same way as HEISENBERG and this problem does not arise. Moreover, if Nambu's $m = 0$ solution is identified with the light lepton, the introduction of a finite bare mass sufficient to explain the pion mass would be expected to lead to an excessive light lepton mass, unless one is lucky.

Because of the finite bare mass, the $\mathscr{L}_{m_0}$ part of the Lagrangian is not invariant under the Pauli-Gürsey transformation so that the four-component ψ is maintained as the canonical variable and remains, as experiment requires, an isoscalar; *i.e.* the isospin transformation for ψ' is $\psi' \to \psi'$, in contrast to eq. (41). This is to be compared to the four-component ψ which is interpreted as two canonical two-component Weyl spinors φ_1 and φ_2. In this fashion, two four-component spinors ψ and ψ', the first with zero bare mass and the second with finite bare mass, may reproduce simultaneously the baryon triplet $(\Lambda, \mathrm{n}, \mathrm{p})$ and the lepton triplet $(\mu^-, \mathrm{e}^-, \nu)$. The BL symmetry principle has led in a natural way to a *two-field* theory of elementary particles.

We recognize that our two-field theory is more of a programme than a theory. It is less ambitious than Heisenberg's one-field theory in that the strangeness is introduced from the start by means of a second field with $m_0 \neq 0$. It differs from HEISENBERG in exploiting the inequivalent representations to differentiate between the baryons and the leptons rather than employ the « scale transformation » with its attendant difficulties. It shares Heisenberg's dilemma that separate P and C invariance of the strong four-baryon interaction can only be achieved by means of an additional assumption (unless Thirring's programme ([25]) of deriving separate P and C invariance from the CP invariance of this type of theory is successful). The two-field theory is more ambitious than Nambu's theory because the isospin, strangeness and lepton quantum numbers are supposed to follow from the group-theoretic properties of only two fields. It differs from NAMBU in seeking the analogy with superconductivity not through the chirality invariance, but rather through the sensitive dependence of the four-fermion interaction upon the physical fermion mass. The common difficulty of all of these theories is that serious calculations are almost impossible. One may only hope that the judicious choice of model calculations may lend support to the qualitative features of one of these theories and suggest certain types of experiments which may be particularly incisive.

* * *

We are indebted to Professors V. GLASER, W. HEISENBERG, L. VAN HOVE and Y. YAMAGUCHI for valuable conversations and to Professor Y. NAMBU for helpful correspondence. We also wish to thank CERN for its hospitality.

([25]) W. E. THIRRING: *Nucl. Phys.*, **10**, 97 (1959); **14**, 565 (1960).

APPENDIX

The group properties of n four-component spinors.

For the purposes of reference, it is useful to record in this Appendix an extension of the work of DÜRR [18] and THIRRING [25] on the group properties of various types of four-fermion interactions among n four-component spinors. Let us consider n four-component spinors ψ_i $(i = 1, \ldots, n)$, and assume invariance under the unitary group U_n among them. We take zero bare mass so that the Lagrangian is:

$$\text{(A.1)} \qquad \begin{cases} \mathscr{L}_0 = -\frac{1}{4}\left[\bar{\psi}\gamma \frac{\partial}{\partial x}\psi - \frac{\partial \bar{\psi}}{\partial x}\gamma\psi + \psi\gamma^T \frac{\partial \bar{\psi}}{\partial x} - \frac{\partial \psi}{\partial x}\gamma^T\bar{\psi}\right], \\ \mathscr{L}_1 = \frac{1}{4} g(\bar{\psi}Q\psi - \psi Q^T\bar{\psi})(\bar{\psi}Q\psi - \psi Q^T\bar{\psi}), \end{cases}$$

where $\psi = (\psi_1, \ldots, \psi_n)$ is a $4n$-component spinor, Q denotes appropriate γ matrices, and

$$\bar{\psi}Q\psi = \sum_{i=1}^{n} \bar{\psi}_i Q \psi_i .$$

Eq. (A.1) is invariant under the unitary group U_n:

$$\text{(A.2)} \qquad \psi_i \to \sum_{j=1}^{n} a_{ij}\psi_j , \qquad \sum_{j=1}^{n} a^*_{ij} a_{kj} = \delta_{ik} .$$

We shall show that for a special choice of Q, eq. (A.1) is invariant under a much larger group.

We decompose ψ_i into two 2-component spinors φ_i and χ_i by means of:

$$\text{(A.3)} \qquad \varphi_i = \tfrac{1}{2}(1+\gamma_5)\psi_i , \qquad \chi_i = \tfrac{1}{2}(1+\gamma_5)C^{-1}\bar{\psi}_i .$$

Then defining:

$$\text{(A.4)} \qquad \varphi = (\varphi_1, \ldots, \varphi_n) , \qquad \chi = (\chi_1, \ldots, \chi_n) .$$

Eq. (41) becomes:

$$\text{(A.5)} \qquad \mathscr{L}_0 = -\frac{1}{4}\left[\bar{\varphi}\gamma \frac{\partial}{\partial x}\varphi - \frac{\partial \bar{\varphi}}{\partial x}\gamma\partial + \varphi\gamma^T \frac{\partial \bar{\varphi}}{\partial x} - \frac{\partial \varphi}{\partial x}\gamma^T\bar{\varphi}\right] - \\ - \frac{1}{4}\left[\bar{\chi}\gamma \frac{\partial}{\partial x}\chi - \frac{\partial \bar{\chi}}{\partial x}\gamma\chi + \chi\gamma^T \frac{\partial \bar{\chi}}{\partial x} - \frac{\partial \chi}{\partial x}\gamma^T\bar{\chi}\right],$$

and

$$\text{(A.6)}\qquad \bar{\psi}Q\psi - \psi Q^T\bar{\psi} = \bar{\varphi}Q\varphi - \varphi Q^T\bar{\varphi} + \bar{\chi}(C^{-1}Q^TC)\chi - \\ - \chi(CQC^{-1})\bar{\chi} - \chi(CQ)\varphi + \bar{\varphi}(QC^{-1})\bar{\chi} - \varphi(Q^TC)\chi + \bar{\chi}(C^{-1}Q^T)\bar{\varphi}\,.$$

Note, furthermore, that:

$$\text{(A.7)}\qquad \gamma_5\varphi = \varphi\,, \qquad \gamma_5\chi = \chi\,.$$

We now specialize Q.

i) $Q = V, A$, then:

$$\gamma_5^T(CQ)\gamma_5 = -CQ\,,$$

so that:

$$\chi(CQ)\varphi = \chi\gamma_5^T(CQ)\gamma_5\varphi = -\chi(CQ)\varphi = 0\,.$$

Thus:

$$\text{(A.8)}\qquad \bar{\psi}Q\psi - \psi Q^T\bar{\psi} = \bar{\varphi}Q\varphi - \varphi Q^T\bar{\varphi} + \bar{\chi}(C^{-1}Q^TC)\chi - \chi(CQC^{-1})\bar{\chi}\,.$$

ii) $Q = S, T, P$, then:

$$\gamma_5 Q\gamma_5 = Q\,,$$

so that:

$$\bar{\varphi}Q\varphi = -\bar{\varphi}\gamma_5 Q\gamma_5\varphi = -\bar{\varphi}Q\varphi = 0\,.$$

Similarly:

$$\bar{\chi}Q\chi = 0\,,$$

so that:

$$\text{(A.9)}\qquad \bar{\psi}Q\psi - \psi Q^T\bar{\psi} = -\chi(CQ)\varphi + \bar{\varphi}(QC^{-1})\bar{\chi} - \varphi(Q^TC)\chi + \bar{\chi}(C^{-1}Q^T)\bar{\varphi}\,.$$

On the basis of eq. (A.8) and (A.9), we have:

i) $Q = A$

$$\text{(A.10)}\qquad \bar{\psi}Q\psi - \psi Q^T\bar{\psi} = \bar{\varphi}Q\varphi + \bar{\chi}Q\chi - \varphi Q^T\bar{\varphi} - \chi Q^T\bar{\chi}\,.$$

ii) $Q = V$

$$\text{(A.11)}\qquad \bar{\psi}Q\psi - \psi Q^T\bar{\psi} = \bar{\varphi}Q\varphi - \bar{\chi}Q\chi - \varphi Q^T\bar{\varphi} + \chi Q^T\bar{\chi}\,.$$

iii) $Q = S$ or P

$$\text{(A.12)}\qquad \bar{\psi}Q\psi - \psi Q^T\bar{\psi} = -\chi(CQ)\varphi - \varphi(CQ)\chi + \bar{\varphi}(QC^{-1})\bar{\chi} + \bar{\chi}(QC^{-1})\bar{\varphi}\,.$$

iv) $Q = T$

$$\bar{\psi}Q\psi - \psi Q^T\bar{\psi} = \bar{\varphi}(QC^{-1})\bar{\chi} - \bar{\chi}(QC^{-1})\bar{\varphi} - \chi(CQ)\varphi + \varphi(CQ)\chi \,. \tag{A.13}$$

Thus for $Q = A$, $\mathscr{L}_1$ is invariant under the $2n$-dimensional unitary group U_{2n}; this is clear if we define:

$$\Phi = \begin{pmatrix} \varphi \\ \chi \end{pmatrix} . \tag{A.14}$$

For $Q = V$, $\mathscr{L}_1$ is invariant under separate n-dimensional groups U_n among the χ and among the φ, *i.e.* it is invariant under $U_n \otimes U_n$. For $Q = S$ or P, let us introduce new variables:

$$\varphi' = \frac{1}{\sqrt{2}}(\varphi + \chi) , \qquad \chi' = \frac{-i}{\sqrt{2}}(\varphi - \chi) , \tag{A.15}$$

then:

$$\bar{\psi}Q\psi - \psi Q^T\bar{\psi} = -\varphi'(CQ)\varphi' - \chi'(CQ)\chi' + \bar{\varphi}'(CQ)\bar{\varphi}' + \bar{\chi}'(CQ)\bar{\chi}' . \tag{A.16}$$

Therefore, $\mathscr{L}_1$ is invariant under the $2n$-dimensional orthogonal group O_{2n}. Finally, for $Q = T$, if we define:

$$\Phi = \begin{pmatrix} \varphi_1 \\ \chi_1 \\ \varphi_2 \\ \chi_2 \\ \vdots \\ \varphi_n \\ \chi_n \end{pmatrix} , \qquad I = \begin{pmatrix} i\tau_2 & & 0 \\ & \ddots & \\ & & i\tau_2 \\ & \ddots & \\ 0 & & i\tau_2 \end{pmatrix} , \tag{A.17}$$

then $\mathscr{L}_1$ is invariant under:

$$\Phi \to U\Phi \qquad \text{where} \qquad U^T I U = I \,. \tag{A.18}$$

This means that $\mathscr{L}_1$ is invariant under the $2n$-dimensional symplectic group $S_p(2n)$. Note that $\mathscr{L}_0$ is invariant under U_{2n}.

We may summarize the results:

$$\begin{cases} Q = A; & U_{2n} , \\ Q = V; & U_n \otimes U_n , \\ Q = S \text{ or } P; & U_{2n} \cap O_{2n} , \\ Q = T; & U_{2n} \cap S_p(2n) . \end{cases} \tag{A.19}$$

The Heisenberg case corresponds to $n = 1$ and $Q = A$ and hence (A.19) the result is invariant under U_2. Also for $n = 1$ and $Q = T$, we have the two-dimensional unitary symplectic group which is equivalent to the two-dimensional unitary unimodular group; this is why $Q = T$ (together with $Q = A$) leads to invariance under the Pauli-Gürsey transformation but not to invariance under the chirality (gauge) transformation. In the case of $n = 2$, our choice, we have various possibilities depending upon the interaction. For the study of the « symmetrical » Sakata model, $n = 3$ and it appears that we have too many invariant quantities if we adopt a pure Q (*i.e.* not a mixture of various types of interactions). This would then be a problem with the « symmetrical » Sakata model ([2,25]).

RIASSUNTO (*)

Si mostra come il principio di simmetria tra il tripletto di barioni (Anp) e il tripletto di leptoni ($\mu\nu$) suggerisca per le particelle elementari una teoria a due campi. Si usa un campo spinoriale per descrivere i nucleoni e i leptoni leggeri e un secondo campo spinoriale con massa nuda finita per descrivere le particelle « strane » Λ e μ. Sotto molti aspetti il modello a due campi è simile alla teoria di Heisenberg e di Nambu ma esistono anche notevoli differenze che si mettono in evidenza.

(*) *Traduzione a cura della Redazione.*

IL NUOVO CIMENTO Vol. XIX, N. 6 16 Marzo 1961

Analytic Properties of Production Amplitudes.

P. V. Landshoff

St. John's College - Cambridge

S. B. Treiman (*)

Churchill College - Cambridge

(ricevuto il 10 Gennaio 1961)

Summary. — It is shown that a production amplitude, considered as a function of a single scalar invariant, inevitably has complex singularities when four other scalar invariants are fixed at physical values. For the process $\mathcal{N}+\pi\to\mathcal{N}+\pi+\pi$, with the nucleon-nucleon momentum transfer as the variable, the singularities can appear close to the pole to which extrapolations have been made when the other scalar invariants are fixed at typical experimental values.

For a variety of obvious reasons, the analytic properties of production amplitudes are currently a matter of considerable interest. It is equally obvious that the subject is bound to be a complicated one. Aside from spins, the number of independent dynamical variables needed to describe a reaction involving n particles is $3n-10$. Even for the simplest production processes, therefore, the number of independent variables, $3n-10=5$, is discouragingly large. Certainly the hope of finding anything so simple as a generalized Mandelstam representation has never appeared reasonable [1].

A more modest question has to do with analyticity properties in a single variable, the other variables being held fixed and physical. This in turn de-

(*) Alfred P. Sloan Foundation Fellow, on leave from Palmer Physical Laboratory, Princeton University.

[1] M. Fowler, P. V. Landshoff and R. W. Lardner: *Nuovo Cimento*, **17**, 956 (1960). There is a printing error in this reference: Fig. 1*b*) should be rotated clockwise through 90°.

pends on how the variables are chosen. From a kinematic point of view the simplest choice would consist of scalar products of four-momenta. We shall find here that production amplitudes, so parametrized, are generally bound to have complicated analyticity properties, *i.e.*, to involve complex contours in their integral representations. Our results are based on elementary examples from perturbation theory.

It must be admitted that these questions are anyhow rather academic for the most part. For even if one could prove simple dispersion relations, the task of identifying the « absorptive parts » would remain formidable (it is peculiar only to simple scattering, $n = 4$, that the absorptive part is the same as the imaginary part; and the latter, at least in the physical region, acquires a simple interpretation through unitarity). It should also be said that our results do not rule out the possibility that production amplitudes have simple analyticity properties when expressed in terms of other variables, not linearly related to the momentum scalar-product variables ([2]).

At the present time the only concrete relevance of analyticity properties for production amplitudes concerns the possibility of extrapolation in a momentum transfer variable to a one-particle pole, in the manner first proposed by Chew and Low ([3]). The question here is whether other singularities can occur in the nearby region. We shall find that this can indeed happen, in particular for the reaction of so much current interest, $\mathcal{N}+\pi \to \mathcal{N}+\pi+\pi$.

It will be enough for us to restrict ourselves to the simplest production processes, $n = 5$. Let us denote the four-momenta of the particles involved by k_i, $i = 1, \ldots, 5$, with $k_i^2 = m_i^2$. For convenience we take allpartic les as « incoming », so that $\sum_i k_i = 0$. One can form ten scalar product variables, $W_{ij} = (k_i + k_j)^2$, $i \neq j$; but only five of these are independent. There are many ways therefore to choose an independent set. Suppose that a particular choice of independent variables has been made; call them V_{ij}. To this there corresponds a definite set of five redundant variables, call them r_{ij}. The V_{ij} and r_{ij} are collectively denoted by W_{ij}, as above. Finally, let us select from among the V_{ij} a particular variable, V, in terms of which we want to discuss analyticity, the remaining V_{ij} being held at fixed, physical values. The physical reaction is: $1+2 \to 3+4+5$. The quantities W_{12}, W_{34}, W_{35}, W_{45} are therefore « energy » variables; whereas W_{13}, W_{14}, W_{15}, W_{23}, W_{24}, W_{25} are « momonentum transfer » variables. For the momentum transfer extrapolation programme, say in the reaction $\mathcal{N}(1)+\pi(2) \to \mathcal{N}(3)+\pi(4)+\pi(5)$, one selects as independent variables the set V_{12}, V_{34}, V_{45}, V_{24}, and $V_{13} = V$ and one

([2]) For example, the variables used in the heuristic derivation of a dispersion relation by J. C. Polkinghorne: *Nuovo Cimento*, **4**, 216 (1956).

([3]) G. F. Chew and F. E. Low: *Phys. Rev.*, **113**, 1640 (1959).

seeks to extrapolate in V from the physical region to a one-particle pole — the one-pion pole at $V = \mu^2$ in the above example (μ = pion mass).

This particular selection of variables seems especially favourable for extrapolation purposes for the following reason. The variable $V_{13} = V$ is linearly related to $\cos\theta$, where θ is the centre of mass angle between incoming and outgoing nucleons. Ascoli [4] has shown that the production amplitude is analytic in the $\cos\theta$ plane within a certain « Lehmann ellipse », with foci at $\cos\theta = \pm 1$. For reasonable energies V_{12}, the pole term lies not too far outside the ellipse, a favourable circumstance for extrapolation purposes. The question however is whether other singularities may also occur near the ellipse, in particular in the vicinity of the pole. Now whatever the situation is with regard to this, a certain practical difficulty can arise, as first noted by Ascoli [5], if one attempts to extrapolate not the purely differential cross-section but rather the latter integrated over V_{24}, V_{34}. The result, call it $\sigma(V_{12}, V_{45}, V_{13})$ will in general have complex singularities in the V_{13} plane even if the amplitude itself does not. This is a kinematic effect, induced by certain real poles (and, we may add, branch points) in the amplitude. For the reaction $\mathcal{N} + \pi \to \mathcal{N} + \pi + \pi$ these extra « unforeseen » singularities happen to be far away from the region of interest. But in any case, this particular problem can always be avoided by carrying out extrapolations in the purely differential cross-section. That is to say, the essential analyticity questions concern the amplitude itself, rather than the integrated cross-section.

We turn to this therefore, taking perturbation theory as a guide. The simplest singularities will consist of one-particle poles. Except for the fact that there can be a great many more of these than appear in ordinary scattering, there is nothing new here. Next consider the singularities produced by diagrams in which there are only two external vertices, two of the external particles joining at one of them, the remaining three joining at the other. Each such diagram depends on a single variable W_{ij} and contributes to the amplitude a term

$$\int_{\tilde{W}_{ij}}^{\infty} \frac{\varrho_{ij}(W')}{W' - W_{ij} - i\varepsilon}\, \mathrm{d}W',$$

where ϱ_{ij} is a real weight function. This is of course the familiar situation encountered for ordinary scattering. But because there are now so many redundant variables, some new complication can arise. A term of the above type will occur for each one of the ten quantities W_{ij}, independent or re-

---

[4] R. Ascoli: *Nuovo Cimento*, **18**, 754 (1960). See also R. Ascoli and A. Minguzzi: *Phys. Rev.*, **118**, 1435 (1960).

[5] R. Ascoli: *Nuovo Cimento*, **18**, 744 (1960).

dundant. Suppose that we are discussing analyticity in a particular variable V, chosen from a particular set of independent variables V_{ij}. Select two variables W_{ij}, call them W_a and W_b, such that each depends on V (W_a, for example, may be the variable V itself, or it may be a redundant variable which happens to depend on V when expressed in terms of the independent set). Thus: $W_a = \alpha_a V + \beta_a$, $W_b = \alpha_b V + \beta_b$. The β's here are linear combinations of the fixed V_{ij} and the squares of the masses of the particles, and the α's, as it turns out, always have the value $+1$ or -1.

Suppose now that the variable V and the remaining independent V_{ij} have been chosen in such a way that there exist two variables, W_a and W_b, with the following properties:

i) $\alpha_a = +1$, $\alpha_b = -1$.

ii) W_a and W_b are « energy » variables in the physical region. From i) it follows that the production amplitude will contain, among others, the term

$$f = \int_{\bar{V}_a}^{\infty} \frac{\varrho_a(V')\,\mathrm{d}V'}{V' - V - i\varepsilon} + \int_{-\infty}^{\bar{V}_b} \frac{\varrho_b(V')\,\mathrm{d}V'}{V' - V + i\varepsilon} \equiv f_a + f_b\,, \tag{1}$$

where $\bar{V}_a$ and $\bar{V}_b$ may depend on the fixed V_{ij}. Notice the alternation of sign of the $i\varepsilon$ in the two terms. Now from ii) it follows that $\bar{V}_b > \bar{V}_a$ and that in the physical region of V we have $\bar{V}_a < V < \bar{V}_b$. Thus, although each of the above integrals defines a function analytic in a whole cut plane, the cuts overlap in the physical region and V approaches the real axis from opposite directions in the two terms. In the first instance, therefore, f need not even have the most elementary property of being the boundary value of an analytic function of V. Whether or not it in fact has this property depends on the singularities of the weight functions themselves; *i.e.*, on whether we can distort one or another of the contours of integration away from the real axis throughout the physical region.

Now in fact some such distortion of contour should certainly be possible. But the resulting integral representation of our analytic function will then involve complex contours, unless it is possible to distort the contour so much that it again is real but runs in the opposite direction so that we can express either f_a of f_b in a representation with only real cuts not extending into the physical region. But this will certainly not be possible if both f_a and f_b have normal threshold branch points in the physical region — as may happen for suitable ranges of values of the fixed V_{ij}. When such branch points do not occur, say for f_a, the above possibility cannot be ruled out: it is equivalent to the assertion that the corresponding weight function ϱ_a, as defined in the physical region, is itself the boundary value of a function analytic in the entire

relevant half plane. Little is known about the analytic properties of the weight functions, but this analyticity seems too much to expect. In fact it is known from a dual diagram analysis that self-energy graphs do yield complex singularities on unphysical sheets, and it is probable that this includes the neighbouring unphysical sheet as needed to give corresponding singularities to ϱ_a.

It is our expectation therefore that for any choice of variables (choice of V_{ij} and choice of a particular V from among them) for which conditions i) and ii) can be met, the physical value of the production amplitude cannot be expressed as the boundary value of an analytic function which has no complex cuts.

We encounter a new class of difficulties, relevant to other sets of variables, when we turn to triangle graphs, in which pairs of external particles are joined at each of two vertices (Fig. 1). Let us denote by α, β, ... the various external particles and by p_{ab}, p_{bc}, p_{ac} the net four-momentum carried in at each vertex by external particles. Define Z_{ab} by

$$p_{ab}^2 = W_{ab} = M_a^2 + M_b^2 - 2M_aM_bZ_{ab}$$

and similarly for Z_{bc}, Z_{ac}, where M_a, M_b, M_c are the internal masses as shown in Fig. 1. If $W_{ab} > (M_a + M_c)^2$ we have $Z_{ab} < -1$ and the vertex is said to be externally unstable; and similarly for the other vertices. In fact at the one external particles vertex (bc) we always have both external and internal stability and thus $|Z_{bc}| < 1$. We are regarding the graph as a function of W_{ab} and W_{ac}, hence of Z_{ab} and Z_{ac}, with Z_{bc} fixed as above.

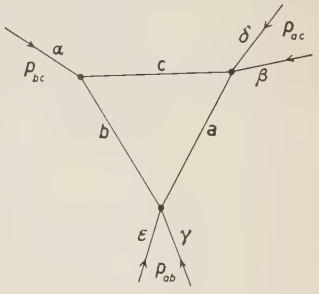

Fig. 1.

Once again, suppose a definite choice of variables has been made and consider a definite triangle graph in which the internal particles, and external particles α, β, ..., are given a specific identification. Suppose that this graph meets the following conditions:

iii) The variable W_{ac} is independent of the variable V, *i.e.*, W_{ac} is a fixed quantity.

iv) The variable W_{ab} depends on V (linearly, necessarily).

v) At the (ac) vertex the condition $Z_{ac} < -1$ holds. In most cases this means that W_{ac} must be an « energy » variable.

We now make the two main points of the present paper.

1) When conditions iii)–v) are satisfied, the graph in question produces a function with a complex singularity in a definite half of the W_{ab} plane, hence

of the V plane. The physical function is the boundary value as V approaches the real axis from one half-plane; the complex singularity lies in the other. This result will be established below. The complex singularity is a branch point, not a pole. It has a cut attached to it.

2) For *any* selection of independent variables V_{ij}, and *any* selection of a distinguished variable V from among them, it is possible to find some graphs, consistent with all selection rules, such that conditions iii)–v) are satisfied, except for certain sets V_{ij} where however the conditions i) and ii) discussed earlier can then be met. Moreover, when the conditions iii)–v) are satisfied this can in fact always be achieved in two ways: for some graphs one has $W_{ab} = V + \beta$, for others $W_{ab} = -V + \beta'$, β and β' being fixed quantities. Since both algebraic signs can occur for the coefficient of V, the net result is that the complex singularities mentioned above in fact occur in both halves of the V-plane, thus ruling out the possibility of representations involving only real contours. All of these kinematic results are a matter of straightforward enumeration and we shall not enter into the details here.

Let us turn now to a proof of the assertions made above concerning the analyticity properties of triangle graphs. For the moment we regard the parameters Z_{ab} and Z_{ac} as complex variables, Z_{bc} being fixed and real, $|Z_{bc}| < 1$. In the first place, we recall that the triangle graph produces normal threshold singularities on the physical sheet at $Z_{ab} = -1$ and $Z_{ac} = -1$. Additional singularities must lie in the manifold defined by

$$\det (Z_{ij}) = 0 , \qquad i, j = a, b, c,$$

where $Z_{ij} = Z_{ji}$, $Z_{ii} = 1$; only a portion of this manifold corresponds to singularities on the physical sheet, and of course it is only such singularities that concern us. The above equation, written out in full is

$$(2) \quad 1 - Z_{bc}^2 + 2 Z_{bc} Z_{ab} Z_{ac} - Z_{ab}^2 - Z_{ac}^2 = 0 .$$

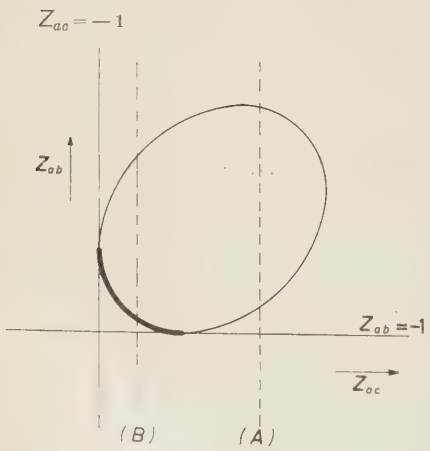

Fig. 2.

In the real (Z_{ab}, Z_{ac}) plane this produces an ellipse, as shown in Fig. 2. The standard analysis of the Feynman representation for the triangle graph function [1] reveals that only that portion of the ellipse (heavily shaded in Fig. 2) which lies between the points of contact with the normal thresholds

corresponds to singularities on the physical sheet. Consider now the roots of eq. (2) regarded as a function of Z_{ab} for fixed real Z_{ac}. When Z_{ac} has a value corresponding to the dashed line labelled (A) in Fig. 2, the two roots Z_{ab} are real but do not represent physical singularities. When Z_{ac} is in position (B), the lower root Z_{ab} has become a physical singularity, the upper root remaining unphysical. At $Z_{ac}=-1$ the two roots Z_{ab} just coincide, but since $Z_{ac}=-1$ is a line of branch points we avoid this value by giving Z_{ac} a small imaginary part. Thereafter, as Z_{ac} moves to the left (Z_{ac} real again and <-1) the two roots Z_{ab} move off into the complex plane, one above and one below the real axis. One root remains a physical singularity, the other remains unphysical; *i.e.*, since no branch cut has been crossed the nature of the singularities cannot have changed. In fact, since Feynman amplitudes contain a small negative imaginary part attached to each internal mass, we conclude that the physically singular root Z_{ab} is that one which lies in the upper half plane, whereas the physical function is obtained as Z_{ab} approaches the real axis from the lower half plane (this determines the sign of the small imaginary part given to Z_{ac} in order to avoid the singularity $Z_{ac}=-1$).

Thus, for graphs in which Z_{ab} depends on our variable V, a complex singularity is produced if at the other vertex the condition $Z_{ac}<-1$ holds. This establishes the result discussed above.

This completes our general discussion. We have seen from a consideration of the most elementary graphs that, with any choice of scalar product variables, the single variable representations for production amplitudes will necessarily involve complex contours. Higher order graphs no doubt only further confound the situation. For the practically important problem of extrapolating in a momentum transfer variable this si in itself not necessarily fatal. The relevant question here is, where do the singularities occur? We cannot say anything about the worst possible outcome, which would require a consideration of all higher order graphs. It will be enough to show here that already the triangle graphs can produce trouble in certain circumstances.

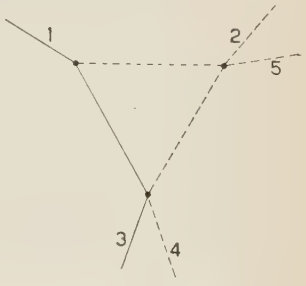

Fig. 3.

In Fig. 3 there is shown a sample graph for the reaction $\mathcal{N}(1)+\pi(2)\rightarrow$ $\rightarrow\mathcal{N}(3)+\pi(4)+\pi(5)$, where the dotted lines represent pions (mass μ), the heavy lines nucleons (mass M). Let us select as variables the customary set, V_{12}, V_{45}, V_{24}, V_{34}, $V_{13}\equiv V$, where, again, $V_{ij}=(k_i+k_j)^2$. This graph depends only on the variables V_{34} and $(k_2+k_5)^2$, where the latter is related to the basic set by

$$(k_2+k_5)^2=V_{13}-V_{45}-V_{24}+3\mu^2\,.$$

In our earlier notation, the vertices (ac), (bc), (ab) are identified respectively with the external particles (34), (1), (25). The physical singularity in V_{13} is now to be located from the solution of eq. (1), and we find for the singular point

$$V_{13} = -\mu^2 + V_{24} + V_{45} - \left(\frac{\mu}{M}\right)\mu^2 Z_{ac} - 2i\mu^2\left\{(Z_{ac}^2 - 1)\left(1 - \frac{\mu^2}{4M^2}\right)\right\}^{\frac{1}{2}}, \tag{3}$$

where

$$Z_{ac} = \frac{-V_{34} + M^2 + \mu^2}{2M\mu}.$$

It is clear that the present graph always has the property $Z_{ac} < -1$ necessary to produce a complex singularity (except in the limiting case $Z_{ac} = -1$ which corresponds to the outgoing nucleon and one outgoing pion being produced with zero relative momentum).

Although the quantities V_{24}, V_{45}, and V_{34} are independent, they cannot be varied unrestrictedly for physical processes. We may remark however on a simple limiting situation: take $V_{34} = (M+\mu)^2$. In the limit $V_{12} \to \infty$ one can achieve $V_{24} + V_{45} \to 2\mu^2 + (\mu^3/M + \mu)$. In this limit the singular point in V_{13} in real and located at $\mu^2\left(1 + (\mu/M) + (\mu/(M+\mu))\right)$ — perilously close to the single particle pole at μ^2. Even for situations where V_{12} and V_{45} are chosen more realistically, V_{34} and V_{24} can be chosen in such a way as to produce a singularity not too far from the pole at μ^2 (6). It is also true that with other physically realistic values one can manage to remove the singularity from the dangerous region. But we do not press this point here, since we have no idea what further singularities may arise from higher order graphs.

* * *

We are grateful to Dr. R. J. Eden and Dr. J. C. Polkinghorne for many useful discussions. One of us (P.V.L.) wishes to thank the D.S.I.R. for a grant.

(6) For example, with $V_{12} = (12\mu)^2$, $V_{45} = 12\mu^2$, $V_{34} = 61\mu^2$, and $V_{24} = -10 \cdot 2\mu^2$ the singularity in V_{13} occurs at $\sim (1-i)\mu^2$.

RIASSUNTO (*)

Si mostra che l'ampiezza di produzione, considerata come funzione di un solo invariante scalare, ha inevitabilmente singolarità complesse quando, entro valori fisici, si fissano quattro altri invarianti scalari. Nel processo $\mathcal{N} + \pi \to \mathcal{N} + \pi + \pi$, prendendo come variabile il trasferimento di impulso nucleone-nucleone, le singolarità possono apparire presso al polo verso il quale si è estrapolato quando agli altri invarianti scalari si assegnano tipici valori sperimentali.

(*) *Traduzione a cura della Redazione.*

IL NUOVO CIMENTO Vol. XIX, N. 6 16 Marzo 1961

S-Matrix, Left-Hand Cut Discontinuity and Potential.

A. Martin

CERN - Geneva

(ricevuto il 23 Gennaio 1961)

Summary. — Assuming a two body potential which is a continuous superposition of exponential potentials we first show in a straightforward way how to get, from the left-hand cut discontinuity of the S-wave scattering amplitude, the scattering amplitude itself, without any ambiguity. On the other hand, we establish a one to one correspondence between the unphysical cut discontinuity and the inverse Laplace transform of the potential. When the discontinuity is known in a certain range of values the inverse Laplace transform of the potential is exactly known in a corresponding range of values. An extention of the treatment when a repulsive hard core is present at short distance is given. The usefulness of the inverse Laplace transform of the potential as an intermediate tool in the calculation of the scattering amplitude is discussed.

1. – Introduction.

In previous studies [1-3] we have established the analytic properties of the scattering matrix in the S-state for two particles interacting through a potential of the family

$$V(r) = \int_{\mu}^{\infty} C(\alpha) \exp[-\alpha r]\, \mathrm{d}\alpha\,, \qquad |C(\alpha)| < M\alpha^{-\varepsilon}\,. \tag{1}$$

It was shown that, in the complex energy plane, in addition to the physical

(1) A. Martin: *Nuovo Cimento*, **14**, 403 (1959).

(2) A. Martin: *Lecture notes at the summer school of Cargèse (Corsica)* (1960), CERN preprint 9432/TH. 120.

(3) R. G. Newton: *Journ. Math. Phys.*, **1**, 319 (1960).

cut, an unphysical cut is present on the real axis from $E \equiv k^2 = -\infty$ to $E = -\mu^2/4$. These properties coincide with those obtained in the field theoretical case by projecting the Mandelstam representation for the nucleon-nucleon scattering matrix on the S-state, if μ is the meson mass.

In the dispersion approach to the nucleon-nucleon problem the discontinuity of the S-matrix across the left hand cut is known at least in a certain region, and from it one can get, if certain assumptions are made, the scattering matrix itself, as it is shown by NOYES and WONG [4]. On the other hand, CHARAP, FUBINI and TAUSNER [5] have studied the problem of defining a potential reproducing the S-matrix, at least when one and two meson intermediate states are considered [5].

We wish to look at these two problems under the assumption that two nucleons interact through a potential of family (1). In this case we prove that the knowledge of the discontinuity across the unphysical cut determines unambiguously both the scattering matrix and the inverse Laplace transform of the potential. If the discontinuity of the S-matrix is not completely known it is still possible to say something about the inverse Laplace transform of the potential. More precisely if the left-hand cut discontinuity is known from $E = k^2 = -\mu^2/4$ to $E = -n^2\mu^2/4$ the inverse Laplace transform of the potential is known from $\alpha = \mu$ to $\alpha = n\mu$ and *conversely*.

However, we could not solve completely the problem to find necessary and sufficient conditions on the left-hand cut discontinuity, assumed to be completely known from $-\mu^2/4$ to $-\infty$, to ensure that the inverse Laplace transform $C(\alpha)$ has the correct behaviour, given by (1) for large α. Only partial results have been obtained. This problem is not physically so important because the left-hand cut discontinuity is never known up to $E = -\infty$.

2. – Basic equations.

We write here the main equations and the main results of reference [1]. A solution of the Schrödinger equation was written as $f(k, r) \exp[-ikr]$ such that $f(k, \infty) = 1$. It has been shown that with a potential of family (1) f may be written

$$f(k, r) = 1 + \int_{\mu}^{\infty} \varrho_k(\alpha) \exp[-\alpha r] \, \mathrm{d}\alpha \,, \tag{2}$$

[4] H. P. NOYES and D. Y. WONG: *Phys. Rev. Lett.*, **3**, 191 (1959).

[5] J. CHARAP and S. FUBINI: *Nuovo Cimento*, **14**, 540 (1959); **15**, 73 (1960); J. CHARAP and M. TAUSNER: *E.F.I.N.S.* 60-26, to be published in *Nuovo Cimento*.

with

$$\alpha(\alpha+2ik)\varrho_k(\alpha) = C(\alpha) + \int_{\mu}^{\alpha-\mu} C(\alpha-\beta)\varrho_k(\beta)\,\mathrm{d}\beta\,. \qquad (C(\alpha)=0 \text{ for } \alpha<\mu). \tag{3}$$

Eq. (2) is an especially simple integral equation from which one cat get $\varrho_k(\alpha)$ for any finite value of α by a finite number of iterations. When k is outside the cut $i(\mu/2)\to i\infty$, $\varrho_k(\alpha)$ is well defined for all the values of α. The S-matrix is just

$$S(k) = \exp[2i\delta(k)] = \frac{f(k,0)}{f(-k,0)}\,, \tag{4}$$

where $f(k,0)$ (*) has a cut along the imaginary k axis from $k=i(\mu/2)$ to $k=i\infty$ and no other singularities. Consequently $f(-k,0)$ has a cut from $k=-i(\mu/2)$ to $k=-i\infty$, and one can further prove that $f(-k,0)$ has no zeros in the upper half plane except on the imaginary axis. We should add the symmetry property $f(k,0)=f^*(-k^*,0)$. The behaviour at infinity is given by

$$\lim_{|k|\to\infty} |k|^{\varepsilon}|f(k,0)-1| \leqslant \text{const}\,. \qquad 0<\varepsilon<1. \tag{5}$$

3. – S-matrix and unphysical cut.

The above mentioned analytic properties and, especially, inequality (5) enable us to write spectral representations for $f(k,0)-1$ and $f(-k,0)-1$ without any subtraction. Hence, S may be written

$$S(k) = \frac{1 - i\int_{\mu/2}^{\infty} w(\varkappa)/(k-i\varkappa)\,\mathrm{d}\varkappa}{1 + i\int_{\mu/2}^{\infty} w(\varkappa)/(k+i\varkappa)\,\mathrm{d}\varkappa}\,, \tag{6}$$

where $-2\pi i\, w(\varkappa)$ is the purely imaginary discontinuity of $f(k,0)$ for $k=i\varkappa$.

Let us call $2\pi i\, D(x)$ the discontinuity of $S(k)$ across the upper cut, which corresponds to the left-hand cut in the variable k^2 (the lower cut corresponds to a cut in the second Riemann sheet of the k^2 plane).

(*) This function was first introduced by R. JOST (6).

(6) R. JOST: *Helv. Phys. Acta*, **19**, 256 (1946).

Then one readily gets from eq. (6)

$$\frac{S(i\varkappa_0+\varepsilon)-S(i\varkappa_0-\varepsilon)}{2i\pi}\equiv D(\varkappa_0)=\frac{w(\varkappa_0)}{1+\int\limits_{\mu/2}^{\infty} w(\varkappa)\,\mathrm{d}\varkappa/(\varkappa+\varkappa_0)}\,,$$

or

$$w(\varkappa_0)=D(\varkappa_0)\left[1+\int\limits_{\mu/2}^{\infty}\frac{w(\varkappa)\,\mathrm{d}\varkappa}{\varkappa+\varkappa_0}\right]. \tag{7}$$

With some changes in the notations this is exactly the Noyes and Wong final Fredholm equation in the non-relativistic case, established without any ambiguity in the case of potential scattering. The Fredholm equation determines the weight function w which, inserted in eq. (6), gives $S(k)$. It is not clear, however, that when $w(\varkappa)$ is inserted in expression (6), $S(k)$ has the right analytic properties. The cuts are in the right place, but nothing prevents $f(-k, 0)$ from vanishing in isolated points of the upper half k plane, outside the imaginary axis. In an actual calculation, starting from a given $D(\varkappa)$, one has to check *a posteriori* that this does not happen. The same difficulty appears in the field theoretical treatment.

If we try to compare our method of solution with that of Noyes and Wong we see that the main difference comes from the fact that they use the variable k^2. Then the cuts are the left-hand cut and the physical cut; S, in their case is separated as $\mathcal{N}/\mathcal{D}$, where $\mathcal{N}$ has a discontinuity across the left-hand cut and $\mathcal{D}$ across the right hand cut. $\mathcal{N}$ and $\mathcal{D}$ are related by two coupled dispersion relations taking into account unitarity and the knowledge of $D(\varkappa)$ In our case, however, where the physical cut is replaced by the lower cut in the k plane, unitarity is automatically fulfilled from the beginning. This is why we directly get a unique integral equation. On the other hand, in our treatment, the subtraction problem does not appear, and, further, the possible bound states should come out of the solution, without being *a priori* postulated.

In the case where the discontinuity across the unphysical cut is not completely known (in practice one can obtain $D(\varkappa)$ from $\varkappa=\mu/2$ to $\varkappa=3\mu/2$, corresponding to the knowledge of the $N\bar{N}\to\pi$ and $N\bar{N}\to 2\pi$ amplitudes) eq. (7) cannot be solved without making phenomenological assumptions on $D(\varkappa)$ for large values of $\varkappa$. However, as we shall see it in the next section, it is nevertheless possible to obtain a partial but accurate information on the potential itself.

4. – Unphysical cut and inverse Laplace transform of the potential.

We shall try first to evaluate the discontinuity $D(\varkappa)$ in terms of the inverse Laplace transform of the potential. For this purpose we must look more carefully at what happens for $k\to i\varkappa$.

For $k = i\varkappa$, the funktion $\varrho_k(\alpha)$, introduced in eq. (3) is well defined provided $\alpha < 2\varkappa$. In the neighbourhood of $\alpha = 2\varkappa$ this is no longer true because a factor in the left-hand side of eq. (3) vanishes. However, from $\alpha = 2\varkappa + \varepsilon$ to $\alpha = 2\varkappa + \mu - \varepsilon$ $\varrho_{i\varkappa}(\alpha)$ is again well defined because the right-hand side of eq. (3) makes use of values of α smaller than $2\varkappa$. When $\varrho_{i\varkappa}(\alpha)$ is not well defined, it is still possible to define $\varrho^+_{i\varkappa}(\alpha)$ and $\varrho^-_{i\varkappa}(\alpha)$ such that

$$\varrho^+_{i\varkappa}(\alpha) = \lim_{\varepsilon \to 0} \varrho_{i\varkappa+\varepsilon}(\alpha) , \qquad \varrho^-_{i\varkappa}(\alpha) = \lim_{\varepsilon \to 0} \varrho_{i\varkappa-\varepsilon}(\alpha) .$$

From eq. (3) one gets, in the neighbourhood of $\alpha = 2\varkappa$

$$\varrho^+_{i\varkappa}(\alpha) - \varrho^-_{i\varkappa}(\alpha) = -i\pi\,\delta(\alpha - 2\varkappa)\,\frac{C(2\varkappa) + \int_{\mu}^{2\varkappa-\mu} C(2\varkappa - \beta)\,\varrho_{i\varkappa}(\beta)\,\mathrm{d}\beta}{\varkappa} . \tag{8}$$

f^+ and f^- can be defined from the corresponding ϱ's. So for $k = i\varkappa$ there are three solutions of the Schrödinger equation:

$$f^+(i\varkappa, r)\exp[\varkappa r] , \quad f^-(i\varkappa, r)\exp[\varkappa r] , \quad f(-i\varkappa, r)\exp[-\varkappa r] ;$$

these solutions are not independent, and since

$$\lim_{r\to\infty} f^+(i\varkappa, r) , \quad f^-(i\varkappa, r) , \quad f(-i\varkappa, r) = 1$$

the only possible relation which can be identically satisfied is

$$[f^+(i\varkappa, r) - f^-(i\varkappa, r)]\exp[2\varkappa r] = A(\varkappa) f(-i\varkappa, r) . \tag{9}$$

If we evaluate eq. (9) at $r = 0$ we get

$$\frac{f^+(i\varkappa, 0)}{f(-i\varkappa, 0)} - \frac{f^-(i\varkappa, 0)}{f(-i\varkappa, 0)} = A(\varkappa) .$$

Therefore $A(\varkappa)$ is just the discontinuity of the S-matrix across the cut. So we can rewrite eq. (9) as:

$$2i\pi\, D(\varkappa) f(-i\varkappa, r) = [f^+(i\varkappa, r) - f^-(i\varkappa, r)]\exp[2\varkappa r]$$

and hence

$$2i\pi\, D(\varkappa) = \lim_{r\to\infty} [f^+(i\varkappa, r) - f^-(i\varkappa, r)]\exp[2\varkappa r]$$

or, expressing f^+ and f^- in terms of ϱ^+ and ϱ^-

$$2i\pi D(\varkappa) = \lim_{r\to\infty} \exp[2\varkappa r] \int_{2\varkappa-\varepsilon}^{2\varkappa+\varepsilon} [\varrho^+_{i\varkappa}(\alpha) - \varrho^-_{i\varkappa}(\alpha)] \exp[-\alpha r]\,\mathrm{d}\alpha +$$

$$+ \lim_{r\to\infty} \exp[2\varkappa r] \int_{2\varkappa+\mu-\varepsilon}^{\infty} \exp[-\alpha r][\varrho^+_{i\varkappa}(\alpha) - \varrho^-_{i\varkappa}(\alpha)]\,\mathrm{d}\alpha\,.$$

The second term vanishes because it behaves like $\exp[-(\mu-\varepsilon)r]$. The first term is the δ-function contribution. Finally

$$-2\varkappa D(\varkappa) = C(2\varkappa) + \int_{\mu}^{2\varkappa-\mu} C(2\varkappa-\beta)\,\varrho_{i\varkappa}(\beta)\,\mathrm{d}\beta\,. \tag{10}$$

Eq. (10) is the key for our problem. First it gives $D(\varkappa)$ in terms of the inverse Laplace transform of the potential. $\varrho_{i\varkappa}(\beta)$ appears in the equation, but the argument β is less than $2\varkappa-\mu$, and ϱ can therefore be obtained from the inverse Laplace transform of the potential by using eq. (3). The important point is that the *reverse* is *true*. Assume we know

$$D(\varkappa) \quad \text{from} \quad \varkappa = \mu/2 \quad \text{to} \quad \varkappa = \varkappa_0 + (\mu/2)$$

and

$$C(\alpha) \quad \text{from} \quad \alpha = \mu \quad \text{to} \quad \alpha = 2\varkappa_0$$

then it is clear that we also know $\varrho_{i\varkappa}(\beta)$ from $\beta = \mu$ to $\beta = 2\varkappa_0$ provided $\varkappa > \varkappa_0$.

Let us now apply eq. (10) for a value

$$\varkappa_0 < \varkappa < \varkappa_0 + (\mu/2)\,.$$

Then $D(\varkappa)$ is known, the quantities appearing in the integral are known and one gets *unambiguously* $C(2\varkappa)$ or $C(\alpha)$ for $2\varkappa_0 < \alpha < 2x_0 + \mu$. So if $D(\varkappa)$ is known up to $x = \varkappa_{\max}$, $C(\alpha)$ is known up to $\alpha = 2\varkappa_{\max}$. We can illustrate this for low values of $\varkappa$:

— for $\varkappa < \mu/2$ $\qquad C(2\varkappa) = D(\varkappa) = 0\,,$

— for $\mu/2 < \varkappa < \mu$ $\qquad C(2\varkappa) = -2\varkappa D(\varkappa)\,,$

— for $\mu < \varkappa < \dfrac{3\mu}{2}$, $\qquad C(2\varkappa) = -2\varkappa D(\varkappa) - \displaystyle\int_{\mu}^{2\varkappa-\mu} D\left(\varkappa - \frac{\beta}{2}\right) D\left(\frac{\beta}{2}\right)\mathrm{d}\beta\,,$

and so on ....

If we look at the expression for $\mu < x < 3\mu/2$ we see that its structure reminds us of the result of CHARAP and FUBINI, namely that to get the fourth order potential one must subtract from the discontinuity of the scattering amplitude for $-\mu^2 > k^2 > -(3\mu/2)^2$ the iteration of the second order result.

In our opinion this approach, though it does not furnish directly the scattering amplitude, is more satisfactory than the one considered in the preceding section because one does not mix known and unknown things concerning the left-hand cut discontinuity. The last step, which unavoidably involves some phenomenology, is to go from the inverse Laplace transform of the potential to the scattering amplitude. Let us first notice that one can work directly with the inverse Laplace transform of the potential as was shown by the author in ref. (1); the method of computation we proposed is rapidly convergent and an upper limit of the error made in the calculation of phase shifts can be obtained. However, one has to assume something about the high components of the inverse Laplace transform, but the assumptions made are easily interpreted because these high components mainly affect the short distance part of the potential. For instance to introduce a short range repulsion one can take $C(\alpha) = \alpha^{1-\varepsilon}$, $C > 0$ for $\alpha > A \gg \mu$. Of course, a limitation of our method is that too singular potentials (even repulsive ones) are excluded because they do not belong to family (1). However, in the case of a hard core, the modifications to be done are almost trivial.

Assume

$$V(r) = +\infty \qquad \text{for} \quad r < a\,,$$

$$V(r) = V'(r-a) \qquad \text{for} \quad r > a\,,$$

where $V'(r)$ belongs to family (1).

Then

$$\delta(k) = \delta'(k) - a$$

and

$$S(k) = S'(k) \exp[-2ika]\,.$$

Hence $S(k)$ and $S'(k)$ have the same analytic properties, except for the behaviour at infinity. One can get the discontinuity $D'(\varkappa)$ of $S'(k)$ by using the relation

$$D'(\varkappa) = D(\varkappa) \exp[-2\varkappa a]\,.$$

Then one obtains the inverse Laplace transform of $V'(r)$ in a range corresponding to the range where $D(\varkappa)$ is known. Clearly things would not be so simple for higher waves.

Let us now come back to the case where the potential belongs to family (1) and say a few words about the *academic* problem of determining the potential when the discontinuity across the unphysical cut is completely known from $k^2 = -\mu^2/4$ to $-\infty$. It is not obvious that this problem has always a solution because the inverse Laplace transform $C(\alpha)$ obtained from $D(\varkappa)$ might not have the property $|C(\alpha)| < M\alpha^{1-\varepsilon}$ for large α. By using upper bounds for $\varrho_{i\varkappa}(\alpha)$ and $C(\alpha)$ one easily gets a *necessary* condition from eq. (10), namely:

$$|D(\varkappa)| < \text{const}\, \varkappa^{-\varepsilon}\,.$$

As an example we give a *sufficient* condition which can be derived in a rather tedious way:

$$|D(\varkappa)| < \frac{\mu}{8\varkappa}\,.$$

However, these difficulties should not be taken too seriously, because, in actual cases, the left-hand cut discontinuity is not known up to infinity.

5. – Concluding remarks.

We believe that the present paper brings some clarification of the connection between the scattering amplitude, the left-hand cut discontinuity and an assumed two body potential. Of course, it would be desirable to extend this treatment to all partial waves. Then appears the problem of finding a unique potential; this problem has been solved by Charap and Fubini in the framework of meson theory for one and two meson intermediate states.

In our opinion, the results we obtained bring some justification for the search for a nucleon-nucleon potential (or its inverse Laplace transform) though it might look old-fashioned since it is at present possible to get directly the scattering amplitude from its left-hand cut discontinuity. The reason for this is our ignorance of the left-hand cut discontinuity for large negative values of k^2. One may prefer to feed in phenomenological assumptions on the high components of the inverse Laplace transform of the potential, which can be easily interpreted, than on the left-hand cut discontinuity of the scattering amplitude.

* * *

The author whishes to thank Professor S. Fubini for many valuable discussions, Professor L. Van Hove for useful criticism and Dr. R. Stora for encouraging him to publish the present work.

RIASSUNTO (*)

Presupponendo fra due corpi un potenziale, sovrapposizione continua di potenziali esponenziali, si mostra dapprima in maniera diretta come ottenere senza ambiguità, dalla discontinuità del taglio sinistro dell'ampiezza di scattering dell'onda S, l'ampiezza di scattering stessa. D'altra parte si stabilisce una corrispondenza univoca fra la discontinuità del taglio non fisico e la trasformazione di Laplace inversa del potenziale. Quando la discontinuità è nota in un certo campo di valori la trasformazione di Laplace inversa del potenziale è esattamente nota in un campo di valori corrispondente. Si dà una estensione del trattamento per il caso in cui sia presente a breve distanza un nocciolo repulsivo. Si discute l'utilità della trasformazione di Laplace inversa del potenziale quale strumento intermedio per il calcolo dell'ampiezza di scattering.

(*) *Traduzione a cura della Redazione.*

LETTERE ALLA REDAZIONE

(La responsabilità scientifica degli scritti inseriti in questa rubrica è completamente lasciata dalla Direzione del periodico ai singoli autori)

Photostar Cross-Section from Coulomb Disintegrations of High Energy Heavy Primaries.

S. T. Butler and C. A. Pearson

The Daily Telegraph Theoretical Department, School of Physics (*), *The University of Sydney - Sydney, N. S. W.*

(ricevuto l'11 Ottobre 1960)

Recently Castagnoli *et al.* [1] have reported the cross-section for photostars in emulsion to be constant for photons between .5 and 1.1 GeV. They found the cross-section per nucleon agreed closely with the sum of the single, double and triple photo-pion cross-sections measured by Bernardini [2] and Sellen [3] except around 1 GeV where it was somewhat larger. Over the same range the mean number of prongs in their photostars increased with energy from 3 to 3.5 suggesting that higher multiplicities in the pion production play an important part in the photostar cross-section above 1 GeV.

It would be interesting to know how this cross-section behaves above 1.1 GeV, as this provides information on the photopion cross-sections at high energies. Some idea of its gross structure up to several GeV may be obtained by examining the tracks of high energy heavy primary cosmic rays in emulsion.

In scanning large stacks of emulsion flown at high altitudes, a number of tracks have been seen of primaries larger than Carbon with energy greater than 10^{12} eV per nucleon. Before striking an emulsion nucleus such primaries have a fair chance of suffering observable disintegrations similar to photostars, the energy of which ranges from .2 to about 25 GeV.

The distinguishing feature of these events is the absence of any low energy tracks. It is well known that in a system fixed on such a primary, the Coulomb field of an emulsion nucleus resembles a packet of photons. When the primary absorbs one of these the momentum is taken up by the whole emulsion nucleus leaving no visible low energy tracks.

The spectrum of the photons which are equivalent to the Coulomb field of the emulsion nucleus for collisions outside a region of radius p can be shown by the familiar Weizsäcker-Williams method to be

$$(1) \qquad N(\nu, p)\,\mathrm{d}\nu = \frac{2}{\pi}\frac{Z^2e^2}{\hbar c}\log\left(\frac{E}{\hbar\nu\alpha}\right)\frac{\mathrm{d}\nu}{\nu},$$

(*) Also supported by The Nuclear Research Foundation within The University of Sydney.

(1) C. Castagnoli, M. Muchnik, G. Ghigo and R. Rinzivillo: *Nuovo Cimento*, **16**, 683 (1960).

(2) G. Bernardini: *Kiev Conference* (1959).

(3) J. M. Sellen, G. Cocconi, V. T. Cocconi and E. L. Hart: *Phys. Rev.*, **113**, 1323 (1959).

where $N(\nu, p)\,\mathrm{d}\nu$ is the number of photons in the frequency interval $\mathrm{d}\nu$, Z the charge on the emulsion nucleus, E the energy per nucleon of the primary in the Lab. system and $\alpha = pmc/\hbar$ where m is the nucleon mass. For a given p the maximum photon energy is $E\hbar/pmc$ showing that the higher energy photons correspond to close collisions.

For incident energies greater than 10^{13} eV/nucleon collisions with a pure Coulomb field outside atomic dimensions can contribute photons with enough energy to produce mesons. Because the Coulomb field is shielded these should be omitted. The spectrum corresponding to the Coulomb field cut off at the Bohr orbit of the innermost electron then becomes

$$N(\nu, p)\,\mathrm{d}\nu = \frac{2}{\pi}\frac{Z^2e^2}{hc}\log\left(\frac{a_0 Z^{-\frac{1}{3}}}{p}\right)\frac{\mathrm{d}\nu}{\nu}, \tag{2}$$

where a_0 is the Bohr radius for hydrogen.

The phase relations between the photons can be neglected and the cross-section for Coulomb disintegration of the primary can be conveniently written in two parts

$$\sigma_c = \int_0^{\nu_{\mathrm{meson}}} N(\nu, p)\sigma(\nu)\,\mathrm{d}\nu + \int_{\nu_{\mathrm{meson}}}^{\nu_{\max}} N(\nu, p)\sigma(\nu)\,\mathrm{d}\nu, \tag{3}$$

where $\sigma(\nu)$ is the photostar cross-section. The first term on the right represents the absorption of photons up to the threshold for meson production. It is dominated by the giant dipole resonance absorption exciting the nucleus to about 15 MeV. Although this term is the larger such excitations would usually result in neutron emission and would not be seen in the emulsion.

The second term on the right hand side of (3) is the cross-section for the absorption of photons from the threshold for single meson production, up to the maximum photon energy in the spectrum, and includes all the events detectable in the emulsion. For primaries with energy above 10^{12} eV/nucleon the spectrum extends beyond 25 GeV.

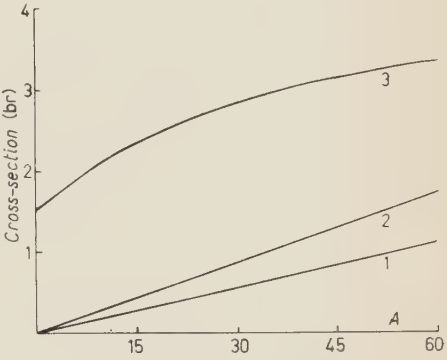

Fig. 1. – In Fig. 1 for primaries interacting with silver, the cross-sections for Coulomb disintegration above meson threshold are compared with the geometric cross-section as a function of the primary size. The Coulomb cross-sections (Curves 1 and 2) assume that the photostar cross-section is zero beyond 1.1 GeV and has the Castagnoli value to 4 GeV respectively. Both are plotted for a primary energy of 10^{12} eV/nucleon.

Because of the fall-off of the spectrum (1) with photon energy the cross-section for Coulomb disintegration of a 10^{12} eV/nucleon primary is insensitive

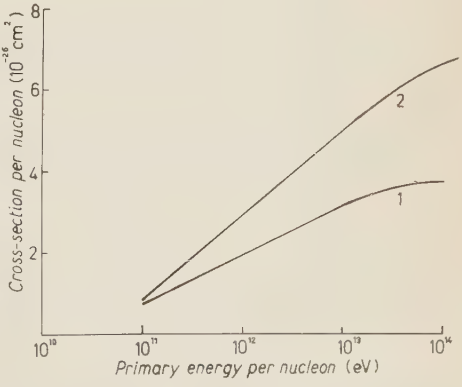

Fig. 2. – Curves 1 and 2 are the cross-sections corresponding to curves 1 and 2 of Fig. 1 plotted as a function of the primary energy.

to the behaviour of the photostar cross-section above several GeV. In Fig. 1 the result of integrating the second part of (3) using the photo-pion cross-sections of Bernardini and Sellen up to .5 GeV and the photostar cross-section of Castagnoli *et al.* from .5 to 1.1 GeV is compared with that found by assuming the photostar cross-section remains constant to 4 GeV. The geometric cross-section is also included for comparison. Already for 10^{12} eV/nucleon primaries bigger than carbon the second Coulomb cross-section is more than one and a half times the first and more than one fifth geometric. In Fig. 2 the Coulomb cross-sections are shown increasing with the logarithm of the primary energy to the point where shielding becomes important. As the primary energy increases there is the possibility that the spectrum even beyond 4 GeV may contribute substantially to the Coulomb disintegration.

It is clear that above 10^{12} eV/nucleon many heavy primaries should suffer Coulomb disintegration in emulsion and that an examination of a number of heavy primary tracks could determine whether the photostar cross-section decreases rapidly with energy above 1.1 GeV.

The Mean Free Path for α-Particles in Nuclear Photographic Emulsion (*).

R. L. English (**)

Department of Physics, Washington University - St. Louis, Mo.

(ricevuto il 31 Ottobre 1960)

In a recent publication, Lohrmann and Teucher (1) summarized the several experimental values of the α-particle mean free path in nuclear emulsion. This parameter has been measured using artificially accelerated particles, having kinetic energies of 90 MeV/nucleon, and cosmic-ray particles, with average energies of several GeV/nucleon. No published data appear for intermediate energies.

As many α-particles tracks in this energy region were observed during an experiment with emulsions flown at geomagnetic latitude 55° N, it was decided to investigate this point. The results are displayed in Table I.

Table I.

	Track length (cm)	No. of interactions	M.F.P. (cm)
$E > 600$ MeV/nucleon	1378.0	75	18.4
$E \leqslant 600$ MeV/nucleon	1044.4	49	21.3
All particles	2422.4	124	19.6

Each track was divided into segments covering 100 MeV/nucleon intervals, and the number of stars and total track length in each interval were noted. With the small sample available, it was felt not justified to effect such a fine breakdown, and the data were combined for Table I.

Combining the data listed by Lohrmann and Teucher with the value given here, and another of $\lambda = (24 \pm 2)$ cm (J. H. Mulvey: private communication), we obtain as the best estimate

$$\lambda = (19.2 \pm 0.4) \text{ cm},$$

where the standard deviation quoted results from the standard deviations listed for the individual values of λ. However, if the distribution of the individual values from the mean be considered, the standard deviation is 0.7 cm.

(*) The work reported here has been supported by the Air Force Office of Scientific Research, the Office of Ordinance Research and the National Science Foundation.

(**) Now at Hughes Ground Systems Laboratories, Fullerton, Calif.

(1) E. Lohrmann and M. W. Teucher: *Phys. Rev.*, **115**, 636 (1959).

IL NUOVO CIMENTO Vol. XIX, N. 6 16 Marzo 1961

Measurements on the π^--He Cross Sections at High Energy.

G. Brautti, L. Chersovani, C. Franzinetti (*),
M. Sedmak-Furlan and R. Tosi-Torelli (*)

Istituto di Fisica dell'Università - Trieste
Istituto Nazionale di Fisica Nucleare - Sezione di Trieste

(ricevuto il 16 Gennaio 1961)

The present letter reports on some results concerning interactions of 0.97 1.67 and 2.26 GeV kinetic energy π^- with Helium nuclei. These interactions have been observed in the liquid helium bubble chamber built by the Duke University group and exposed by Dr. M. M. Block to high energy pion beams produced by the Berkeley Bevatron.

The experiment was designed to provide information on the following quantities observed in π^--^{4}He collisions:

1) total cross section;

2) cross section for elastic scattering;

3) strange particle production;

4) multiple production of pions.

In what follows we present our results concerning points 1, 2 and 3. Point 4 will be dealt with in a subsequent publication.

1. – Experimental procedure.

The analysis of the film has been carried out selecting only the events inside a determined volume which excluded the peripheral regions of the chamber. This volume had the shape of a truncated rectangular pyramid having a volume of about 1350 cm^3.

During the exposure to the 1.67 and 2.26 GeV pion beams, the chamber was equipped with a magnetic field of 14.3 kG.

The events have been analyzed and measured following the methods described in detail by Borelli *et al.*[1].

The total track length, included in the accepted volume, has been deduced from measurements carried out on a sample of photograms corresponding to 20% of the total number of available photos.

We have taken as « elastic scatters » all those coplanar 2-prong stars for which angles and ranges (whenever measurable) were consistent with the values required to conserve momentum and energy.

When the range of the ^{4}He-recoil was too short to be appreciated we required that no significant variation of ionization was observed on the π^--track before and after the collision.

(*) Present address: Istituto di Fisica della Università, Pisa.

(1) V. Borelli, P. Franzini, I. Mannelli, A. Minguzzi-Ranzi, R. Santangelo, F. Saporetti, V. Silvestrini, P. Waloschek and V. Zoboli: *Nuovo Cimento*, **10**, 525 (1958).

Neutral strange particles could be identified with certainty only when their origin was visible within the sensitive volume of the chamber and a magnetic field was available. Without a magnetic field the identification is more difficult. An estimate of the relevant parameters is often possible on the basis of the measured angle and ionization of decay products, following well known standard methods. However, the uncertainty on the cross section thus deduced is large, mainly because of the difficulty in establishing the efficiency of the method.

2. – Results.

2·1. *Total cross section.* – The experimental results are listed in Table I.

In Fig. 1 our data regarding the total cross section have been plotted and compared with those of FOWLER *et al.* (2). KOZODAEV *et al.* (3), obtained using cloud chambers.

σ_{π^-p} is the total cross section for interaction of π^- on free protons as obtained

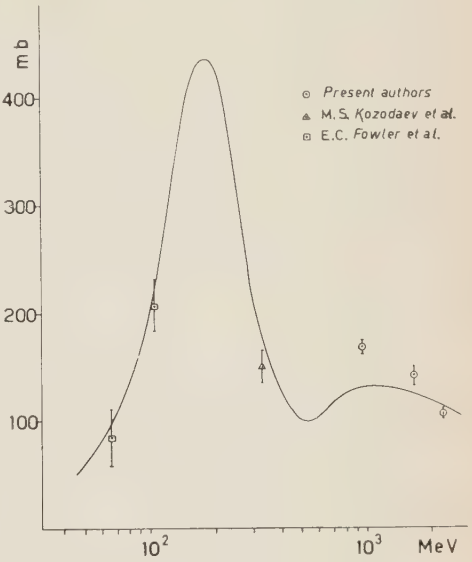

Fig. 1. – π^--^{4}He total cross sections, as obtained by the present authors (0.97; 1.67; 2.26 GeV π^- kinetic energy); by FOWLER *et al.* (0.068 and 0.105 GeV); and by KOZODAEV *et al.* (0.330 GeV).

TABLE I. – *Total cross section for* π^--He *interactions.*

Kinetic energy of the π^- (GeV)	Scanned track lenght (km)	Observed numbers of interactions	Detection efficiency	Corrected total cross section (*) (mb)
0.97	4.502	1353	0.897	167.4 ± 5.4
1.67	5.900	1423	0.855	140.7 ± 8.1
2.26	5.010	817	0.779	104.7 ± 1.5

(*) The errors quoted here are only statistical.

The continuous curve drawn on the experimental points represents the function

$$\bar{\sigma} = 2[\sigma_{\pi^-p} + \sigma_{\pi^-n}] ;$$

experimentally by YUAN and PICCIONI (4). σ_{π^-n} has been deduced assuming charge symmetry, *i.e.* taking $\sigma_{\pi^-n} = \sigma_{\pi^+p}$.

The sum has then been averaged with respect to energy, in order to take into account the motion of the nucleons inside the ^{4}He-nucleus. To do this, the

(2) E. C. FOWLER, W. B. FOWLER, R. P. SHUTT, A. M. THORNDIKE and W. L. WITTEMORE: *Phys. Rev.*, **91**, 135 (1953); see also *Phys. Rev.*, **85**, 929 (1952).

(3) M. S. KOZODAEV, R. M. SULAEV, A. I. FILIPPOV and IU. A. SHOHERBAKOV: *Sov. Phys. J.E.P.T.*, **4**, 580 (1957).

(4) L. C. L. YUAN: *CERN Symposium* (1956); R. COOL, O. PICCIONI and D. CLARK: *Phys. Rev.*, **103**, 1082 (1956).

TABLE II.

π^- kinetic energy (GeV)	f	Reference
0.068	-0.141 ± 0.274	FOWLER *et al.* [2]
0.105	-0.070 ± 0.116	FOWLER *et al.* [2]
0.330	-0.143 ± 0.092	KOZODAEV *et al.* [3]
0.970	$+0.270 \pm 0.053$	Present authors
1.666	$+0.110 \pm 0.071$	Present authors
2.265	-0.077 ± 0.041	Present authors

function:

$$P(\beta)\,\mathrm{d}\beta = 3.41 \exp[-36.4\beta^2]\,\mathrm{d}\beta\,,$$

has been assumed to represent the velocity distribution of the bound nucleons.

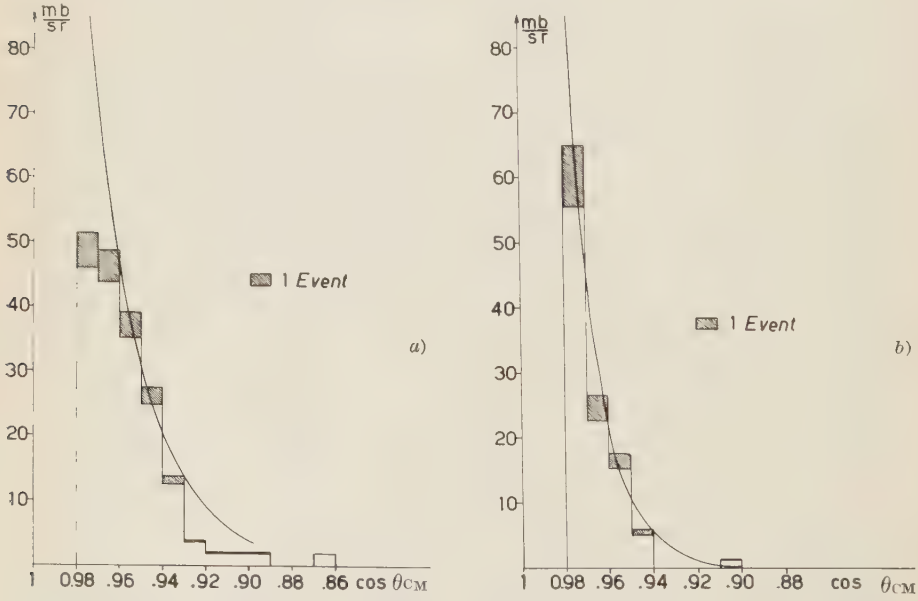

Fig. 2. – Angular distribution of elastically scattered π^- from helium. Fig. 2*a* refers to 0.97 GeV and Fig. 2*b* to 1.67 GeV π^-'s: the continuous lines have been calculated using Belenky's formula (see text).

This corresponds to an average energy of $\bar{E}_{\mathcal{N}} = 19.3$ MeV (see BLOCK and HARTH [5]). Such a procedure, certainly inadequate at low energies, may be acceptable in the energy range which concerns the present experiment. From Fig. 1 we see, however, that a discrepancy between our data and the values thus deduced exists just in the high energy regions. Such a discrepancy is better shown in Table II where the quantity

$$f = \frac{(\sigma_{\mathrm{tot}})_{\mathrm{obs}} - \bar{\sigma}}{\bar{\sigma}}\,,$$

is calculated for various energies.

[5] M. M. BLOCK and E. M. HARTH: *Phys. Rev.*, 100, 324 (1955).

2·2. *Elastic scattering* $\pi^- + {}^4\mathrm{He}$. *Differential cross section.* – The experimental angular distributions have been plotted in Fig. 2. The non shaded parts of the hystograms represent the observed distributions. These had to be corrected to take into account systematic losses due to the unfavourable geometry of part of the events. The correction is indicated by the shaded parts. The observations at 2.26 GeV were too scarce to be significant.

The experimental data thus obtained indicate that $\mathrm{d}\sigma/\mathrm{d}\Omega$ has a pronunced peak at small angles. Unfortunately the corrections associated with angles for which $\cos\theta_{\mathrm{CM}} \geqslant .98$ were too large to give any significance to our small angle observations.

On the basis of the distributions for $\cos\theta_{\mathrm{CM}} \leqslant .98$ an analysis in terms of diffraction scattering was attempted,

TABLE III.

Kinetic energy (GeV)	Identity of the particle	Momentum of the detected particle (GeV/c)	Angle of emission with respect to the primary direction $\theta^\circ_{\mathrm{lab}}$	Observed lifetime τ (10^{-10} s)
0.97	Λ^0	0.790	31.0°	2.41
	K^0	1.050	36.2°	0.47
	or Λ^0	0.630	36.2°	1.77
	K^0	0.270	17.8°	2.70
	K^0	0.100	59.6°	1.23
	K^0	1.150	37.8°	0.08
	or Λ^0	0.550	37.8°	0.37
	K^0	0.400	46.0°	1.23
1.67	Λ^0	0.192	42.0°	3.47
	Λ^0	0.500	44.0°	5.95
	Λ^0	0.314	26.5°	0.19
	K^0	0.370	30.5°	1.01
2.26	Λ^0	0.850	24.2°	1.53
	K^0	1.648	2.6°	0.37
	K^0	0.380	64.7°	0.21
	K^0	0.660	26.8°	1.29
	K^0	0.780	23.5°	0.21
	Λ^0	0.850	32.1°	0.90

using Belenky's approximate formula [6]

$$\frac{\mathrm{d}\sigma_{\mathrm{el}}}{\mathrm{d}\Omega} = \frac{\alpha^2 R^4}{4\lambda^2} \exp\left[-\frac{R^2}{2\lambda^2}\theta^2_{\mathrm{CM}}\right],$$

where R is the radius of the Helium nucleus, $\alpha = \sigma_{\mathrm{tot}}/2\pi R^2$, λ the wave length of the π^- in the c.m. system, θ_{CM} the deflection of the π^-. This formula could

[6] S. Z. BELENKY: *Sov. Phys. JETP*, **3**, 813 (1956).

be made to fit the experimental results only by taking different values for R: $R = 1.45 \cdot 10^{-13}$ cm for 0.97 GeV and $1.3 \cdot 10^{-13}$ cm for 1.67 GeV π^- scattering data.

Table III reports all the relevant data on the 16 events which could be identified as neutral K or Y particles.

For the K-mesons account has been taken of the long lived component which excaped detection. For both neutral hyperons and K-mesons, the data have been corrected for loss of events due to neutral decays.

TABLE IV. – *Cross section for* $\Lambda^0(\Sigma^0)$ *and* K^0 *production.*

π^- kinetic energy (GeV)	$\sigma(\Lambda^0+\Sigma^0)$ (mb)	$\sigma(K^0)$ (mb)
0.97	0.62 ± 0.44	1.76 ± 0.88
1.67	0.74 ± 0.43	0.35 ± 0.35
2.26	0.64 ± 0.45	1.82 ± 0.91

2·3. *Strange particle production.* – The importance associated with the study of reactions leading to the production of K-mesons from ^{4}He has been pointed out in a previous paper (7).

The determination of the cross section for production of K^0's from π^--^{4}He collisions, compared with those relative to production of K^+'s from π^+-^{4}He collisions can give indications on the K^0-K^+ relative parity.

The cross sections for production of K^0, which one obtains from our observations, are listed in Table IV.

* * *

We wish to thank Dr. M. M. BLOCK and his colleagues of the Duke, Johns Hopkins, Oak Ridge, Syracuse Universities for giving us the film taken with their Helium Bubble Chamber exposed at the Berkeley π^- beams. We also wish to thank Dr. M. M. BLOCK for proposing the experiment, for his constructive remarks and for the assistance given to us during the period which he spent in our Institute.

(7) M. M. BLOCK, B. BRUCKER, C. CHANG, T. KIKUCHI, C. MELTZER, F. ANDERSON, A. PEVSNER, H. COHN, E. HARTH, J. LEITNER, G. BRAUTTI, C. FRANZINETTI and R. TOSI: *Nuovo Cimento*, **12**, 642 (1959).

Spin-Lattice Relaxation in Cerous Magnesium Nitrate.

R. P. Hudson (*) and R. S. Kaeser

Cryogenic Physics Section, National Bureau of Standards - Washington, D. C.

(ricevuto il 18 Gennaio 1961)

It has been demonstrated recently [1] that the extreme temperature-dependent behaviour of the spin-lattice relaxation time, τ, in cerous magnesium nitrate (CMN) in the region of 2 °K [2] can be explained in terms of a direct two-phonon process between the ground doublet and the first excited doublet at a separation, δ_1, of about 24 cm^{-1} ($\delta_1/k = 34$ °K). The latter figure is in quite good agreement with the (37 ± 3) °K found by Leask and Wolf [3] by measurement of the departures of the susceptibility, χ, from Curie's Law between 10 °K and 20 °K. An independent study [4] of the χ-T function (between 4 °K and 300 °K) undertaken to derive information on the separations δ_1 and δ_2 to the two excited doublet yielded a rather higher value for δ_1/k (43 °C), while $\delta_2/k \approx 300$ °K.

In the course of a general investigation of the low temperature behaviour of CMN we also used the Casimir-Du Pré [5] relaxation method, but chiefly to obtain the interaction contribution to the specific heat [6]. Since the data simultaneously provide information on τ, we have used the approach of Finn, Orbach and Wolf [1] to compute a value for δ_1 in order to help fix a best value within the present experimental spread of (34 ÷ 43) °K.

Measurements were made in a field of 50 G (and one or two points at 100 G) in the temperature range 1.64 °K to 2.12 °K, using seven different measuring frequencies between 20 Hz and 1000 Hz. Three typical χ''-χ' plots (where $\chi = \chi' - i\chi''$) are shown in Fig. 1, for $H = 50$ G. Reasonably good semicircles were obtained, demonstrating that it is valid to deduce a relaxation time from the Casimir-Du Pré theory. Below 1.6 °K, χ'' became too small to measure, even at our lowest frequency and above 2.12 °K *a*) the experimental points did not

(*) Temporary address: Clarendon Laboratory, Oxford.

(1) C. B. Finn, R. Orbach and W. P. Wolf (in course of publication); see Abstract 8-2, *7th. International Conf. Low Temp. Phys.*, (Toronto, Aug.-Sept. 1960).

(2) A. H. Cooke, H. J. Duffus and W. P. Wolf: *Phil. Mag.*, **44**, 623 (1953).

(3) M. J. M. Leask and W. P. Wolf (to be published).

(4) W. R. Hosler and R. P. Hudson (submitted for publication in the *Phys. Rev.*).

(5) H. B. G. Casimir and F. K. Du Pré: *Physica*, **5**, 507 (1938).

(6) R. P. Hudson, R. S. Kaeser and H. E. Radford: Abstract 8-3, *7th. International Conf. Low Temp. Phys.* (Toronto, Aug.-Sept. 1960).

extend far enough towards the adiabatic susceptibility, χ_S, to enable us to fit a semi-circle with confidence, and *b*) the bath temperature (controlled by a Sommers-type electronic stabilizer (7)) tended to drift.

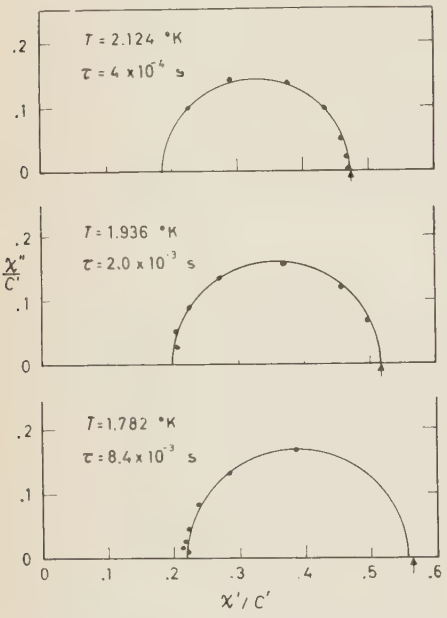

Fig. 1. – Imaginary part of susceptibility, χ'', as a function of the real part, χ'. for applied steady field $H = 50$ G. C' is the Curie constant. Arrow for each curve indicates the isothermal susceptibility, χ_0, as measured in zero field.

The derived values of τ are shown on a semilog plot against T^{-1} in Fig. 2. They show an approach to exponential behaviour ($\tau = A \exp(\delta_1/kT)$) above 2 °K, as was found by Finn and colleagues. These authors made measurements in fields of 1000. 600 and 300 G and observed that A decreased with decreasing field. Our results, for $H = 100$ and 50 G, fit this general trend. From the slope of the curve near 2 °K (dotted line) we estimate $\delta_1/k = 36$ °K (the line is actually $1.595 \cdot 10^{-11} \exp[36.27/T]$) which must be regarded as a lower limit, since a slight curvature probably persists beyond our range of measurement above 2.12 °K. Below 2 °K a second relaxation process is evidently becoming important: a T^{-1} dependent process was suggested by Finn *et al.* If we write

$$\frac{1}{\tau_{\text{meas.}}} = \frac{1}{\tau_{\text{expon.}}} + \frac{1}{\tau'},$$

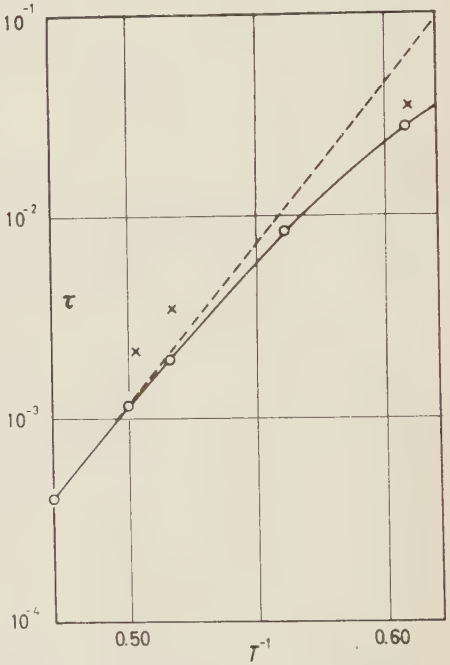

Fig. 2. – Relaxation time, τ, in seconds as a function of the inverse of the absolute temperature: ○, measurements with $H = 50$ G; ×, measurements with $H = 100$ G. Dashed line is tangent to the curve at the highest temperature (see text).

and use the departure of the curve from the straight line in Fig. 2 to calculate τ', we find a T^{-5} dependence for $0.55 < T^{-1} < 0.62$ (1.82 °K $> T > 1.61$ °K). The points fit very well to $1/\tau' = 1.63\ T^5$.

Normally, two relaxation mechanisms compete in paramagnetic salts (8), a

(7) H. S. Sommers: *Rev. Sci. Instr.*, **25**, 793 (1954).

(8) J. H. Van Vleck: *Phys. Rev.*, **57**, 426 (1940); *Quantum Electronics*. Ed. C. H. Townes (New York. 1960), p. 392.

direct process with $\tau \propto T^{-1}$ and a « Raman-type » process with $\tau \propto T^{-9}$, for ions with an odd number of electrons. The latter is usually negligible at liquid helium temperatures (but not, apparently, in cobalt salts [9] and cesium titanium alum [10]). We have attempted to decompose $1/\tau'$ further into two such components and although the fit is not quite as good as for the single T^5 variation, the experimental results may be represented rather well by

$$\frac{1}{\tau'} = 6.0T + 0.111T^9 . \tag{2}$$

Finally, we shown in Fig. 3 how the experimental points fit the complete equation for τ, viz.

$$\frac{1}{\tau} = 0.627 \cdot 10^{11} \exp[-36.27/T) + 6.0T + 0.111T^9 . \tag{3}$$

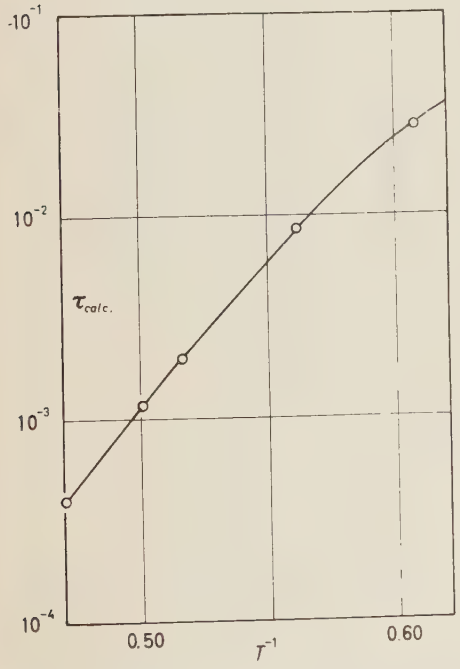

Fig. 3. – Relaxation time, τ, calculated from eq. (3) of the text, together with the experimental points for $H = 50$ G.

Although eq. (3) is in almost exact accord with our data, in drawing conclusions one must not ignore the experimental errors (which are largest at the low temperature end of the range, where χ'' is very small) nor the possibly misleading versatility of a three-term expression such as eq. (3). It seems safe to conclude, at least, that below 2 °K the direct two-phonon relaxation process is overtaken by a second-order mechanism such as is found in the majority of paramagnetics at higher temperatures. It would be interesting, if this type of measurement could be extended to still lower temperatures, to look for the term in T^{-1} as it, in turn, becomes dominant.

For similar reasons, it will be valuable to measure τ in neodymium magnesium nitrate in the range 1 °K to 20 °K. τ has been found to vary approximately as T^{-1} [11], while Dieke and Heroux [12] obtained $\delta_1 = 33.13$ cm^{-1} from optical spectrometry. Hence it would appear that the entire transition from $\exp[1/T]$ via T^{-9} to T^{-1} dependence of τ may be accessible to measurement in the low temperature region.

Confirmation has been obtained for a value of δ_1/k in the neighbourhood of 37 °K. The value of 43 °K appears, on the sum of the evidence, to be too high — unless CMN exhibits properties varying significantly from specimen to specimen, which would not be altogether surprising.

We are indebted to R. Orbach for informative discussions and for kindly making available a preprint of his publication [1].

[9] J. van den Broek, L. C. van der Marel and C. J. Gorter: *Physica*, **25**, 371 (1959).

[10] R. J. Benzie and A. H. Cooke: *Proc. Roy. Soc.*, A **209**, 269 (1951).

[11] A. H. Cooke, H. Meyer and W. P. Wolf: *Proc. Roy. Soc.*, A **237**, 395 (1956).

[12] G. H. Dieke and L. Heroux: *Phys. Rev.*, **103**, 1227 (1956).

IL NUOVO CIMENTO Vol. XIX, N. 6 16 Marzo 1961

The Coulomb Scattering of Neutral Hyperons and the Lifetime of the Σ^0.

W. S. C. Williams

Department of Natural Philosophy, The University of Glasgow - Glasgow

(ricevuto il 3 Febbraio 1961)

The decay of the neutral Σ hyperon

$$\Sigma^0 \to \Lambda + \gamma ,$$

can be reversed by the scattering of Λ hyperons in the electric field of a nucleus. The differential scattering for this process is inversely proportional to the lifetime of the decay and is peaked in the forward direction. This last feature may permit the process to be separated from meson exchange scattering and hence permit a measurement of the Σ^0 lifetime to be made, or a lower limit to be put on this lifetime.

The decay process was assumed to proceed via an effective interaction of the type

$$\eta\bar{\psi}_\Sigma(\gamma_\mu\gamma_\nu - \gamma_\nu\gamma_\mu)\left(\frac{\partial A_\mu}{\partial x_\nu} - \frac{\partial A_\nu}{\partial x_\mu}\right)\psi_\Lambda .$$

The lifetime, τ, was calculated using first order perturbation theory and is given by

$$\frac{1}{\tau} = \frac{4\eta^2 k^3}{\pi} ,$$

where k is the energy of the decay photon (units: $\hbar = c = m_e = 1$). The differential scattering cross-section was also calculated using the Born approximation and assuming the same effective interaction at the $\Sigma\Lambda\gamma$ vertex. The result is:

$$\frac{\mathrm{d}\sigma}{\mathrm{d}\Omega} = \frac{8\eta^2 Z^2}{137\pi}\frac{1}{q^4}\frac{p_2}{p_1}\left\{p_1^2(p_2^2 + E^2 - m_1 m_2) + p_2^2(p_1^2 + E^2 - m_1 m_2) - \right.$$
$$\left. - p_1 p_2 \cos\theta\,(p_1^2 + p_2^2 + 2E^2 - 2m_1 m_2)\right\}.$$

The nucleus Z is assumed infinitely heavy. q is the momentum transfer, given by

$$q^2 = p_1^2 + p_2^2 - 2p_1 p_2 \cos\theta .$$

E is the total energy of the incoming Λ and of the outgoing Σ^0. m_1 and m_2 are masses of the Λ and Σ^0 respectively.

It is evident that the scattering cross-section can be expressed in terms of τ and the figure shows $\tau(d\sigma/d\Omega)$ plotted as a function of $\cos\theta$ for Λ hyperons of momentum 1000 MeV/c incident upon lead. For example, if the lifetime is 10^{-18} s the differential scattering in the forward direction is 139 mb/sr.

The detection of this process is difficult. However, if the Λ are produced in a hydrogen filled cloud chamber by π^--mesons at an energy below the threshold for producing Σ^0 hyperons, many of the Λ will have energy above the threshold for Coulomb scattering into Σ^0. Judiciously placed lead plates could intercept many of the Λ. The decay characteristics of the final Λ observed will distinguish between various possible histories which can occur between production and decay. The processes which are confusable with the process to be observed are inelastic scattering of Λ and the nuclear scattering which converts Λ into Σ^0. If the lifetime is very short, the strong forward Coulomb scattering may be distinguishable, provided the experimental conditions are carefully chosen.

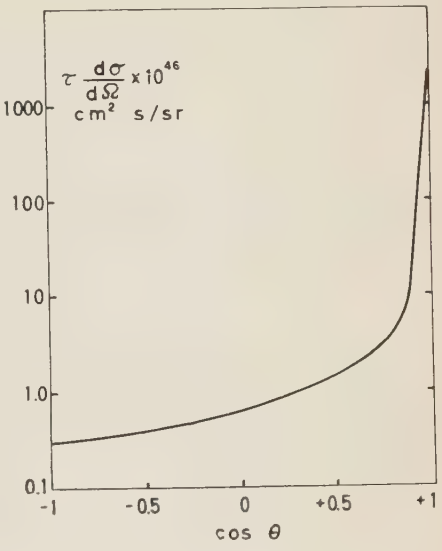

Fig. 1. – $\tau(d\sigma/d\Omega)$ plotted as a function $\cos\theta$ for 1000 MeV/c Λ hyperons incident upon lead.

The effects of the nuclear form factor and of any form factor at the $\Sigma\Lambda\gamma$ vertex have not been included in the calculation given above.

* * *

I am indebted to Dr. R. G. Moorhouse for assistance with the perturbation calculations.

On a Schrödinger Equation for a Radiating Electron.

G. Valentini

Istituto di Scienze Fisiche dell'Università - Milano

(ricevuto il 20 Febbraio 1961)

In a note appeared in 1959 (1) P. Caldirola points out the possibility to treat by means of the Lagrangian and Hamiltonian formalism the system of an electron subjected to electrodynamic reaction forces, which are not derivable from a potential function. Starting from the consideration of the Newtonian equations of motion for a particular model of rigid finite electron (in classical non-relativistic approximation) of the form

$$m\left(\ddot{x}_h - \frac{\tau}{2}\dddot{x}_h + \alpha^2 \ddddot{x}_h\right) = -\frac{\partial U}{\partial x_h}, \qquad (h = 1, 2, 3); \qquad \alpha = \frac{\tau}{4},$$

he comes to the Lagrangian function

$$\mathscr{L} = -\exp\left[-\frac{4}{\tau}t\right]\left\{\frac{\tau^2}{32}m\ddot{x}_h\ddot{x}_h + U\right\}.$$

With the introduction of generalized canonical variables according to Ostrogradsky:

$$q_h = x_h, \qquad p_h = \frac{\delta\mathscr{L}}{\delta\dot{q}_h} = \frac{\partial\mathscr{L}}{\partial\dot{q}_h} - \frac{\mathrm{d}}{\mathrm{d}t}\frac{\partial\mathscr{L}}{\partial\ddot{q}_h},$$

$$Q_h = \dot{x}_h, \qquad P_h = \frac{\delta\mathscr{L}}{\delta Q_h} = \frac{\partial\mathscr{L}}{\partial\ddot{q}_h} - \frac{\mathrm{d}}{\mathrm{d}t}\frac{\partial\mathscr{L}}{\partial\dddot{q}_h},$$

the equations of motion can be written in the Hamiltonian form, the Hamiltonian being

$$H = p_h Q_h - \frac{8}{m\tau^2}\exp\left[\frac{4}{\tau}t\right]P_h P_h + \exp\left[-\frac{4}{\tau}t\right]U(q, t).$$

(1) P. Caldirola: *Rend. Ist. Lomb. Sc.*, A **93**, 439 (1959).

In order to write the corresponding Schrödinger equation, let us assume the canonical variables $q_\hbar$, $Q_\hbar$ to be independent variables and associate to these the operators $\cdot q_\hbar$ and $\cdot Q_\hbar$ and to the conjugate variables $p_\hbar$, $P_\hbar$ the operators $-i\hbar(\partial/\partial q_\hbar)$ and $-i\hbar(\partial/\partial Q_\hbar)$, which obey the commutation rules: $[q_\hbar, p_\hbar] = i\hbar$; $[Q_\hbar, P_\hbar] = i\hbar$.

Then the time evolution of any state Ψ of the system will be given by the Schrödinger equation

$$i\hbar \frac{\partial \Psi}{\partial t} = \mathscr{H}\Psi , \tag{1}$$

where $\mathscr{H}$ coincides with H if for $q_\hbar$, $p_\hbar$, $P_\hbar$ we mean the corresponding operators.

From eq. (1), by means of a suitable generalization of the usual boundary conditions on Ψ, we are able to derive a continuity equation [2]. In fact let us define

$$\varrho = \int \Psi\Psi^* \, \mathrm{d}Q_{123} , \qquad j_\hbar = \int \Psi Q_\hbar \Psi^* \, \mathrm{d}Q_{123} ,$$

which can be respectively interpreted as a probability density and probability current density; they turn out to be connected through the equation

$$\frac{\partial \varrho}{\partial t} + \operatorname{div} j = -\frac{i\hbar 8}{m\tau^2} \exp\left[\frac{4}{\tau} t\right] \int_{S(Q_{123})} \left(\Psi^* \frac{\partial \Psi}{\partial Q_\hbar} - \Psi \frac{\partial \Psi^*}{\partial Q_\hbar} \right) \times \boldsymbol{n} \, \mathrm{d}S(Q_{123}) .$$

Now if we suppose that Ψ and its gradient vanish at the boundary of the Q-space (this is equivalent to require that the probability of finding a particle with infinite velocity be zero), then we have

$$\frac{\partial \varrho}{\partial t} + \operatorname{div} j = 0 ,$$

whence it follows that we can normalize Ψ and interpret $\Psi^*\Psi$ according to the usual meaning of probability density.

We show now that it is possible to reduce eq. (1), at least in the case of an elastic or constant potential function, to a Schrödinger equation with time-independent coefficients [3]. To this purpose we express the state $\Psi(q, Q, t)$ of our system by means of another state $\psi(q, Q, t)$ related to it through a unitary transformation: $\Psi(q, Q, t) = \exp[iS(t)]\, \psi(q, Q, t)$, on the condition that at $t = t^0$ be $\Psi(qQt_0) = \psi(qQt_0)$ and $S = 0$. Thus we come to the following Schrödinger equation for the state ψ:

$$i\hbar \frac{\partial \psi}{\partial t} = \left\{ \exp[-iS] \left[p_\hbar Q_\hbar - \frac{8}{m\tau^2} \exp\left[\frac{4}{\tau} t\right] P_\hbar P_\hbar + \exp\left[-\frac{4}{\tau} t\right] U \right] + \hbar \frac{\partial S}{\partial t} \right\} \psi .$$

---

[2] A continuity equation formally similar to the one here derived has been used by L. WALDMANN [*Zeits. f. Naturwiss.*, **8a**, 583 (1953)] in a study on the Schrödinger equation corresponding to the classical equation (without dissipative terms): $m[\ddot{x}_\hbar - (1/\omega^2)\dddot{x}_\hbar] = -\partial U/\partial x_\hbar$.

[3] The transformation here applied has been used by K. W. STEVENS [*Proc. Phys. Soc.*, **72**, 1027 (1958)] in a study of the Schrödinger equation for a damped harmonic oscillator.

We put now $S=\Gamma_1+\Gamma_2$

$$\Gamma_1=\gamma_1\frac{(p_h q_h+q_h p_h)}{4\hbar}(t-t_0)\,,\qquad \Gamma_2=\gamma_2\frac{(P_h Q_h+Q_h P_h)}{4\hbar}(t-t_0)\,;$$

as a consequence of the commutation rules between q, p and Q, P the following relations hold:

$$\exp[-i\Gamma_1]\,p_h\exp[i\Gamma_1]=p_h\exp\left[\gamma_1\frac{(t-t_0)}{2}\right],$$

$$\exp[-i\Gamma_1]\,q_h\exp[i\Gamma_1]=q_h\exp\left[-\gamma_1\frac{(t-t_0)}{2}\right],$$

$$\exp[-i\Gamma_1]\,p_h p_h\exp[i\Gamma_1]\;=p_h p_h\exp[\gamma_1(t-t_0)]\,,$$

$$\exp[-i\Gamma_1]q_h q_h\exp[i\Gamma_1]=q_h q_h\exp[-\gamma_1(t-t_0)]\,,$$

and other similar relations concerning P, Q and Γ_2.

If we make $\gamma_1=\gamma_2=-4/\tau$, that is

$$S=-\frac{(t-t_0)}{\hbar\tau}\,(p_h q_h+q_h p_h+Q_h P_h+P_h Q_h)\,,$$

we come to the equation

$$i\hbar\frac{\partial\psi}{\partial t}=\left\{p_h Q_h-\exp\left[\frac{4}{\tau}t_0\right]\frac{8}{m\tau^2}P_h P_h+\exp\left[-\frac{\tau}{4}t\right]\exp[-iS]\,U\exp[iS]-\right.$$
$$\left.\frac{1}{\tau}(p_h q_h+q_h p_h+P_h Q_h+Q_h P_h)\right\}\psi\,,$$

where the whole burden of the explicit time-dependence is now in the only term containing the potential $U(q_h,t)$. In order to have a time-independent coefficient equation for the state ψ, it must necessarily be

$$\exp\left[-\frac{4}{\tau}t\right]\exp[-i\Gamma_1]\,U\exp[i\Gamma_1]=R\,,$$

R being a time-independent operator. This happens for instance if $U(q,t)$ is an elastic potential (we neglect the trivial case $U=k$); then we have

$$\exp\left[-\frac{4}{\tau}t\right]\exp[-i\Gamma_1]\,U\exp[i\Gamma_1]=\frac{k}{2}q_h q_h\exp\left[-\frac{4}{\tau}t_0\right],$$

and we obtain for the state ψ the Schrödinger equation

$$(2) \qquad i\hbar \frac{\partial \psi}{\partial t} = \left\{ p_\hbar Q_\hbar - \exp\left[\frac{4}{\tau} t_0\right] \frac{8}{m\tau^2} P_\hbar P_\hbar + \right.$$

$$\left. + \frac{k}{2} \exp\left[-\frac{4}{\tau} t_0\right] q_\hbar q_\hbar - \frac{1}{\tau} (p_\hbar q_\hbar + q_\hbar p_\hbar + P_\hbar Q_\hbar + Q_\hbar P_\hbar) \right\} \psi ,$$

where t_0 can also be assumed equal to zero.

To conclude this brief note we want to remark that the study of an equation of form (2) can give useful information on the behaviour of the radiating electron, even if, as it is obvious, the physical problem requires, for a complete study, together with eq. (2) for the electron, the simultaneous consideration of the system (electromagnetic field) coupled with the electron [4].

* * *

I wish to thank Prof. P. CALDIROLA for helpful discussions and suggestions.

---

[4] This situation is analogous to the one pointed out by I. R. SENITZKY [*Phys. Rev.*, **119**, 670 (1960)] in the study of the radiation field of a cavity by means of a damped harmonic oscillator.

LIBRI RICEVUTI E RECENSIONI

Libri ricevuti.

R. C. Koch: *Activation Analysis Handbook*, vol. I, Academic Press Inc., Publishers, New York, 1960; pp. x-219, 64 s.

A. F. Ioffe: *Physics of Semiconductors*, Infosearch Ltd., London, 1961; pp. xi-436, 84 s.

Orear: *Fundamental Physics*, J. Wiley and Sons Inc., New York, 1961; pp. 381, $ 6.75.

H. B. Barlow *et al.*: *Kibernetik*, Band I, Heft 1, Springer-Verlag, Berlin-Göttingen, Heidelberg, 1961; pp. 56, D.M. 12,80.

E. Segrè: *Annual Review of Nuclear Science*, vol. X, Annual Reviews Inc., Palo Alto, Cal., 1960; pp. vii-617, $ 7.50.

T. E. Sterne: *An Introduction to Celestial Mechnics*, vol. IX, Interscience Publishers Inc., New York-London, 1961, pp. vii-206, $ 2.50.

J. H. Sanders: *The fundamental Atomic Constants*, Oxford University Press, 1961; pp. vi-88, 10 s.

S. S. Drell and F. Zachariasen: *Electromagnetic Structure of Nucleons*, Oxford University Press, 1961; pp. viii-111, 12 s. 6 d.

H. E. Duckworth: *Proceedings of the International Conference of Nuclidic Masses*; University of Toronto Press, Toronto, 1960; pp. xi-540; $ 10.00.

D. Kastler: *Introduction à l'Electrodynamique Quantique*; Dunod, Paris, 1961; pp. xxxiii-333; N. F. 69.

C. Brown and N. Clarke: *International Education in Physics*; The Technology Press and John Wiley and Sons Inc., New York, 1960; pp. xvi-191.

Recensioni.

G. Friedlander et J. W. Kennedy – *Chimie Nucléaire et Radiochimie* Tradotto dall'americ. da J. Guizerix e P. Martinelli. Dunod ed., Paris, 1960; pp. 496; NF 58.

È significativa la circostanza che, tra gli ormai numerosi testi che trattano questo argomento, si sia ritenuto opportuno tradurre in francese il lavoro di Friedlander e Kennedy, tanto più che la letteratura francese dispone su questo argomento di una solida tradizione e di una produzione molto aggiornata e di notevole valore. Ciò costituisce un'ulteriore prova, ammesso che ve ne fosse bisogno, a favore di questo libro il cui successo è legato alla chiarezza e alla semplicità con cui vengono trattati i diversi argomenti.

Altra caratteristica positiva di quest'opera è costituita dalla successione razionale con cui le diverse parti vengono sviluppate: il testo risulta pertanto di notevole valore didattico ed è facilmente accessibile anche allo studioso che si accosti per la prima volta a tali argomenti, tanto più che ogni capitolo è corredato da esercizi numerici con relative soluzioni.

Nella traduzione francese, curata da J. Guizerix e P. Martinelli, ed edita per i tipi della Casa Editrice Dunod, tali caratteristiche permangono e di questo si deve dare atto alla competenza e alla capacità dei traduttori. Sarà bene a questo punto osservare come in Italia si sia alieni dal tradurre nella nostra lingua libri stranieri ed anzi si noti una sempre crescente tendenza a leggere e studiare su testi scritti in altre lingue. Ciò, pur presentando l'innegabile vantaggio di una maggiore padronanza in una lingua straniera, ingenera peraltro una spiacevole tendenza ad usare correntemente una terminologia straniera o, cosa ancor più deprecabile, italianizzata (di cui « targhetta » e « splittamento » sono esempi ormai classici). Non credo infatti di affermare cosa nuova nel sottolineare la necessità, sempre più sentita in vasti strati della cultura italiana, di avere una traduzione corretta dei vocaboli tecnici usati negli altri Paesi. Sarebbe quindi auspicabile incoraggiare e promuovere la traduzione in italiano dei libri scientifici che vanno per la maggiore perchè ciò rappresenterebbe un primo passo per la soluzione di tale problema.

Il libro è talmente noto che non mi sembra opportuno dilungarmi sul suo contenuto; parecchie edizioni americane, a partire dal 1949, gli avevano già assicurato una ben giustificata notorietà. Desidero piuttosto rimarcare la concezione base su cui è costruito il testo: esporre i vari argomenti più da un punto di vista concettuale, che rigorosamente matematico.

Solo nel capitolo in cui vengono trattati statisticamente il fenomeno della radioattività e la sua misura, si può notare un diverso stile di testo, da parere addirittura trapiantato da un'altra fonte che contrasta nettamente con tutto l'assieme. Non vedo infatti perchè si sia voluto sviluppare con tale eccessivo formalismo quest'argomento, quando molte altre parti di Chimica Nucleare e Radiochimica, pure ampiamente svolte, siano notoriamente suscettibili di una trattazione altrettanto rigorosa.

Desidero inoltre sottolineare in questa sede l'eccellente stile con cui sono esposti argomenti quali le leggi del decadimento radioattivo, la parte riguardante la natura e la produzione delle reazioni nucleari, l'interazione delle radiazioni con la materia e le applicazioni dell'energia nucleare e dei radioisotopi nell'economia e nella ricerca moderna.

Per finire vorrei aggiungere che tale libro, di fondamentale importanza per tutti coloro che iniziano gli studi di Radiochimica, non dovrebbe mancare nella biblioteca di coloro che in tale materia non sono più principianti, perchè in esso si trova sempre qualcosa di nuovo ed una risposta alle incertezze che, nello studio, si possono molto spesso presentare.

Limitati ma ben selezionati riferimenti bibliografici facilitano il lavoro di perfezionamento del lettore negli argomenti trattati dai singoli capitoli del testo.

G. Semerano

Progress in Elementary Particle and Cosmic Ray Physics, vol. V; J. G. Wilson e S. A. Wouthuisen, Editor; North Holland Pubblishing Company - Amsterdam, 1960; pp. XII-461. Fl. 45.

Il quinto volume accentua ulteriormente, rispetto al precedente, l'interesse riservato nella collezione, alla Fisica delle Particelle Elementari, e l'aggiunta al titolo indica esplicitamente il nuovo orientamento. I volumi futuri, come viene preannunciato dagli editori nella preparazione, verranno dedicati alternativamente ai due campi distinti delle particelle elementari e dei problemi di natura astrofisica e geofisica riguardanti i raggi cosmici.

Il presente volume contiene i seguenti articoli: *Interazioni deboli* di

A. Lundby; *Fenomenologia dell'interazione nucleone-nucleone* di J. L. Gammel e R. M. Thaler; *Teoria degli antinucleoni* di J. McConnel; *Osservazione delle interazioni di raggi cosmici di tipo « jet » nelle emulsioni nucleari* di D. H. Perkins; *Assorbimento e decadimento di mesoni μ negativi* di R. M. Tennent.

Il primo articolo è una rassegna degli esperimenti che sono stati compiuti nel campo delle interazioni deboli (essenzialmente decadimenti leptonici) dopo la scoperta della non conservazione della parità. Assieme ad una chiara formulazione dei risultati teorici, sono descritti vari esperimenti di correlazione e asimmetria nel decadimento β dei nuclei e del neutrone e nei decadimenti dei mesoni π e μ; sono riportati risultati aggiornati al Febbraio del 1959. Vengono quindi descritti i metodi usati per la produzione di fasci polarizzati di neutroni ed elettroni e per le misure di polarizzazione nei raggi β e γ.

Il secondo articolo dà un quadro organico e completo della fenomenologia delle interazioni tra due nucleoni. Dopo una breve storia delle tappe più importanti nello studio delle forze nucleari e considerazioni generali sulla natura del potenziale, basata sui principi di conservazione usuali, viene riportata un'analisi accurata dei dati relativi allo scattering p-p e n-p a basse e ad alte energie (fino a 310 MeV). Viene quindi riportato il « best fit » per i parametri relativi ai vari termini del potenziale fenomenologico di Gammel e Thaler, e viene discusso il potenziale semi-teorico di Gartenhaus e i suoi perfezionamenti ulteriori. Vengono infine trattati i processi radiativi della fotodisintegrazione del deutone e della cattura n-p. L'articolo dovrebbe essere particolarmente utile sia per i fisici teorici che sperimentali che lavorano in questo campo.

Il terzo articolo è una rassegna del materiale teorico che si è venuto rapidamente accumulando negli ultimi anni sulle proprietà degli antinucleoni. Per i processi di produzione di coppie $\mathcal{N}\overline{\mathcal{N}}$ nelle collisioni $\mathcal{N}$-$\mathcal{N}$ e π-$\mathcal{N}$ e di annichilazione vengono riportati risultati generali basati sui principi di conservazione e risultati specifici di calcoli perturbativi e statistici. Vengono quindi riportati, per l'interazione degli antinucleoni nei nuclei e con nucleoni liberi, risultati ottenuti mediante applicazione del modello ottico. Il quadro generale rivela l'aspetto frammentario della conoscenza attuale in tale campo.

Il quarto articolo è connesso con i raggi cosmici; esso costituisce un'analisi approfondita dello studio degli eventi di altissima energia (maggiore di 1000 GeV) mediante la tecnica delle emulsioni nucleari. Vengono trattati i problemi della identificazione delle particelle nei « jets » e delle loro distribuzioni angolari ed energetiche, della determinazione della energia della particella primaria e della anelasticità nella collisione. L'articolo presenta una descrizione esauriente dei metodi di indagine dei risultati sperimentali; inoltre si fa cenno alle teorie più importanti sulla produzione dei mesoni.

Nell'ultimo articolo l'autore riprende il problema dell'assorbimento dei mesoni μ^- in vari materiali, già trattato nel volume II della serie (Sard e Crouch); assieme ai risultati di nuovi esperimenti di raggi cosmici, vengono riportati i risultati di esperimenti effettuati con le macchine acceleratrici. Viene data una descrizione dei vari processi che hanno luogo nella cattura dei mesoni μ^-, e vengono descritti i metodi usati per le misure. Tabelle aggiornate fino ai primi mesi del 1959 riportano le probabilità di scomparsa e interazione dei μ^+ in una trentina di elementi. L'articolo si conclude con un confronto dei dati sperimentali con la teoria.

G. Costa